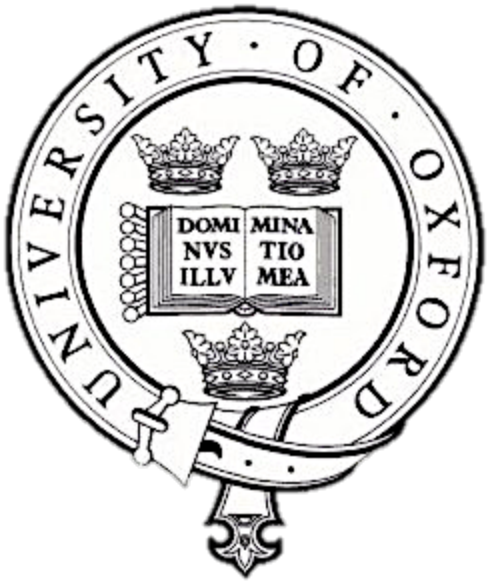
# Imaging-based analysis of antibody superagonism




**Meike Christina Aßmann**

**St. Edmund Hall**

Supervisor: Simon J. Davis

Thesis submitted for the degree of Doctor of Philosophy

Trinity Term, 2016

The work described in this thesis was supported by the Medical Research Council [grant number 1238220].






## Abstract

### Imaging-based analysis of antibody superagonism

Meike Christina Aßmann, St. Edmund Hall
Thesis submitted for the degree of Doctor of Philosophy
Trinity Term, 2016

Activating antibodies against the T-cell costimulator CD28 fall into two categories: those that require an additional stimulus, such as an anti-TCR antibody, to fully active a T cell are termed "conventional antibodies" (CAs), and those that induce such strong signalling that T cells become activated in the absence of TCR ligation are referred to as "superagonists" (SAs). It was proposed that SAs are particularly potent because they sterically exclude large phosphatases such as CD45 more efficiently from signalling receptors *versus* CAs. To test this, we stimulated T-cell lines with an anti-CD28 SA or CA immobilised on glass surfaces. Although no TCR ligand is present, we confirmed that the expression of the TCR is nevertheless required for SA-induced signalling on glass. We showed that the SA is only active on glass when it is immobilised *via* its Fc, and that signalling is sensitive to the dimensions of the antibody/CD28 complex relative to those of CD45. We then visualised the organisation of these proteins by imaging. When treated with the SA, T cells form contacts with the glass slide that exclude CD45 ~ 2-fold more efficiently *versus* CA treatment, and both antibody-bound CD28 and CD45 slow down their diffusion to a greater extent under SA *versus* CA treatment. Both the exclusion of CD45 and the restriction of CD28 and CD45 diffusion appear to be steric effects, caused by the SA bridging a narrow gap between cell and glass surface. We hypothesize that SAs induce particularly potent signalling by protecting CD28 from dephosphorylation by CD45 *via* (1) spatially segregating the two proteins, and (2) reducing their encounter rate by slowing them down, while kinases continue to diffuse and have access to CD28. In summary, our results provide evidence that antibody superagonism is driven by size-dependent local perturbations in kinase and phosphatase organisation and diffusion.

*Für Gerd*

## Acknowledgements

First and foremost, I would like to thank my supervisor, Simon Davis, for giving me the opportunity to be part of a very exciting research project, for your example in being a brilliant and enthusiastic scientist, for many enlightening discussions, and for your patience in supervising me.

David Klenerman and Steven Lee, for many fruitful discussions that lead to great imaging data. Anna Lippert, for coming up with a brilliant way to analyse our data and for many fun hours at the microscope. James McColl, for being the Lord of the Rings of superagonism. Matthieu Palayret, for the prettiest super-resolution images, and for answering all my questions on analysis even all the way from France. Marco Fritzsche, for teaching me how to use Matlab and for all your time spent on a personalised CalQuo version. Mai Vuong, for being my right hand in all things IL-2 and cell culture, and for your cheerfulness and energy. Mafalda Santos, for taking over the Lck story of superagonism, for all your advice on science and on life, and for being like a second big sister. Rachel Knox, for all your hard work cloning, growing cells and doing IL-2 assays alongside me, for your friendship, and for making me feel at home in Cambridge. Jiandong Huo, for teaching me how to use the BIAcore and for cooking the most delicious hotpot and dumplings. James Felce, for getting me started in the lab and for being an unbeatable example of efficiency and excellence. Ricardo Fernandes, for smart advice every time my experiments got stuck, and for being the best example of a relaxed attitude towards science and life that I still need to achieve. Janet Fennelly, for showing me how to produce proteins and for your wisdom and support through the ups and downs of a PhD and life in general. Oliver Lui, for all your practical help and many fun chats in the office, and for sharing your emergency chocolate supply. Martin, Jemma, Heather, Elizabeth, Susan, Chris, Debbie, Hideo, Veronica, for many fun times in the lab and all your support.

Nothing would be possible without the support of my family and closest of friends. My parents, grandparents, and sister, for encouraging me at every stage of my life, and for your frequent visits to Oxford. Laura, Sina, Sophie, for your friendship. Joni, for introducing me to the excitement of science, you are missed. Niko, for the most precious memories of friendship, laughter, and an easiness in life that always keep me going.

## Contents

**Chapter 1 General introduction ..... 1**

1.1. Overview of the immune system ..... 1

1.2. Innate immunity and the inflammatory response ..... 1

1.3. The adaptive immune response ..... 3

1.3.1. Antigen presentation ..... 3
1.3.2. The source of variability and specificity in adaptive immunity ..... 4
1.3.3. Functional antigenic receptors are selected for that do not bind to self ..... 5
1.3.4. T-cell mediated immunity ..... 6
1.3.5. B-cell mediated immunity ..... 8

1.4. Structural and functional properties of antibodies ..... 8

1.4.1. Fc receptors ..... 10

1.5. The immunological synapse ..... 12

1.6. Immunoreceptors ..... 13

1.6.1. The TCR ..... 14
1.6.2. CD28 ..... 15

1.7. The triggering problem ..... 18

1.7.2. Aggregation models ..... 23

1.8. Triggering receptors with antibodies ..... 30

1.9. Application of antibodies against immunoreceptors in therapy ..... 32

1.10. Aims of this thesis ..... 34

**Chapter 2 General materials and methods ..... 35**

2.1. Cell Culture ..... 35

2.2. Flow Cytometry ..... 36

2.3. Molecular Cloning ..... 37

2.4. Sodium Dodecyl Sulphate – Polyacrylamide Gel Electropheresis (SDS-PAGE) ..... 42

2.5. Western blot ..... 44

2.6. Transduction of cell lines with lentivirus for stable expression ..... 45

2.7. Production and purification of soluble His-tagged protein in mammalian cell lines ..... 46
2.7.1. Protein production in CHO cells with a glutamine synthetase selection system ..... 47
2.7.2. Protein production in CHO cells with a lentiviral system ..... 51
2.7.3. Purification of soluble His-tagged protein from cell culture supernatant with affinity chromatography ..... 53
2.8. Purification of antibody from hybridoma culture supernatant ..... 54
2.9. Digest of antibody with papain for Fab production ..... 55
2.10. Labelling of antibodies and Fab fragments with fluorescent dyes ..... 56
2.11. IL-2 *in vitro* stimulation assay ..... 57
2.11.1. IL-2 enzyme-linked immunosorbent assay (ELISA) ..... 59
2.11.2. IL-2 stimulation data analysis and presentation ..... 59
2.12. Surface plasmon resonance-measurements on the BIAcore ..... 61
2.13. Antibodies used throughout the thesis ..... 63

**Chapter 3 The mitogenic potential of JJ316 is not explained by affinity 66**

3.1. Introduction ..... 66
3.2. Materials and methods ..... 67
3.2.1. Measuring whole antibody binding kinetics to cell-bound receptors 67
3.3. Results ..... 68
3.3.1. JJ319 and JJ316 have similarly low off-rates when bound to rmCD28 expressed on the cell surface ..... 68
3.3.2. JJ319 binds to rmCD28 expressed on the cell surface with a higher on-rate than does JJ316 ..... 69
3.3.3. Surface plasmon resonance-based affinity measurements ..... 69
3.3.4. JJ316 and JJ319 soluble binding affinities and kinetics are identical . 72
3.3.5. Comparing BIAcore to flow-cytometry measurements ..... 87
3.4. Discussion ..... 91

**Chapter 4 Antibody superagonism can be studied on glass surfaces 94**

4.1. Introduction ..... 94
4.2. Materials and methods ..... 95
4.2.1. Harvest of primary mouse CD4+ T-cells ..... 95

4.2.2. Calcium flux assay ..... 96
4.3. Results ..... 99
4.3.1. JJ316 is superagonistic on glass whereas JJ319 is costimulatory ..... 99
4.3.2. JJ316 is most active when immobilised on glass indirectly ..... 106
4.3.3. Superagonism is a phenomenon of weak, tonic signalling ..... 108
4.3.4. Superagonistic signalling differs on glass *versus* on EIA plastic ..... 114
4.4. Discussion ..... 123

**Chapter 5 The requirements for antibody superagonism are compatible with a "kinetic-segregation" based theory of signalling... 126**

5.1. Introduction ..... 126
5.2. Materials and methods ..... 127
5.2.1. Immobilisation of His-tagged mFcγRIIb on Ni-NTA-coated plastic ..... 127
5.3. Results ..... 128
5.3.1. The activity of soluble JJ316 is not abrogated by "silencing" its Fc region ..... 128
5.3.2. JJ316-induced superagonism is Fc-dependent ..... 129
5.3.3. Superagonism is crosslinking-dependent ..... 134
136
5.3.4. Superagonism is dependent on receptor dimensions ..... 138
5.3.5. Superagonism is sensitive to phosphatase dimensions ..... 141
5.3.6. Superagonism is sensitive to antibody dimensions ..... 144
5.3.7. The extended JJ316 antibodies are demonstrably larger ..... 149
5.3.8. Superagonism may be a quantitative phenomenon ..... 154
5.4. Discussion ..... 164

**Chapter 6 Imaging-based analysis of the effects of antibodies on receptor diffusion and phosphatase segregation ..... 167**

6.1. Introduction ..... 167
6.2. Materials and methods ..... 168
6.2.1. Culturing of the YW62.3.20 hybridoma for anti-mCD45-Fab production ..... 168
6.2.2. Photoactivated localization microscopy (PALM) imaging [271] ..... 169
6.2.3. Diffusion analysis ..... 169
6.2.4. Bulk-labelling experiments ..... 170
6.3. Results ..... 171

6.3.1. Principles of PALM and TIRFM imaging ..... 171
6.3.2. Super-resolved images indicate that CD28 distribution or diffusion is altered by the superagonist ..... 174
6.3.3. Single-particle tracking reveals that the superagonist constrains CD28 diffusion ..... 178
6.3.4. Production of labelled anti-mCD45-Fab ..... 188
6.3.5. Single-molecule imaging reveals that CD28 and CD45 do not colocalize ..... 190
6.3.6. JJ316, but not JJ319 constrains CD45 diffusion ..... 194
6.3.7. The superagonist constrains CD28 diffusion partially by steric effects ..... 194
6.3.8. Bulk-labelling experiments reveals that JJ316 induces the local segregation of CD45 more efficiently than JJ319 ..... 197
6.4. Discussion ..... 201

**Chapter 7 General discussion ..... 205**

7.1. Results from this thesis ..... 205

7.2. Future work ..... 216

7.3. Concluding remarks ..... 219

## List of Figures

Figure 1-1: Space-filling model of the human IgG structure. ..... 11

Figure 1-2: The T-cell signalling machinery. ..... 16

Figure 1-3: Downstream signalling pathways of CD28. ..... 18

Figure 1-4: The mechanism behind TCR triggering according to the kinetic-segregation model. ..... 29

Figure 1-5: Superagonistic antibodies form compact complexes with receptors. ..... 33

Figure 2-1: Vector map for pHR-SIN-CSGWdNotI/dEcoRI (pHR) ..... 37

Figure 2-2: Vector map for pEE14 (Lonza Biologics). ..... 48

Figure 3-1: Association and dissociation curves of whole antibodies binding to cell-bound receptors. ..... 71

Figure 3-2: Design of a His-tagged soluble rat CD28 - mouse Fc fusion protein. ..... 74

Figure 3-3: Transfected CHO-K1 clones produce rCD28-mFc-His. ..... 75

Figure 3-4: Western blot confirms expression of rCD28-mFc-His. ..... 77

Figure 3-5: Purification of soluble rCD28-mFc-His with size exclusion chromatography. ..... 78

Figure 3-6: SDS-PAGE of purified soluble rCD28-mFc-His[8]. ..... 78

Figure 3-7: Characterisation of the Fab-containing protein G elution for the JJ316 papain test digest with size exclusion chromatography. ..... 80

Figure 3-8: Purification of JJ316 Fab fragments with size exclusion chromatography. ..... 81

Figure 3-9: SDS-PAGE of JJ316 Fab fragments. ..... 82

Figure 3-10: Purification of JJ319 Fab fragments with size exclusion chromatography. ..... 83

Figure 3-11: SDS-PAGE of JJ319 Fab fragments. ..... 84

Figure 3-12: Equilibrium measurement of mouse B7-1 3D affinity for rat CD28 at 37 ºC (BIAcore). ..... 85

Figure 3-13: Kinetic measurement of JJ316 soluble affinity at 37 ºC (BIAcore). ..... 89

Figure 3-14: Kinetic measurement of JJ319 soluble affinity at 37 ºC (BIAcore). ..... 90

Figure 4-1: Design of chimeric CD28 receptors. ..... 100

Figure 4-2: Experimental set-up for the IL-2 stimulation assay. ..... 102

Figure 4-3: JJ316 induces superagonistic signalling in murine T-cell hybridoma lines on glass, whereas JJ319 is costimulatory. ..... 104

Figure 4-4: JJ316 induces T-cell activation in the absence of a second stimulus whereas JJ319 does not. ..... 105

Figure 4-5: Indirectly immobilised JJ316 induces signalling more efficiently than when soluble or directly immobilised. ..... 107

Figure 4-6: Experimental procedure in the calcium flux assay. ..... 110

Figure 4-7: Microscopy-based calcium flux assay. ..... 111

Figure 4-8: Indirectly immobilised superagonist does not induce an early calcium flux. ..... 112

Figure 4-9: Primary C57BL/6 $CD4^+$ splenocytes respond to KT3 stimulation with an early calcium flux. ..... 113

Figure 4-10: Superagonism is partially independent of CD28 signalling on EIA plastic, but not on glass, and dependent on the presence of the TCR on both EIA plastic and glass. ..... 117

Figure 4-11: Superagonism is dependent on both TCR and CD28 expression levels. ..... 120

Figure 4-12: EIA plastic immobilises 5-fold more antibody as compared to glass. . 121

Figure 4-13: Superagonising truncCD28, but not rmCD28 is sensitive to the amount of antibody immobilisation. ..... 122

Figure 5-1: SDS-PAGE analysis of a PNGaseF-digest of JJ316. ..... 130

Figure 5-2: SDS-PAGE analysis of a ficin digest of JJ316. ..... 131

Figure 5-3: Deglycosylated and "Fc-silent™" JJ316-derivatives are active in solution. ..... 132

Figure 5-4: The $F(ab')_2$ fragment of JJ316 is only active when immobilised. ..... 133

Figure 5-5: Design of a monomeric PDCD28 chimera. ..... 135

Figure 5-6: Crosslinking CD28 is required for superagonistic signalling. ..... 136

Figure 5-7: PDCD28 signalling induced by crosslinking is TCR-dependent. ..... 137

Figure 5-8: Design of an extended FcCD28 chimera. ..... 139

Figure 5-9: Extending the CD28 extracellular domain abrogates superagonism. ..... 141

Figure 5-10: Design of chimeric full-length and truncated phosphatases. ..... 143

Figure 5-11: JJ316-induced superagonistic signalling is sensitive to the CD148 and CD45 phosphatase dimensions. ..... 146

Figure 5-12: Schematic depiction of an extended JJ316 form. ..... 147

Figure 5-13: Design of a JJ316 antibody extended in the hinge region. ..... 148

Figure 5-14: Custom-engineered extended JJ316 antibodies are demonstrably larger. ..... 149

Figure 5-15: Extended JJ316 forms bind cells-surface expressed rmCD28. ..... 151

Figure 5-16: Extended JJ316 antibodies bind to plate-bound secondary antibody. ..... 152

Figure 5-17: Extended JJ316 antibodies are costimulatory, but not superagonistic. 153

Figure 5-18: Design of a His-tagged soluble mFcγRIIb construct. ..... 155

Figure 5-19: Western blot confirms expression of mFcγRIIb-His[34] ..... 156

Figure 5-20: Purification of soluble mFcγRIIb-His with size exclusion chromatography[35] ..... 157

Figure 5-21: SDS-PAGE of purified soluble mFcγRIIb-His. ..... 158

Figure 5-22: mFcγRIIb binds mIgG1 and rIgG2a with low to intermediate affinity. ..... 160

Figure 5-23: Ni-NTA plastic immobilises His-tagged protein more efficiently than antibody-coated glass or EIA plastic. ..... 162

Figure 5-24: JJ319 is superagonistic when immobilised densely *via* a His-tagged Fc receptor on Ni-NTA-coated plastic. ..... 163

Figure 6-1: Schematic explanation of the principle behind PALM/STORM super-resolution imaging. ..... 173

Figure 6-2: Schematic depiction of the principle behind TIRFM. ..... 174

Figure 6-3: Design of chimeric CD28-mEos3.2 fusion proteins. ..... 175

Figure 6-4: Super-resolved images of truncCD28-mEos stimulated with JJ316 or JJ319. ..... 177

Figure 6-5: Single-particle tracking of CD28 in live cells. ..... 180

Figure 6-6: JJ316 constrains CD28 diffusion under both signalling and non-signalling conditions. ..... 181

Figure 6-7: JJ316 does not affect CD86 diffusion. ..... 183

Figure 6-8: Anti-PD1 antibodies constrain truncPDCD28-mEos3.2 diffusion. ..... 185

Figure 6-9: Diffusional effects of antibodies are dependent on their concentration. ..... 187

Figure 6-10: SDS-PAGE analysis of protein G-purified anti-mouse CD45 Fab after size exclusion chromatography. ..... 189

Figure 6-11: YW62.3.20-Fab specifically binds to CD45 endogenously expressed in BW5147 cells. ..... 190

Figure 6-12: Simultaneous dual-colour single-particle tracking of Fab-labelled CD45 and CD28-mEos. ..... 192

Figure 6-13: CD45 and CD28 localizations are anti-correlated for all stimulation conditions. ..... 193

Figure 6-14: JJ316 constrains both CD28 and CD45 diffusion. ..... 195

Figure 6-15: Experimental set-up for measuring the diffusion of non-immobilised, antibody-bound CD28. ..... 196

Figure 6-16: Non-immobilised, antibody-bound CD28 slows its diffusion when a close cell/glass contact is created *via* a PD1/antibody interaction. ..... 196

Figure 6-17: Areas depleted of CD45 are observed under both JJ316 and JJ319 treatment. ..... 199

Figure 6-18: CD45 intensity is decreased under JJ316 *versus* JJ319 treatment across the cell-glass contact as well as in antibody-enriched areas. ..... 200

Figure 6-19: Differential Amplitude Vector Intensity Signal (DAVIS) plots visualise the increased anti-correlated receptor distribution under A JJ316 *versus* B JJ319 treatment..... 201

Figure 7-1: Antibody immobilisation *via* secondary antibody or Fc receptor. ..... 212

Figure 7-2: Segregation on a spatial or a temporal scale can lead to signalling. ..... 215

## List of Tables

Table 2-1: Antibodies used in this thesis. ..... 64

Table 3-1: Known soluble affinities and kinetics of control antibodies, as measured by BIAcore* ..... 69

Table 3-2: Apparent association and dissociation rates of antibodies binding to cell-bound receptors ..... 69

Table 3-3: Properties of transfected CHO-K1 clones that produce rCD28-mFc-His ..... 75

Table 3-4: mouse B7-1 affinity for rat CD28 at equilibrium at 37ºC ..... 85

Table 3-5: Kinetic measurements of JJ316 and JJ319 soluble 1:1 affinity ..... 86

Table 3-6: Comparing binding rates measured with BIAcore and flow cytometry. ..... 88

Table 4-1: Non-linear regression with a binding model* quantifies superagonistic and costimulatory activities of JJ316 and JJ319, respectively ..... 104

Table 4-2: Surface expression of CD3 and CD28 in BW5147 cells ..... 118

Table 5-1: Surface expression of CD3 and CD28 in BW5147 cells ..... 141

Table 5-2: Surface expression of CD45 and CD148 in BW5147 cells. ..... 144

Table 5-3: Non-linear regression with a binding model† quantifies suppression of superagonistic signalling by truncated phosphatases ..... 144

Table 5-4: Flow cytometry quantifies the binding of unmodified *versus* extended JJ316 to cells-surface expressed rmCD28 ..... 151

Table 5-5: Non-linear regression with a binding model† quantifies the costimulatory activities of the extended JJ316 antibodies. ..... 154

Table 5-6: Non-linear regression with a binding model† confirms superagonistic signalling induced by JJ319 when immobilised at high density. ..... 164

Table 6-1: Quantification of the fraction of CD28 receptors that are grouped into the faster, "mobile" population. ..... 180

Table 6-2: Quantification of the fraction of CD28 or CD86 receptors that are grouped into the faster, "mobile" population. ..... 182

Table 6-3: Quantification of the fraction of PDCD28 receptors that are grouped into the faster, "mobile" population. ..... 184

Table 6-4: Estimation of the molar ratio of antibodies to CD28 homodimers for varying the antibody concentration. ..... 186

Table 6-5: Quantification of the fraction of CD28 receptors that are grouped into the faster, "mobile" population. ..... 188

Table 6-6: Quantification of YW62.3.20-Fab binding to CD45 endogenously expressed in BW5147 cells. ..... 190

## Abbreviations

| | |
|---|---|
| APC | Antigen-presenting cell |
| BCR | B-cell receptor |
| BLAST | Basic local alignment search tool |
| BTLA | B and T lymphocyte attenuator |
| BW | BW147 |
| c | central |
| C-terminus | Carboxy-terminus |
| CA | Conventional antibody |
| CBC | Coordinate-based colocalisation analysis |
| CD | Cluster of differentiation |
| CD200R | CD200 receptor |
| cDNA | Complementary DNA |
| CDR | Complementary-determining region |
| CF | Correction factor |
| CHO | Chinese hamster ovary |
| CMV | Cytomegalovirus |
| CTLA4 | Cytotoxic T-lymphocyte-associated protein 4 |
| d | distal |
| DAM | Donkey anti mouse Fc antibody |
| DAVIS | Differential Amplitude Vector Intensity Signal |
| DC | Dendritic cell |
| DMEM | Dulbecco's modified eagle medium |
| DNA | Deoxyribonucleic acid |
| dNTP | Deoxynucleotide |
| DRiP | Defective ribosomal product |
| EC50 | Median effective concentration |
| ECL | Enhanced chemiluminescence |
| EDTA | Ethylenediaminetetraacetic acid |

| | |
|---|---|
| EGFR | Epidermal growth factor receptor |
| EIA | Enzyme-immunoassay |
| ELISA | Enzyme-linked immunosorbent assay |
| ER | Endoplasmic reticulum |
| extJJ316 | Extended JJ316 |
| Fab | Fragment antigen-binding |
| FACS | Fluorescence-activated cell sorting |
| Fc | Fragment crystallisable |
| FcCD28 | Chimeric human Fc - mouse CD28 protein |
| FcR | Fragment crystallisable receptor |
| FPLC | Fast protein Liquid Chromatography |
| GAH | Goat anti human Fc antibody |
| GPCR | G-protein coupled receptor |
| h | Human |
| HA | Human influenza hemagglutinin |
| HBS | HEPES-buffered saline |
| HEK | Human embryonic kidney |
| HEPA | High-efficiency particulate air |
| HEPES | (4-(2-hydroxyethyl)-1-piperazineethanesulfonic acid |
| hi | High |
| His | Histidine |
| HIV | Human immunodeficiency virus |
| HRP | Horse radish peroxidase |
| HT | Hypoxanthine - thymidine |
| ICOS | Inducible T-cell costimulator |
| Ig | Immunoglobulin |
| IL-2 | Interleukin-2 |
| ITAM | Immunoreceptor tyrosine-based activation motif |
| ITIM | Immunoreceptor tyrosine-based inhibitory motif |
| ITSM | Immunoreceptor tyrosine-based switch motif |

| | |
|---|---|
| JD | Jump distance |
| $K_D$ | Dissociation constant |
| $k_{off}$ | Association rate constant |
| $k_{on}$ | Dissociation rate constant |
| KS | Kinetic segregation |
| LAT-CD148 | Chimeric mouse LAT – mouse CD148 protein |
| LAT-CD45 | Chimeric mouse LAT – mouse CD45 protein |
| Lck | Lymphocyte-specific protein tyrosine kinase |
| lo | Low |
| m | Mouse |
| me | Medium |
| MFI | Mean fluorescence intensity |
| MHC | Major histocompatibility complex |
| MSD | Mean square displacement |
| MSX | Methionine sulphoximine |
| n | Hill-slope |
| N-glycan | Amine-linked glycan |
| N-terminus | Amine-terminus |
| NA | Numerical aperture |
| NFAT | Nuclear factor of activated T-cells |
| NFκB | Nuclear factor kappa-light-chain-enhancer of activated B cells |
| NHS-ester | N-hyrdroxysuccinimide ester |
| Ni-NTA | Nickel-nitrilotriacetic acid |
| O-linked | Oxygen-linked |
| p | peripheral |
| PALM | Photoactivated localization microcopy |
| PBS | Phosphate-buffered saline |
| PCR | Polymerase chain reaction |
| PD1 | Programmed cell death 1 |
| PD1 | Programmed cell death 1 |
| PDCD28 | Chimeric human PD1 – mouse CD28 protein |

| | |
|---|---|
| PDCD28 | Chimeric human PD1 – mouse CD28 protein |
| pH | Potential hydrogen |
| pHR | pHR-SIN-CSGWdNotI/dEcoRI |
| PKC θ | Protein kinase C θ |
| pMHC | peptide-bound MHC protein |
| PSF | Point-spread function |
| r | Rat |
| RICM | Reflection interference contrast microscopy |
| rmCD148 | Chimeric rat – mouse CD148 protein |
| rmCD28 | Chimeric rat – mouse CD28 protein |
| rmCD45 | Chimeric rat – mouse CD45 protein |
| RPMI | Roswell Park Memorial Institute medium |
| SA | Superagonistic antibody |
| SDS-PAGE | Sodium dodecyl sulphate polyacrylamide gel electrophoresis |
| SH2 | Src homology |
| sJJ316 | Soluble JJ316 |
| sJJ319 | Soluble JJ319 |
| SLB | Supported lipid bilayer |
| SMAC | Supramolecular activation cluster |
| spt | Single-particle tracking |
| STORM | Stochastic optical reconstruction microscopy |
| TAP | Transporter associated with antigen presentation |
| Tapasin | TAP-associated glycoprotein |
| Taq | *Thermus aquaticus* |
| TCR | T-cell receptor |
| TIRF | Total internal reflection fluorescence |
| TIRFM | Total internal reflection fluorescence microscopy |
| truncCD28 | Truncated chimeric rat – mouse CD28 protein |
| truncCD86 | Truncated human CD86 protein |
| truncFcCD28 | Truncated chimeric human Fc - mouse CD28 protein |

| | |
|---|---|
| truncPDCD28 | Truncated chimeric human PD1 – mouse CD28 protein |
| TSS | Transformation and storage solution |
| ZAP-70 | Zeta-chain associated protein of 70 kDa |

# Chapter 1 General introduction

## 1.1. Overview of the immune system

Immunity is often thought of as an apparently never-ending arms race between pathogens and hosts, and is thereby central to biology as it shapes how organisms evolve and interact [1-4]. Arguably, some form of "immunity" co-evolved with even the simplest forms of life: prokaryotes counteract being infected and re-programmed by bacteriophages [3], such as by degrading non-self DNA with restriction enzymes [5-8] and the CRISPR/CAS system [9]. Also eukaryotic organisms, including humans, possess an innate intracellular immunity that pre-dates a system of specialised immune cells, such as by recognising and degrading invasive viral DNA and RNA [10, 11]. However, the term "immune system" typically describes the complex orchestration of specialised immune cells that evolved in higher organisms as a defence to pathogens [12]. These immune cells scan their environment *via* cell-surface receptors and recognise foreign structures for destruction while ignoring self [13]. They differ in the expression of specific receptors, and thus targets, as well as in their effector functions [12], as outlined in more detail in the following sections. Immunology, therefore, is predominantly focused on processes of the cell surface [14, 15], which conveniently are well-suited to being visualised in great detail by advanced microscopy techniques that help to enlighten our understanding of the molecular mechanisms underlying immunity [15-17].

## 1.2. Innate immunity and the inflammatory response

Considering the time course of the immune response, it is the so-called innate, and evolutionarily older, arm of immunity that responds to an infection first [12]. Innate immune cells express germ-line encoded pattern recognition receptors that bind to structures that are shared by many pathogens but not present on self, including cell wall components such as lipopolysaccharide [13]. Binding of Toll-like receptors (TLRs) to their targets results in the activation of the innate immune cell [18].

Macrophages are tissue-resident cells that survey their local environment, and typically encounter pathogens at the site of an infection first [19, 20]. Upon their activation they start the inflammatory response by secreting chemokines and cytokines that attract other immune cells, and by stimulating the division of precursors in the bone marrow that differentiate into neutrophils [12]. Neutrophils home to the infected tissue *via* chemotaxis, attachment to the endothelial wall with the help of adhesion molecules, and transendothelial migration [12]. They engulf and phagocytose pathogens and degrade them in the phagolysosome *via* toxic oxygen reactive species and enzymes [12]. Neutrophils can clear pathogens much more efficiently that have previously been opsonised with complement or antibody, which they recognise *via* specific cell-surface receptors. The complement system consists of humoral glycoproteins that are recruited to non-self surfaces or substances in a cascade, with each step amplifying the previous one, culminating in direct cytolysis, or the opsonisation of a pathogen or infected cell [12, 21].

While the innate and adaptive immunity are often referred to as separate arms, they are highly interconnected, and the adaptive immune response depends upon the innate [12, 22]. For example, innate immune cells such as dendritic cells (DCs) endocytose foreign substances upon binding them with their pattern recognition receptors, and process them for presentation to the adaptive immune cells [12]. DCs travel to lymph nodes from the site of infection, where they interact with and prime T cells to start the adaptive immune response [19].

The innate immune response prompts inflammation, which is initiated by the release of cytokines into the blood stream [19, 23]. While it strengthens the immune response by increasing the flow of blood (and thereby immune cells) to the infected tissue and the flow of lymph, carrying dendritic cells to the lymph nodes, by promoting adhesion of immune cells to the endothelial wall and permeability for transendothelial migration, and by recruiting effector cells of the adaptive arm to the site of infection, it runs the risk of also being damaging to healthy tissue, and can become life-threatening [12, 19].

## 1.3. The adaptive immune response

Adaptive immunity, which is unique to higher animals, is characterised by: (1) highly variable antigen receptors that result from somatic rearrangement of germline-encoded genes, and that bind to their targets with unparalleled specificity; (2) a delayed onset of the response (days to weeks); and (3) a memory for a previously encountered foreign structure, such that a much faster response can be launched [12, 13]. The highly specific recognition makes it difficult for a pathogen to evade the immune system by hiding or avoiding expression of pathogen-associated molecular patterns, and protects the host tissue from damage due to an unspecific inflammatory response [12, 13].

A major advantage of adaptive immunity is that a highly specific and effective response can be launched very quickly when infection with the same pathogen occurs a second time. Memory T- and B-cells, primed for a specific antigen, survive in a dormant state (*i.e.* in a state of unresponsiveness as well as low metabolic activity and cell-cycle progression [24]) and for long periods of time (up to decades), and undergo rapid activation and clonal expansion upon re-encountering their antigen [25].

### 1.3.1. Antigen presentation

In the interaction at the very heart of adaptive immunity, a T cell scans the surface of an antigen-presenting cell (APC) for foreign peptides presented on specialised receptors, the major histocompatibility complex (MHC) class I and class II proteins [26]. They bind peptides *via* specific interactions between peptide anchor residues and pockets in the MHC protein binding groove [26]. Human individuals typically express six different alleles of the highly polymorphic class I and eight of class II that each bind $10^3$-$10^4$ unique peptides [27], such that virtually any protein can be presented. The peptides, which are derived from degraded pathogen- and self-proteins, are selected, processed, and then trafficked to the cell surface *via* MHC [28]. They may originate from engulfed and degraded microbes and be taken up by MHC class II *via* the endocytic compartment, or from virus-encoded as well as self-proteins that are degraded and imported into the endoplasmic reticulum (ER) *via* the transporter

associated with antigen presentation (TAP), where they are loaded onto MHC class I with the help of TAP-associated glycoprotein (tapasin) [26]. The antigenic peptide is, in fact, an integral part of the quaternary structure of the MHC protein, helping it to fold into a stable complex. In the ER, MHC class I proteins gradually exchange low affinity peptides for high affinity ones with the help of tapasin, and are only permitted to travel to the cell surface once stably folded such that they can escape recycling into the ER *via* calreticulin [29]. To date, it is not completely resolved where the peptides destined for antigen presentation *via* MHC class I originate from [30]. Initially, it was believed that they stem from "retired" proteins that are degraded at the end of their life time. However, this model failed to explain the high speed of the pMHC-dependent immune response upon viral infection. It was then proposed that an estimated 30-80 % of nascent proteins, the so-called defective ribosomal products (DRiPs), are immediately targeted for degradation *via* the (immuno-) proteasome, and thereby antigen presentation, such that virtually the entire proteome of the APC is presented at its surface in due time [31, 32]. Although an involvement of the ubiquitin-proteasome pathway in antigen presentation has been established, many of the peptides appear to be generated proteasome-independently by some unknown pathway [30]. Probably in response to viruses evading antigen presentation by downregulating MHC class I, its ubiquitous surface expression by all nucleated cells is required for their survival by inhibiting the cytotoxic activity of natural killer cells [33, 34]. MHC class II, on the other hand, is expressed only by professional APCs, such as DCs, macrophages and B cells [26].

### 1.3.2. The source of variability and specificity in adaptive immunity

The antigenic receptors of T and B cells, the T-cell receptor (TCR) and B-cell receptor (BCR), respectively, are characterised by their remarkable variability. Each T- or B-cell clone expresses a unique receptor as the result of somatic rearrangement of germline-encoded genes, such that particular non-self structures can be recognised with very high specificity [12]. The final gene encoding the unique receptor is built up of four gene segments, the variable (V), diversity (D), joining (J) and constant (C) regions [12,

35]. A number of genes (25+) are encoded in the germline for the V, D and J segments that can be combined randomly, creating combinatorial diversity [12]. More junctional diversity is generated by ligating the segments together in an imprecise manner that allows for a frameshift to occur, and nucleotides can be added or removed at the junctions by DNA polymerases and nucleases in a random process [12, 35]. In the case of the BCR, further diversification occurs after antigen recognition in a process called somatic hypermutation [12]. Somatic mutations in the variable regions of the antibody will by chance generate some antibodies with an increased affinity for their antigen, and these clones will be selected for (*i.e.* they will proliferate and differentiate into memory B-cells and antibody-producing plasma cells) because of increased signalling through the BCR. Therefore, the process of somatic hypermutation generates a more diverse pool of B-cell clones and facilitates production of high-affinity antibodies [12].

### 1.3.3. Functional antigenic receptors are selected for that do not bind to self

Both B and T cells arise from precursors in the bone marrow. While B cells undergo maturation in the bone marrow, T cell precursors, *i.e.* thymocytes, migrate to the thymus at an early developmental stage where they mature [12]. Because the antigen binding site of the T- and B-cell receptors is generated in a random gene rearrangement process, self-specific receptors naturally arise, and clones recognising self need to be eliminated in a process called negative selection [19]. At the same time, clones bearing unproductive receptors that are incapable of usefully binding antigen (*e.g.* TCRs that are not MHC-restricted) are deleted during positive selection [19]. In the thymus, thymocytes interact with APCs that present self-antigen *via* MHC class I and II. Antigens specific to certain peripheral tissues are also presented because such proteins are expressed ectopically, and a fraction of these proteins depend on the transcription factor AIRE [36, 37]. Thymocytes that bind weakly to self-peptide presented on MHC survive, whereas self-reactive ones that bind strongly and unproductive non-binding ones undergo apoptosis [36]. Immature B-cells undergo a similar selection process in the bone marrow that, however, permits a small fraction of weakly self-reactive B-cells

to reach the periphery, perhaps to balance the disadvantage of self-targeted immunity against the need for a wide spectrum of BCRs that recognise foreign structures [38].

In addition to ignoring self-structures, the immune system (innate and adaptive) also needs to tolerate commensal microbes, such as the microbiota in the gut, the importance of which becomes evident in the breakdown of tolerance during inflammatory bowel disease. It is still incompletely understood what causes the balance to tip from homeostasis to inflammation, and both genetics and environmental factors are thought to play a role. Current research involves dissecting the roles of different subsets of T cells (regulatory T-cells, T-helper 17, T-helper 1 and T-helper 2 cells), the role of cytokines such as IL-23 and IL-17, and the breakdown of the intestinal mucosal barrier leading to a "leaky gut" [39, 40].

### 1.3.4. T-cell mediated immunity

A limitation of the humoral (*i.e.* antibody and complement-mediated) immune response is that intracellular pathogens or cancer antigens are inaccessible. T-cell-mediated immunity, on the other hand, fulfils this function with the help of antigen presentation *via* MHC, as described above. More precisely, αβT-cells expressing the co-receptor CD8 that contacts MHC class I, which are also termed "cytotoxic T-cells", are responsible for directly killing infected or transformed cells [41]. Cytotoxic T-cells can kill their target by the directed release of cytotoxic granules in a particularly structured contact formed between the two cells, called the immunological synapse [42, 43]. Alternatively, they can induce apoptosis of their target cell *via* surface expression of the Fas ligand, which binds to the Fas receptor on the surface of the target cell, triggering an apoptotic signal [42].

αβT-cells expressing the co-receptor CD4, which are called T helper ($T_H$) cells, recognise MHC class II-presented antigen. A number of functionally diverse $T_H$ subsets exist, characterised by the expression of certain surface receptors and the secretion of particular cytokines [44]. $T_H$ cells can, for example, stimulate macrophages to degrade intracellular bacteria ($T_{H1}$ cells), promote the survival, proliferation, and

differentiation of B cells, induce B cells to undergo hypermutation of the BCR gene and immunoglobulin class switching, and attract B cells *via* chemotaxis ($T_{H2}$ cells) [45]. Regulatory T-cells ($T_{regs}$), which are characterised by the expression of the transcription factor *foxp3*, have an anti-inflammatory function that contributes to maintaining tolerance, but assists tumours to evade the immune response [44]. Thymocytes may differentiate into $T_{regs}$ upon binding to self-antigen with high affinity rather than undergoing apoptosis, and peripheral T-cells may differentiate into induced $T_{regs}$, for example under conditions of chronic inflammation, or during TCR activation in the absence of costimulation [46]. $T_{H17}$ cells, which are characterised by their secretion of IL-17, are pro-inflammatory T-cells responsible for orchestrating immune responses against extracellular bacteria and fungi, but have also been implicated in autoimmunity [47]. It should be noted that a categorisation of T cells into distinct subsets is an imprecise science, as many more subsets could in principle be created with more detailed descriptions. With the advent of single-cell biology, it is now possible to identify the heritage and function of individual cells, as well as to map cellular fate, more accurately than was possible using a limited number of surface receptors or secreted cytokines [48].

The majority of thymocytes express an αβTCR and eventually mature into either $CD4^+$ or $CD8^+$ T-cells following initial double-negative ($CD4^-CD8^-$) and then double-positive ($CD4^+CD8^+$) developmental stages, depending on their preference for binding MHC class I or II [49, 50]. Some thymocytes, however, express an alternative TCR originating from separate gene loci, which is also the result of VDJ recombination, and mature into γδT-cells. In contrast to αβT-cells, γδT-cells are not restricted to binding MHC-presented antigen, and are thought to resemble the B-cell compartment in its ability to recognise virtually any structure [51]. While being part of the adaptive arm of the immune response, they are thought to also resemble innate immune cells in their ability to respond to an infection at very early stages [51]. In their effector functions, they can act alike αβT-cells and orchestrate immune responses with the secretion of cytokines, such as IFNγ, TNF, IL-13, and IL-17, specific to the subset they belong to [51]. However, their functional repertoire is broader: they can provide

B-cell help, lyse infected or stressed cells, act as APCs to prime αβT-cells, provide growth factors to stromal cells, and aid DCs in their maturation [51]

### 1.3.5. B-cell mediated immunity

Upon binding antigen and becoming activated, B cells differentiate into antibody-secreting plasma cells. Antibodies comprise soluble forms of the BCR, which unlike the TCR is not restricted to MHC-presented antigen but can recognise virtually any structure, be it an organic or inorganic molecule, *e.g.* a soluble toxin, or a structure on the surface of a pathogen or cell. Toxins are thereby neutralised, microbes are opsonised for phagocytosis by neutrophils, and the complement system is activated [12, 52]. When antigens on the surface of an abnormal (*i.e.* infected or transformed) cell are bound by antibody, NK cells or other Fc-receptor bearing cells are induced to kill the target cell in a process called antibody-dependent cell-mediated cytotoxicity [53].

Unlike T cells, B cells are not activated directly upon binding their antigen, but require signals from a $T_H$ cell [45, 54-56]. B cells predominantly reside in lymph nodes, where they sample their environment with their BCR, and upon binding antigen internalise it for processing and presentation to a $T_H$ cell *via* MHC class II. The primed $T_H$ cell, having previously been activated by the same antigen, then secretes cytokines that cause the B cell to divide and differentiate into a plasma cell [12, 45]. Memory B-cells can, however, become activated without T-cell help when they recognise complexed antigen bound to Fc receptors by follicular dendritic cells, which also secrete cytokines and trophic factors to aid in B-cell activation and clonal expansion [12, 57].

## 1.4. Structural and functional properties of antibodies

Antibodies are comprised of two heavy (~ 55 kDa) and two light (~ 25 kDa) chains that are arranged in a homodimeric structure stabilised by disulphide bonds (Figure 1-1). The functional elements making up an antibody have been studied by enzymatic digestion: papain treatment yields three fragments, two identical fragments responsible for antigen binding (Fabs), and one mediating effector functions, the fragment

crystallisable (Fc; Figure 1-1). Each heavy chain is made up of a variable and three or four constant domains ($C_{H1}$-$C_{H4}$) while each light chain consists of one variable and one constant domain. The variable domains of both heavy and light chain contribute to the antigen binding site of the Fab [52]. Structurally, each of the domains are immunoglobulin (Ig) folds, comprised of two sandwiched, disulphide-bonded beta sheets [52]. The interchain disulphide bonds locate to the hinge region of the antibody, which connects Fabs and Fc, *i.e.* C-terminally of the $C_{H1}$ domain. Antibodies are glycoproteins, and N- and O-linked (in the hinge region [58]) glycans contribute to antibody stability as well as effector function; *e.g.* they contribute to - and are in some cases essential for - binding to Fc receptors, and have been implicated in the efficacy of HIV-neutralising antibodies [52]. Figure 1-1 displays the conserved glycan at Asn-297 that is required for binding to FcγR.

Immunoglobulins are expressed in essentially two states: a membrane-bound, the BCR, and a secreted form, the antibody, and each are produced by alternative splicing of the heavy chain constant domain [52]. Two separate gene loci exist, κ and λ, which encode different light chain constant domains [52]. Whereas VDJ recombination of the variable regions creates the vast diversity among immunoglobulins that enables the compartment to recognise a multitude of antigens, some diversity exists also among constant regions of heavy chains ($C_H$) such that different effector functions can be performed. Astonishingly, antibodies can also incorporate gene segments from distant chromosomes by a mechanism that is incompletely understood, as described for the case of a *LAIR1* insertion, which even contributes to antigen binding [59]. Immunoglobulins can switch between different $C_H$ genes, splicing the VDJ heavy chain variable domain in front of the respective gene, in a process called class switch recombination [52]. Here, antigenic specificity is retained while the effector function changes, and the resulting different immunoglobulins are called isotypes. Five isotypes exist called IgM, IgD, IgG, and IgA. Early in their development, all B cells express IgM BCRs. IgM is of relatively low affinity, and is often able to bind to several distinct epitopes (*i.e.*, it is polyreactive), allowing a broader range of antigens to be detected in the early immune response [52]. IgM antibodies are typically secreted in a multivalent

form, most prominently as pentamers stabilised by an additional polypeptide, the J chain [52]. This balances their relatively poor affinity by increasing avidity, and makes them very efficient at opsonising pathogens [52], suggesting that their main function is to act on immobilised antigens. An activated B cell then switches to expressing IgD, which is often co-expressed with IgM [52]. IgD can bind bacterial proteins *via* its constant region, activating the B cell [52]. Activation *via* binding antigen, as well as *via* cytokine signalling, can induce B cells to then switch to expressing IgG, IgA, or IgE. The BCR gene also undergoes somatic hypermutation, which eventually, under conditions of selection *via* antigen-mediated activation, leads to the secretion of antibodies with increasingly higher affinity, a process that is called affinity maturation [52]. IgG antibodies predominate in the serum and have a particularly long serum half-life; they are also the best-studied isotype [52]. Several subclasses exist, differing in their flexibility and effector function, and in their affinity for Fc receptors [52]. IgA antibodies are mostly found in the mucosa, where there are often expressed in dimeric form [52]. They neutralise toxins and viruses and prevent the binding of pathogens to the mucosa, and are implicated in antigen-dependent cell-mediated cytotoxicity [52]. IgE is implicated in allergies, and plays a role in immunity against parasites and worms [52].

### 1.4.1. Fc receptors

Fc receptors (FcRs) are transmembrane proteins that bind to the Fc portion of antibodies. Thereby, they connect humoral and cell-mediated immunity [52]. They are expressed by a number of immune cells of both the innate and adaptive arm, including B cells, T cells, natural killer cells, macrophages, neutrophils, and DCs [61]. They differ in the isotype and subclass of antibody they bind to, the affinity with which they bind, their expression pattern, and the responses they induce, which can be both activating and inhibitory [61]. Some of them contain signalling motifs that are phosphorylated by external kinases for signal propagation, whereas others associate with adapter proteins carrying such motifs [61]. FcR signalling can lead to immune cell activation, differentiation, cytokine or chemokine production, changes in migratory behaviour,

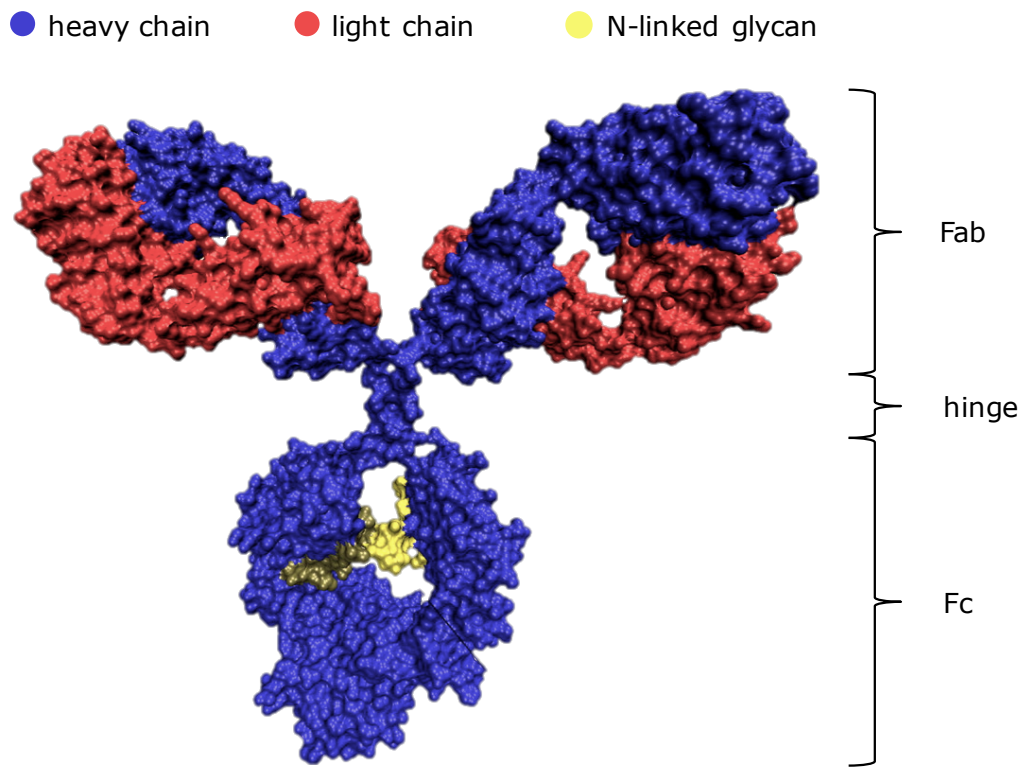



Figure 1-1: Space-filling model of the human IgG structure. Modified from [60] and based on a model submitted to the Protein Data Bank by M. Clark, University of Cambridge.

phagocytosis, degranulation, antibody-dependent cell-mediated cytotoxicity, and internalisation for processing and presentation of the antigen [62]. Additionally, some Fc receptors can also mediate the uptake and transport of antibody [52]. X-ray crystallography of FcRs bound to antibodies revealed that they form particularly compact complexes: they bind to the lower hinge region of the antibody, forcing it into a configuration in which the Fc region faces downward (see Figure 7-1, page 212 [63, 64]), and there is evidence that FcR signalling depends on the small dimensions of the complex (personal communication with James Felce, Davis and Dustin laboratories, University of Oxford).

## 1.5. The immunological synapse

T-cell activation drives cytoskeletal rearrangements that culminate in the formation of the "immunological synapse" (IS), a highly organised structure at the centre of the T-cell/APC contact [65]. Transmembrane proteins accumulate in the IS where they are compartmentalised in a specific "bull's-eye" pattern [66]. Three separate concentric regions, or "supramolecular activation clusters" (SMACs), were described: the central (c), peripheral (p), and distal (d) SMACs [43, 67, 68]. The TCR as well as Lck accumulate in the cSMAC, CD28 locates to the peripheral cSMAC, integrins locate to the pSMAC, and the phosphatase CD45 is found in the dSMAC [43, 67-69]. Upon its discovery, the IS was described as the engine that drives and sustains T-cell signaling [70]. However, since TCR signalling precedes and is necessary for IS formation, the IS cannot be the site of initial signalling [71, 72]. Formation of a mature IS is not strictly required for T-cell activation, and the formation of a typical IS is not observed at the T-cell/DC contact, where several clusters (*i.e.* a multifocal IS) are observed rather than one central one [67, 73, 74]. The central cSMAC was revealed to be a site where signalling is terminated and downregulated by endocytosis of TCRs [67, 75]. It was recently discovered that the IS is also a site of exocytosis, and that TCR/pMHC complexes are sorted into vesicles that bud off [76]. This process is thought to further downmodulate signalling, but has also been implicated in cell-to-cell communication [76]. When a cytotoxic T-cell kills a target cell, the IS plays a structural role in the controlled polarized delivery of granules, and this may be its main function [67, 72, 77, 78]. Interestingly, an IS-like structure termed the "anti-synapse" also forms at the opposite pole of the T cell as the consequence of adhesion, wherein signalling proteins accumulate and become phosphorylated [79]. It therefore appears that T-cell adhesion causes global cytoskeletal and membrane protein rearrangements [79]. The formation of an IS is not unique to T-cells, but also occurs in other lymphocytes such as natural killer cells [80], and in B cells, where its primary function appears to be the internalisation and subsequent processing of antigen for presentation [81, 82], utilising the cytoskeleton as a tool to mechanically probe antigen affinity and to selectively internalise high-affinity antigen [81, 83].

## 1.6. Immunoreceptors

Immunoreceptors (also known as non-catalytic tyrosine-phosphorylated receptors [84]) comprise a subset of leukocyte receptors that share four characteristics: (1) they have no intrinsic enzymatic activity and therefore rely on external kinases to phosphorylate tyrosine residues in their signalling motifs for initiating a signalling cascade [84]; (2) their ectodomains have small dimensions [84, 85]; (3) they are activated by cell-surface bound ligands [84]; and (4) they are characterised by relatively weak yet specific interactions with their ligands [85]. They differ by their diverse ligands and share little sequence homology, but engage a shared downstream signalling machinery, and it has been proposed that they may be triggered *via* a common mechanism [84, 86]. Immunoreceptors can initiate either activating or inhibitory signalling, depending on which signalling motifs they or their associated adaptors express, recruiting downstream signalling proteins that propagate the different types of signalling. Many receptors express semi-conserved motifs containing the tyrosine residues that are phosphorylated by extrinsic kinases upon ligand binding; these are called immunoreceptor tyrosine-based activation, inhibitory, or switch motifs (ITAMs, ITIMs, and ITSMs) [87-90]. The action of kinases is balanced by receptor-type protein tyrosine phosphatases that are expressed at the cell surface in high numbers [86], and also by highly expressed cytosolic phosphatases recruited to the membrane post-triggering*, e.g. via* programmed cell death 1 (PD1) [91]. A number of immunoreceptors are typically engaged simultaneously or within a short period of time, and their synergistic or antagonistic signalling is integrated downstream [84, 92-94]. The TCR, the BCR, the Fc receptor family, PD1, and the CD28 family (with CD28, CTLA4, BTLA, ICOS), among others, are all immunoreceptors [84, 86]. The following sections introduce the TCR and CD28, the principal subjects of this thesis, in greater detail, focusing on the structural basis of their function in T-cell signalling.

### 1.6.1. The TCR

**Structural properties**

The TCR is comprised of two polypeptide chains, α and β, that are covalently associated *via* a disulphide bond in the stalk region of their extracellular domains [95]. Each chain is built up of a very short cytoplasmic region, a helical transmembrane domain, and a two Ig domains that are attached to the transmembrane domain *via* a stalk in the extracellular region [85]. The membrane-distal variable Ig domains, Vα and Vβ, contact their ligand, the pMHC complex, *via* three flexible loops, the complementarity-determining regions (CDRs) [85]. Interactions to both the peptide and the MHC contribute to the binding interface and energy of the TCR/pMHC interaction, with the MHC-directed contacts dominating [85, 96-98]. Comparing solved crystal structures of the complex, the CDRs and particularly CDR3 show remarkable conformational flexibility [99-101], enabling one TCR to recognise, it is claimed, in the range of $10^5$ different pMHC ligands [85, 102], and there are no conserved contacts between the CDRs and specific MHC residues [96]. The overall geometry of the TCR/pMHC interaction, however, appears to be conserved [85, 103]. The thermodynamics of the TCR/pMHC interaction in solution is characterised by slow kinetics and an affinity that is relatively high in comparison to other immunoreceptor/ligand interactions [85]. The TCR itself bears neither signalling motifs nor enzymatic activity, but associates with the CD3 complex that propagates a downstream signal upon the phosphorylation of its cytoplasmic ITAMs by lymphocyte-specific protein tyrosine kinase (Lck), a Src kinase (Figure 1-2; [84, 86]). Expression of the TCR at the cell surface depends on the assembly of the TCR/CD3 complex, which appears to be mediated by interactions between the transmembrane as well as extracellular domains of the polypeptide chains [95, 104-106]. While the stoichiometry of the TCR/CD3 complex is resolved, with each αβTCR associating with one CD3εγ heterodimer, one CD3εδ heterodimer and one CD3ζζ homodimer, the spatial organisation of the subunits with respect to each other is disputed [95]. Controversy also exists regarding the valency of the TCR: while some report that

αβTCR/CD3 complexes are monovalent in the resting state [107, 108], others propose that oligomeric forms prevail, or that monovalent and multivalent forms co-exist [109], and a similar controversy surrounds the valency of the pMHC ligands [110, 111].

**Downstream signalling**

Phosphorylation of the ITAMs in the CD3 cytoplasmic tails by Lck activates the cellular signalling machinery, which is reviewed in detail elsewhere [112]. The kinase zeta-chain associated protein of 70 kDa (ZAP-70) is recruited to the phosphorylated ITAMs and forms a stable interaction that protects the tyrosine residues from dephosphorylation. This is considered the decisive step in the cascade that determines whether a T-cell response is launched or whether signalling remains sub-threshold [112-114]. Phosphorylation of downstream signalling proteins by ZAP-70 results in calcium signalling, cytoskeletal rearrangements and polarisation, an arrest in cellular migration and adhesion, and eventually altered gene transcription effecting cellular proliferation, differentiation, and cytokines secretion (Figure 1-2;[112, 115]).

### 1.6.2. CD28

**Structure and function**

CD28 is the dominant costimulatory receptor of the T cell, providing a second signal alongside TCR ligation such that activation results rather than anergy [116-119]. As such, it has both pro- and anti-inflammatory effects because its signalling sustains the survival, activity, differentiation, and proliferation of both regulatory and effector T cells, making it a particularly complex therapeutic target [119-123]. It forms a homodimer that is stabilised with a disulphide bond in the stalk region of its extra cellular domain [124, 125]. Each monomer is comprised of an immunoglobulin domain attached to a single transmembrane domain through a stalk, and a cytoplasmic tail that propagates a signalling cascade by recruiting downstream signalling molecules to its signalling motifs *via* their Src homology (SH) 2 and 3 domains (Figure 1-3;[118, 119, 125]). The membrane-proximal YMNM and the membrane-distal PYAP motifs

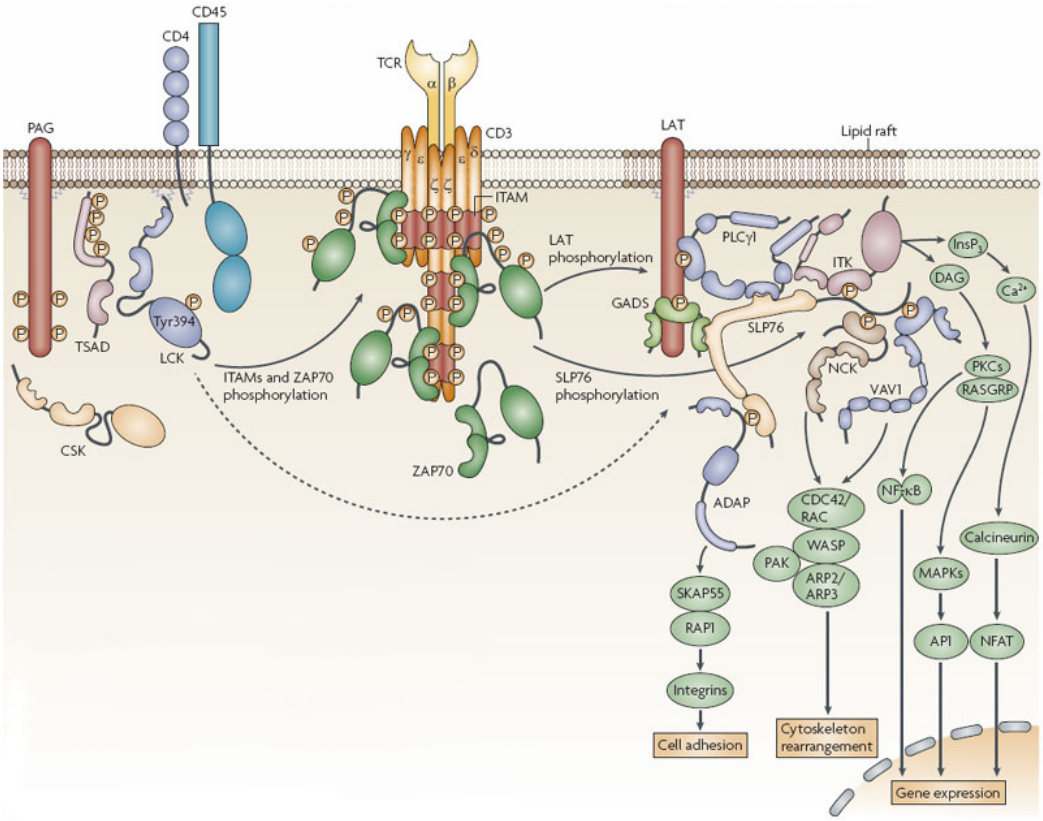



Figure 1-2: The T-cell signalling machinery. Modified from [112]. Phosphorylation of the CD3 ITAMs recruits ZAP-70, which becomes activated and initiates a downstream signalling cascade that results in calcium signalling, changes in cellular migration and adhesion, cytoskeletal rearrangements and polarisation, and changes in gene expression.

have been well characterised in terms of the proteins they recruit and their downstream effects [118, 119]. Downstream signalling is initiated by phosphorylation of the tyrosine residues in the motifs by Lck [119, 126-128]. Interestingly, however, some downstream effectors are recruited even to the unphosphorylated motifs [119, 129]. This may explain why mutating the tyrosines in both motifs does not completely abrogate CD28 signalling, or alternatively, additional, thus far undescribed motifs may contribute to signalling [119, 130]. The predominant physiological ligands for CD28 are CD86 and CD80, both of which are transmembrane proteins expressed on the surfaces of antigen presenting cells [119, 125, 131]. CD28 competes for these ligands with CTLA4, a receptor that shares sequence homology with CD28 but antagonises

its effects [119]. CD28 interacts monovalently with both CD86 and CD80, despite being a dimer, owing to steric effects [119, 132].

**Downstream effects**

Figure 1-3 summarises the downstream signalling pathways of CD28 and their effects. The dominant outcome of CD28 signalling is an increased IL-2 production, effected both by upregulation of its transcription through the transcription factors nuclear factor kappa-light-chain-enhancer of activated B cells (NF$\varkappa$B) and nuclear factor of activated T-cells (NFAT), and the stabilisation of IL-2 messenger RNA [118, 133]. CD28 has been implicated in actin remodelling *via* recruiting Vav1 [134, 135], and the stabilisation and compartmentalisation of the IS [114, 136, 137]. CD28 also stimulates glycolysis, enhancing metabolism for cellular growth and proliferation [138], and sustains cellular survival by upregulating Bcl-$x_L$, an inihibitor of apoptosis [139].

**CD28 as an amplifier of TCR signalling or an independent signalling receptor?**

CD28 has been described as both an amplifier of TCR signalling, acting quantitatively [140, 141], *e.g.* by recruiting protein kinase C θ (PKCθ) to TCR-containing microclusters and the IS, feeding into TCR-proximal signalling [142], and as a source of signals that are distinct to, but complementary to TCR signalling [118, 134]. Although normally T-cell activation requires both receptors to signal synergistically [143], particular "superoptimal" conditions have been described for which either receptor was active on its own, stressing their ability to act independently [135, 144]. TCR and CD28 signalling pathways appear to converge early [140], which is consistent with the observation that their physical proximity is necessary for optimal costimulation [145].

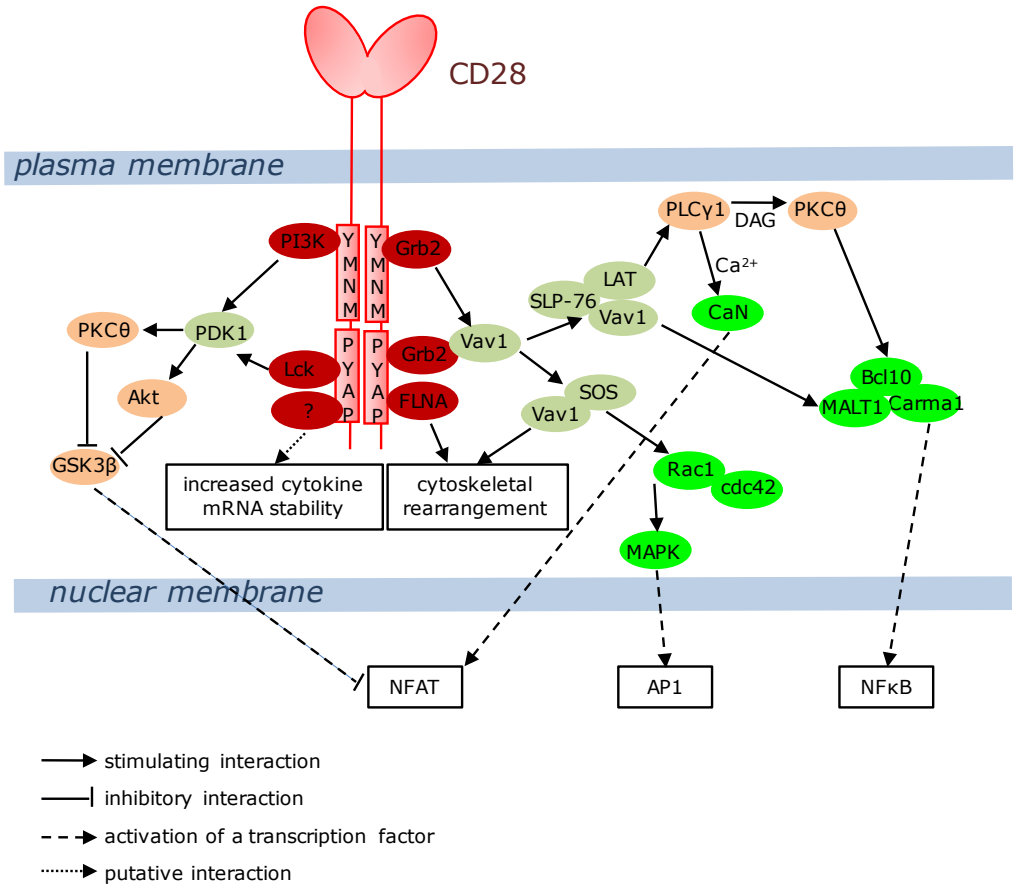



Figure 1-3: Downstream signalling pathways of CD28. Drawn after [119], Figure 2 and [118], Figure 3. Lck is recruited to CD28 and phosphorylates PDK1, which activates PKCθ that effects an increase in the transcription of NFAT-regulated genes via inhibiting GSK3β. Grb2, an adapter, binds both CD28 signalling motifs, and recruits Vav1 and Sos, which results in a signalling casade activating MAPK and thereby AP1-regulated transcription. *Via* recruiting the scaffold proteins SLP-76 and LAT, Vav-1 also effects the formation of the MALT1-Bcl10-CARMA1 complex that activates the NFκB transcription factor.

## 1.7. The triggering problem

While our understanding of the downstream signalling that follows the phosphorylation of immunoreceptors is detailed, it remains uncertain how ligand binding in the extracellular space translates into cytoplasmic phosphorylation, initiating the signalling cascade. Despite the fundamental importance of this process and much effort into studying it, the mechanistic principle underlying immunoreceptor triggering

is to date incompletely understood, with a number of competing models aiming to explain it. The TCR is by far the best studied immunoreceptor, and most investigations into the immunoreceptor triggering mechanism focused on this receptor. When considering evidence for and against the various models of activation, the functional properties of the receptor should be kept in mind. The TCR is highly sensitive and potent, with a single ligand being sufficient to induce T-cell activation [73, 146, 147]. At the same time, it is discriminatory, and able to discern even subtle differences in ligand affinity [148, 149]. Notably, agonist pMHC ligands are presented in a vast excess of non-agonist (self-) pMHC [149].

Historically, two different groups of receptors have served as models for triggering: the epidermal growth factor receptor (EGFR) family, and the G-protein coupled receptor (GPCR) family. EGFRs possess internal kinase activity, and trans auto-phosphorylate upon ligand-induced dimerization [150]. GPCRs, on the other hand, undergo a conformation change upon ligand binding that renders them active [151]. Neither of these types of receptors, however, are good models for immunoreceptor triggering. Immunoreceptors do not have enzymatic activity, and thus trans auto-phosphorylation cannot occur. Immunoreceptors also do not structurally resemble GPCRs, which bear seven transmembrane domains that re-organise upon ligand binding, resulting in the release and activation of the Gα protein [151]. It is particularly interesting that immunoreceptors have been shown to trigger ligand-independently under certain conditions, such as when phosphatase activity is inhibited [152], and when cells are brought into contact with artificial surfaces [153]. Therefore, a mechanism requiring immunoreceptor activity to be strictly dependent on a change that is specifically induced by the ligand, be it dimerization or a conformational change, cannot adequately explain triggering. The following sections discuss the main proposals that are still debated today, some of which are based on the initial EGFR/GPCR models, as well as alternative models that consider the particular properties of immunoreceptors and aim to bridge the discrepancies surrounding the initial models. It should be noted that the individual models are not mutually exclusive, and that TCR triggering may well result from a complex interplay of several molecular

events, although this seems unlikely given that triggering of so many distinct immunoreceptors has to be explained.

### 1.7.1. Conformational change models

In the case of the TCR, it is not trivial how a binding event involving the αβTCR chains would propagate and induce the associated CD3 chains to adopt a different conformation. The decisive questions are: What are the active and inactive forms of the TCR? How do they differ structurally? How does the conformational change propagate from one polypeptide chain to the other given that their interaction is non-covalent? How is the active conformation induced by a ligand, and how would it be induced ligand-independently? Given that the TCR:pMHC binding interface is structurally variable, how could a conserved conformational change be propagated? How can ligand discrimination be accounted for given that a conformational change represents a binary response? Therefore, the models detailed below should be scrutinized asking these questions.

Given that the fine structure of the TCR:pMHC interface is poorly conserved, it is unsurprising that no large conserved conformational changes of the αβTCR could be identified [149, 154], and that motions propagated to the constant regions of the αβTCR are not conserved [155]. A small structural rearrangement was reported concerning the AB loop of the Cα domain, but more data is needed to confirm whether it is in fact conserved and what its functional significance is [149, 156, 157]. Another study found that the TCR rigidifies upon ligand binding, which promotes the lateral association with neighbouring proteins and thereby complex formation, which may favour signalling [158].

The CD3ε subunit was suggested to undergo a conformational change upon αβTCR ligand binding that initiates TCR signalling [159]. A molecular dynamics study identified two residues in the stalk region as responsible for the conformational change, and mutating these impaired T-cell activation [159]. A shortcoming of this study was, however, that intracellular rather than surface staining was used to confirm

expression of the mutants, and therefore the activation defect could stem from a lack of TCR surface expression.

Since both mitogenic antibodies and pMHC ligands are capable of inducing T cell activation, any conserved conformational changes occurring as an essential part of the triggering mechanism should be observable analysing antibody-bound and unbound receptors. However, in the case of CD3ε, no large structural rearrangements occurred, and a mutational analysis suggested that novel interfaces for interacting with other CD3 subunits do not form [160]. It therefore appears that a conformational change is not required to induce signalling.

It was proposed that the cytoplasmic tails of CD3ε [161], CD3ζ [162], and CD28 [163] associate with the plasma membrane at resting state, rendering them inaccessible to Lck, such that ligand binding needs to induce their dissociation during receptor triggering by some unknown mechanism, perhaps because the receptor locates to an environment with an altered lipid composition [164]. An NMR structure showed that CD3ε associates with acidic lipids *via* a stretch of basic residues in its tail, and that mutating these favoured dissociation [161]. Others showed, however, that mutating the basic residues to "release" the cytoplasmic tail from the membrane did not result in its phosphorylation unless when phosphatase activity was blocked with pervanadate [165]. This suggested that both forms are in fact accessible to Lck, and sequestering of the CD3ε cytoplasmic tail is not responsible for keeping phosphorylation levels sub-threshold at resting state [165]. Phosphorylation by Lck of the CD3ζ cytoplasmic tail precedes dissociation, and would therefore have to be a consequence of rather than a requirement for receptor triggering [162].

Sanchez-Lockhart *et al* report that TCR signalling causes the CD28 homodimers residing in the IS to reorient their cytoplasmic tails, and that it promotes the relocalisation of CD28 to the IS [144]. It remained unclear, however, if and in what way these two observations are causally related, and by what mechanism the TCR interferes with CD28 localisation and conformation. It was also not reported whether

CD28 phosphorylation and downstream signalling was affected by the TCR-induced changes. Sanchez-Lockhart *et al* furthermore suggest that the TCR promotes CD28 signalling by stabilising a conformation that enables bivalent ligand binding, possibly as a consequence of reorienting the cytoplasmic tails [166]; however, sufficient mechanistic detail as to how this would occur is lacking. While it was concluded that bivalent binding of ligand by CD28 in a CTLA4-like dimer is sterically prevented based on the CD28 crystal structure [131], Sanchez-Lockhart *et al* propose a CTLA4 dissimilar dimer based on MD simulations used to explore possible CD28 conformations.

Binding to surface-immobilised pMHC, the TCR experiences mechanical forces that have been suggested to induce a conformation change that propagates to the CD3 cytoplasmic domains [167, 168]. Pulling forces may be generated by cytoskeletal movements of both the APC and the T cell, or alternatively forces may be exerted on the pMHC-TCR complex in the form of the resistance of large glycocalyx-forming transmembrane proteins to compression in or segregation from close-contact areas [149, 169, 170]. Only interactions of sufficiently high affinity are thought to sustain such forces whereas low-affinity bonds break, offering an explanation for ligand discrimination [149, 168]. Several observations are in agreement with such a model: (1) an intact actin cytoskeleton appears to be required for triggering [170]; (2) the extracellular and transmembrane domains of the TCR/CD3 complex may be rigid, allowing for propagation of the force [106, 149, 171, 172]; (3) surface-immobilised ligands are more active than soluble ones [149, 173, 174]; (4) elongated ligands are less active, potentially because they reduce mechanical force [149, 175-177]; and (5) the TCR can be triggered by applying mechanical forces [149, 178-180]. The nature of the conformational change that would be induced, however, remains unclear. The "force" model also falls short of accounting for ligand-independent TCR triggering as reported by Chang *et al,* which occurs when a "close-contact" is created between the T-cell and a supported lipid bilayer *via* a CD2/CD48 interaction, leaving the TCR suspended [153].

In conclusion, several studies claim to show a structural change in the TCR upon ligand binding. However, many mechanistic questions remain unanswered, and none of the studies gave enough detail to derive a general triggering mechanism for immunoreceptors. Moreover, while conformational rearrangements may accompany TCR triggering, they do not appear to be strictly required.

### 1.7.2. Aggregation models

Although immunoreceptors cannot trans auto-phosphorylate upon consolidating due to their lack of enzymatic activity, a local concentration of signalling motifs would increase the probability of receptor triggering. Should a single receptor become triggered and then recruit kinases and other crucial signalling proteins, this greatly enhances the chance of its neighbouring receptors being phosphorylated as well. This effect adds cooperativity to the system, which would help explain the speed and magnitude of T-cell activation [149, 153]. Interestingly, such cooperativity appears to be implemented even in single TCR/CD3 complexes, which express a large number of ITAMs [181], and the motifs of the CD3ζ chain are reported to be phosphorylated sequentially, *i.e.* in a non-random, cooperative fashion [182]. Further support comes from the observation that artificially induced aggregation suffices to induce T-cell activation [149]. A general criticism is, however, that the formation of aggregates is limited by speed of diffusion of transmembrane proteins, and thus aggregation may be insufficient to account for the speed at which receptor triggering occurs [87]

As a T cell becomes activated, both signalling and adhesion proteins consolidate into organised structures called microclusters [183, 184], in an actin-dependent manner [75, 185], and eventually the microclusters migrate to the centre of the T-cell/APC contact where they form the cSMAC of the immunological synapse after 5-15 minutes [186]. Signalling is thought to be sustained in these clusters [75, 187], but it is unclear whether they are also the sites of signal initiation. ZAP-70 recruitment and clustering at the membrane appears to precede (detectable) TCR cluster formation [187], suggesting that clustering may in fact depend on initial receptor triggering, rather than *vice versa*. Support for the role of microclusters in signalling comes from the observation that the

number of antigens available within a cluster is predictive of T-cell sensitivity [188]. CD28 and the TCR colocalise in microclusters, while they segregate in the cSMAC [142], and therefore microclusters are thought to be the ideal sites for costimulation [189], given that close proximity of CD28 and TCR is needed for signal integration [145]. Some signalling models suggest that signalling proteins are pre-clustered separately in the resting state, and that these nanoclusters consolidate during activation to form signalling machines [190], but the functional significance has been debated in the case of LAT clusters [191]. Using total internal reflection fluorescence microscopy (TIRFM; see Section 6.3.1) of T cells in contact with artificial surfaces, it has been proposed that protein islands form independently of and prior to ligand binding, and increase in size and number upon activation [192]. However, surfaces like those used in TIRFM (*i.e.,* coated glass) were demonstrated to change the mobility of TCRs, suggesting caution in the interpretation of TIRFM data [107]. Furthermore, some of the studies that report nanoclustering of signalling proteins in the resting state, *e.g.* for the TCR [190], LAT [190], and Lck [193], have used photoactivated localisation microscopy (PALM; see Section 6.3.1) or stochastic optical reconstruction microscopy (STORM; see Section 6.3.1) to detect and quantify clustering, a method that makes use of stochastically blinking fluorophores to achieve non-diffraction limited resolution (*i.e.* < 200 nm). However, a recent analysis pointed out that PALM and related methods are not suitable to characterise clustering because blinking events of the same fluorophore are wrongly assigned to separate, clustered fluorophores, overestimating fluorophore density ([194]; also see Section 6.3.2). Furthermore, since the formation and orchestration of microclusters is an active, actin-driven process [75, 185], it remains unclear by what passive event this process would be initiated; *i.e.* which event would initially drive cluster formation, and how ligand binding would cause the formation of clusters.

Whether aggregation of the TCR occurs by crosslinking with its natural ligands is subject to controversy, because conflicting reports exist on the valency of both the pMHC ligands on the APC, and the resting TCR, as discussed in Section 1.6.1. It is conceivable that while the TCR is monomeric in its true resting state, it may be pre-

clustered following tonic, low-level signalling that occurs physiologically, and thereby pre-disposed to forming higher order aggregates or clusters upon triggering with a productive pMHC ligand [149]. In agreement with this hypothesis, the TCR appears to be pre-clustered to a greater extent in memory as compared to naïve T cells, increasing their sensitivity to activation [195]. The BCR, which constitutes a homodimeric structure, can be crosslinked with multivalent soluble antigen resulting in B-cell activation [196, 197]. However, activation is also induced by antigens that are unable to crosslink the BCR, making crosslinking an insufficient model to generally explain BCR triggering [196, 197].

Any plausible aggregation model needs to be able explain how a single productive TCR-pMHC interaction would lead to activation [147]. It has been proposed that TCRs bound by weak agonists, *e.g.* self-pMHC, which are known to induce weak signalling, associate with productive, high-affinity TCR-pMHC complexes to form signalling units, perhaps mediated by the co-receptors, and this hypothesis is supported by the observation that a higher abundance of self-pMHC enhances T-cell activation [149, 198, 199]. It should be noted, however, that T-cell activation occurs even in the absence of coreceptor expression [200, 201], and the affinity of *e.g.* CD4 interactions is astonishingly weak [202]. Other models suggest that a ligand-induced conformational change disposes the TCR [158], or the BCR [196, 203], to laterally associate with other receptors, such as by rigidifying the receptor complex [158], or by exposing new interfaces for interaction [203]. It is, however, difficult to envisage how a ligand-induced conformational change could provide a general mechanism for immunoreceptors, given their (and their ligands') diversity in sequence and structure. Furthermore, ligand-independent triggering would not be accounted for, questioning whether a conformational change could present a general triggering mechanism.

### 1.7.3. Segregation models

Phosphorylation of the immunoreceptor signalling motifs is regulated by the action of kinases, such as Lck and Fyn, and receptor-type protein-tyrosine phosphatases, such as CD45 and CD148. Therefore, the net levels of immunoreceptor phosphorylation

are governed by the local balance of kinase to phosphatase activity, and altering this balance in favour of kinase activity would result in signalling. It has also been proposed that the regulation of Lck activity is decisive for signalling [204-206]. Phosphorylation of the C-terminally located Y505 creates an intramolecular binding site for the SH2 domain, causing Lck to adopt an auto-inhibited conformation, whereas phosphorylation of Y394 is activating, and protects Lck from becoming auto-inhibited [181, 207]. The kinase Csk negatively regulates T-cell activation by phosphorylating Y505, and Lck self-regulates by phosphorylating both Y394 and Y505 in *trans* [181], whereas CD45 dephosphorylates both sites [207]. This rather complex regulatory system involving Lck, Csk, and CD45 is able to change Lck activity by a factor of 10 [181].

However, Lck was reported to be constitutively active, and the proportion of active Lck does not appear to change significantly during T-cell activation [208]. Furthermore, inhibiting phosphatase activity with the drug pervanadate sufficed to induce T-cell activation [209], supporting the notion that Lck is active in resting T-cells and that phosphatase activity is necessary to keep CD3 phosphorylation levels below the signalling threshold in the absence of stimulation with a ligand. This may explain why T cells express such large amounts of CD45, *i.e.* in the range of $10^5$ proteins per cell and 2-3 CD45 proteins per TCR complex [210], at a high energetic cost. Receptor-type protein-tyrosine phosphatases are estimated to have much higher (10-100 fold) enzymatic activity as compared to tyrosine kinases [211], which together with their larger abundance supports the case that they are dominant over kinases in the resting state. Although CD45 is broadly specific [212], it preferentially binds and dephosphorylates CD3ζ rather than Lck, suggesting that its primary function is to downregulate CD3 phosphorylation rather than to tune Lck activity (*via* dephosphorylating Y505 and Y394) [181]. The question then arises of how ligand binding would alter the kinase/phosphatase balance in a way that would lead to receptor triggering.

In the kinetic-segregation model, it is postulated that receptor-type protein tyrosine phosphatases are segregated from TCR/pMHC complexes in the T-cell/APC contact based on their large dimensions, while Src kinases such as Lck continue to diffuse, shifting the local kinase/phosphatase balance towards phosphorylation [86]. CD45 and CD148 are heavily glycosylated glycocalyx proteins with no known ligands that possess large extracellular regions consisting of four (CD45) and eight to ten (CD148) fibronectin type-3 domains that are arranged like beads on a string and an N-terminal mucin-like domain (see Figure 5-10; [65, 153, 213, 214]). The sequence of the extracellular region of CD45 is poorly conserved across species, and conserved residues locate to the domain interfaces rather than the surface, indicating that its overall structural properties are evolutionary important [153]. These observations support the hypothesis that the extracellular regions of CD45 and CD148 function as molecular levers, and that their structures may be important in moving their associated phosphatase activity around the cell. Src kinases, on the other hand, do not possess extracellular domains but are cytoplasmic proteins that associate with the plasma membrane *via* lipid tails [215]. In the kinetic-segregation model, ligand discrimination is thought to occur based on the half-life of the TCR/pMHC interaction: the TCR is protected from phosphatase activity while engaged, but diffuses out of the close-contact upon releasing its ligand and is then quickly dephosphorylated [86]. A signalling cascade is initiated if the TCR/pMHC complex persists for a sufficient time span to recruit co-receptors such as CD4, and key downstream signalling proteins including ZAP-70 (Figure 1-4). The model is supported by a number of observations: (1) the CD45 extracellular domain has dimensions sufficiently large to effect its passive segregation from TCR/pMHC, and is predicted to stand upright on the membrane [153]; (2) the exclusion of CD45 and CD148 from signalling receptors has been visualised by imaging, in the IS [214, 216], microclusters [75], "close-contacts" [153], and a reconstituted giant unilamellar vesicle system [217]; (3) sterically-driven exclusion of CD45 at "close contacts" that form between T cells and artificial surfaces is sufficient to induce ligand-independent calcium signalling [153]; (4) the truncation of phosphatases abrogated TCR-mediated signalling as well as their exclusion from close

contacts [149, 153, 216, 218]; (5) TCR- and CD28-mediated signalling is sensitive to the dimensions of their ligands [175, 176, 219]; (6) surface-immobilised ligands are more active than soluble ones [149, 173, 174]; (7) chimeric TCRs induce activity most potently when engaging a membrane-proximal epitope on their target cell [149, 214, 220, 221]; and (8) phosphorylation of CD3ζ is affected by local phosphatase density more so than by kinase availability [181]. Additional support comes from the observation that adhesion molecules such as CD2, spanning similar dimensions to TCR/pMHC complexes when bound to their ligands, will likely promote the formation of close-contacts between T cells and APCs [86]. Moreover, the resistance of the plasma membrane against bending is thought to drive the steric exclusion of glycocalyx proteins energetically [217], and mathematical modelling predicts that a single TCR/pMHC interaction suffices for passive size-based segregation [87]. Because these passive rearrangements are not dependent on receptor diffusion, they can account for a very high speed of T-cell activation [87].

Since CD45 exclusion from microclusters was observed, it has been proposed that segregation may also result from aggregation rather than from steric exclusion. Support comes from the observation that aggregation suffices to effect the exclusion of bystander proteins [217]. Lck was described to co-cluster with the TCR while excluding CD45 [193], a setting that lead to strong TCR phosphorylation in a reconstituted system [181]. An alternative and somewhat controversial model suggests that the TCR transitions to a different lipid environment, or membrane compartment, upon ligand binding, although how such a transition is triggered is unknown. Transmembrane proteins are thought to locate to either the "ordered" (*i.e.* lipid rafts) or "disordered" phase in the membrane, as has been shown to occur at room temperature in giant plasma membrane vesicles [222]. The TCR is thought to reside in the disordered phase in resting T-cells [223], and to partition into the ordered phase upon ligand binding, a compartment that is enriched in Lck but depleted of CD45, but this relocation has not yet been confirmed conclusively [186, 224].

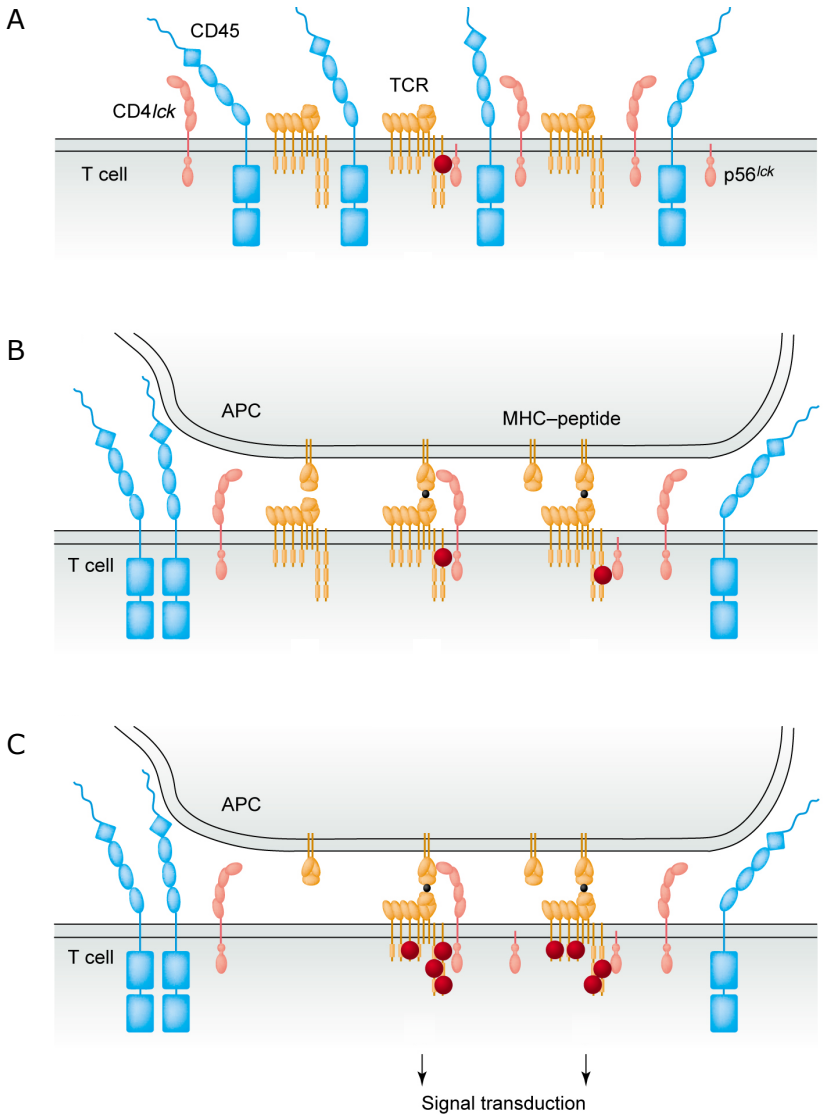



Figure 1-4: The mechanism behind TCR triggering according to the kinetic-segregation model. Modified from [225]. **A** In the resting state, Lck constitutively phosphorylates the TCR, but phosphorylation levels remain subthreshold due to the dominant phosphatase activity by CD45. **B** The TCR-pMHC interaction brings the membranes of the T cell and APC into very close opposition, sterically excluding CD45. In "close-contact" areas thereby protected from phosphatase activity, TCRs remain phosphorylated. **C** Specificity results from strongly bound TCRs remaining in the contact sufficiently long such that co-receptors and downstream signalling proteins are recruited, while unbound or weakly bound TCRs diffuse out. Unbound Lck also phosphorylates the TCR, though less efficiently than co-receptor bound Lck, explaining co-receptor independent signalling.

Lateral associations and complex formation are also thought to be favoured in lipid rafts, such that receptor triggering results from its confinement to a dynamic substructure of the membrane [186], and as outlined in Section 1.7.1, a change in lipid environment has been suggested to induce productive conformational changes. It has been observed that LAT and other signalling proteins downstream of the TCR partition into a dynamic membrane compartment that excludes CD45 based on charge repulsion and that helps to sustain signalling; this process is, however, dependent on initial TCR signalling and can therefore not constitute the initial step in receptor triggering [226, 227].

## 1.8. Triggering receptors with antibodies

In addition to their natural ligands, immunoreceptors are triggered by other stimuli, such as agonistic antibodies, or even ligand-independently, *e.g.* due to interactions with artificial surfaces [153] or by chemically switching off phosphatase activity [209]. These alternative stimuli act upon the same signalling apparatus, achieving responses like the natural ligands, and are subject to the same physical and structural limitations, likely utilising the same mechanism. Any plausible triggering mechanism thus needs to be able to explain these epi-phenomena as well as triggering with natural ligands.

The phenomenon of antibody superagonism was first discovered among anti-CD28 antibodies. Agonistic, or "conventional", anti-CD28 antibodies induce costimulatory signalling; *i.e.,* an additional stimulus needs to be present to achieve full T-cell activation, such as an anti-CD3 antibody. "Superagonistic" antibodies, however, are mitogenic when used on their own, inducing full activation in the absence of additional stimuli [228]. Interestingly, the epitopes of the superagonistic antibodies all map to the side of CD28 close to the membrane, whereas conventional antibodies bind at the top of CD28 as do its natural ligands [229]. Four potential mechanisms were initially suggested to underpin the greater potency of superagonists: (1) CD28 may exist in two or more states that differ in their signalling competency, and superagonist antibodies may preferentially bind to the more competent subgroup. The states may differ in their

extent of oligomerisation; *i.e.* the superagonist may be able to bind to pre-clustered CD28 whereas the conventional antibody may be sterically prevented from doing so, binding instead to unclustered, perhaps less signalling-competent, CD28. This model is, however, very vague, and it has not been demonstrated that CD28 exists in different oligomerisation states in the resting T-cell. Furthermore, the superagonist binds to a membrane-proximal epitope that is expected to be less rather than more accessible, particularly in protein clusters. (2) Alternatively, one could envisage that CD28 may exist in different conformations, and that the superagonist perhaps stabilises a more signalling-competent conformation. This hypothesis was, however, ruled out by x-ray crystallography [131]. (3) Another hypothesis was that the superagonistic antibody may crosslink CD28 more efficiently because it adopts a "parallel" conformation [132, 228, 230]. It should be noted, however, that a conventional antibody (clone 7.3B6) was shown to be able to crosslink CD28 and form arrays similarly to a superagonist (clone 5.11A1) [131], and the CD28 crystal structure implies that a "parallel" conformation, as observed for CTLA4, is not sterically permitted in the case of CD28 [131]. (4) It was suggested that binding a membrane-proximal *versus* membrane-distal epitope may differentially affect the accessibility of the CD28 signalling motifs for downstream signalling proteins such as kinases. This model assumes that the CD28 cytoplasmic tail cannot rotate freely relative to the extracellular domain, such that extracellular binding events translate into cytoplasmic effects. This interpretation is possible, but would require a more in depth analysis to be confirmed.

Intrigued by the structural correlation and wanting to explore the signalling mechanism, previous work on the problem began in this laboratory with the determination of the crystal structure of an antibody superagonist bound to CD28 [131]. This revealed that the superagonist forms a more compact complex, binding with a near horizontal geometry. In contrast, conventional antibodies were observed to form more extended V-shaped complexes, with a resulting 75 Å height difference between the two types of antibody complexes (Figure 1-5; [131]). A new, kinetic-segregation model-based hypothesis was put forward, suggesting that large phosphatases segregated from superagonist-bound CD28 more efficiently than from

conventional antibody-bound CD28. In regions thereby depleted of phosphatases, the kinases dominate, and the half-life of receptor phosphorylation increases, initiating a signalling cascade [131]. Although TCR ligation was not required, and CD3 phosphorylation was not observable, anti-CD28 superagonism was nevertheless dependent on surface expression of the TCR and on its proximal signalling network [228, 231, 232]. How the TCR is involved in the signalling mechanism, however, is not known.

### 1.9. Application of antibodies against immunoreceptors in therapy

Not only are antibodies a valuable research tool, but they are being increasingly used as biologic therapeutics. Due to their unparalleled specificity, they are well suited to minimising off-target effects. Therapeutic antibodies can be used to engage a target cell *via* binding to a surface antigen and to then recruit an effector immune cell for directed killing, either *via* its Fc, or in the case of engineered bispecific antibodies expressing two separate Fabs, *via* their antigen binding site [233]. In this way, tumour cells can be made visible to the immune system. Perhaps most successfully, antibodies are also being used to block ligand/receptor interactions by targeting either the ligand, or the receptor at or near the ligand binding site, or by stabilising an inactive receptor conformation [234]. Blocking antibodies against the checkpoint inhibitor PD1 are a very successful example in cancer immunotherapy. PD1 carries both an ITIM and an ITSM in its cytoplasmic tail, and recruits phosphatases upon becoming triggered that negatively regulate TCR signalling [235]. PD1 engagement by its natural ligands, which are highly expressed on the surface of many tumour cells, prevents the activation of cytotoxic T-cells and induces anergy, and can cause activated T-cells to undergo apoptosis, such that the tumour evades destruction by the immune system [236]. PD1 signalling also suppresses anti-tumour immune responses by inducing T cells to secrete IL-10, an anti-inflammatory cytokine, and by inducing effector T-cells to differentiate into anti-inflammatory, regulatory T-cells [236]. Using blocking antibodies, ligand binding is sterically prevented by engaging PD1 near the ligand binding site. Nivolumab and pembrolizumab are FDA-approved anti-PD1 antibodies for the treat-

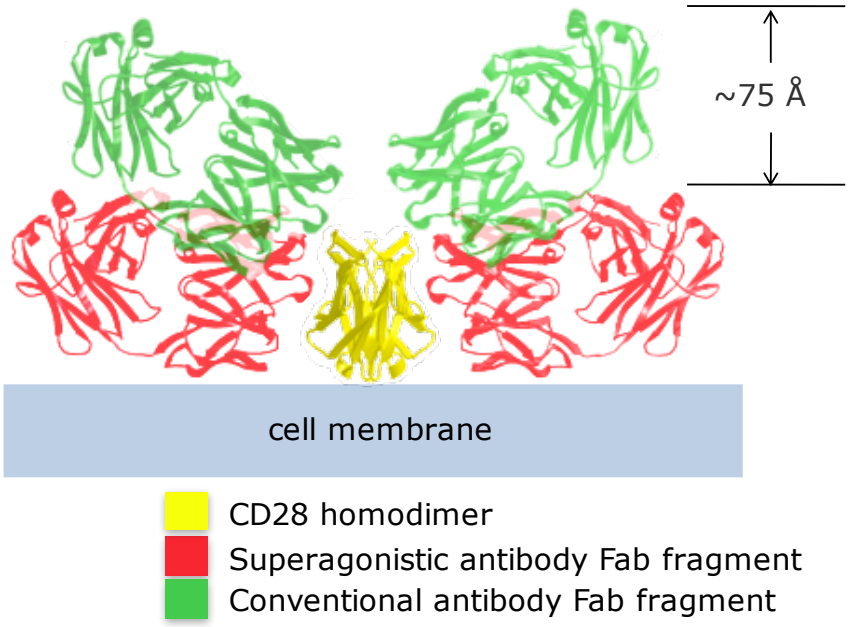



Figure 1-5: Superagonistic antibodies form compact complexes with receptors. Modified from [131]. A model of the Fab fragment of the 5.11A1 superagonist (red) in complex with the soluble human CD28 homodimer (yellow) is displayed, based on x-ray crystallography [131]. Overlaid is a model of the Fab fragment of the 7.3B6 conventional antibody (green) in complex with human CD28 (yellow), based on cryo electron microscopy [131].

ment of melanoma, and have been shown to be superior to standard chemotherapy in clinical trials [236]. They were shown to cause tumours to regress, and to increase patient survival, and their effects were long-lived [236]. Importantly, and in contrast to conventional chemotherapy, they were reasonably well-tolerated in terms of toxicity [236].

However, another application would be to trigger receptor signalling by targeting it with an antibody. Agonistic antibodies induce signalling, which may switch on or off immune responses, depending on the nature of the target receptor (*i.e.* one that expresses ITAMs or ITIMs). The therapeutic aim of anti-CD28 superagonists was to selectively activate regulatory, but not effector T-cells, which seemed like a promising approach in preclinical *in vitro* and *in vivo* studies. In a phase I clinical study, however, an unexpectedly severe cytokine storm was induced in healthy volunteers [237-239],

and only at a much lower dose was the desired effect observed in humans without severe side effects in a later study [240, 241]. Despite the fact that the use of antibodies in therapy is becoming increasingly common, and that the number of novel antibody-based biologics is ever increasing, in the case of the agonists the exact mode of their activity is relatively poorly understood. Most data address their effects at the physiological level, and their safety, efficacy and toxicology, but their effects at the molecular level are only vaguely known. The design of novel therapeutics, and especially their safety, would benefit from a detailed knowledge of how antibodies trigger immunoreceptors.

### 1.10.Aims of this thesis

The goal of this thesis is to determine how antibodies trigger immunoreceptors, with a particular focus on superagonistic anti-CD28 antibodies. This is expected to add to our current understanding of how immunoreceptors are triggered generally, since a general model needs to account for all possible ways in which these receptors are triggered. However, antibodies that modulate immune responses have in principle great therapeutic potential, with applications in autoimmune disease and cancer, and the work of this thesis ought to assist with the design of new, safe treatments based on the use of antibody agonists. At the centre of the analysis, fluorescence imaging will be used to directly test the hypothesis that superagonistic antibodies are more potent *versus* conventional, non-mitogenic antibodies simply because they more efficiently exclude large receptor-type protein tyrosine phosphatases from CD28.

# Chapter 2 General materials and methods

## 2.1. Cell Culture

### General cell culture

Cell culture was performed using standard antiseptic technique in HEPA filtered cell culture cabinets. All substances were bought sterile or were filter-sterilised before they were introduced to cell culture. Cell lines were grown at 37 ºC in a 5% $CO_2$ atmosphere. Cell viability and density were monitored by regular microscopy and by counting them in a haemocytometer. Trypan blue (0.4%, SigmalAldrich), a dye that penetrates dead but not viable cells, was mixed 1:1 with a 30 μL aliquot of cells before counting.

### Subculturing of cell lines

Mouse leukaemia T-cell hybridomas DO11.10 [242], Yae5b3k [243], and BW5147 [244] were cultured in JMEM medium (RPMI-1640 medium supplemented with 10% foetal calf serum, 10 mM HEPES, 1 mM sodium pyruvate, 2 mM L-glutamine and antibiotics [50 units penicillin, 50 μg streptomycin and 100 μg neomycin per mL]). They were split ~ every two to three days to keep them at a density between $1*10^5$ and $1*10^6$ cells per mL.

HEK-293T cells [245] were grown in 293T medium (DMEM medium (Gibco) supplemented with 10 % foetal calf serum, 2 mM glutamine and antibiotics [50 units penicillin and 50 μg streptomycin per mL]). They were split when they reached 70-90 % confluency. The medium was discarded and the adherent cells of one T75 flask (Greiner flask, tissue culture treated, Sigma-Aldrich) were washed with 10 mL PBS. The cells were detached by incubation in 5 mL trypsin-EDTA at 37 ºC for 2-5 minutes. The flask was shaken to detach all cells, and 10 mL fresh medium was added. The cells

were pelleted at 1300 rcf for 5 minutes. They were resuspended in 10 mL fresh medium and split 1/5 into a fresh flask with fresh medium.

**Liquid nitrogen storage of cell lines**

For long-term storage, cell lines were kept in liquid nitrogen tanks. Typically, three to six vials containing $1*10^6$ cells each were stored. 30-60 mL cell culture at a density of ~ $1*10^6$ cells/mL was pelleted by centrifugation at 1300 rfc, 4 minutes, 4 ºC. Pellets were resuspended in 3-6 mL freezing solution (90% foetal calf serum (Sigma-Aldrich)), 10% DMSO (Sigma-Aldrich) and aliquoted to 1 mL per vial. Vials were transferred to isopropanol-filled freezing chambers (Mr. Frosty™ Freezing Container, Thermo Fisher Scientific) that ensure an even decrease in temperature of about 1 ºC per minute, and kept in a freezer at -80 ºC overnight. The next day vials were transferred to liquid nitrogen.

## 2.2. Flow Cytometry

Flow cytometry was used to assess whether and at which levels endogenous as well as stably transfected receptors were expressed. This analysis provided information of single-cells as well as statistical information across a large number of cells.

The flow cytometer creates a current of cells passing through the analyser one at a time. It records the fluorescence of each cell. Cells fluoresce either because they were transfected with a fusion protein with a fluorescent protein, or because they were stained with fluorophore coupled-antibodies against a surface receptor. In the first case overall expression in the cytoplasm as well as at the cell surface is measured, whereas in the latter case only expression at the cell surface is accounted for. Intracellular staining with antibodies upon permeabilisation of the cell is of course also possible but was not employed in the work described in this thesis. Because fluorescence can be detected in multiple channels at a time, two or more different receptors can be stained in different colours in one experiment.

Per condition $5*10^5$ cells were washed with 3 mL PBS-azide 0.05%, and centrifuged at 1200 rcf in polypropylene tubes. Cells were incubated for 45 minutes at 4 ºC with 5 µg/mL of monoclonal antibody, specific for the receptor of interest, in PBS-azide. Cells were then washed and centrifuged as above. Cells were incubated with Alexa647®-coupled secondary antibody at 2 µg/mL in PBS-azide for 30 minutes at 4 ºC. Controls were included in which incubation with either antibody was omitted. Cells were washed and centrifuged as above and resuspended in 2% paraformaldehyde/PBS-azide for fixation.

Cells were analysed on a Cyan APP (Dako) fluorescence-activated cell sorting (FACS) flow cytometer. Compensation was applied where more than one channel was analysed simultaneously to correct for bleed-through between the channels.

Data analysis was performed with the FlowJo software (version 9). Expression levels were compared according to the mean florescence intensity for cells gated as viable in the forward and side scatter. Cell lines with multiple populations (*i.e.* showing more than one peak for expression of the gene of interest) were discarded.

## 2.3. Molecular Cloning

### Overview

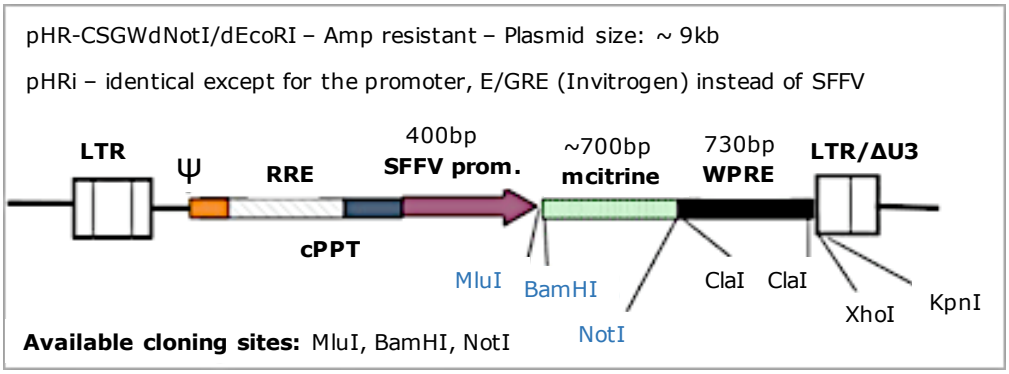



Figure 2-1: Vector map for pHR-SIN-CSGWdNotI/dEcoRI (pHR)

For lentiviral transduction, the gene of interest was inserted into the pHR vector (Figure 2-1) *via* the MluI/BamHI/NotI cloning sites. Typically, untagged genes were inserted between the MluI and NotI cloning sites. For tagged genes, the desired tag (e.g. a fluorescent protein gene) was inserted between the BamHI and NotI cloning sites prior to inserting the gene of interest between the MluI and BamHI cloning sites. The gene of interest was amplified by polymerase chain reaction (PCR), followed by digest of vector and insert (*i.e.* PCR product) to create sticky ends. Purified vector and insert deoxyribonucleic acid (DNA) fragments were then ligated. Competent bacteria were transformed with the ligate, and plasmid DNA was purified from bacterial culture. Because the pHR vector confers ampicillin resistance, transformed bacteria can be selected for by adding ampicillin. Once the DNA sequence was confirmed, plasmids were used to transfect a packaging cell line for virus production. Cell lines of interest were then transduced with the lentivirus to stably express the gene of interest.

**Template preparation**

Genes of interest were amplified by PCR either from complementary DNA (cDNA), or from a plasmid if available. Tags such as fluorescent proteins were expressed as C-terminal fusion proteins unless specified otherwise. Where ligation to a tag gene was desired, the stop codon of the gene of interest was omitted and primers were designed to ensure an in-frame ligation to the tag.

**Primer design**

Primers complementary to the 5' or '3 ends of the sequence of interest, respectively, and containing the desired restriction sites were designed to have matching melting temperatures in the range of ~ 65-70 ºC. Primer properties were verified with the Sigma-Aldrich custom oligo online tool prior to purchase from Sigma-Aldrich.

**Polymerase chain reaction**

The PCR protocol was optimised for each gene of interest and set of primers. A typical protocol was as follows:

Mixture for one 40 µL reaction

| | |
|---|---|
| MilliQ water | 28.4 µL |
| 5x Phusion-HF buffer | 8 µL |
| 10 mM dNTP mix | 2 µL |
| 10 µM forward primer | 0.4 µL |
| 10 µM reverse primer | 0.4 µL |
| Phusion polymerase | 1 µL |

PCR machine programme

| | | |
|---|---|---|
| 95 ºC (denaturation) | 3 minutes | |
| 95 ºC (denaturation) | 30 seconds | 34 cycles |
| 55ºC (annealing) | 30 seconds | |
| 72ºC (extension) | 20 seconds | |
| 72ºC (final extension) | 5 minutes | |

PCR products were separated at 80 mA on ethidium bromide-stained 1% agarose gels in 0.1M Tris/0.1 M borate/2 mM EDTA buffer (percentage may be varied for very large or very small products). When the PCR product was of the correct size and no contaminant bands were visible, the band was excised and DNA was extracted with the QiaQuick gel extraction kit (Qiagen).

**Restriction digest**

The PCR product and the pHR vector were digested with the appropriate restriction enzymes at 37 ºC for 1-1.5 hours.

Pipetting scheme for one 20 µL digest (PCR product)

| | |
|---|---|
| PCR product | 16 µL of a 30 µL elution from gel extraction |
| 10x NEB buffer 2/3/4 | 2 µL |
| Restriction enzyme 1 | 1 µL |
| Restriction enzyme 2 | 1 µL |

Pipetting scheme for one 20 µL digest (vector plasmid)

| | |
|---|---|
| Vector | 5 µL (for a 200 ng/µL plasmid) |
| 10x NEB buffer 2/3/4 | 2 µL |
| Restriction enzyme 1 | 1 µL |
| Restriction enzyme 2 | 1 µL |
| MilliQ water | 11 µL |

Digests were separated on an agarose gel as above. Vector and insert bands were excised and extracted as above.

**Ligation of vector and insert**

Ligation reactions were prepared with varying ratios of insert to vector DNA. Ligation was at 16 ºC, typically over night or for 5 hours.

Pipetting scheme for one 20 µL ligation

| | Reaction 1 | Reaction 2 | Reaction 3 |
|---|---|---|---|
| Vector | 5 µL | 5 µL | 5 µL |
| Insert | 0 µL | 1 µL | 10 µL |
| 10x T4 DNA ligase buffer (NEB) | 2 µL | 2 µL | 2 µL |
| T4 DNA ligase (NEB) | 1 µL | 1 µL | 1 µL |

**Transformation of competent bacteria**

Competent Top10 bacteria were transformed with the ligations. A 30 mL culture in liquid broth medium (LB Lennox, Sigma-Aldrich) was grown at 37 ºC to an $OD_{600}$ between 0.3 and 0.6. Bacteria were harvested at 3,000 rcf for 10 minutes at 4 ºC. The supernatant was discarded and bacteria were resuspended in residual broth. 2.5 mL of chilled transformation and storage solution (TSS; liquid broth with 5% DMSO, 10% PEG6000, 50 mM magnesium chloride) was added. The suspension was shaken gently and chilled on ice for 10 minutes. 100 µL of suspended bacteria were added to the chilled ligation tubes and gently shaken. The mixture was incubated on ice for 10

minutes and then transferred to the 37 ºC water bath for 4.5 minutes. Then, the tubes were immediately returned to ice and quickly topped up with 400 µL fresh liquid broth. The bacteria were allowed to recover for 30-45 minutes in the 37 ºC water bath before the mixture was plated out on liquid broth agar plates containing 100 µg/mL ampicillin. The pHR vector carries an ampicillin resistance gene. Plates were incubated at 37 ºC overnight. Colonies were counted. For ligation reaction 1 very few colonies are expected because no insert was present, and vectors cut with two different restriction enzymes do not tend to re-ligate. Colonies present for reaction 1 correspond to undigested vector. For reactions 2 and 3 a much higher number of colonies is anticipated. Typically, the plate for reaction 2 was chosen for picking colonies.

**Colony PCR**

Typically, eight colonies were picked for colony PCR. More colonies were picked if the number of colonies for reaction 1 and 2 or 3 did not differ greatly. Colony PCR was carried out to test for the presence of the desired insert. The protocol was as follows:

Pipetting scheme for one 20 µL colony PCR reaction

| | |
|---|---|
| MilliQ water | 16.5 µL |
| 10x thermo buffer | 2 µL |
| 10 mM dNTP mix | 0.5 µL |
| 10 µM forward primer | 0.4 µL |
| 10 µM reverse primer | 0.4 µL |
| NE biolabs Taq polymerase | 0.2 µL |

A colony was picked with a sterile plastic tip that was immersed in the PCR mix and then streaked on a reference liquid broth agar plate with 100 µg/mL ampicillin. The plate was incubated at 37 ºC for several hours. The PCR machine programme was typically performed as described above. Extension time was adjusted for very large

inserts. PCR products were separated on an agarose gel as described above. Two colonies that gave a PCR product of the correct size were typically chosen.

**Plasmid purification**

20 mL liquid broth with 100 μg/mL ampicillin was inoculated with bacteria from the reference plate, and incubated at 37 ºC overnight. The bacteria were pelleted at 4,000 rcf for 10 minutes at 4 ºC. Plasmids were isolated with the HiPure plasmid mini-prep kit (invitrogen). DNA concentrations were determined by spectrophotometry (NanoDrop, Thermo Fisher Scientific), measuring absorbance at 260 nm. A $A_{260}/A_{280}$ ratio > 1.8 indicated DNA purity.

**DNA sequencing**

DNA sequencing with suitable primers was carried out by the Sequencing Unit of the Weatherall Institute of Molecular Medicine (University of Oxford). Sequences were read automatically with the 4Peaks software. Sequence identity and integrity was confirmed with a Basic Local Alignment Search Tool (BLAST) found at:

https://blast.ncbi.nlm.nih.gov/Blast.cgi?PAGE_TYPE=BlastSearch.

The UniProt data base was used to confirm appropriate protein sequence and isoform, as found at

http://www.uniprot.org.

## 2.4. Sodium Dodecyl Sulphate – Polyacrylamide Gel Electropheresis (SDS-PAGE)

Electrophoresis is employed to separate proteins of different masses on a gel. First, proteins are treated with sodium dodecyl sulphate (SDS), which denatures them and gives them a negative charge that is proportional to their molecular mass. Then, proteins are loaded onto a porous gel and subjected to a current. The proteins migrate towards the cathode at a speed that is proportional to their negative charge, and thus to their molecular mass. Subsequently, protein bands are visualised, for example by

staining with a protein dye such as Coomassie Brialliant Blue, by a Silver Stain, or by blotting them onto a nitrocellulose membrane followed by immunodetection (Western blot, see 2.5). The position of the band on the gel identifies the mass of the protein relative to protein markers of known sizes. The width or strength of the band reveals the amount of protein.

10 μL protein sample (at no more than 0.5 mg/mL) was diluted 1:1 in either reducing or non-reducing 2x loading buffer. Samples were boiled at 95 ºC for 5 minutes. 15 μL was loaded per well of a 15-well, 12% SDS-PAGE gel. Electrophoresis was carried out at 150 V in a Tris/glycine/SDS-PAGE running buffer (National diagnostics). 12% SDS-PAGE gels consisted of a separating and a stacking gel:

Recipe for a 0.75 mm 12% Separating Gel

| | |
|---|---|
| Deionised water | 1.75 mL |
| Tris-HCl pH8.8 SDS buffer (ProtoGel) | 1.25 mL |
| 30% acrylamide/bis-acrylamide | 2 mL |
| 10% ammonium persulphate | 25 μL |
| TEMED | 5 μL |

Recipe for a 0.75 mm Stacking Gel

| | |
|---|---|
| Deionised water | 1.55 mL |
| Tris-HCl pH6.8 SDS buffer (ProtoGel) | 625 μL |
| 30% acrylamide/bis-acrylamide | 325 μL |
| 10% ammonium persulphate | 12.5 μL |
| TEMED | 5 μL |

Recipe for 2x loading buffer

| | |
|---|---|
| 0.5 M Tris-HCL pH 6.8 | 1 mL |
| glycerol | 0.8 mL |
| 10% SDS | 1.6 mL |
| Bromophenol blue | to colour |
| β-mercaptoethanol (reducing buffer only) | 0.4 mL |

Typically, the gel was subsequently subjected to Western blotting (see 2.5), or stained with Coomassie Brilliant Blue. The gel was placed in 0.1 % Coomassie Brilliant Blue in a 10 % acetic acid, 40 % methanol solution for 15 minutes under shaking. It was then destained under shaking in a 10 % acetic acid, 12 % methanol solution until no background was visible.

### 2.5. Western blot

Western blotting is employed to detect proteins already separated by size *via* SDS-PAGE with very high specificity. SDS-PAGE followed by a protein stain alone is not sufficient to identify a specific protein with certainty, because it cannot be distinguished from other proteins of a similar mass. In addition, Western blotting is very sensitive and can detect a small amount of protein in a vast excess of contaminant protein.

On the SDS-PAGE the Amersham ECL Rainbow Molecular Weight Markers (GE life sciences) were used because they can be visualised on the Western blot membrane without staining.

As a first step, the proteins were transferred from the acrylamide gel onto a nitrocellulose membrane. Blotting paper and a nitrocellulose membrane were soaked in blotting buffer (2 mM Tris, 150 mM glycine, 20 % methanol). The membrane was set onto the gel and blotting paper was placed on top and below. The assembly was placed in a transfer chamber filled with blotting buffer, and an electric current at 100 V was applied such that the negatively charged protein migrate towards the cathode and onto the membrane. The transfer was performed at 4 ºC and under stirring to prevent overheating.

The membrane was blocked in blocking buffer (1 % skim milk in PBS) overnight under shaking at 4 ºC to prevent unspecific binding of antibody.

Second, an antibody specific to the protein of interest was added to the blocking buffer, typically diluted 1/2000, and incubated at 4 ºC for 45 minutes under shaking.

The membrane was then washed in PBS-Tween 0.05% three times for five minutes under shaking. Typically, a secondary antibody was used to amplify the signal, diluted 1/1000 in blocking buffer. It was incubated at 4 ºC for 30 minutes under shaking, and the membrane was washed as above.

Detection of signal was typically achieved by using a secondary antibody that is coupled to horse radish peroxidase (HRP). A luminescent substrate (Pierce ECL Western blotting substrate, Thermo Fisher Scientific) was added and incubated for two minutes, and the membrane was exposed to an x-ray film. The position of the detected protein bands identified the molecular mass of the protein relative to protein markers of known sizes, and the strength of the bands corresponded to the amount of detected protein.

### 2.6. Transduction of cell lines with lentivirus for stable expression

Stable transfection of cell lines was achieved by transducing them with lentivirus, and was confirmed by flow cytometry. A human immunodeficiency virus (HIV)-derived system was used consisting of three separate plasmids that produce self-inactivating virus driving the expression of the gene of interest. HEK-293T cells [245] were transfected with the p8.91 vector, containing the structural proteins and enzymes needed to generate infectious viral particles [246], the pMDG vector, containing viral coat proteins for packaging [246], and the pHR-CSGWdNotI/dEcoRI (pHR) vector, containing the gene of interest, flanked by long terminal repeats, under control of the cytomegalovirus (CMV) promoter [246] (Figure 2-1). $6*10^5$ HEK-293T cells were seeded in a 9 $cm^2$ tissue culture plastic dish in 2 mL medium. The following day, a mixture of 100 µL unsupplemented DMEM, 0.5 µg p8.91, 0.5 µg pMDG, 0.5 µg pHR and 3µL GeneJuice® transfection reagent (Merck) was incubated at room temperature for 30 minutes and then added to the HEK293T cells. 48 hours later the virus was harvested. HEK293T cells were pelleted by centrifugation at 3,000 rcf for 5 minutes. The supernatant, which contained the virus, was filtered with a 0.45 µL syringe filter and added to $1*10^6$ cells of the desired T-cell hybridoma in 0.5 mL JMEM. The

following day the medium was replaced with fresh JMEM. After 5-7 days of culturing the expression of the gene of interest was tested by flow cytometry. Stable expression was followed up by flow cytometry before experiments were carried out. Expression was matched for different constructs within one experiment. Rather than sorting cell lines for a specific surface expression, levels were adjusted by varying the amount of virus used to transduce the cells, or by subjecting cells to multiple rounds of transduction until the desired expression level was achieved. Cells were promptly frozen to be stored in liquid nitrogen, and freshly thawed cells were used for experiments. Expression was confirmed after freeze-thawing cell lines and was found to be very stable.

## 2.7. Production and purification of soluble His-tagged protein in mammalian cell lines

To produce soluble forms of transmembrane proteins of the Ig superfamily, such as CD28 and Fc receptors, a mammalian expression system was chosen to ensure correct folding and glycosylation. Chinese hamster ovary (CHO) cells were selected because large yields can be achieved. A stable transfection system was chosen because, albeit it is more laborious and time-consuming, better yields can be achieved and once made the cell line can be stored long-term should future experiments require more or fresh protein.

To make a soluble, His-tagged form of the desired protein, a short DNA sequence encoding a His-tag followed by a STOP codon was inserted just before the transmembrane domain. The N-terminal signal peptide was maintained to ensure secretion of the protein.

Two different ways of stably transfecting CHO cells were employed, depending on the particular protein and application in question: Either the more laborious and time-consuming glutamine synthetase selection system, which allows for selection of a single high-expressing clone, or the faster lentiviral system, which omits the selection step.

Expression and secretion of the desired protein into the cell culture supernatant was confirmed by Western blot (see 2.5) once a stably transfected cell line was made.

Typically, two Corning® HYPER*Flask*® cell culture vessels were seeded with ~ $2*10^7$ transfected CHO cells in 500 mL medium. After two to three weeks in culture the protein was harvested and purified.

### 2.7.1. Protein production in CHO cells with a glutamine synthetase selection system

To select for CHO clones that express large amounts of protein, a glutamine synthetase selection system was employed. Glutamine is an essential amino acid that is synthetized from glutamate by glutamine synthetase, which is endogenously expressed in CHO cells. To increase selective pressure, cells are grown in glutamine-free medium in the presence of a glutamine synthetase inhibitor, methionine sulphoximine (MSX). A single clone is isolated that secretes large amounts of the desired protein.

**Insertion into the pEE14 expression vector**

The protein of interest is inserted into an expression vector, pEE14 (Lonza Biologics), that contains a glutamine synthetase minigene under the same promoter that drives expression of the gene of interest. Transfected CHO cells that express the protein of interest in large amounts thus have an advantage over untransfected or low-expressing cells, and are selected for.

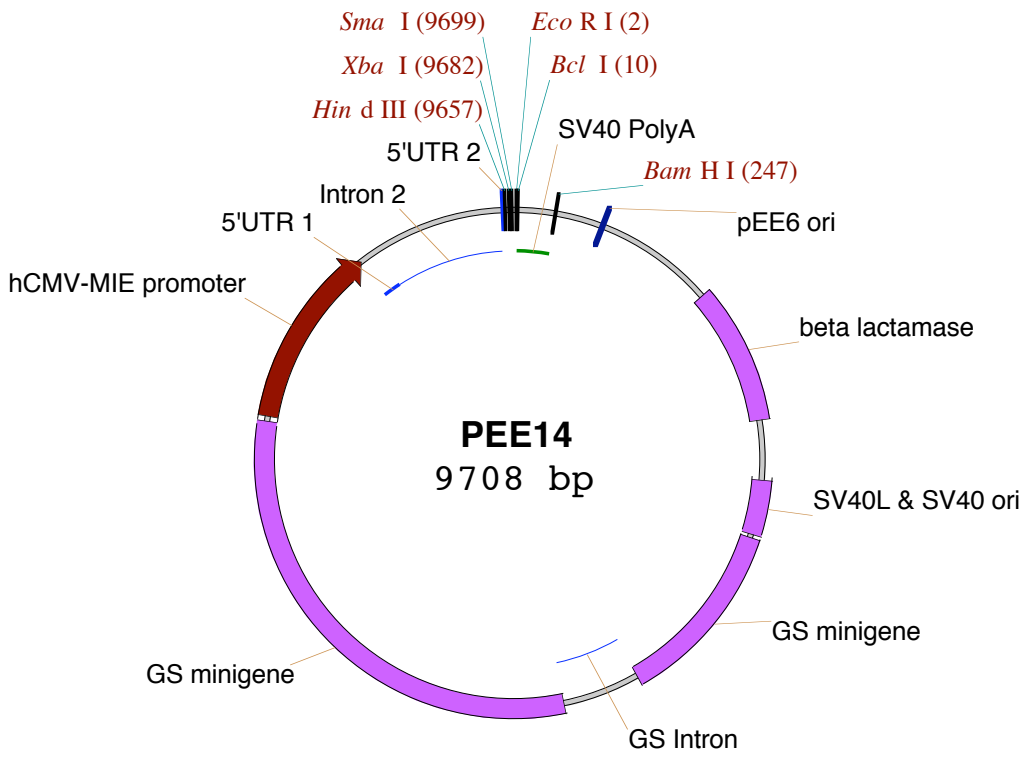



Figure 2-2: Vector map for pEE14 (Lonza Biologics), generated with VectorNTI® (ThermoFisher Scientific).

The protein of interest was expressed as a fusion protein with a mouse Fc domain containing a C-terminal hexahistidine-tag for convenient purification. To allow for cleavage of the mouse Fc domain should it be desired, a thrombin cleavage site (LVPRGS) was included. A modified pEE14 vector was obtained (Heather Brouwer, Davis laboratory, University of Oxford) with the thrombin cleavage site, mouse Fc domain and His-tag genes inserted between the SmaI and the BclI cloning sites (Figure 2-2). The gene of interest, containing one N-terminal signal peptide sequence and ending just before the transmembrane domain omitting a stop codon, was inserted between the XbaI and SmaI cloning sites, as explained in 2.3.

**Transfection of CHO cells with pEE14**

Two T75 flasks (Greiner flask, tissue culture treated, Sigma-Aldrich) were inoculated with $4*10^6$ CHO-K1 cells in DMEM medium (Gibco) supplemented with 10% foetal

calf serum (Sigma-Aldrich), 2 % nucleoside and amino acid supplement (0.35 mg/mL adenosine, 0.35 mg/mL cytidine, 0.35 mg/mL guanosine, 0.35 mg/mL uridine, 0.12 mg/mL thymidine, 0.1 mg/mL asparagine, 0.1 mg/mL glutamic acid), 1 mM sodium pyruvate, 2 mM L-glutamine and antibiotics (50 units penicillin, 50 μg streptomycin and 100 μg neomycin per mL). The next day, cells were transfected with the pEE14 plasmid containing the tagged gene of interest. The CHO-K1 medium was replaced with glutamine-free CHO-K1 medium (glutamine-free DMEM medium (Gibco) with 10% dialysed, glutamine-free foetal calf serum (Sigma-Aldrich), 2 % nucleoside and amino acid supplement as above, 1 mM sodium pyruvate, and antibiotics as above. First, the plasmid was sterilised. An equal volume of ether was added to the tube followed by centrifugation at 1100 rcf for one minute at room temperature. In the cell culture cabinet, the organic layer was removed with a pipette, and the remainder was allowed to evaporate. 10 μg plasmid was added to 1 mL unsupplemented glutamine-free DMEM medium (Gibco) and mixed, followed by addition of 30 μL GeneJuice® transfection reagent (Merck). The solution was mixed and incubated at room temperature for 20 minutes and then added to one CHO-K1 flask. To the other flask, 1 mL unsupplemented glutamine-free DMEM medium (Gibco) was added as a mock transfection. After 48 hours, the cells were trypsinised. The medium as discarded and the flask was washed with 10 mL PBS. 4 mL 1x trypsin in PBS (from trypsin solution 10x, Sigma-Aldrich) was added and incubated at 37 ºC for 3-5 minutes. 10 mL glutamine-free DMEM medium (Gibco) supplemented as above was added, and the cells were harvested at 1200 rcf. The transfected cells were plated out in nine 96-well plates (Nunc®) at $1*10^5$ cells/mL, 100 μL/plate, in glutamine-free DMEM medium (Gibco) supplemented as above. The mock cells were plated out in three 96-well plates (Nunc®) as above. A seeding density is desired that will result in one cell per well to separate single clones. Cells were cultured for ~ 24 hours.

**Selection of a highly expressing clone with MSX**

The next day, MSX, the glutamine synthetase inhibitor, was added to select for transfected and highly expressing clones. Three different concentrations of MSX were chosen (25, 30 and 35 μM) because the ideal concentration that will allow growth of transfected but prevent growth of untransfected clones can vary slightly. For the transfected cells, three 96-well plates (Nunc®) were used per MSX concentration; for the mock cells one plate was used per concentration. 100 μL MSX in glutamine-free CHO-K1 medium was added per well. Cells were cultured for one week, and then 100 μL volume was removed from each well and replaced with 100 μL glutamine-free CHO-K1 medium containing one-half the original MSX concentration (*i.e.* 12.5, 15 and 17.5 μM). Cells were cultured for two to three weeks. Wells were screened for clones that had expanded, and counts of positive wells were compared between MSX concentrations and mock *versus* transfected cells. Clones from the most suitable MSX concentration (*i.e.* producing the highest number of positive wells) were screened for production of the desired protein by dot blot.

**Dot blot to identify highly expressing clone**

100 μL of each well to be screened was transferred to a fresh 96-well plate (Nunc®). 5 μL of each was pipetted onto a nitrocellulose membrane with the help of a grid. The membrane was blocked in 1 % skim milk in PBS overnight. Alike in a Western blot (see 2.5), the membrane was probed with a horse radish peroxidase-coupled anti-mouse Fc secondary antibody (Sigma-Aldrich, A1063), 1/2000 in 1 % skim milk PBS. Because the protein of interest was expressed as a fusion protein with mouse Fc, it will be detected by the secondary antibody. The membrane was developed with Pierce™ ECL Western blotting substrate (Thermo Fisher Scientific) and exposed to an X-ray film. Highly expressing clones were identified by a strong signal on the dot blot. Typically, three clones were chosen for further characterisation. Wells corresponding to the chosen clones were treated with trypsin as above (50 μL 1x trypsin, then 100 μL glutamine-free CHO-K1 medium with the respective MSX concentration were added),

then transferred to 4 $cm^2$ wells (12-well plate, Nunc®) and cultured in glutamine-free CHO-K1 medium with the respective MSX concentration. When confluent, clones were trypsinised and transferred to 9 $cm^2$ wells. Once they were confluent in 9 $cm^2$ wells (6-well plate, Nunc®), the supernatant was characterised by Western blot (see 2.5), and cells were seeded into a T25 flask (Greiner flask, tissue culture treated, Sigma-Aldrich) for subculturing. The Western blot was used to confirm that a protein of the correct size was secreted, and to judge which clone expressed the largest amounts. Probing with secondary antibody was as in the dot blot above.

**Long-term storage and large-scale culturing of the selected clone for protein production**

The best clone was expanded by culturing in the presence of MSX, trypsinising and seeding into a larger flask as above. Cells cultured to confluency in a T175 flask (Greiner flask, tissue culture treated, Sigma-Aldrich) were trypsinised and cells were harvested for long-term liquid nitrogen storage. A second T175 flask was used to inoculate a Corning® HYPER*Flask*® cell culture vessel, culturing the transfected cells of the selected clone in glutamine-free DMEM medium (Sigma-Aldrich) supplemented with 10 % foetal calf serum (regular, not dyalised; Sigma-Aldrich), 2 % nucleoside and amino acid supplement (0.35 mg/mL adenosine, 0.35 mg/mL cytidine, 0.35 mg/mL guanosine, 0.35 mg/mL uridine, 0.12 mg/mL thymidine, 3.1 mg/mL asparagine, 3.05 mg/mL glutamic acid, 1.78 mg/mL alanine, 2.65 mg/mL aspartic acid, 2.3 mg/mL proline), 1 mM sodium pyruvate, and antibiotics [50 units penicillin, 50 μg streptomycin and 100 μg neomycin per mL]). Culturing for protein production was for 3-5 weeks.

### 2.7.2. Protein production in CHO cells with a lentiviral system

Where selection of a single, highly expressing clone was not necessary and time-efficient protein production was preferred, stably transfected CHO-K1 cell lines were achieved with a lentiviral system. Omitting the selection step makes this protocol ~ six weeks faster than the glutamine synthetase selection system.

**Virus production in HEK293T cells**

The protocol in Section 2.6 was followed, inserting the gene of interest followed by a His-tag into the pHR vector. A T75 flask (Greiner flask, tissue culture treated, Sigma-Aldrich) was inoculated with $3*10^5$ HEK293T cells in 16 mL 293T medium and cultured. The following day, the cells were transfected with pHR, p8.91 and pMDG plasmids as in Section 2.6, using eight times the amounts and volumes to scale up from a 9 $cm^2$ well to a 75 $cm^2$ flask. Cells were cultured for 48 hours for virus production.

**Transduction of CHO-K1 cells with virus**

CHO-K1 cells were seeded in a T75 flask (Greiner flask, tissue culture treated, Sigma-Aldrich) at $4*10^6$ cells/mL in 16 mL DMEM medium (Sigma-Aldrich) supplemented with 10% foetal calf serum (Sigma-Aldrich), 1 mM sodium pyruvate, 2 mM L-glutamine, 2 % nucleoside and amino acid supplement (0.35 mg/mL adenosine, 0.35 mg/mL cytidine, 0.35 mg/mL guanosine, 0.35 mg/mL uridine, 0.12 mg/mL thymidine, 3.1 mg/mL asparagine, 3.05 mg/mL glutamic acid, 1.78 mg/mL alanine, 2.65 mg/mL aspartic acid, 2.3 mg/mL proline) and antibiotics (50 units penicillin, 50 μg streptomycin and 100 μg neomycin per mL).

The virus was harvested as in Section 2.6. The CHO-K1 cellculture supernatant was discarded and replaced with the filtered virus-containing supernatant. The next day, the virus-containing cell culture supernatant was discarded and replaced with fresh medium as above. The following day, cells were washed with PBS and trypsinised with 5 mL 1x trypsin in PBS (from 50x Trypsin solution, Sigma-Aldrich) for 3-5 minutes at 37 ºC. 10 mL medium supplemented as above was added and cells were harvested at 1200 rcf for 5 minutes. Cells were resuspended in medium supplemented as above and seeded into a T175 flask (Greiner flask, tissue culture treated, Sigma-Aldrich) and cultured.

**Quality control of protein production by Western blot**

Secretion of the desired protein into the cell culture supernatant was confirmed by Western blot (see Section 2.5), probing the nitrocellulose membrane with an anti-penta-His antibody (Qiagen, 34660) used at 1/2000. Both the correct size of the protein on reducing and non-reducing gels as well as a good amount of protein were examined.

**Long-term storage and large-scale culturing of the selected clone for protein production**

Once the transfected CHO-K1 cells were confluent in a T175 flask (Greiner flask, tissue culture treated, Sigma-Aldrich), they were trypsinised as above with 2x volumes and seeded in a Corning® HYPER*Flask*® cell culture vessel in 500 mL medium supplemented as above. They were cultured for 3-5 weeks for protein production. A second T175 flask (Greiner flask, tissue culture treated, Sigma-Aldrich) was harvested for long-term storage in liquid nitrogen.

### 2.7.3. Purification of soluble His-tagged protein from cell culture supernatant with affinity chromatography

His-tagged proteins were purified by affinity chromatography, making use of the high-affinity interaction between bivalent metal ions and histidine residues. "Nickelated" sepharaose beads were employed to capture the secreted protein *via* its His-tag. Imidazole, having a higher affinity for nickel, was subsequently used replace the His-tag and thereby free the protein of interest from the beads.

To remove cells and debris, the cell culture supernatant was centrifuged at 3000 rcf for 20 minutes at 4 ºC. In a large conical flask, the supernatant was diluted in an equal volume of PBS-azide 0.05%, 0.5 M sodium chloride, pH 8.0. 1-2 mL nickel-charged resin (Ni-NTA agarose, QIAGEN), equilibrated with PBS, was added. The solution was slowly stirred over night at 4 ºC.

When resin was reused, it was washed with 5 column volumes 250 mM imidazole, 5 column volumes MilliQ, and 5 column volumes 100 mM EDTA pH 8.0. It was then recharged with 2 column volumes 100 mM nickel sulphate and washed with 5 column volumes MilliQ, and finally equilibrated with 5 column volumes PBS.

To harvest the resin, the diluted supernatant was centrifuged at 1200 rcf for 5 minutes at 4 ºC. Most of the supernatant was siphoned into a flask and kept for a second extraction if desired. The last 500 mL, containing the resin, was passed through a small column that retains Sepharose. The column was washed with 20 mL PBS. To remove unspecifically bound contaminant protein, the captured protein was pre-eluted with 10 mM imidazole, pH 8.0. Typically, ten 1.5 mL fractions were collected and protein concentration was determined by spectrophotometry (NanoDrop, Thermo Fisher Scientific), measuring UV absorbance at 280 nm. If the last fractions still contained measurable amounts of protein, more fractions were collected. The captured protein was then eluted with 250 mM imidazole, pH 8.0 to purify the His-tagged protein of interest. Typically, ten 1 mL fractions were collected, and protein concentration was determined as above. More fractions were collected if there was still measurable protein in the last fraction

Protein-containing fractions of both pre-elution and elution were separated on a 12 % acrylamide gel, as described in Section 2.4.

### 2.8. Purification of antibody from hybridoma culture supernatant

Production of antibody was confirmed by Western blot of the hybridoma culture supernatant (see Section 2.5). Two to four Corning® HYPER*Flask*® cell culture vessels were seeded with 550 mL of a hybridoma culture at a density of $2*10^5$ cells per mL. ~ three weeks later the supernatant was harvested and diluted it 1:1 with PBS-azide 0.05%, pH 7.4. The antibody was extracted with 20 mL protein-G coupled Sepharose over night at 4 ºC under gentle stirring. After extraction, the beads were loaded on a column and washed with 100 mL MilliQ water, followed by a wash with 200 mL PBS 0.5 M NaCl pH 7.4. Elution was with 0.1 M glycine pH 2.5. Ten fractions

of 5 mL each were collected into 15 mL falcon tubes with a volume (~ 225 µL) of 2 M Tris pH 8.5 that neutralise the pH. The ten fractions were measured for absorption at 280 nm to determine their protein content. To test for the purity of the fractions, they were separated on reducing and non-reducing sodium dodecyl sulphate polyacrylamide gel electrophoresis (SDS-PAGE) gels. In this case, there were no contaminant bands visible for any of the fractions. Thus, all fractions of one extraction were pooled and centrifuged in Vivaspin 20 columns (Sartorius Stedium Biotech) that concentrate proteins larger than 10 kDa.

In the next step, the antibody was purified by fast protein liquid chromatography (FPLC). The SuperDex 200 HR column was used in an ÄKTA FPLC system to separate proteins by size exclusion chromatography. First, column and pumps were washed with filtered 0.5 M sodium hydroxide, then with filtered MilliQ water. Then, the system was calibrated with filtered PBS. The injection loop, with a volume of 2 mL, was also flushed with filtered PBS. Before injection, the antibody was centrifuged at 13,000 rpm in a table-top centrifuge for 5 minutes to pellet any aggregated protein. For each round, no more than 10 mg protein was injected in a volume of 500-1000 µL. The antibody was eluted with filtered PBS. 500 µL fractions were collected and measured for absorption at 280 nm. Again, purity was tested by SDS-PAGE as above. All pure antibody-containing fractions, *i.e.* those that showed no contaminant bands, were pooled, concentrated to 0.5-2 mg/mL as above, aliquoted and frozen. Protein concentrations were determined by spectrophotometry (NanoDrop, Thermo Fisher Scientific), dividing absorbance at 280 nm by the respective extinction coefficient.

### 2.9. Digest of antibody with papain for Fab production

The antibody was buffer-exchanged to 20 mM sodium phosphate 10 mM EDTA pH 7.0 on the FPLC system. The antibody-containing fractions were pooled and concentrated as above to ~ 1.2 mg/mL in 500 µL. They were topped up with 500 µL digestion buffer (20 mM sodium phosphate 10 mM EDTA 20 mM cysteine-HCl pH 7.0). 500 µL of immobilised papain slurry (in 50% glycerol, 0.1 M sodium acetate

0.05% azide pH 4.4, ThermoScientific) was washed twice with digestion buffer and centrifuged at 3,000 rfc for 5 minutes. The slurry was then resuspended in 500 μL digestion buffer, and added to the antibody mixture. The mixture was incubated under shaking at 37 ºC overnight. The slurry was pelleted at 3,000 rcf for 5 minutes. The supernatant was collected. The slurry was washed twice with 2 mL 10 mM Tris-HCl pH 7.5. The washes were collected. 3 mL protein-G coupled Sepharose was loaded on a column and washed first with 8 mL MilliQ water, then with 8 mL 10 mM Tris-HCl pH 7.5. Then the papain digest supernatant and washes were loaded. The flow-through was collected and re-loaded five times; also the last round of flow-through was collected. Beads were washed with 8 mL 10 mM Tris-HCl pH 7.5 and the wash was collected. Elution was with 3 mL 0.1 M glycine pH 2.5 as above; again fractions were neutralised. Twelve 500 μL fractions were collected. Flow-through, wash and fractions were measured for absorption at 280 nm and separated by SDS-PAGE as above. The fragment crystallisable (Fc) regions (> 30 kDa on the gel) were found in the flow-through and wash whereas the desired fragment antigen-binding (Fab) regions (<30 kDa on the gel) were found in the elution. Pure elution fractions, *i.e.* those not showing any contaminant Fc bands, were pooled and purified on the FLPC. A SuperDex 75 HR column was used. Fab fragments were eluted with filtered HBS (10mM Hepes, 150mM NaCl). Purify of the Fab fragments was confirmed by SDS-PAGE as above. Pure elution fractions, *i.e.* those not showing any contaminant bands, were pooled and either frozen for storage or kept at 4 ºC for prompt use. Protein concentrations were determined by spectrophotometry (NanoDrop, Thermo Fisher Scientific), dividing absorbance at 280 nm by the respective extinction coefficient.

### 2.10. Labelling of antibodies and Fab fragments with fluorescent dyes

For labelling antibodies and Fab fragments with Alexa488® or Alexa647®, the Molecular Probes® Antibody Labeling Kits (Thermo Fisher Scientific) were used. The AlexaFluor® dyes are provided as N-hyrdroxysuccinimide esters (NHS-esters) that undergo a covalent reaction with primary amines (*i.e.* lysine side chains) to form very stable conjugates. 100 μL of antibody or Fab fragment was used at 1 mg/mL in PBS.

A 1 M sodium bicarbonate (Sigma-Aldrich) solution was prepared, and 10 μL was added to the antibody to achieve a pH of ~ 8.3. The antibody was then added to the vial containing the dye and incubated for 1-2 hours protected from light. Unbound dye was removed with gel filtration columns from the kit. The concentration and degree of labelling of the antibody-dye conjugate was determined by spectrophotometry (NanoDrop, Thermo Fisher Scientific). The following formulae were used:

Protein concentration (M) = $(A_{280} – (A_{dye} \times CF_{280}))/203{,}000$

Degree of labelling = $A_{dye} / (\varepsilon_{dye} * \text{protein concentration (M)})$

Where CF = correction factor for absorption readings at 280 nm

$CF_{Alexa647®=}$ 0.03; $CF_{Alexa488®}$=0.11; $CF_{Atto655}$=0.08

ε = extinction coefficient at $\lambda_{max}$ in $cm^{-1}$ $M^{-1}$

$\varepsilon_{Alexa647®=}$ 239,000; $\varepsilon_{Alexa488®}$=71,000; $\varepsilon_{Atto655}$=125,000

For labelling antibodies and Fab fragments with Atto655, the Atto655 protein labelling kit (SigmaAldrich) was used with an optimised protocol. To 100 μL of Fab at 1 mg/mL in HBS, I added 5 μL freshly made 0.2 M sodium bicarbonate pH 9.0 to achieve a final pH of 8.3. 6.7 nmol Atto655-NHS ester in PBS was added. The reaction was incubated for two hours at room temperature, protected from light. Unbound dye was removed with gel filtration columns from the Antibody Conjugate Purification Kit (Thermo Fisher Scientific). Concentration and degree of labelling was determined as above. Good and specific binding of the labelled anti-mCD45 Fab was confirmed by flow cytometry as above.

### 2.11.IL-2 *in vitro* stimulation assay

In this *in vitro* assay, T-cell hybridoma lines stably transfected with different receptors were stimulated with antibodies immobilised on glass or plastic plates. As a read-out

the levels of IL-2 secreted in the cell culture supernatant were assessed, which is a bulk rather than a single-cell measurement. This assay determines full T-cell activation in the time frame of days rather than early T-cell activation.

Thermo Scientific™ Nunc™ MicroWell™ 96-well optical-bottom plates with coverglass base (glass plates), or Costar® flat-botttomed 96-well EIA-RIA plates (EIA plastic plates) were used as specified. Plates were wet-coated in 1x coating buffer (from the Mouse IL-2 ELISA Ready-SET-Go!® kit, eBioscience) overnight at 4 ºC with donkey anti-mouse polyclonal secondary antibody at 500 μg/mL, or KT3 at the specified concentration diluted in 500 μg/mL donkey anti-mouse. JJ316 and JJ319 were not typically wet-coated directly on the plate unless stated otherwise.

Wells were washed three times with 250 μL sterile PBS. It was tested whether blocking the wells for one hour at room temperature (with 1x Assay diluent from the Mouse IL-2 ELISA Ready-SET-Go!® kit, eBioscience) followed by three more PBS washes would affect results, in particular the production of IL-2 by cells stimulated with soluble JJ316. Results were not affected (data not shown), and thus the blocking step was subsequently omitted.

Appropriate expression levels of the transfected receptors were ensured by flow cytometry. The required number of cells for each cell line was harvested at 1,300 rcf for 5 minutes and cells were resuspended in appropriate volumes of fresh medium to achieve a concentration of $1*10^7$ cells/mL. Resuspended cells were then mixed 1:1 with medium containing the stimulating antibodies in appropriate concentrations (except for KT3, which was pre-coated onto the plate, see above. For KT3 stimulation or no stimulation, the cell suspension was mixed 1/2 with fresh medium). Cells were incubated at room temperature for ~ 15 minutes. Each condition was performed in technical duplicates or triplicates. Each well received $5*10^5$ cells in 100 μL medium/antibody mixture. Wells were then incubated at 37 ºC in 5 % atmospheric $CO_2$ for 24-72 hours.

### 2.11.1. IL-2 enzyme-linked immunosorbent assay (ELISA)

ELISA is a sensitive and highly specific quantitative assay that detects the presence of a soluble substance with the help of antibodies. A colour reaction provides the read-out. In a sandwich ELISA, an antibody specific to the substance of interest is immobilised on a surface before the sample is applied. Subsequently, a second antibody specific to the substance of interest is applied, which is coupled to an enzyme that catalyses a colour reaction when its substrate is added.

The cell supernatant was analysed for released IL-2 with the Mouse IL-2 ELISA Ready-SET-Go!® kit (eBioscience), according to the kit protocol. An EIA plastic plate was wet-coated with an anti-mouse IL-2 capture antibody in 1x coating buffer provided in the kit. After washing the plate with PBS-Tween and blocking with 1x assay diluent from the kit, the undiluted cell supernatant was transferred to the plate, along with a serial dilution of a mouse IL-2 standard from the kit. Samples were incubated over night at 4 ºC or for two hours at room temperature. After another washing step, an anti-mouse IL-2 detection antibody coupled to biotin was applied and incubated. Another washing step followed, and an avidin-horse radish peroxidase reagent was applied and incubated. Substrate solution was applied and incubated, resulting in a colour reaction, which was stopped with 2 M sulphuric acid. The plate was analysed by measuring absorption at 450 nm.

### 2.11.2. IL-2 stimulation data analysis and presentation

A standard curve was prepared that correlated the concentration of IL-2 standard to absorbance at 450 nm. The standard curve was applied to calculate IL-2 concentrations for the cell supernatant samples. When comparing experiments that were carried out on different days, the overall IL-2 concentrations varied up to 2-4-fold, but the relative trends between conditions did not.

For producing bar diagrams displaying error bars, several (2-4) independent repeats were combined in one graph. Within each experiment, IL-2 concentrations of each condition were typically divided by the IL-2 concentration of the 10 μg/mL KT3

condition, and thereby converted to relative units. This way, the results across several experiments could be displayed in the same graph as mean values with error bars, and relative IL-2 units were listed on the y-axis. To be able to display IL-2 concentration in pg/mL on the y-axis of the combined graph, relative units were then multiplied with the average experimental IL-2 concentration achieved by stimulation with 10 μg/mL KT3. All error bars display the standard error of the mean unless states otherwise. A student's t-test was used to determine whether conditions differed with statistical significance.

Diagrams displaying curves show one representative of 2-4 repeats rather than the average of several repeats. Where suitable, data points were fitted with a binding model by non-linear regression, and an F-test was used to confirm that this model fits the data better than a horizontal line. Goodness of fit was also confirmed visually, and by a high $R^2$ value. Where a horizontal line was the more suitable fit, as was normally the case for negative control conditions (*e.g.* stimulation with isotype control only), the horizontal line fit was displayed rather than the fit with the binding model. Where fitting with neither the nonlinear regression nor the horizontal line was suitable, or fitting was ambiguous and did not meet the quality requirements in terms of goodness of fit, a curve was drawn by connecting the data points rather than fitting them with a model.

The binding model used for nonlinear regression, based on the Hill equation, was:
$Y = \text{Maximum} * X^n/(EC50^n + X^n) + \text{Minimum}$

Where:
Y = [IL-2] in pg/mL
X = [stimulating antibody] in μg/mL
EC50 = X corresponding to ½ $Y_{max}$ in μg/mL
n = Hill slope (a measure of cooperativity, or how "switch-like" a response is)
Maximum = Y at infinite [X] in pg/mL
Minimum = Y for X=0 in pg/mL

To determine whether two curves differed from each other with statistical significance, an F-test was performed for each parameter (EC50, n, maximum, minimum) that may differ between the curves. Identifying which parameter differs rather than merely discriminating that two curves differ gives mechanistic insight. For instance, costimulatory activity of an antibody is defined as lowering the EC50 of the response to a second stimulus.

### 2.12. Surface plasmon resonance-measurements on the BIAcore

For the measurements presented in this thesis, a BIAcore 3000 machine (GE Healthcare) was used. All measurements were undertaken at 37 ºC.

The purity of the ligand was confirmed with SDS-PAGE and size exclusion chromatography. Ligands were immobilised directly on a CM5 sensor chip *via* amine coupling. The chip was activated with 75 mg/mL 1-Ethyl-3-(3-dimethylaminopropyl) carbodiimide hydrochloride and 11.5 mg/mL N-Hydroxysuccinimide mixed in a 1:1 ratio. The ligand was diluted in 10 mM sodium acetate pH 5.0 (GE Healthcare), typically to 5 μg/mL. A small volume of ligand was injected to achieve a low level of ligand immobilisation of ~ 100 response units. The chip was then inactivated with ethanol amine chloride to prevent unspecific binding of the analyte. On a reference chamber of the chip, a negative control ligand was immobilised, such that a control sensorgram could be created to assess the background response. This was subtracted from the sample sensorgrams to achieve background-corrected sensorgrams. It was important to ensure that direct immobilisation did not inactivate the ligand. This was confirmed by assessing the interaction with a known binding partner.

The purity of the analyte was confirmed with SDS-PAGE and size exclusion chromatography. It was buffer-exchange to HBS-azide 0.05 % during gel filtration to match the running buffer used in the BIAcore. It was centrifuged at 1100 rcf for six minutes at 4 ºC to remove any remaining aggregate. Its concentration was determined spectrophotometrically, measuring absorbance at 260 nm. A dilution series was prepared, and samples were pulse-centrifuged to remove any air bubbles.

For equilibrium measurements, the flow rate was set to 20 μL/min. The injection volume was 20 μL. For kinetic measurements, the flow rate was set to 30 μL/min. The injection volume was 60 μL. 360 seconds were allowed for dissociation to occur. Because dissociation of the analyte was not complete, the chip was regenerated between injections. Any bound analyte was eluted with 5 μL 10 mM glycine-HCl, pH 2.5 (GE Healthcare) at 10 μL/min.

**Analysis**

GraphPad Prism was used to analyse equilibrium measurements. Non-linear regression was performed with the "one site –specific binding" model that assumes a 1:1 binding stoichiometry:

$R = R_{max} * [analyte] / (K_D + [analyte])$

where R is the response in relative units measured at equilibrium, $R_{max}$ is maximal binding in response units extrapolated to very high concentrations of the analyte, and $K_D$ is the dissociation constant.

A Scatchard plot was created as well to assess the quality of the data, and to judge whether a 1:1 model is suitable. In a Scatchard plot, the ratio of bound to unbound analyte is plotted against the concentration of bound analyte. A linear relationship indicates that the data is of good quality, and confirms a 1:1 binding stoichiometry. Linear regression was carried out, determining the slope and axes intercepts.

The BIAevaluation software (GE Healthcare) was used to analyse kinetic measurements. The curves for one analyte, representing different analyte concentrations, were overlaid in one graph plotting response against time, and aligned to the start of injection. Association and dissociation rates for all curves were fitted together. If necessary, curves were cleaned for disturbances such as air bubbles by cutting out the corresponding data points. The background response was adjusted to zero. Injection time was adjusted manually. The Langmuir model for a 1:1 binding

stoichiometry was selected for the mathematical fit, which aimed to minimise $Chi^2$ [247].

## 2.13. Antibodies used throughout the thesis

Table 2-1 lists all antibodies that are referred throughout this thesis with their properties.

Table 2-1: Antibodies used in this thesis.

| antibody | antigen | species | subclass | clone | catalog no. | source | comment |
|---|---|---|---|---|---|---|---|
| JJ316 | rat CD28 | mouse | IgG1 | JJ316 | 554992 | BD Biosciences | |
| JJ319 | rat CD28 | mouse | IgG1 | JJ319 | 16-0280-85 | eBioscience UK Ltd | |
| KT3 | mouse CD3ε | rat | IgG2a | KT3 | MCA500EL | Bio-Rad AbD Serotec | |
| HP6091 | human IgG1 (Fc) | mouse | IgG2a | 8c/6-39 | MCA514G | Bio-Rad AbD Serotec | |
| IC-10 | human IgG1 (Fc) | mouse | unknown | IC-10 | n.a. | kind gift from John Young, Compton | |
| GAH | human IgG (L+H) | goat | polyclonal | n.a. | 109-001-003-JIR | Stratech Scientific | |
| DAM | mouse IgG (L+H) | donkey | polyclonal | n.a. | 715-001-003-JIR | Stratech Scientific | |
| MOPC-21 | unknown | mouse | IgG1 | MOPC-21 | M5284 | Sigma-Aldrich Co Ltd | isotype control |
| MOPC-21 | unknown | mouse | IgG1 | MOPC-21 | 400153 | BioLegend® | isotype control |
| HB.96 | human Ia | mouse | IgG1 | HB.96 | n.a. | Human Immunology Unit, Oxford | isotype control |
| OX7 | rat Thy-1 | mouse | IgG1 | OX7 | n.a. | Human Immunology Unit, Oxford | initially used as isotype |
| anti-HC | mouse IgG1 | rat | IgG1 | LO-MG1-13 | MCA1289 | Bio-Rad AbD Serotec | |
| anti-k LC | mouse IgG (kappa LC) | rat | unknown | RMK-12 | 407202 | BioLegend | |

| antibody | antigen | species | subclass | clone | catalog no. | source | comment |
|---|---|---|---|---|---|---|---|
| anti-FcR | mouse CD16/CD32 | rat | IgG2a | clone 93 | 101302 | BioLegend | |
| anti-mCD45 | mouse CD45 (all isoforms) | rat | IgG2b | YW 62.3.20 | n.a. | kind gift from Herman Waldmann, Oxford | Watt et al (1987); Kong et al (1989) |
| clone 2 | human PD1 | mouse | IgG1 | clone 2 | n.a. | Simon Davis, Oxford | |
| clone 19 | human PD1 | humanised | IgG1 | clone 19 | n.a. | Simon Davis, Oxford | |
| clone 10 | human PD1 | humanised | IgG1 | clone 10 | n.a. | Simon Davis, Oxford | |
| hclone 2 | human PD1 | humanised | IgG1 | hclone 2 | n.a. | Simon Davis, Oxford | |
| hclone 19 | human PD1 | humanised | IgG1 | hclone 19 | n.a. | Simon Davis, Oxford | |
| hclone 10 | human PD1 | humanised | IgG1 | hclone 10 | n.a. | Simon Davis, Oxford | |
| JJ316 | rat CD28 | mouse | IgG1 | JJ316 | Ab00284-1.1 | Absolute Antibody | |
| Fc-silent™ | rat CD28 | mouse | IgG1 | JJ316 | Ab00284-1.4 | Absolute Antibody | no longer binds to CD16/CD32 |
| extJJ316 +50 | rat CD28 | mouse | IgG1 | JJ316 | Ab00284-c224 | Absolute Antibody | extended hinge |

* found to cross-bind to mouse Thy-1 and thus no longer used as a mIgG1 isotype control with mouse cells

# Chapter 3 The mitogenic potential of JJ316 is not explained by affinity

## 3.1. Introduction

A number of hypotheses have been suggested to explain the mechanism underlying superagonistic signalling. These include more efficient receptor crosslinking or aggregation by the superagonist, more efficient steric exclusion of the phosphatase CD45, stabilising a more active receptor conformation, preferentially binding to a subgroup of functionally distinct, more active receptors, and affecting the ability of downstream molecules such as kinases to bind [131, 132, 228, 229, 248]. This thesis aims to contribute to elucidating the mechanism that determines superagonism, examining the whether one of the suggested hypotheses, of a combination thereof, or a thus far undescribed contribution, hold true.

The examples of the anti-rat CD28 antibodies JJ316, a superagonist, and JJ319, a conventional antibody are chosen, the model where antibody superagonism was first discovered [228]. In addition to mapping their epitopes, JJ316 and JJ319 have been functionally characterised; their differential ability to activate both T-cell hybridoma lines and primary T-cells is well-documented [228]. However, our knowledge of their CD28 binding affinity and kinetics is limited. To date, only somewhat semi-quantitative data exist that compare avidities of the antibodies for cell-bound CD28 [3]. These data are lacking off-rate measurements, and are thus unable to conclusively compare binding strength. In disentangling how superagonists work it is important to characterise the thermodynamic properties of both antibodies, because it may impose constraints on the mechanism. Based on the evidence available to date one could propose that JJ316 is a more potent antibody simply because of an increased affinity for CD28.

This chapter examines the binding kinetics and affinity of the two antibodies with two different methods, addressing the hypothesis that affinity differences contribute to their differences in potency. First, multivalent binding avidities for cell surface-bound CD28 were quantified in a cell-binding assay. Second, monovalent binding affinities for soluble CD28 protein were measured in solution, making use of the BIAcore.

## 3.2. Materials and methods

### 3.2.1. Measuring whole antibody binding kinetics to cell-bound receptors

A flow cytometry-based analysis of antibody kinetics binding to cell-bound receptors was performed, as in general methods (see Section 2.2) with the following changes:

No labelled secondary antibody was used. Instead, the primary antibodies JJ316, JJ319, clone 10 and clone 19 were directly conjugated to Alexa647® and used to stain rmCD28-expressing BW5147 cells (see Figure 4-1, page 100). To determine the association kinetics, incubation time with the antibody at 37 ºC was varied, followed by one wash in 3 mL PBS-azide and fixation. To determine dissociation kinetics, the incubation time was constant at 30 minutes, 4 ºC, followed by one quick wash as above, and one long wash at 37 ºC for varying amounts of time. As a reference, anti-PD1 antibodies with known affinity and kinetics were included. Those were used to stain PDCD28-expressing BW5147 cells (see Figure 5-5, page 135).

The FlowJo software was used to calculate mean fluorescence intensity (MFI) values of each sample by determining the geometric mean of the fluorescence intensity distribution. MFI values were plotted and fitted with binding models in GraphPad Prism. The F-test was used to determine if two curves differed significantly. On-rate and off-rate values were derived from the fitted models.

The following model was fitted to the dissociation curves:

$$MFI = (MFI_0 - NS) * \exp(-k_{off} * time) + NS$$

where $MFI_0$ is the MFI at 0 minutes dissociation, NS is non-specific binding at infinite times, and $k_{off}$ ist the dissociation rate constant.

The following model was fitted to the association curves:

$MFI = MFI_{max} * (1-exp(-1*(k_{on}*L+k_{off})*time))$

where the $k_{off}$ values were input from the dissociation measurements as determined by flow cytometry, L is the antibody concentration (in M) and $MFI_{max}$ is the maximal MFI value.

## 3.3. Results

### 3.3.1. JJ319 and JJ316 have similarly low off-rates when bound to rmCD28 expressed on the cell surface

Because no information on the dissociation kinetics of JJ316 and JJ319 was available to date, it was important to assess whether there were large differences between the off-rates of the two antibodies. A flow-cytometry based approach was chosen to quantify the binding of fluorescently-labelled JJ316 or JJ319 antibody to rmCD28[1]-expressing BW5147 cells. Interactions with known soluble affinities as determined by BIAcore were included as controls: the binding of anti-human PD1 antibodies clone 19 and clone 10 to human PD1-expressing BW5147 cells was assessed in parallel (Figure 3-1A). Clone 10 has an off-rate that is two orders of magnitude higher than that of clone 19 (Table 3-1), and this difference was highly significant ($p<0.0001$) in the flow cytometry analysis used in this thesis, validating the approach (Table 3-2). No significant differences in off-rate were detected for JJ316 *versus* JJ319 in the flow cytometry approach, and both antibodies had off-rates similar to that of clone 19 (Table 3-2). The off-rates for both antibodies were small, confirming good and stable binding to cell-expressed rat CD28.

[1] rmCD28 is a chimeric rat - mouse CD28 protein; see Figure 4-1.

### 3.3.2. JJ319 binds to rmCD28 expressed on the cell surface with a higher on-rate than does JJ316[2]

Using the same approach, the on-rates for bivalent JJ316, JJ319 and the anti-PD1 control antibodies binding to cell-bound receptors were quantified (Figure 3-1B). As previously shown in relative terms [228], JJ316 binds cell-bound rat CD28 with a smaller on-rate. Quantified here, the difference is as large as an order of magnitude, and highly significant (p=0.0006; Table 4-1).

Table 3-1: Known soluble affinities and kinetics of control antibodies, as measured by BIAcore*

| | Clone 19/hPD1 | Clone 10/hPD1 |
|---|---|---|
| $k_{off}$ (min-1) | 7.02E-02 | 1.30E+01 |
| $k_{on}$ ($M^{-1}$ $min^{-1}$) | 1.93E+06 | 1.61E+06 |
| $K_D$ (M) | 3.63E-08 | 8.03E-06 |

* measured by Sara Morgan, Davis group, University of Oxford [249]

Table 3-2: Apparent association and dissociation rates of antibodies binding to cell-bound receptors

| | JJ316/ rCD28 | JJ319/ rCD28 | Clone 19/ hPD1 | Clone 10/ hPD1 |
|---|---|---|---|---|
| Apparent $k_{off}$ (min-1) | 3.67E-02* | 2.84E-02 | 3.93E-02 | 1.13E-01** |
| Apparent $k_{on}$ ($M^{-1}$ $min^{-}$ | 3.30E+05*** | 2.90E+06 | 8.29E+06 | 6.83E+06 |

* not different from JJ319 p=0.3578 (F-test)
** different from clone 19 p<0.0001 (F-test)
*** different from JJ319 p=0.0006 (F-test)

### 3.3.3. Surface plasmon resonance-based affinity measurements

No significant differences were detected between the off-rates of JJ316 and JJ319 with the flow-cytometry approach. The approach is capable of detecting large differences, since it discriminated between the off-rates of clone 10 and clone 19. Small differences may exist, however, that may contribute to the larger potency of JJ316 but that the method is not sensitive enough to detect. JJ316 and JJ319 likely interact bivalently with

[2] Confirming published results .

the cell-expressed CD28 homodimer, and avidity effects may mask small differences in affinity. Therefore, it was important to validate the results with a more sensitive approach, and to study monovalent interactions to remove avidity effects.

**Principle**

Surface plasmon resonance is a label-free method to detect and quantify protein-protein interactions with very high sensitivity. It is possible to measure the affinity, kinetics, and enthalpy of an interaction in real time. One binding partner, which is referred to as the the ligand, is immobilised on a gold-coated surface at the bottom of a flow chamber. The other binding partner, called the analyte, is injected into the flow chamber, under a constant flow of buffer. Optics are used to detect binding of the analyte to the ligand. Accumulation of protein changes the refractive index of the surface, which is quantified by the phenomenon of surface plasmon resonance. When light hits the surface at the angle of total internal reflection, some energy is absorbed by the electrons in the gold layer, inducing the formation of an evanescent wave that extends a few hundred nanometres on either side of the interface. The refractive index of the surface, and thus the amount of immobilised protein, affects the angle of the reflected light, and changes in this angle are measured by the detector. The response, reflecting the refractive index change, which in turn reflects the mass change due to binding in this case, is expressed in relative units called response units. A sensorgram is created plotting response against time. Following the injection of analyte, the response increases as the analyte binds to the ligand; this is referred to as the association phase. When the analyte starts to detach, the response drops, giving the dissociation phase.

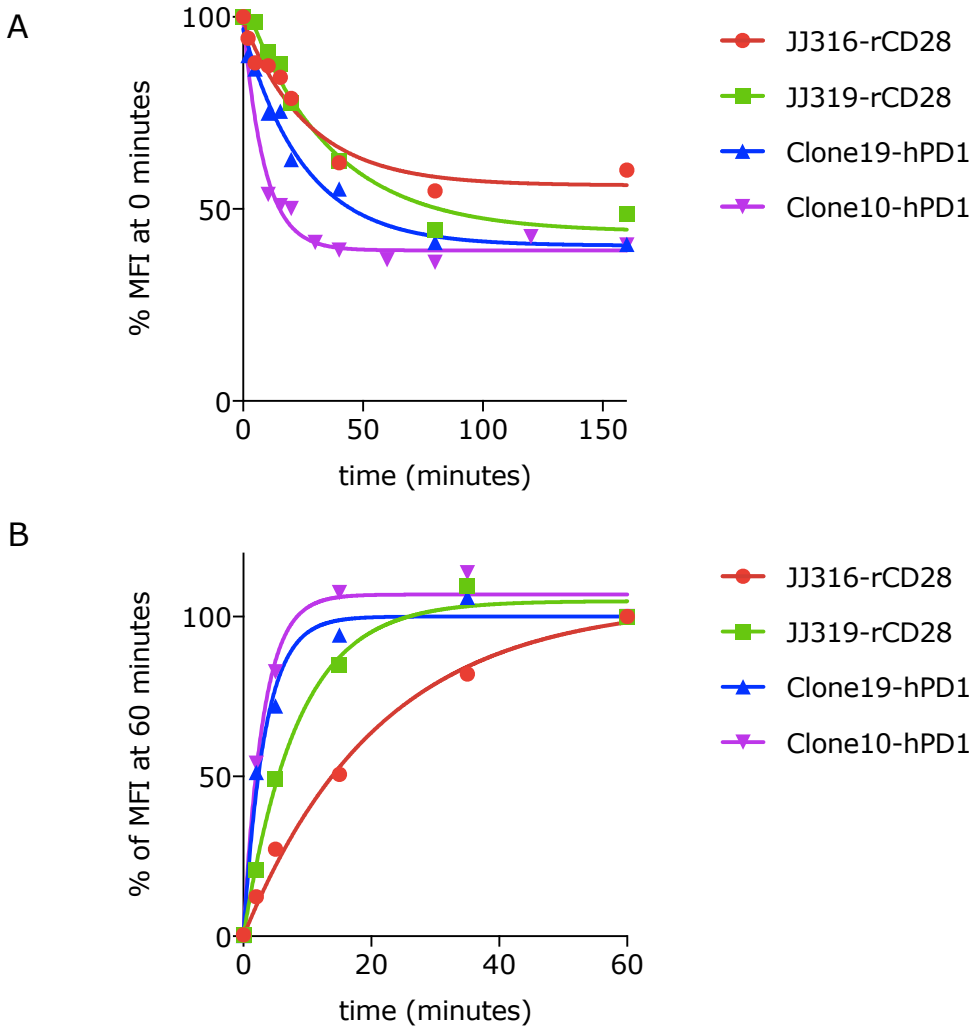



Figure 3-1: Association and dissociation curves of whole antibodies binding to cell-bound receptors. A flow cytometry-based approach was carried out to quantify binding of fluorescently labelled antibodies to transmembrane receptors stably expressed in cells. Measurements were carried out at 37 ºC. Data points are averages of three independent repeats. MFI= mean fluorescence intensity. **A** Incubation time in the wash step after antibody binding was varied to quantify dissociation. Curves were fit with a dissociation model. **B** Incubation time with the antibodies was varied to quantify association. Curves were fit with an association model**.

*MFI = $(MFI_0 - NS) * \exp(-k_{off}*time) + NS$; where NS is non-specific binding at infinite times
**MFI = $MFI_{max} * (1-\exp(-1*(k_{on}*L+k_{off})*time))$ where L is the antibody concentration (in M)

**Affinity and kinetic measurements**

The affinity of a protein-protein interaction is determined with an equilibrium measurement. The analyte is injected at different concentrations over a range of several orders of magnitude. Response units at equilibrium are plotted against concentration, and a mathematical fit with a binding model is employed to calculate the dissociation constant. Care needs to be taken to ensure that the model is suitable for the data. Any statements referring to affinity or real rate constants based on quantitative measurements on the BIAcore are only valid for interactions with a 1:1 binding stoichiometry. Equilibrium measurements are often not suitable for interactions with a very low off-rate because equilibrium is not reached within an appropriate time frame. For such interactions, kinetic measurements can be undertaken instead. Here, the rate of association and dissociation is measured to derive the dissociation constant. However, even more care needs to be taken to prevent artefacts and to ensure that the fitting model is suitable. Limitations include an underestimation of the association rate where the rate of transport of analyte to the ligand binding site is lower than the association rate, and an underestimation of the dissociation rate when re-binding of analyte occurs. Both can be improved by immobilising a minimal amount of ligand, and by increasing the flow rate in the flow chamber [250].

### 3.3.4. JJ316 and JJ319 soluble binding affinities and kinetics are identical

Affinities and kinetics of JJ316 and JJ319 binding to rat CD28 were quantified using surface plasmon resonance as implemented by BIAcore. To determine affinities rather than avidities, a 1:1 binding stoichiometry was required. Fab fragments of JJ316 and JJ319 were therefore produced, which interact monovalently with the CD28 homodimer.

**Production of a soluble rCD28-mFc-6His fusion protein**

For immobilisation on the BIAcore chip, the rat CD28 extracellular domain was expressed as a fusion protein with the mouse IgG1 Fc region and a hexahistidine tag (Figure 3-2). The construct was designed in the example of a soluble human CD28

construct successfully expressed for crystallography [251]. To ensure the correct formation of the disulphide bond in the stalk region of the extracellular domain, which is important for the formation of the homodimer and thus for protein stability and folding, the entire sequence of the extracellular domain was included, not omitting any amino acids that precede the transmembrane domain. The native signal peptide was included to ensure secretion of the protein. Primers were designed that introduce a XbaI restriction site ay the 5' end preceding the start codon, and a SmaI restriction site at the 3' end following the codon corresponding to the final amino acid of the extracellular domain; a stop codon was not included. The XbaI and SmaI restriction sites were used to insert the sequence into the pEE14 expression vector (see Figure 2-2; Lonza Biologicals). The pEE14 vector had been modified[3] to encode a mouse IgG1 Fc region followed by a hexahistidine tag and a stop codon after the SmaI restriction site (see Figure 2-2), such that the soluble CD28 protein would be expressed as a fusion protein with mouse Fc and hexahistidine to facilitate purification (Figure 3-2). A mammalian expression system was chosen to ensure correct folding and glycosylation of the soluble CD28 construct, which is essential for studying and quantifying its interaction with the antibodies. A stable transfection system was chosen because, albeit it is more laborious and time-consuming, better yields can be achieved and transfected the cell line can be stored long-term should future experiments require freshly purified protein.

A Chinese hamster ovary (CHO)-K1 cell line was stably transfected with the expression vector for protein production. A glutamine synthetase selection system was used for stable transfection.

[3] Performed by Heather Brouwer, Davis laboratory, University of Oxford.

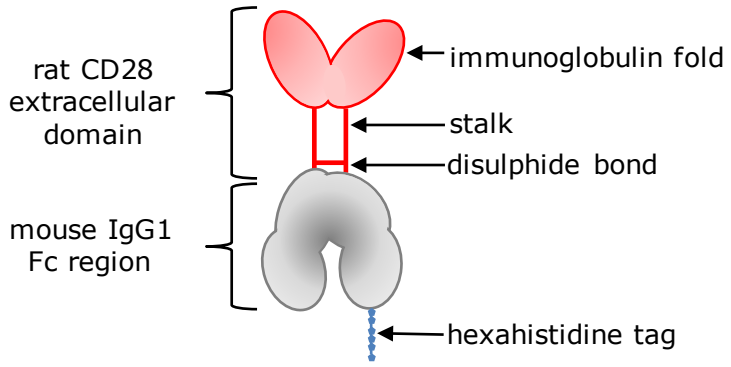



Figure 3-2: Design of a His-tagged soluble rat CD28 - mouse Fc fusion protein.

pEE14 encodes a glutamine synthetase minigene that provides transfected cells with an advantage when glutamine is limited. To select for transfected cells, the CHO-K1 cells were cultured in glutamine-free medium and serum, and L-methionine sulfoximine (MSX) was added, a chemical that inhibits the cellular glutamine synthetase. A concentration of MSX was chosen that inhibits the proliferation of untransfected cells but allows transfected cells, which express larger amounts of glutamine synthetase, to proliferate. Because the ideal MSX concentration can vary, three different concentrations were chosen; 20, 25 and 30 μg/mL MSX. Single cells were seeded in 288 repeats per MSX concentration; as a negative control untransfected cells were seeded in 96 repeats per MSX concentration. The presence of colonies, corresponding to a single clone, was assessed after four weeks. Out of the three times 288 repeats, colonies were observed for 138 clones. For the untransfected cells that served as a negative control, colonies were observed for 13 out of three times 96 clones. A dot blot was performed to characterise the clones further and to assess how efficiently they produce the CD28 fusion protein. 90 transfected clones and 3 untransfected clones were included, along with purified human CD28-mFc-His protein[4] as a positive control. The blot was probed with an anti-mouse Fc antibody that was conjugated with horse radish peroxidase (Sigma-Aldrich, A1063). Nine transfected clones expressed rCD28-mFc-His, while no signal was observed for the untransfected clones (Figure 3-3).

[4] Purified by Edward Evans, Davis laboratory, University of Oxford; as used in [251]

Table 3-3: Properties of transfected CHO-K1 clones that produce rCD28-mFc-His

| clone | dot blot signal (0-4) | colony size (% of well area) | [MSX] in µg/mL | number of colonies |
|---|---|---|---|---|
| A7 | 2 | 5 % | 25 | single |
| A9 | 1 | 15 % | 25 | single |
| B4* | 1 | 15 % | 25 | single |
| B6* | 2 | 7 % | 25 | single |
| E6 | 0.5 | 5 % | 30 | multiple |
| E9 | 4 | 15 % | 30 | single |
| F12* | 3 | 15 % | 30 | single |
| G1 | 4 | 50 % | 30 | multiple |
| G10 | 0.5 | 80 % | 30 | multiple |

* selected for further characterisation

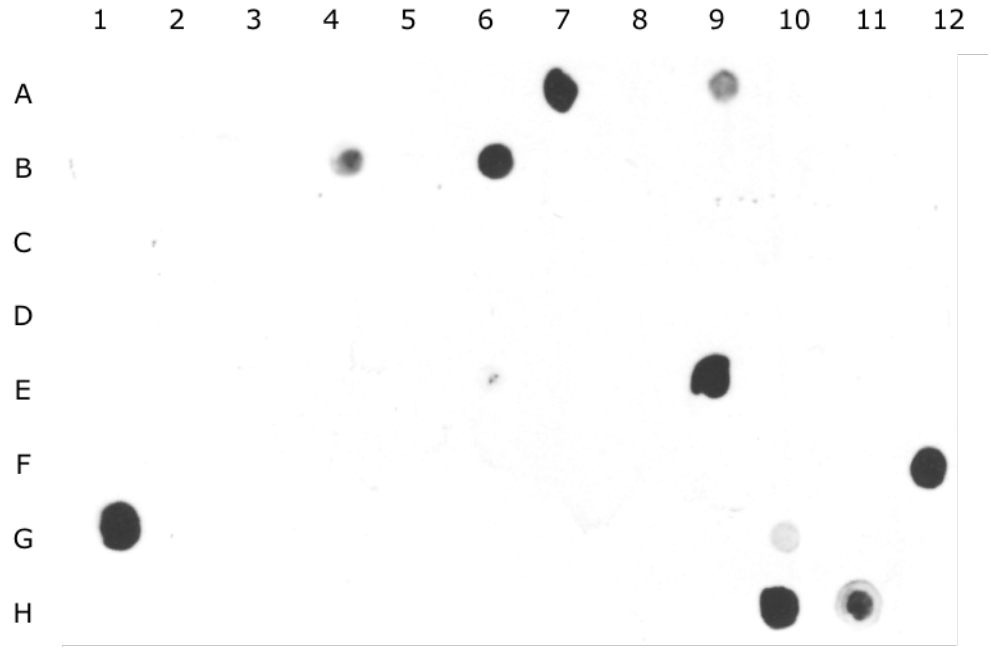



Figure 3-3: Transfected CHO-K1 clones produce rCD28-mFc-His. The cell culture supernatant of colonies corresponding to single CH-K1 clones was blotted on a nitrocellulose membrane. Clones A1-H6 were transfected with rCD28-mFcHis in a pEE14 expression vector. Clones H7-H9 were untransfected. H10 corresponds to 5 µg/mL purified hCD28-mFcHis, H11 to 2.5 and H12 to 1 µg/mL. The membrane was probed with an anti-mouse Fc antibody that was conjugated with horse radish peroxidase (Sigma-Aldrich, A1063) and incubated with Pierce ECL Western blotting substrate. Luminescence was detected on an x-ray film.

Three clones were selected for further characterisation based on high expression of rCD28-mFc-His, and a large colony size indicating fast proliferation. Clones that were potentially contaminated with a second clone were excluded. Table 3-3 summarises the properties of the nine expressing clones. Clones B4, B6, and F12 were expanded and their supernatants were examined by Western blot to confirm that the expressed protein is of the correct mass (Figure 3-4). Purified hCD28-mFc-His[5] was included as a positive control. Expression was confirmed for all three clones. A band at ~ 150 kDa was observed for all three clones as well as for the positive control under non-reducing conditions (Figure 3-4), which likely corresponds to the glycosylated CD28 homodimer. This is indicative of good protein quality and correct disulphide bond formation, as misfolded protein would not likely form a dimer and would not likely be expressed in large amounts. A weaker band between 76 and 150 kDa (Figure 3-4) likely corresponds to the unglycosylated CD28 homodimer. Under reducing conditions, bands were observed at ~ 50 kDa (Figure 3-4), corresponding to the monomeric form of CD28. Bands that were observed at ~ 20 kDa for the clones but not the positive control (Figure 3-4) likely correspond to contaminant protein present in the cell culture supernatant.

Clone B4 was chosen for protein production because it proliferated quickly and expressed a good amount of protein. A 500 mL culture was inoculated. The chimeric protein was purified from the cell culture supernatant by affinity chromatography, using Ni-NTA-coupled sepharaose that binds to the hexahistidine-tagged protein, and the protein was eluted with imidazole[6]. Elution fractions were characterised by SDS-PAGE (data not shown)[6].

[5] Purified by Edward Evans, Davis laboratory, University of Oxford; as used in [251]
[6] Performed by Shirley Yang, Princeton University, under the author's supervision.

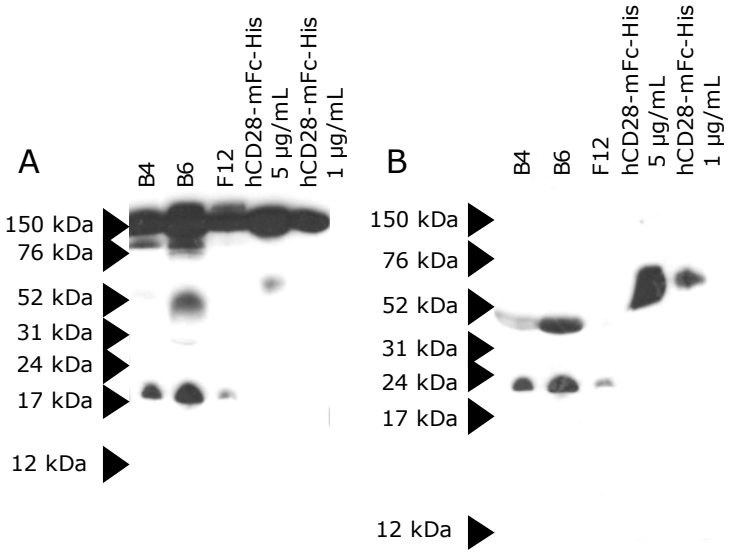



Figure 3-4: Western blot confirms expression of rCD28-mFc-His. Samples were separated on a 12 % acrylamide gel. 7.5 µL cell culture supernatant was loaded, under either **A** non-reducing or **B** reducing conditions. The protein was transferred onto a nitrocellulose membrane and probed with an HRP-conjugated anti-mouse Fc antibody (Sigma-Aldrich, A1063) and incubated with Pierce ECL Western blotting substrate. Luminescence was detected on an x-ray film.

The fractions were pooled and subjected to size exclusion chromatography[7]. A single peak indicated pure protein free from aggregates (Figure 3-5). Purity of the size exclusion chromatography fractions was confirmed by SDS-PAGE (Figure 3-6).[7] The size shift from non-reducing to reducing conditions conforms with the homodimeric nature of rat CD28. A size of ~ 50 kDa as seen in the reducing gel is as expected for a glycosylated CD28 monomer. Weaker bands on top and below of the main bands conform with different glycosylation forms. Faint bands corresponding to the size on the non-reducing gel indicate that reduction of the disulphide bond was not complete.

[7] Performed by Shirley Yang, Princeton University, under the author's supervision.

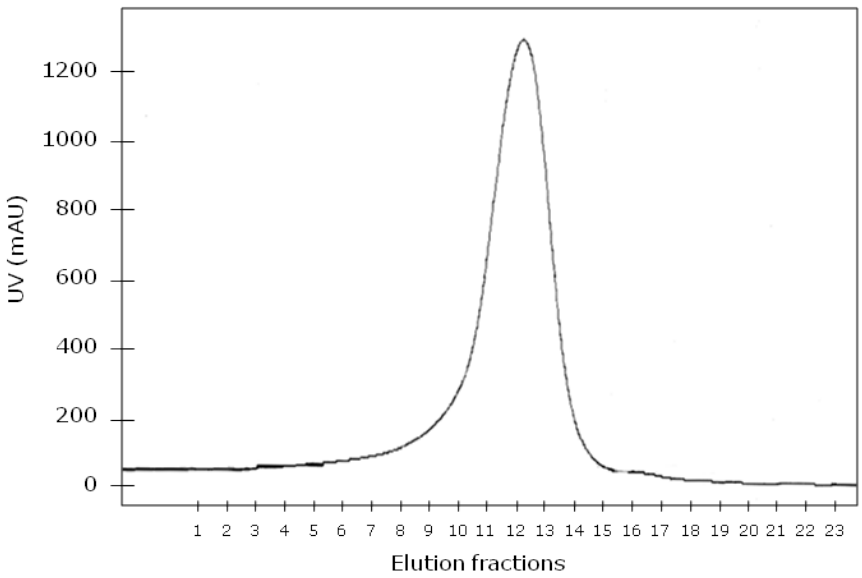



Figure 3-5: Purification of soluble rCD28-mFc-His with size exclusion chromatography[8]. An Äkta FPLC system was used, fitted with a Sepharaose 200 column of size 10/300. The protein was eluted with HBS-azide 0.05 %, and 500 µL fractions were collected.

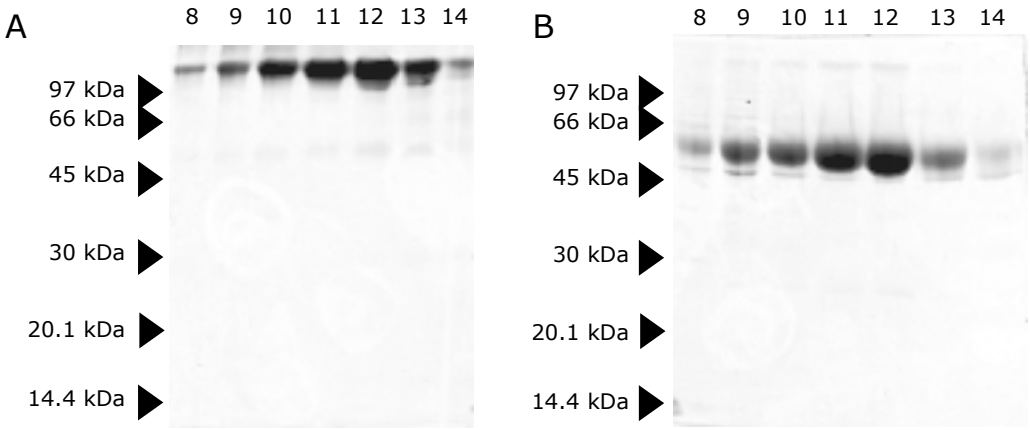



Figure 3-6: SDS-PAGE of purified soluble rCD28-mFc-His[8]. Samples were separated on a 12 % acrylamide gel. 10 µL of each FPLC elution fraction was loaded, under either **A** non-reducing or **B** reducing conditions.

[8] Performed by Shirley Yang, Princeton University, under the author's supervision.

Fractions 9-13 were pooled and stored at 4 ºC until the BIAcore measurements were performed. ~ 3 mg protein was purified from the 500 mL culture.

**Production of JJ316 and JJ319 Fab fragments**

JJ316 and JJ319 Fab fragments were generated by digesting the antibodies with papain. The reaction was first optimised with YW62.3.20, a rat IgG2b antibody that was purified from a large-scale hybridoma culture in large quantities (see Section 6.3.4). In brief, the antibody was incubated with sepharaose-immobilised papain enzyme (Sigma-Aldrich, P4406). To separate Fab fragments from Fc fragments, the digest was purified with sepharaose-immobilised protein G. Flow-through, wash and elution fractions were characterised by SDS-PAGE. The Fab fragments were present exclusively in the elution fractions whereas the Fc fragments were present exclusively in the flow-through and wash, resulting in very clear separation and indicating that protein G has an affinity for the Fab rather than the Fc fragments. It was necessary to adapt the protocol for the mouse IgG1 antibodies JJ316 and JJ319 because smaller quantities of these commercial antibodies were available, and because there may be species or antibody subclass-specific differences that require somewhat different experimental conditions. A test digest using 250 μg JJ316 antibody as the starting material was carried out under the conditions optimised for YW62.3.20. Separation of Fab and Fc fragments was very clear; pure Fab fragments were present in the protein G elution (data not shown). The yield of purified Fab, however, was very poor: less than 10 μg pure Fab was recovered (fractions 8-12, Figure 3-7), and size exclusion chromatography of the protein G elution (Figure 3-7) followed by SDS-PAGE analysis (data not shown) indicated that a large part of the starting material was degraded (fractions 18-22) while another part remained undigested (fractions 1-6). To prevent degradation, the reaction time was shortened from 14 hours to 8 hours and to improve the reaction efficiency, the reaction volume was decreased from 2 mL to 0.5 mL while doubling the amount of starting material to 500 μg.

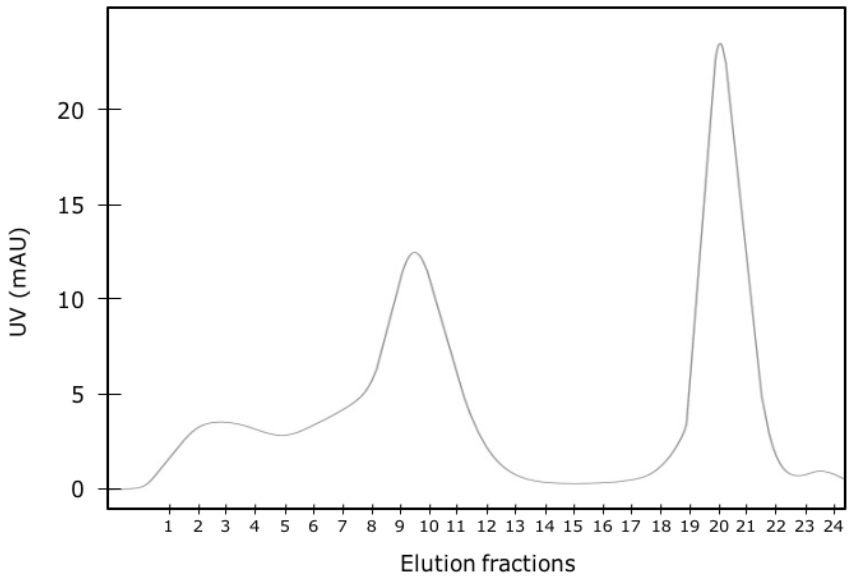



Figure 3-7: Characterisation of the Fab-containing protein G elution for the JJ316 papain test digest with size exclusion chromatography. An Äkta FPLC system was used fitted with a sepharaose 75 column of size 10/300. The protein was eluted with HBS-azide 0.05 % and 500 µL fractions were collected.

JJ316 and JJ319 were therefore digested with papain using the adapted protocol. The yield could be improved: only a very small amount of starting material remained undigested or was degraded (Figure 3-9, Figure 3-11). 122 µg JJ316-Fab and 72 µg JJ319-Fab were purified from 500 µg whole antibody. The Fab fragments were purified using protein G affinity chromatography. Flow-through, wash and elution fractions were analysed by SDS-PAGE (Figure 3-9, Figure 3-11). The double bands at ~ 25 kDa under reducing conditions that were observed for the pooled elution fractions are indicative of Fab fragments, while the bands at ~ 30 kDa present only in the flow-through and wash under both non-reducing and reducing conditions are characteristic for Fc fragments (Figure 3-9, Figure 3-11). This indicated that the separation of Fab from Fc was very successful, and that pure Fab was found in the protein G elution. The pooled elution fractions were subjected to size exclusion chromatography (Figure 3-8, Figure 3-10). Purity of gel filtration fractions was confirmed by SDS-PAGE (Figure 3-9, Figure 3-11). For JJ316-Fab as well as for JJ319-Fab, fractions 7-12 were

pooled and stored at -20 ºC for use in the binding assay, as they showed a single peak indicative of pure unaggregated protein (Figure 3-8, Figure 3-10). Fractions 3-6 likely correspond to aggregated protein, and fractions 18-21 likely correspond to degraded protein (Figure 3-8, Figure 3-10).

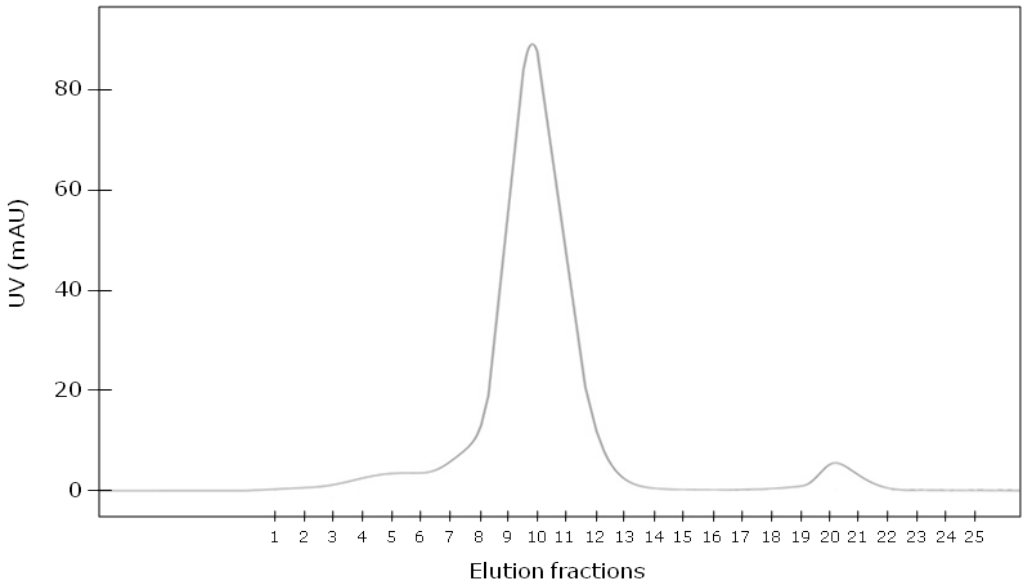



Figure 3-8: Purification of JJ316 Fab fragments with size exclusion chromatography. An Äkta FPLC system was used fitted with a sepharaose 75 column of size 10/300. The protein was eluted with HBS-azide 0.05 % and 500 µL fractions were collected

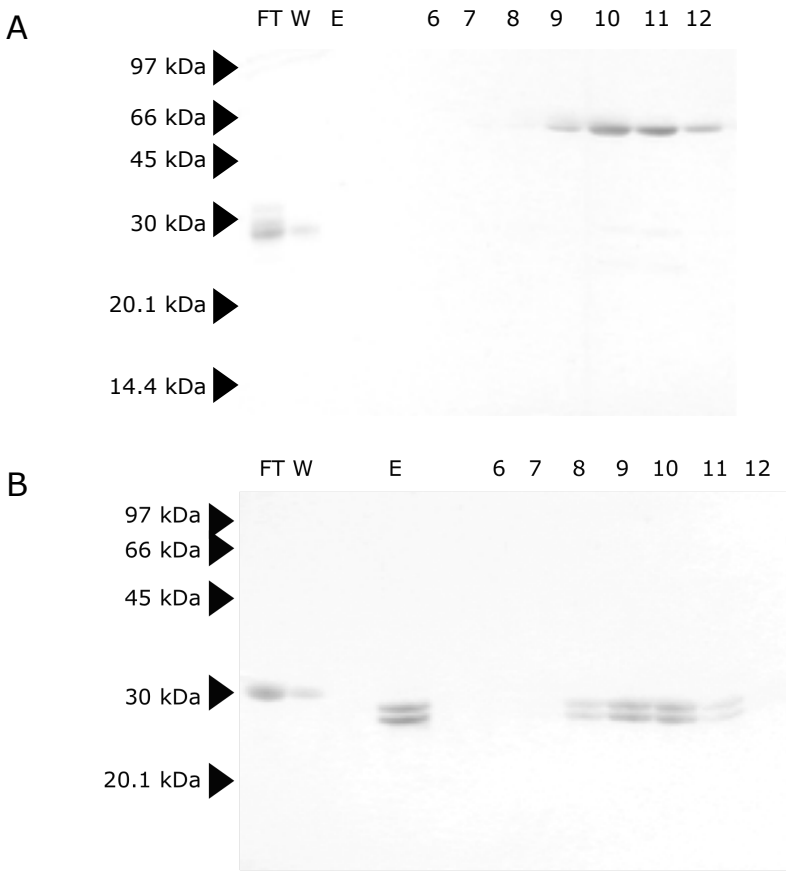



Figure 3-9: SDS-PAGE of JJ316 Fab fragments. FT = Protein G flow-through, W = Protein G wash, E = pooled Protein G elution fractions, 6-12 = FPLC fractions. Samples were separated on a 12 % acrylamide gel. 7.5 μL of each sample was loaded, under either **A** non-reducing or **B** reducing conditions.

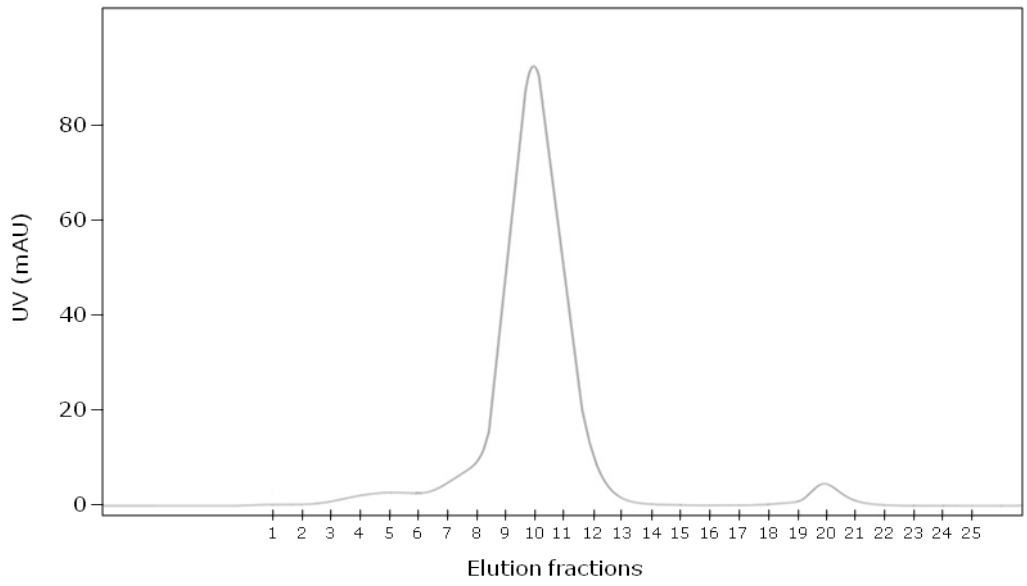



Figure 3-10: Purification of JJ319 Fab fragments with size exclusion chromatography. An Äkta FPLC system was used fitted with a sepharaose 75 column of size 10/300. The protein was eluted with HBS-azide 0.05 % and 500 μL fractions were collected

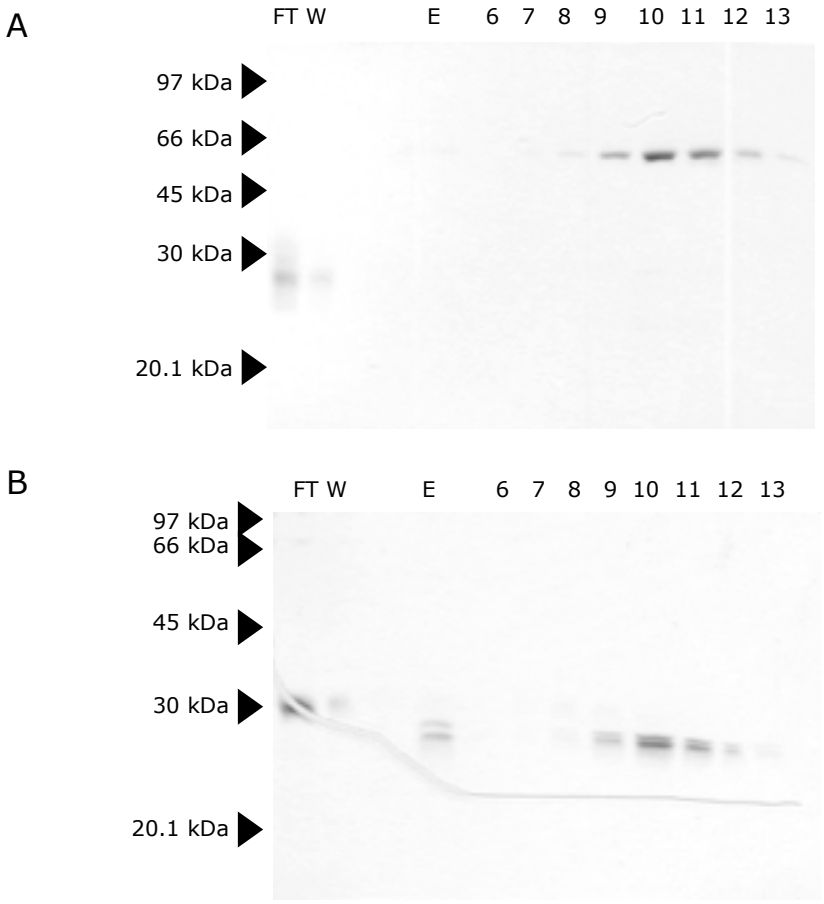



Figure 3-11: SDS-PAGE of JJ319 Fab fragments. FT = Protein G flow-through, W = Protein G wash, E = pooled Protein G elution fractions, 6-13 = FPLC fractions. Samples were separated on a 12 % acrylamide gel. 7.5 μL of each sample was loaded, under either **A** non-reducing or **B** reducing conditions.

**Confirming functionality of rat CD28 ligand with B7-1 analyte**[9]

To test the quality of the immobilised CD28 ligand, its interaction with a native ligand was measured. Soluble mouse B7-1 protein was obtained from frozen stock[10] and subjected to gel filtration to remove any aggregate (data not shown). An equilibrium affinity measurement was carried out. Mouse B7-1 was injected into the flow chamber at increasing concentrations, allowing it to bind to homodimeric rat CD28, which was

[9] Assistance from Jiandong Huo, Davis laboratory, University of Oxford.
[10] Cloned and purified from transiently transfected HEK293T cells by Andrea Iaboni, Davis laboratory, University of Oxford.

directly immobilised on the BIAcore chip, until saturation was reached. The dissociation constant $K_D$ of 6.3 μM measured in this way (Figure 3-12) was in good agreement with published data [252]. The relatively fast kinetics that were observed are typical of the interaction with a native ligand, indicating that the immobilised CD28 was correctly folded and functional.

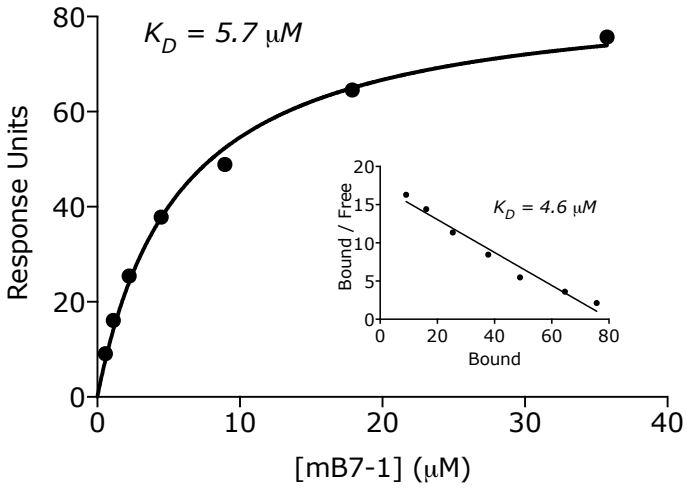



Figure 3-12: Equilibrium measurement of mouse B7-1 3D affinity for rat CD28 at 37 ºC (BIAcore). One out of two repeats is displayed. Nonlinear regression analysis with a 1:1 Langmuir binding model as well as a Scatchard plot (inlay) are shown. The derived $K_D$ values are displayed.

Table 3-4: mouse B7-1 affinity for rat CD28 at equilibrium at 37ºC

| | Scatchard $K_D$ (M) | nonlinear fit $K_D$ (M) | nonlinear fit $R^2$ |
|---|---|---|---|
| Repeat 1 | 4.64E-03 | 5.71E-03 | 0.9938 |
| Repeat 2 | 5.71E-03 | 6.93E-03 | 0.9988 |
| Average | 5.2E-03 | 6.3E-03 | |

**Kinetics-based measurement of solution affinities for JJ316 and JJ319 interacting with rCD28 monovalently**[11]

Because of the relatively low off-rates of the Fab fragments, initial binding did not reach saturation, meaning that an equilibrium affinity measurement was not possible (data not shown). Instead, a kinetics-based measurement of the affinity was performed at 37 ºC. JJ316 and JJ319 Fab fragments were injected into the flow chamber at increasing concentrations, allowing them to bind homodimeric rat CD28 immobilised on the BIAcore chip. The surface was regenerated at low pH in between injections to elute non-covalently bound Fab fragments. A reference flow chamber was included that was functionalised with IgG to determine the background response. JJ316 and JJ319 binding curves were created by subtracting the reference sensorgram from the JJ316 and JJ319 sensorgrams. A 1:1 Langmuir binding model was fitted to the data to determine association and dissociation rates for JJ316 (Figure 3-13) and JJ319 (Figure 3-14). Affinities were calculated in terms of the dissociation constant, $K_D$, which is defined as the quotient of dissociation rate constant ($k_{off}$) and association rate constant ($k_{on}$) (Table 3-5). The goodness of fit was judged with a $Chi^2$ model, which was relatively high for both measurements, indicating that the fit was not perfect (Table 3-5).

Soluble affinities measured for JJ316 and JJ319 were remarkably similar, with $K_D$ values of $9.61^{-8}$ and $9.41^{-8}$ M, respectively (Table 3-5). These measurements confirm that both antibodies bind rat CD28 with similarly high affinity, and with similar kinetics.

Table 3-5: Kinetic measurements of JJ316 and JJ319 soluble 1:1 affinity.

| | $k_{on}$ ($M^{-1}$ $s^{-1}$) | $k_{off}$ ($s^{-1}$) | $K_D$ (M) | $Chi^2$ |
|---|---|---|---|---|
| JJ316 | | | | |
| Repeat 1 | 2.83E+04 | 3.14E-03 | 1.11E-07 | 18.6 |
| Repeat 2 | 3.50E+04 | 2.84E-03 | 8.12E-08 | 18.6 |
| Average | 3.17E+04 | 2.99E-03 | 9.61E-08 | |

[11] Assistance from Jiandong Huo, Davis laboratory, University of Oxford.

| | $k_{on}$ ($M^{-1}$ $s^{-1}$) | $k_{off}$ ($s^{-1}$) | $K_D$ (M) | $Chi^2$ |
|---|---|---|---|---|
| JJ319 | | | | |
| Repeat 1 | 3.61E+04 | 3.21E-03 | 8.91E-08 | 3.91 |
| Repeat 2 | 3.39E+04 | 3.36E-03 | 9.90E-08 | 5.49 |
| Average | 3.50E+04 | 3.29E-03 | 9.41E-08 | |

### 3.3.5. Comparing BIAcore to flow-cytometry measurements

Finally, it was of interest to compare the apparent binding rates of the antibodies measured in the flow-cytometry approach to the binding rates measured by BIAcore. Because PD1 is monomeric in the plasma membrane, the interactions with clone 19 and clone 10 as assessed by flow-cytometry are of a monovalent nature. Off-rate values for clone 19 were similar in absolute terms between the two approaches, whereas the off-rate for clone 10 was largely underestimated by flow-cytometry (Table 3-6). JJ316 and JJ319 had off-rates one order of magnitude smaller for the interaction with cell-bound receptors *versus* the monovalent interaction in solution, indicating that both antibodies were able to bind bivalently (Table 3-6). The differences in on-rate between JJ316 and JJ319 are only apparent when measuring bivalent binding in the physiological context with the target receptor expressed on the cell surface; JJ316 and JJ319 showed identical on-rates when binding rat CD28 monovalently on the BIAcore chip (Table 3-6). This highlights the advantage of assessing binding to the receptor *in situ* in addition to measurements with purified proteins on the BIAcore: the flow cytometry approach analyses binding as it occurs under the experimental conditions when the cellular response to the antibodies is studied, as done in Chapters 4, 5, and 6.

Table 3-6: Comparing binding rates measured with BIAcore and flow cytometry.

| Affinities and binding rates as determined by BIAcore | | | | |
|---|---|---|---|---|
| | JJ316/ rCD28 | JJ319/ rCD28 | Clone 19/ hPD1* | Clone 10/ hPD1* |
| $k_{off}$ (min-1) | 1.79E-01 | 1.97E-01 | 7.02E-02 | 1.30E+01 |
| $k_{on}$ ($M^{-1}$ $min^{-1}$) | 1.90E+06 | 2.10E+06 | 1.93E+06 | 1.61E+06 |
| $K_D$ (M) | 9.61E-08 | 9.41E-08 | 3.63E-08 | 8.03E-06 |
| Apparent binding rates of antibodies interacting with cell-bound receptors | | | | |
| | JJ316/ rCD28 | JJ319/ rCD28 | Clone 19/ hPD1 | Clone 10/ hPD1 |
| Apparent $k_{off}$ (min-1) | 3.67E-02 | 2.84E-02 | 3.93E-02 | 1.13E-01 |
| Apparent $_{on}$ ($M^{-1}$ $min^{-1}$) | 3.30E+05 | 2.90E+06 | 8.29E+06 | 6.83E+06 |

* measured by Sara Morgan, Davis group, University of Oxford

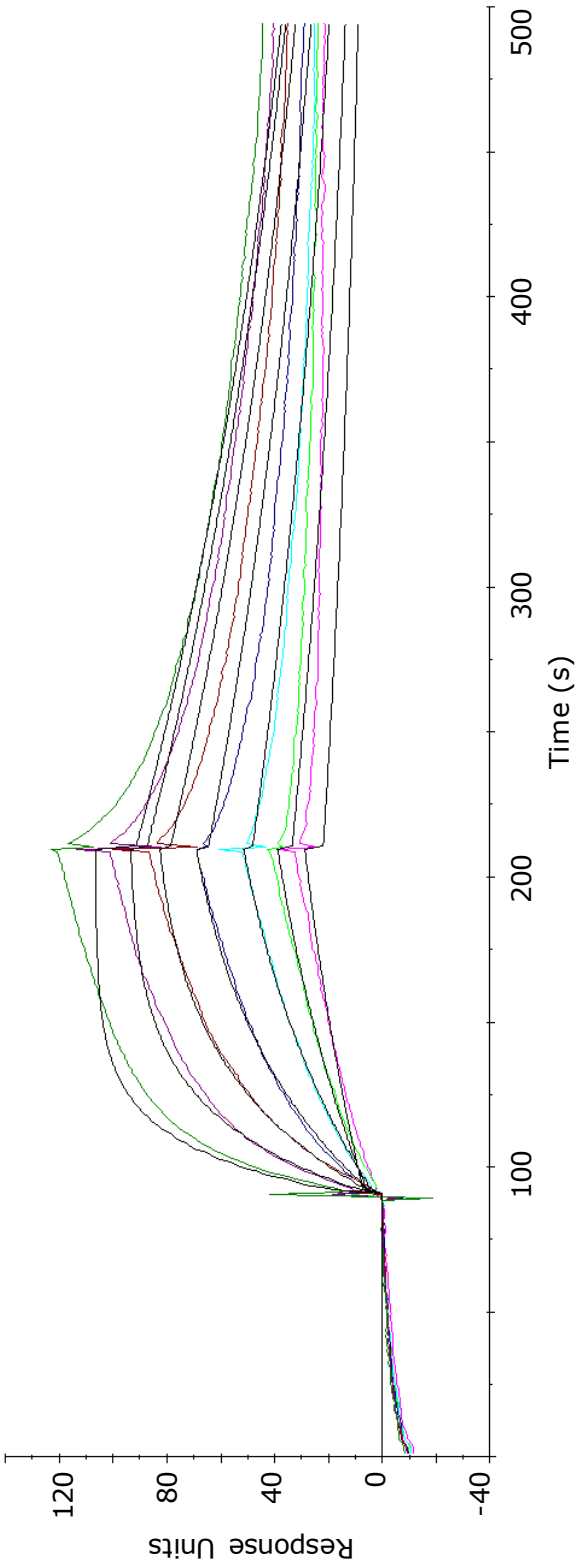



Figure 3-13: Kinetic measurement of JJ316 soluble affinity at 37 °C (BIAcore). Each coloured line corresponds to one analyte concentration, which ranged from $9.33*10^{-8}$ M to $2*10^{-6}$ M. Black lines represent the fit of a 1:1 Langmuir binding model. One out of two similar repeats is shown.

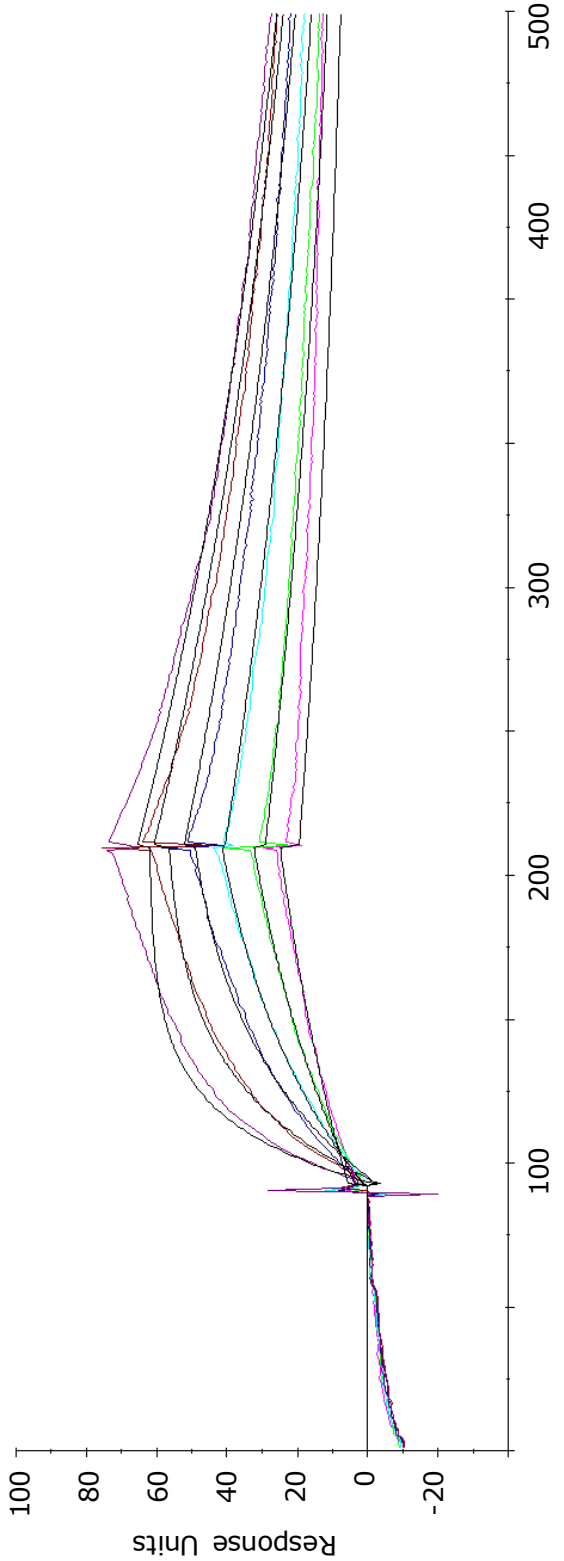



Figure 3-14: Kinetic measurement of JJ319 soluble affinity at 37 °C (BIAcore). Each coloured line corresponds to one analyte concentration, which ranged from $9.33*10^{-8}$ M to $1.2*10^{-6}$ M. Black lines represent the fit of a 1:1 Langmuir binding model. One out of two similar repeats is shown.

## 3.4. Discussion

The data presented in this chapter rule out binding affinity as a potential explanation for the differences between superagonistic and non-superagonisitic anti-CD28 antibodies. Both JJ316, the mitogenic CD28 antibody, and JJ319, which is costimulatory, have identical affinities for rat CD28, as determined by BIAcore.

BIAcore is a highly sensitive method to quantify soluble protein-protein interactions with a 1:1 binding stoichiometry. Affinity is ideally assessed with an equilibrium measurement. However, the Fab/CD28 interactions studied here are not suitable for this approach because their dissociation rates are too low to reach equilibrium within an appropriate time frame. Instead, a kinetic measurement was performed, which requires more care and comes with a number of potential limitations, which include mass transport as the rate-limiting step during association, and re-binding of analyte during dissociation. Association and dissociation rates for the JJ316 and JJ319 antibodies are in a range that is well-suited for a kinetic assessment [250] and experimental conditions were optimised, minimising such problems. Because the ligand can potentially become inactivated during direct immobilisation *via* amine coupling, an equilibrium measurement with a positive control analyte, mouse B7-1, was included, confirming that the rat CD28 used in the measurements was active and able to bind its ligand. The quality of the analyte, *i.e.* the Fab fragments used here, is of great importance for any BIAcore experiment, and for kinetic measurements in particular. It needs to be pure, homogenous and of a known concentration. The high quality and purity of the Fab fragments was demonstrated here by gel filtration and SDS-PAGE. However, a problem in this setting – that may well be responsible for the less-than-perfect model fitting here – was freeze-thawing of the Fab fragments between their purification and use in the binding assay. Although the analyte sample was centrifuged immediately before the assay was undertaken, some aggregate resulting from freeze-thawing may still have been present, introducing heterogeneity in the analyte. In this case, aggregates may bind CD28 multivalently, introducing an error because the model assumes monovalent binding. This could explain the relatively poor

fitting of the curves corresponding to the higher analyte concentrations in particular. Unfortunately, the yield for the Fab digest was small and did not allow the freeze-thawed sample to be subjected to gel filtration a second time. Ideally, measurements should be repeated with freshly purified Fab. The suboptimal fitting with a monovalent binding model may result in an error in the absolute rate constant and affinity values that are reported in this chapter. However, when drawing a conclusion on the mechanistic differences between JJ316- and JJ319-induced signalling, the relative comparison between their affinities is important rather than the accuracy of the absolute values. The binding curves for the two antibodies, *i.e.* the raw data, look very similar, and it is reasonable to assume that the same source of error produced the poor fitting. It is most probable that the same artefact, such as partial aggregation of the ligand introduced by freeze-thawing, caused the suboptimal data, and it is highly unlikely that two separate factors with an opposite effect on the experiment produced the error in a way that affinity differences would be masked. Despite whatever small errors there might have been in the affinity and kinetic measurements, the important point is that the two antibodies did not exhibit largely different behaviour in the two assays that could have accounted for their different signalling activities.

To complement the kinetic affinity assessment in solution, a second experiment was included that is closer to the experimental conditions used to study cellular responses to stimulation with antibodies, such as in Chapters 4, 5, and 6. Interestingly, a difference in association kinetics was observed when the binding of undigested antibody to cell-surface expressed rmCD28 was assessed, as had been reported previously in relative terms [228]. In this setting, the antibody needs to penetrate the densely packed cellular glycocalyx to reach its target. It is conceivable that JJ316 shows delayed binding because its epitope is buried more deeply inside the glycocalyx. In order to bind rat CD28 so close to the cellular membrane, it would need to overcome steric hindrance from neighbouring receptors, which are often heavily glycosylated at the base. However, in this setting avidities rather than affinities were determined: bivalent antibodies were allowed to interact multivalently with a homodimeric receptor.

*In toto*, the hypothesis that JJ316 is a more potent antibody because of an increased affinity for its target receptor was disproven in this chapter. If at all, its avidity for CD28 presented within the cell surface may be lower, as evident from its delayed binding kinetics.

# Chapter 4 Antibody superagonism can be studied on glass surfaces

## 4.1. Introduction

The experiments of the previous chapter ruled out the simple explanation that an increased affinity is responsible for the superagonistic activity of JJ316. Therefore, other differences between JJ316 and JJ319 had to be considered when attempting to explain their different behaviour. The one striking difference that has been described thus far is in the topology of the complexes that these antibodies form, as has been discussed in Chapter 1. Based on the observation that JJ316 forms a more compact complex, a "kinetic segregation" (KS)-based mechanism has been suggested to underlie its greater potency. Previous work on this problem had tested some of the predictions made by this model *in vitro*. T-cell lines were generated that expressed chimeric forms of CD28 and the phosphatases CD45 and CD148 that differed in the dimensions of their extracellular domains, and these cells were stimulated with JJ316 immobilised on plastic surfaces. It was shown that anti-CD28 superagonism is sensitive to the dimensions of both the CD28 receptor and the phosphatases. Either extending CD28 [249] or truncating the phosphatases (Sara Morgan *et al*, unpublished) abrogated superagonistic signalling, consistent with the predictions of the KS model.

Recent developments in high- and super-resolution fluorescence microscopy present the possibility to further test the KS model with an imaging approach in live T-cells. Chang *et al* [153] have produced microscopy-based evidence for sterically driven rearrangement of surface receptors as T cells interact with glass surfaces, leading to activation in the absence of ligand. Therefore, should such rearrangements also occur as part of the mechanism behind antibody superagonism, as suggested by the KS model, they should be detectable with a suitable imaging approach. In addition to testing the KS model in particular, an imaging approach may well be able to reveal other processes that potentially occur as part of the mechanism, such as receptor

aggregation, or the formation of a CD28 lattice because of particularly efficient crosslinking with the superagonist, both of which have been proposed to play a role in signalling [228, 231], or effects on diffusion of the receptors and/or phosphatases. Fluorescence microscopy experiments, however, generally have to be performed on glass surfaces, whereas superagonism had thus far been studied in *in vitro* experiments undertaken on plastic surfaces [228, 229, 249].

This chapter aimed to establish an *in vitro* stimulation assay on glass, and to confirm that JJ316 also induces superagonistic signalling in this setting. As in an assay optimised on high protein-binding plastic [249], IL-2 production was chosen as the read-out for superagonistic activity. The IL-2 response takes place over the course of days, whereas receptor rearrangements potentially leading to signalling take place within seconds or minutes [153]. In addition to the IL-2 stimulation assay, the calcium signalling response to superagonistic and costimulatory antibodies was assessed in this chapter, in order to characterise signalling events that takes place within seconds to minutes of stimulation; *i.e.* a time frame that can be studied with high-resolution fluorescence microscopy.

## 4.2. Materials and methods

### 4.2.1. Harvest of primary mouse CD4+ T-cells

The spleens of wild-type C57BL/6 mice were harvested by Consuelo Anzilotti, Ph.D., Richard Cornall group, University of Oxford. Per round of experiments two spleens were used, with a yield of ~ 1-3*$10^6$ CD4+ T-cells, such that ~ 20 calcium flux measurements could be performed. CD4+ T-cells were isolated by depletion of all other cell types (MACS CD4+ T cell Isolation Kit, mouse, Milteny Biotec). The commercial kit protocol was followed. In brief, the splenocytes were suspended in buffer with the help of a cell strainer, and a cocktail of biotion-conjugated antibodies was added and incubated at 4 ºC, followed by a washing step. Second, magnetic avidin-loaded beads were added and incubated at 4 ºC, followed by a washing step. The mixture was then passed through a column placed in a magnetic separator that retains

the magnetic beads, and washed with buffer. CD4+ T-cells elute whereas all other cell types are retained.

The purified CD4+ T-cells were harvested at 1200 rcf, 4 ºC for 5 minutes and resuspended in JMEM medium. They were incubated at 37 ºC, 5 % $CO_2$ for an hour before proceeding with experiments.

### 4.2.2. Calcium flux assay

An early calcium flux response was measured in real time with the help of a spinning disk confocal microscope as live T-cells interacted with functionalised glass surfaces. The method allowed to analyse cellular activation at single-cell level combined with statistical information on a large number of cells. An automated analysis was carried out that measured time point of and amplitude of the calcium flux, and statistically evaluated the fraction of fluxing cells as well as the average lag time of fluxing. In contrast to the IL-2 measurements, early activation is analysed, in a time frame of minutes rather than days.

**Imaging calcium fluxes on the spinning disk confocal microscope**

Optical glass-bottom dishes with a ø 10 mm well (FD3510-100, World Precision Instruments) were coated with 200 µL antibody at 1-500 µg/mL in 1x coating buffer (from ELISA Ready-SET-Go!®, eBioscience) overnight at 4 ºC. 200 µL poly-L-lysine (0.1% in $H_20$, Sigma-Aldrich) was coated undiluted at 4 ºC overnight.

Imaging was performed on a spinning disk confocal microscope (Carl Zeiss) fitted with a Yogokawa spinning disk unit and an AxioCam camera, and directed with the ZEN software (Carl Zeiss). A 10x air objective was used. The microscope was fitted with an incubator and heating plates that allowed imaging at 37 ºC. Atmospheric $CO_2$ was not controlled.

Cells were suspended in JMEM medium, containing HEPES for improved pH buffering, at $1*10^6$ cells/mL and kept at 37 ºC. They were kept outside of a 5 % $CO_2$-controlled environment for no longer than one hour.

To visualise calcium fluxing, cells were stained with Fluo-4 (F14201, Thermo Fisher Scientific; 50 μg dissolved in 12 μL DMSO and stored in 1 μL aliquots at -20 ºC), a cell permeant dye that increases its fluorescence at 488 nm ~ 100-fold upon binding bivalent calcium. It was stored in DMSO at -20ºC. Probenecid was added to prevent rapid efflux of the dye.

$1*10^6$ cells were centrifuged at 1200 rcf for 90 seconds and resuspended in 200 μL unsupplemented RPMI medium (Sigma-Aldrich). They were then mixed with 200 μL 20.8 μg/mL Fluo-4 in HBS-probenecid (2.5 μM, pH 7.4) and incubated in the dark for 20 minutes. To wash, cells were centrifuged as above and resuspended in HBS-probenecid three times. Cells were either applied to the dishes directly when stimulation with directly coated antibodies was assessed, or they were resuspended in 10 μg/mL antibody in HBS-probenecid and incubated for 30 minutes where stimulation with indirectly immobilised antibody was assessed, and then applied to a secondary antibody coated dish. One batch of stained cells was used for two experiments where stimulation with direct antibodies was assessed, and for one experiment where indirect immobilisation was used.

The coated glass-bottom dishes were washed with 200 μL HBS-probenecid three times, leaving a residual amount of buffer in the last wash to prevent the dish from drying out. To focus on the correct confocal plane, a small number of stained cells was applied to the dish first: cells were diluted 1/50 in HBS-probenecid and 20 μL was added. Then, 40 μL undiluted cells were added, and images were collected for 7-11 minutes in the 488 nm channel as the cells landed on the dish, at 0.5-1 frames per second, 300-800 ms exposure, 100 % laser power (488 nm).

As a positive control, ionomycin (Sigma-Aldrich, I0634, stored at 10 mM in DMSO in 20 μL aliquots at -20 ºC) was used in some experiments. It is a drug that reversibly

binds to bivalent calcium and catalyses transport across lipid bilayers, causing rapid release of calcium from the endoplasmic reticulum into the cytoplasm. It was added to the experiment towards the last two minutes of data collection at a final concentration of ~ 1 μM, from a stock at 10 μM in HBS-probenecid.

**Statistical analysis with CalQuo**

Automated analysis was performed with the MatLab-based CalQuo software as outlined in [253]. The software identifies cells at a reference frame (typically the second to last frame) and follows them throughout the movie, calculating a fluorescence intensity profile for each cell. A function is fitted to identify the landing event as the cell falls into the confocal plane causing an increase in fluorescence readings above background, and the fluxing event as fluorescence peaks sharply. In a custom version of the software used for this thesis, the overall fluorescence intensities were normalised from 0 to 1 across all movies because there was heterogeneity in the raw data sets. Dead cells were excluded from the analysis by applying a threshold that rejects very bright cells. This threshold also excluded cells that were fluxing at the reference, *i.e.* second to last, frame. Thresholds defining the fitted function were optimised by the user, such as the minimum amplitude of the fluxing peak, the minimum lag time between landing and fluxing event, and the minimum amplitude of the landing plateau. Once optimised, they were applied to all data sets collected under equal experimental conditions. The software automatically discriminates between fluxing and non-fluxing cells and outputs a fraction of fluxing cells. It also outputs the average lag time between landing and fluxing event, or "triggering time". Because the software reported both false positive and false negative fluxing events, there was a relatively large error of ~ 10-15 % associated with the fraction of fluxing cells. For this reason, the fraction of fluxing cells was determined manually. The fluorescence profiles as produced by the software were judged by eye as either fluxing or non-fluxing profiles for 200 cells per experiment. The software then calculated a fraction based on the judgements entered by the user, which was associated with an error of ~ 5 % only. Typically, four

experiments were carried out for each stimulation condition. Average fractions of fluxing cells with the standard error of the mean were calculated.

## 4.3. Results

### 4.3.1. JJ316 is superagonistic on glass whereas JJ319 is costimulatory

Before proceeding to imaging studies, it was important to determine whether the antibodies induce superagonistic and costimulatory activity, respectively, on glass surfaces. An *in vitro* stimulation assay was established in which JJ316 and JJ319 antibodies were immobilised on glass surfaces suitable for fluorescence imaging. To allow for cross-linking of CD28 (see Section 5.3.3; [249]), the antibodies were not bound to glass directly, but were instead immobilised indirectly. The glass surface was coated with an anti-mouse Fc secondary antibody (DAM) at very high concentrations. CD28-expressing cells were incubated with JJ316 or JJ319 in solution, and then allowed to interact with the DAM-coated glass surface. Cells were cultured on the surface for 24 to 48 hours, and IL-2 secretion into the cell culture supernatant was assessed with an ELISA. The experimental set-up and procedure are illustrated in Figure 4-2.

$TCR^+$ murine BW5147 hybridoma cells were transfected with a chimeric form of CD28 comprising the extracellular region of rat CD28 and the transmembrane and cytoplasmic domains of mouse CD28 (rmCD28; Figure 4-1). First, co-activation with an anti-CD3 antibody, KT3, and the anti-CD28 antibodies was examined. Cell lines were stimulated with a titration of plate-bound KT3, and a fixed concentration of either JJ316 or JJ319 or isotype antibody was added to the cells, and indirectly immobilised *via* DAM (Figure 4-2B). Both JJ316 and JJ319 increased IL-2 production when co-immobilised on glass with KT3 at suboptimal concentrations, indicating that the antibodies were active on the glass surface (Figure 4-3B). Gaining mechanistic insight into the effects of the antibodies required a more quantitative analysis.

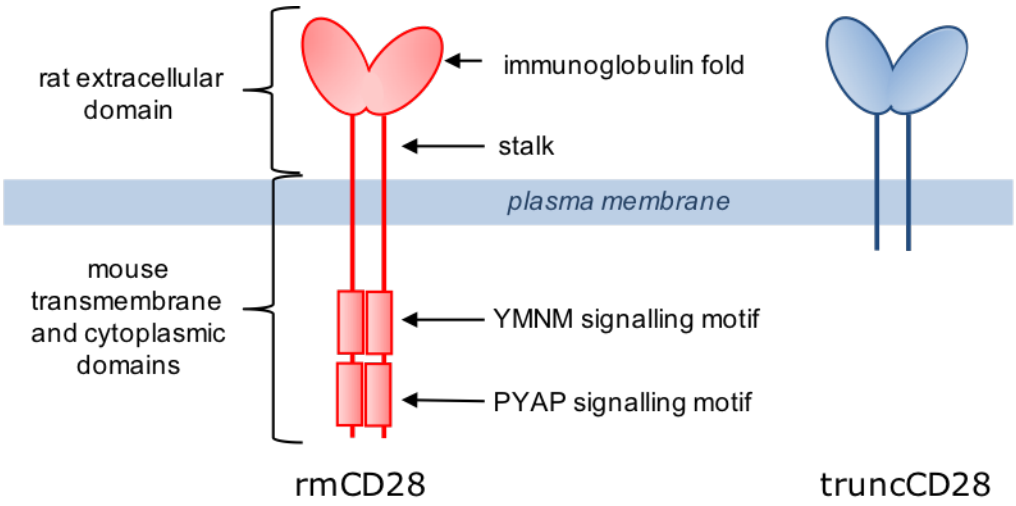



Figure 4-1: Design of chimeric CD28 receptors. rmCD28 constitutes the full-length sequence of the rat CD28 extracellular domain fused to the mouse CD28 transmembrane and cytoplasmic domains. truncCD28 is a truncated form of rmCD28, lacking the intracellular signalling motifs.

Fitting with a biochemical model was used to characterise in what way the anti-CD28 antibodies altered the responses of the cells to KT3. A biochemical binding model based on the Hill equation was chosen:

$$[\text{IL-2}] = \text{Maximum} * [\text{KT3}]^n/(\text{EC50}^n + [\text{KT3}]^n) + \text{Minimum}$$

where Maximum = [IL-2] at maximal [KT3]
EC50 = [KT3] that gives half-maximal [IL-2]
n = Hill-slope, describing cooperativity or "switch-likeness" of the curve
Minimum = [IL-2] at [KT3] = 0

When this analysis was applied to the dose-response curves in Figure 4-3, it was apparent that JJ319 significantly ($p<0.0001$) decreased the EC50 (*i.e.* the KT3 concentration that induces half-maximal IL-2 secretion), confirming its costimulatory activity. JJ316, in contrast, significantly increased the "Minimum" value (*i.e.* the levels of IL-2 secretion at zero KT3), from background to near-maximal levels, confirming its superagonistic activity (Table 4-1). Because it was necessary to plot the data on a

logarithmic scale x-axis for visualisation, the 0 μg/mL KT3 data point could not be displayed (Figure 4-3); it was, however, included in the curve fitting and analysis to extrapolate the "Minimum" value that characterises superagonism. Data displaying IL-2 production for JJ316 stimulation at 0 μg/mL KT3 co-activation can be found in Figure 4-4. It was important to demonstrate that the differences between the antibodies in their ability to activate T cells are not an artefact specific to the BW5147 cell line. Murine T-cell hybridoma lines DO11.10 and Yae5B3K were therefore likewise transfected with the rmCD28 construct and subjected to co-activation with KT3 and the anti-CD28 antibodies, and very similar observations were made (Figure 4-3A, C; Table 4-1).

Having confirmed that JJ316 but not JJ319 induced superagonistic activity when used at a constant concentration, the question remained whether this difference was robust over a range of concentrations. Hence, the dose-response behaviour of rmCD28-transfected cells to a titration of either JJ316 or JJ319 as assessed. The anti-CD28 antibodies were again immobilised indirectly *via* DAM secondary antibody, this time in the absence of co-activation by KT3 (Figure 4-2B). When immobilised alone, JJ3116 induced IL-2 production at a level comparable to, if not greater than, that of KT3 alone, whereas JJ319 was inactive even at high concentrations (Figure 4-4). Therefore, superagonistic signalling could not induced by JJ319 on glass by increasing its concentration.

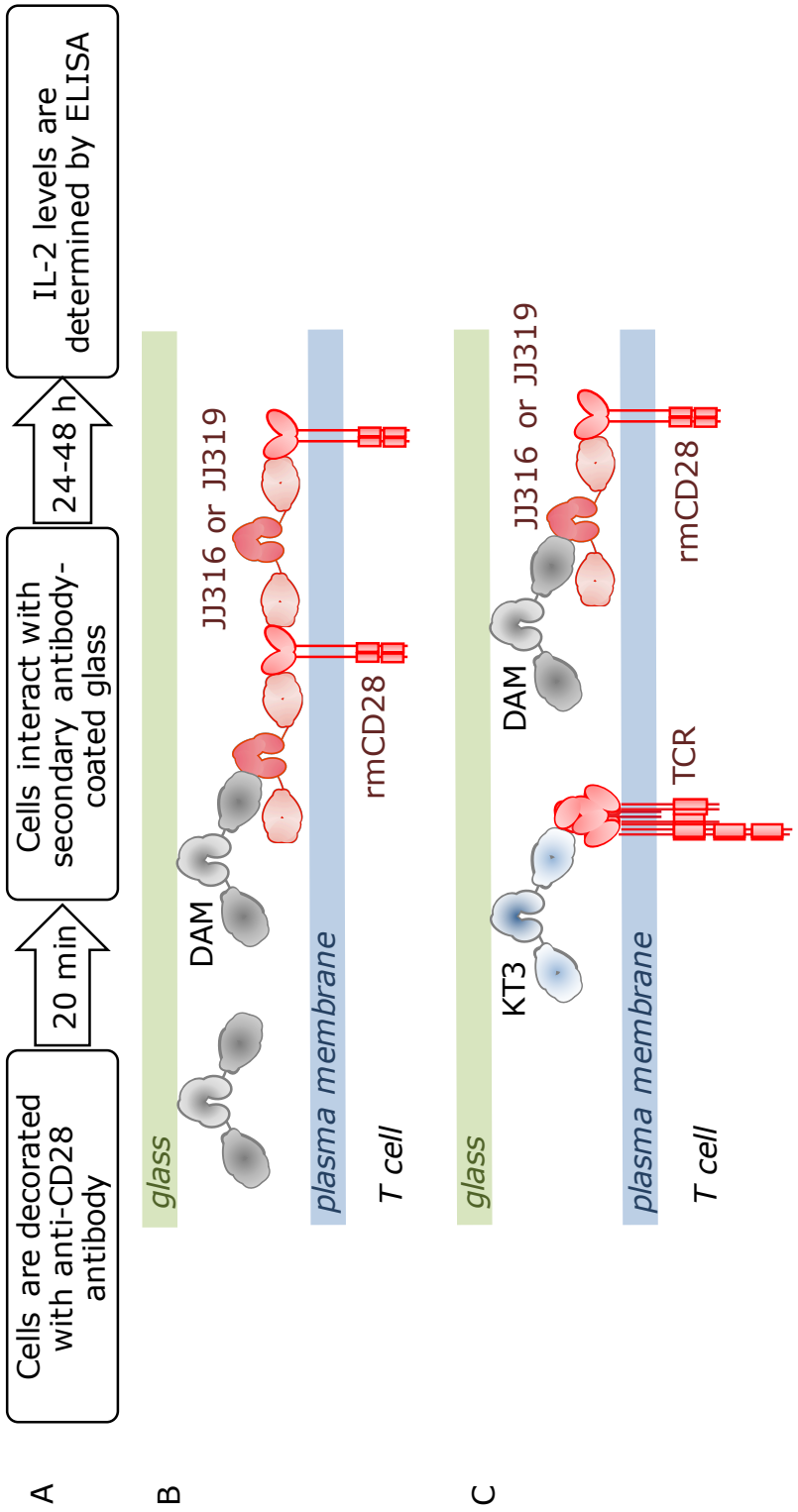



Figure 4-2: Experimental set-up for the IL-2 stimulation assay. **A** A flow chart of the experimental procedure is displayed. **B** A cartoon illustrates the experimental set-up for stimulation with the anti-CD28 antibodies on the molecular level. **C** A cartoon illustrates the experimental set-up for co-activation with the anti-CD3 antibody KT3 and the anti-CD28 antibodies on the molecular level

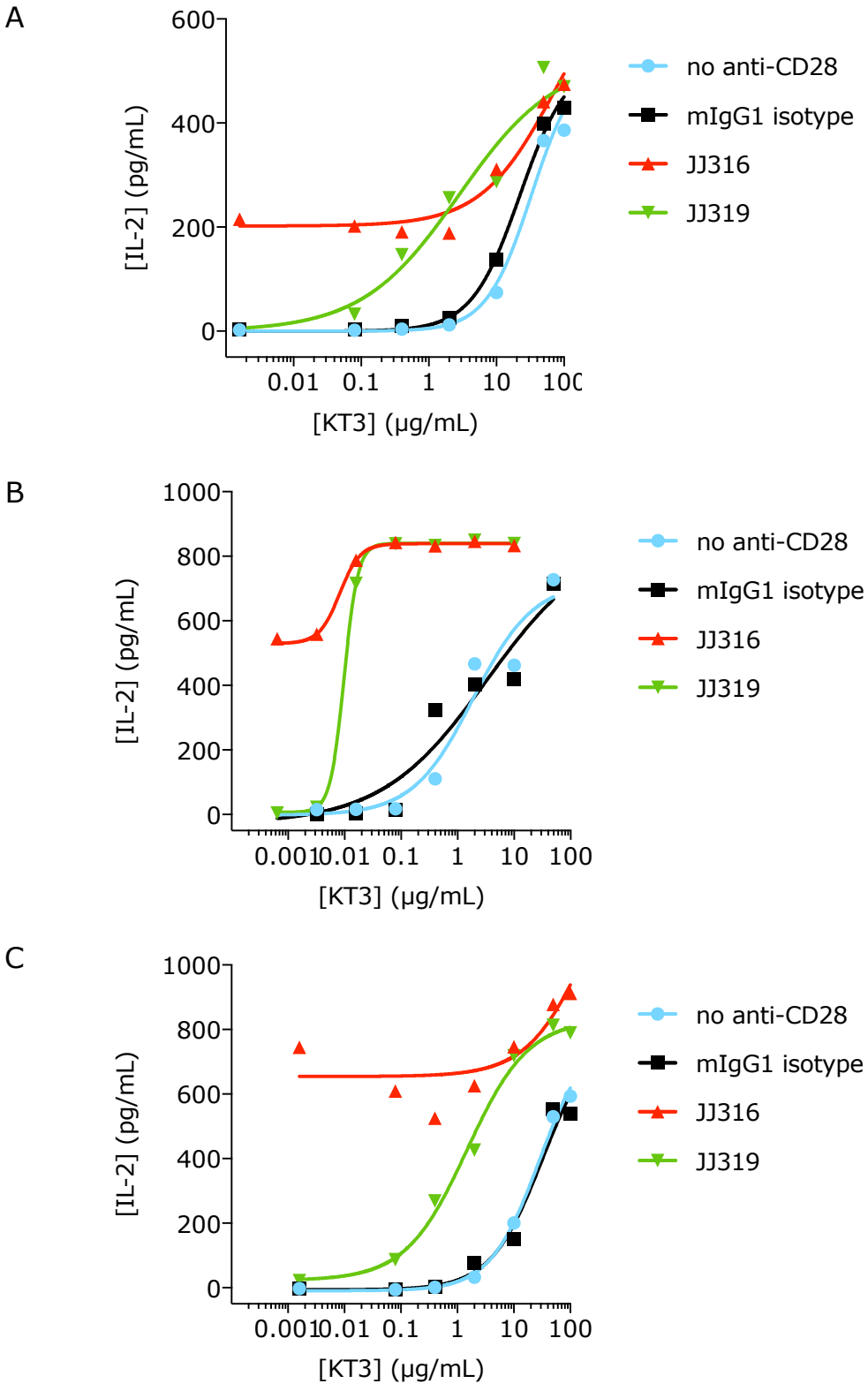

A
600
400
200
0
[IL-2] (pg/mL)
0.01
0.1
1
10
100
[KT3] (µg/mL)
no anti-CD28
mIgG1 isotype
JJ316
JJ319
B
1000
800
600
400
200
0
[IL-2] (pg/mL)
0.001
0.01
0.1
1
10
100
[KT3] (µg/mL)
no anti-CD28
mIgG1 isotype
JJ316
JJ319
C
1000
800
600
400
200
0
[IL-2] (pg/mL)
0.001
0.01
0.1
1
10
100
[KT3] (µg/mL)
no anti-CD28
mIgG1 isotype
JJ316
JJ319

Figure 4-3: JJ316 induces superagonistic signalling in murine T-cell hybridoma lines on glass, whereas JJ319 is costimulatory. **A** Yae5b3k, **B** $TCR^+$ BW5147, or **C** DO11.10 lines were transfected with rmCD28 and stimulated with a titration of KT3 that was directly coated on glass together with DAM secondary antibody. Cells were incubated with 10 μg/mL JJ316, JJ319, or isotype control as indicated in the right-hand legends. IL-2 secretion was assessed. Curves were fitted with a binding model*. For more convenient visualisation data are shown on a logarithmic scale, thus not showing zero on the x-axis. The zero values were, however, included in the fitting and analysis.

Table 4-1: Non-linear regression with a binding model* quantifies superagonistic and costimulatory activities of JJ316 and JJ319, respectively

| Yae5b3k rmCD28 | | | | |
|---|---|---|---|---|
| | no anti-CD28 | isotype | JJ316 | JJ319 |
| Maximum | constrained | constrained | constrained | constrained |
| n | 1.383 | 1.301 | 0.8145 | 0.6414 |
| EC50 | 29.82 | 20.67 | 66.94 | 2.762** |
| Minimum | -2.176 | 1.454 | 202.1*** | 9.148 |
| **DO11.10 rmCD28** | | | | |
| | no anti-CD28 | isotype | JJ316 | JJ319 |
| Maximum | constrained | constrained | constrained | constrained |
| n | 0.9894 | 0.945 | 0.8109 | 0.8006 |
| EC50 | 28.64 | 32.25 | 213.8 | 1.492**** |
| Minimum | -9.275 | -6.292 | 654.4† | 22.4 |
| **BW5147 CD3δζ rmCD28** | | | | |
| | no anti-CD28 | isotype | JJ316 | JJ319 |
| Maximum | 722.9 | 890.6 | 309.4 | 833.3 |
| n | 0.8151 | 0.4672 | 2.398 | 3.553 |
| EC50 | 1.888 | 3.312 | 0.008186 | 0.009791‡ |
| Minimum | -2.135 | -28.46 | 529.7§ | 6.886 |

* model: $[IL\text{-}2] = Maximum * [KT3]^n/(EC50^n + [KT3]^n) + Minimum$; where Maximum = [IL2] at maximal [KT3]; EC50 = [KT3] that gives half-maximal [IL-2]; n = Hill-slope, describing "switch-likeness" ; Minimum = [IL-2] at [KT3] = 0
** different from isotype p=0.0381 (F-test)
*** different from isotype p<0.0001 (F-test)
**** different from isotype p<0.0001 (F-test)
† different from isotype p<0.0001 (F-test)
‡ different from no anti-CD28 p<0.0001 (F-test)
§ different from isotype p=0.0002 (F-test)

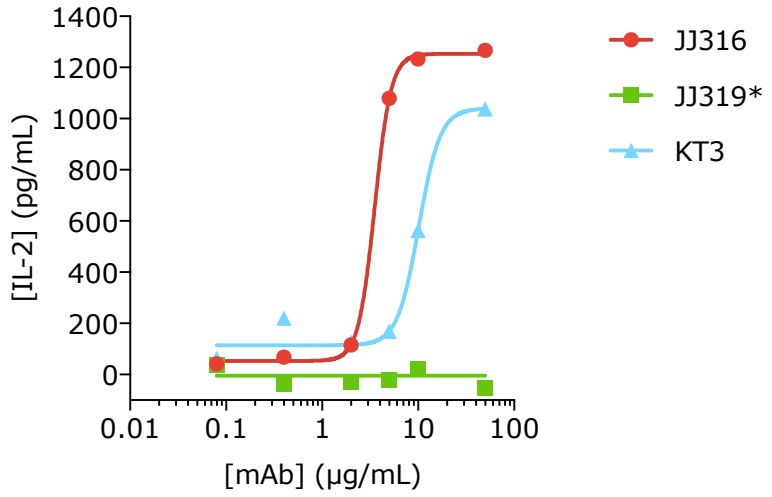



Figure 4-4: JJ316 induces T-cell activation in the absence of a second stimulus whereas JJ319 does not. DO11.10 cells were transfected with rmCD28 and stimulated with a titration of either JJ316 or JJ319 indirectly immobilised on glass *via* DAM secondary antibody, or with a titration of KT3 that was directly coated on glass. IL-2 secretion was assessed. KT3 and JJ316 curves were fitted with a binding model† or, where indicated with an asterisk, with a horizontal line because it was the preferred fit as determined by an F-test.

† [IL-2] = Maximum * $[mAb]^n/(EC50^n + [mAb]^n)$ + Minimum; where Maximum = [IL2] at maximal [mAb]; EC50 = [mAb] that gives half-maximal [IL-2]; n = Hill-slope, Minimum = [IL-2] for [mAb] = 0

### 4.3.2. JJ316 is most active when immobilised on glass indirectly

Having confirmed that JJ316 was active as a superagonist in the *in vitro* assay on glass, it was of interest to assess which mode of immobilisation was optimal to generate superagonistic signalling, and whether immobilisation was necessary at all. A number of formats were compared alongside one another, including indirect immobilisation *via* secondary antibody, or directly coating the superagonist on the glass surface. When JJ316 was bound directly to the plate, a ~ 20-fold higher concentration (100 μg/mL) was necessary to generate similar levels of IL-2 secretion *versus* indirect immobilisation (5 μg/mL) (Figure 4-4, Figure 4-5). JJ316 directly coated as a second layer on top of immobilised DAM was inactive, as was JJ316 directly coated in an excess of DAM in one step (Figure 4-5). Incubating cells with JJ316 in solution and then allowing them to interact with DAM-coated glass was most efficient; adding a washing step before applying the cells to the coated surface greatly reduced the IL-2 response (Figure 4-5). JJ316-stimulated cells that were incubated on uncoated glass also produced IL-2, albeit at a reduced level (~ 50 %) and this response was not abrogated by co-incubating the cells in an excess of isotype control antibody (Figure 4-5). Therefore, soluble JJ316 is superagonistic, and its immobilisation does not appear to be strictly required to induce full T-cell activation. Blocking the glass plate prior to addition of the cells did not alter the results (data not shown). Because it elicited an IL-2 response most efficiently, the setting in which cells were first incubated in JJ316 and then allowed to interact with DAM-coated glass was chosen for all subsequent *in vitro* stimulation experiments.

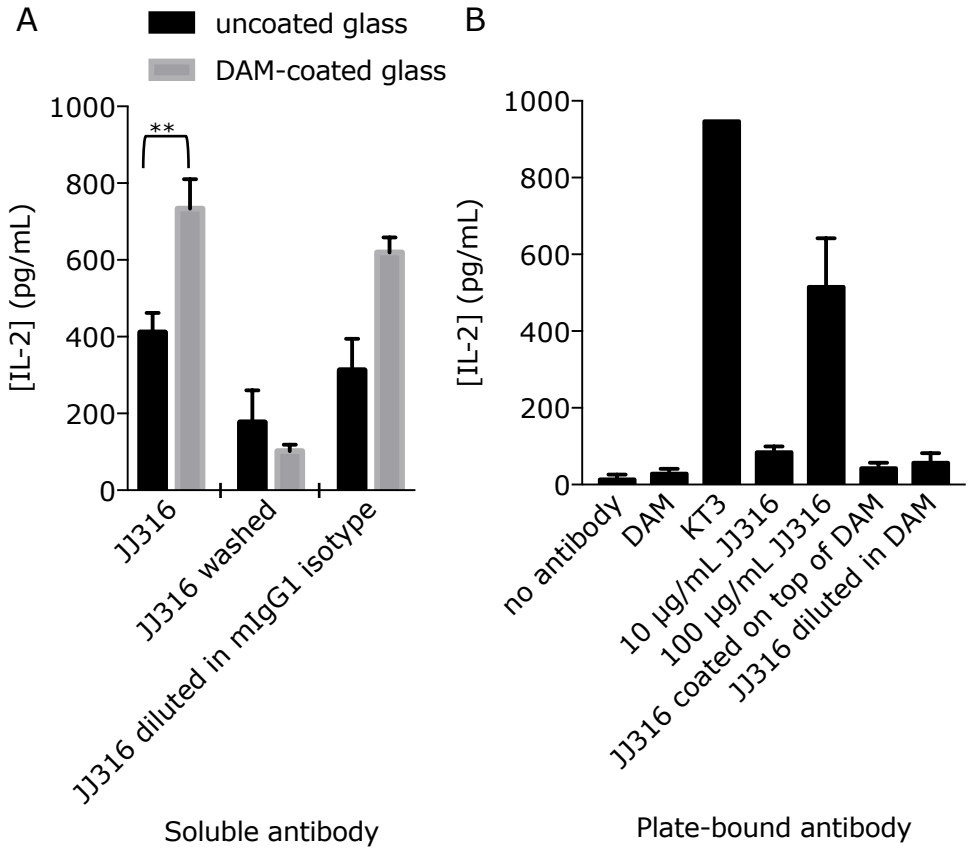



Figure 4-5: Indirectly immobilised JJ316 induces signalling more efficiently than when soluble or directly immobilised. In **A**, $TCR^+$, rmCD28-transfected BW5147 cells were incubated with soluble antibody and then allowed to interact with either uncoated or DAM-coated glass; DAM was coated at 500 µg/mL. Where indicated, JJ316 was used at 10 µg/mL and mIgG1 isotype was used at 100 µg/mL. In **B**, $TCR^+$, rmCD28-transfected BW5147 cells were allowed to interact with antibody-coated glass. 10 µg/mL KT3 and 500 µg/mL DAM coats were applied where indicated. A 100 µg/mL JJ316 coat was applied on top of a 500 µg/mL DAM coat where indicated. 100 µg/mL JJ316 diluted in 500 µg/mL DAM was coated in one step where indicated. In A and B, IL-2 production was assessed after 24 hours. Error bars display the standard error of the mean of four independent repeats. Within each repeat, [IL-2] was normalised to [IL-2] for 10 µg/mL KT3; as a result, the KT3 condition has no error bar. A two-tailed Welch-corrected t-test was employed to determine statistical significance (** here corresponds to $p=0.0072$).

### 4.3.3. Superagonism is a phenomenon of weak, tonic signalling

Whereas the IL-2 response takes place over a period of days, fluorescence imaging of live cells characterises their behaviour in a time frame of seconds to minutes. To help to bridge this gap in the analysis, a read-out was required that allowed superagonist-induced signalling to be assessed within minutes. A microscopy-based calcium flux assay was chosen, and used to determine whether superagonist-induced IL-2 production is preceded by an early calcium flux.

Changes in cytoplasmic calcium levels were measured in real time with the help of a spinning disk confocal microscope, as live T-cells interacted with functionalised glass surfaces. The method allowed analysis of cellular activation at a single-cell level combined with statistical information based on the analysis of a large numbers of cells. An automated analysis was carried out that measured the time point and the amplitude of the calcium flux, and statistically evaluated the fraction of triggering cells as well as the average lag time of triggering.

Figure 4-7 illustrates how the software, CalQuo [253], detects and quantifies cellular triggering from microscopy images with an example movie. Panels A-E show a section (~ 10 %) of the field of view at different time points in chronological order. Fluo-4 loaded cells fluoresce dimly in the 488 nm channel as they land in the field of view. Upon triggering, cells appear brightly fluorescent. Ionomycin added towards the end of the movie induces a simultaneous calcium flux across all viable cells, functioning as an internal positive control for each movie. The software identifies the position of each cell in the final frame of the movie, and then calculates a fluorescence profile for each cell, plotting intensity against time, as shown for two exemplarily cells in panel F. The software fits a mathematical model to the curve to discriminate between triggering and non-triggering cells, and to identify the time point of triggering. First, the "landing" event is identified, as fluorescence levels plateau above background when a dimly fluorescent cell appears in the field of view. Second, the software searches for a peak in fluorescence above a defined threshold to identify a "triggering" event. When such a peak is identified, the cell is recorded as a triggering cell. The time period

between landing and triggering is recorded as the "lag triggering time". After this analysis is performed for each cell, the software outputs statistical information.

To assess whether JJ316 and JJ319 induce an early calcium response, three rmCD28-transfected murine T-cell hybridoma lines were loaded with the calcium reporter Fluo-4 and then stimulated with soluble anti-CD28 antibody. They were then imaged as they made contact with a glass surface coated with DAM, and followed over a period of 11 minutes. The experimental set-up is outlined in Figure 4-6A. No calcium signalling was detected over 11 minutes when the cells were stimulated with indirectly immobilised JJ316 or JJ319, although this had led to strong IL-2 production in the case of JJ316 (see Figure 4-5). No calcium signalling was detected either while the cells were incubating with soluble JJ316 or JJ319 prior to dropping them onto secondary-antibody coated glass (data not shown). These data suggest that superagonist-induced IL-2 production is not preceded by an early calcium flux. As a positive control, cells were stimulated with KT3 directly immobilised on glass (Figure 4-6). ~ 50 % of rmCD28-transfected DO11.10 and Yae5B3K hybridoma cells showed strong calcium signalling within ~ 2-3 minutes upon landing (Figure 4-8). In contrast to the Yae5b3k and DO11.10 hybridoma cell lines, rmCD28-transfected $TCR^+$ BW5147 cells did not produce a calcium flux when stimulated with directly immobilised KT3 (Figure 4-8). Adding ionomycin to the experiment elicited an immediate strong calcium response, however, confirming that the cells were properly loaded with Fluo-4 and able to flux (Figure 4-8). Because of the deviating behaviour of this one cell line, it was important to determine which type of behaviour represents the authentic physiological response. Similarly to rmCD28-transfected DO11.10 and Yae5b3k cell lines, ~ 50 % of freshly harvested primary $CD4^+$ splenocytes calcium fluxed as they interacted with KT3-coated glass (Figure 4-9). Although BW5147 cells give strong distal superagonistic antibody responses, the proximal signalling pathways in these cells appear to be less sensitive to conventional stimuli than in other cells.

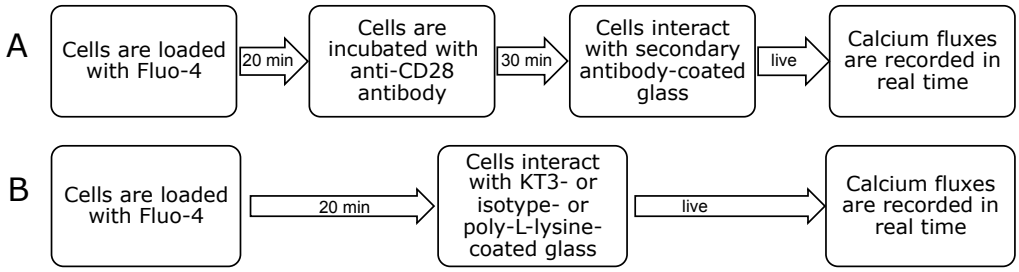



Figure 4-6: Experimental procedure in the calcium flux assay. Flowcharts are depicted that explain the experimental procedure for assessing stimulation with **A** indirectly immobilised anti-CD28 antibodies or **B** directly immobilised positive (KT3, poly-L-lysine) and negative (isotype) controls by calcium flux assay.

Figure 4-7: Microscopy-based calcium flux assay. Cells were loaded with Fluo-4, a reporter whose fluorescence increases ~ 100-fold upon binding calcium. Cells were imaged with a spinning disk confocal microscope as they interacted with functionalised glass. **A** Cells land in the field of view. **B, C, D** Cells fluoresce brightly as they calcium flux. **E** All cells calcium flux simultaneously upon the addition of ionomycin. **F** Fluorescence profiles of individual cells over 13 minutes. The "landing" event is characterised by a plateau above background-level fluorescence. "Triggering" is identified as a peak in fluorescence subsequent to landing. 1 µM ionomycin was added after 11 minutes, inducing a calcium flux in all viable cells, as identified by a peak in fluorescence.

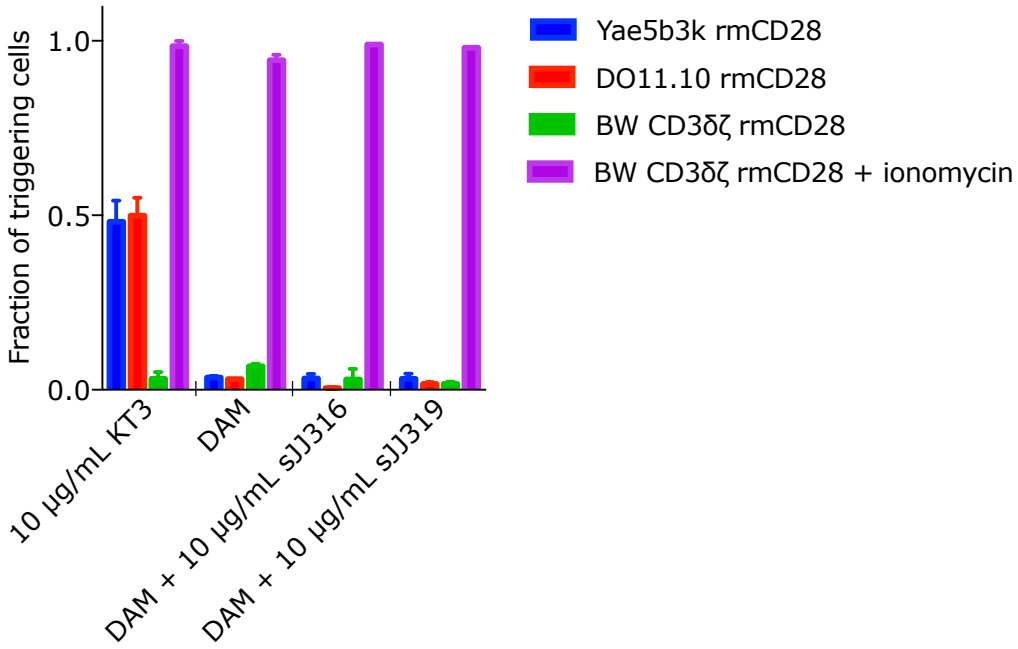



Figure 4-8: Indirectly immobilised superagonist does not induce an early calcium flux. rmCD28-transfected Yae5b3k, DO11.10 and TCR$^+$ BW5147 T-cell hybridoma lines were loaded with Fluo-4 and subsequently stimulated with KT3 directly immobilised on glass, or with soluble (s) JJ316 or JJ319 indirectly immobilised on glass *via* DAM. Cells were imaged for 11 minutes to record calcium signalling as they contacted the glass surface. Where indicated in the right-hand legend, 1 µM ionomycin was added after 11 minutes and images were recorded for a further 2 minutes. The fraction of calcium-fluxing cells is displayed on the y-axis, representing the mean of four independent repeats. Error bars display the standard error of the mean.

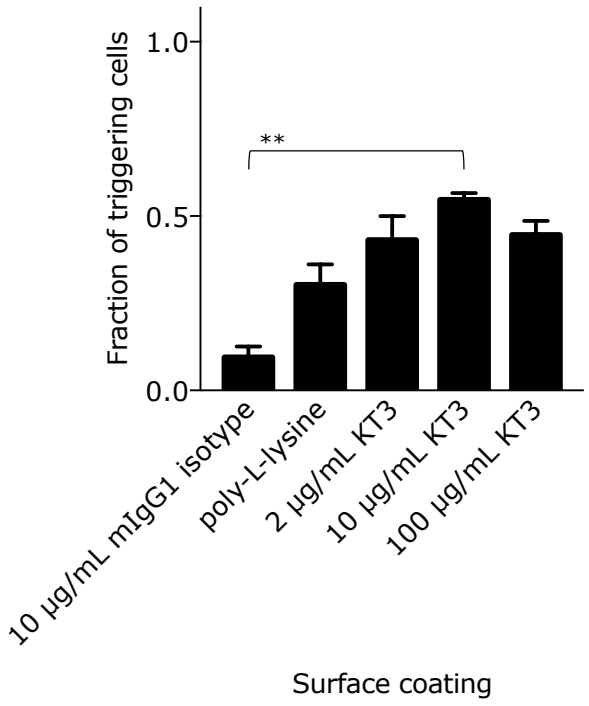



Figure 4-9: Primary C57BL/6 $CD4^+$ splenocytes respond to KT3 stimulation with an early calcium flux. Primary C57BL/6 $CD4^+$ cells were isolated from spleens and loaded with Fluo-4. Cells were imaged for 11 minutes to record calcium signalling as they contacted a functionalised glass surface. The x-axis legend indicates the surface coating condition. The fraction of calcium-fluxing cells is displayed on the y-axis, representing the mean of three independent repeats. Error bars display the standard error of the mean. Statistical significance was determined with a paired two-tailed t-test (** here corresponds to p=0.0073).

### 4.3.4. Superagonistic signalling differs on glass *versus* on EIA plastic

Although anti-CD28 superagonists induce full T-cell activation in the absence of any TCR ligand, it was previously reported that the presence of the TCR at the cell surface is necessary for superagonistic signalling [231]. Because this observation had been made on plastic surfaces, it was of interest to confirm that superagonistic signalling on glass is TCR-dependent. For this purpose, BW5147 cells were used, which lack TCR surface expression because they do not express the CD3 δ and ζ genes. TCR expression was then rescued by lentiviral transduction with CD3 δ and ζ, and confirmed by flow cytometry (Table 4-2). $TCR^-$ and $TCR^+$ BW5147 cell lines were transfected with rmCD28, and an IL-2 stimulation assay was performed. Whereas $TCR^+$ cell lines produced IL-2 in response to JJ316 stimulation on both glass and EIA plastic, $TCR^-$ cell lines did not (Figure 4-10), confirming the dependence on TCR expression of antibody-induced superagonistic signalling on glass [231].

These data prompted the question of whether the superagonist-induced signalling observed on glass and plastic is fully or partially CD28- or TCR-mediated. It was thus necessary to design an experimental setting that would distinguish CD28-dependent from TCR-mediated signalling. To achieve this, a signalling-disabled CD28 construct, truncCD28, was used that is bound by JJ316 but does not initiate a signalling cascade. The extracellular and transmembrane domains were left intact, but the cytoplasmic domain was truncated. The six amino acids following the transmembrane domain were left in place to ensure correct insertion of the protein into the membrane. The signalling motifs, including all tyrosine residues that would become phosphorylated upon receptor triggering, were removed completely.[12] Figure 4-1 illustrates the design of the truncated CD28 receptor. Flow cytometry confirmed that JJ316 binds truncCD28 expressed in BW5147 cells (Table 4-2).

[12] Molecular cloning was performed by Rachel Knox, Davis laboratory, University of Oxford.

Strikingly, on EIA plastic, IL-2 production was observed also when truncCD28 was ligated with JJ316. The response was reduced to ~ 30 % of that elicited by signalling-competent, full-length rmCD28 expressed at equal levels (Figure 4-10). These data suggest that, on EIA plastic, both the TCR and CD28 contribute to superagonism, although no TCR ligand was present. Signalling induced by JJ316 immobilised on glass, in contrast, was entirely CD28 signalling-dependent since removing the cytoplasmic domain of CD28 completely abrogated IL-2 production (Figure 4-10). To further characterise the interplay between the two receptors, the surface expression of both the TCR and CD28 was titrated by transducing cell lines with a dilution series of lentivirus[13]. Table 4-2 lists the different cell lines with their expression levels of TCR and rmCD28 or truncCD28, as assessed by flow cytometry. Stimulation with JJ316 indirectly immobilised on either glass or EIA plastic revealed that superagonism is dependent on the relatively high expression of both the TCR and CD28, and signalling elicited by ligating truncCD28 is dampened in comparison to rmCD28 (Figure 4-11). On EIA plastic, more signalling was observed than on glass for both rmCD28- and truncCD28-expressing cells. In particular, signalling induced by ligating truncCD28 expressed at "medium" levels in combination with "medium" CD3 levels was negligible on glass, whereas ligating rmCD28 expressed at equivalent levels in combination with "medium" CD3 levels induced near-maximal signalling on glass. Therefore, by choosing "medium-level" rmCD28- and TCR- expressing BW5147 cells, entirely CD28-dependent signalling can be studied. Unless specified otherwise, all subsequent experiments were performed with CD28 constructs expressed at levels corresponding to the "medium-level" cell line in this experiment, in "medium-level" CD3-expressing BW5147 cells. On EIA plastic, and particularly with cell lines expressing high levels of both TCR and CD28, and even on glass at the highest CD3- and CD28 expression levels, superagonist-induced signalling is not entirely CD28-dependent. We assume that the signalling observed under these conditions is driven

[13] Lentiviral transductions were performed by Mai Vuong, Davis laboratory, University of Oxford.

by the TCR since it disappears when the TCR is absent. In these circumstances, it is not possible to study CD28-dependent signalling *per se*.

These results motivated further characterisation of the two surfaces. A hypothesis emerged that perhaps the two surfaces differ in their efficiency to immobilise DAM secondary antibody. A luminescence-based ELISA assay was performed in which equal amounts of DAM secondary antibody were directly coated on glass and EIA plastic surfaces. A horse radish peroxidase (HRP)-coupled mouse antibody was added, resembling the indirect immobilisation of JJ316 or JJ319, and the efficiency of its immobilisation *via* DAM was assessed by luminescence. Comparisons showed that EIA plastic immobilised ~ 5-fold more antibody than did glass (Figure 4-12; $p<0.0001$).[14]

Having confirmed that the two surfaces indeed immobilise different amounts of antibody, it remained to be shown whether this effect is responsible for the different outcomes in the IL-2 stimulation assay. It was therefore examined whether TCR-mediated *versus* CD28-dependent signalling depends on levels of secondary antibody immobilisation. Lowering the amount of secondary antibody on EIA plastic dampened signalling induced by ligating truncCD28 with JJ316 more so than rmCD28 (Figure 4-13). Therefore, the observed qualitative differences in signalling on glass *versus* EIA plastic likely result from their differential ability to bind protein. It is also striking that the levels of signalling generated by ligating truncCD28 reach the levels of rmCD28 (Figure 4-13), suggesting that TCR-mediated signalling becomes dominant, or that the signalling capacity is saturated.

[14] A similar experiment that measured fluorescence rather than luminescence, making use of fluorophore-coupled secondary antibody, did not detect any differences in antibody immobilisation between glass and EIA plastic (see Section 5.3.8).

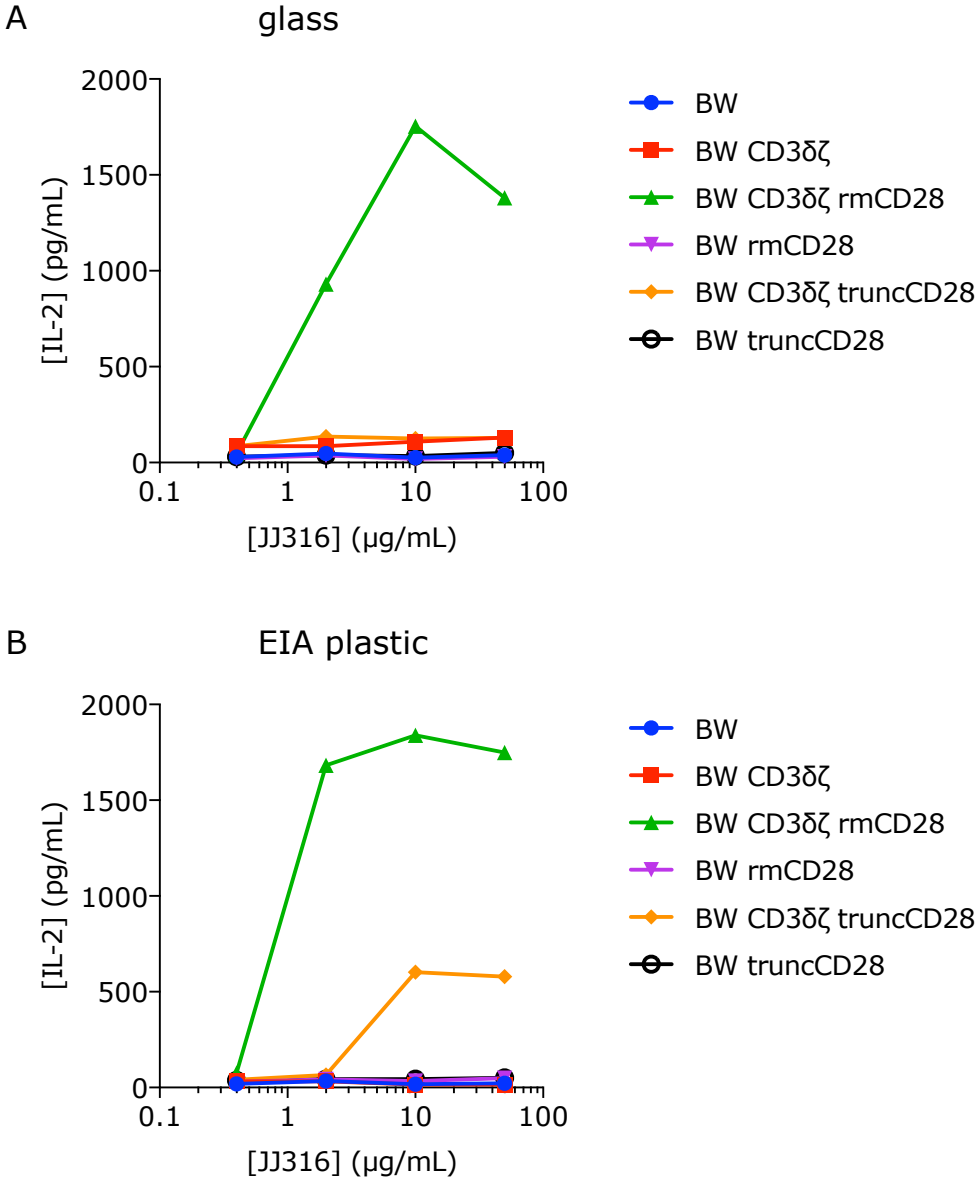


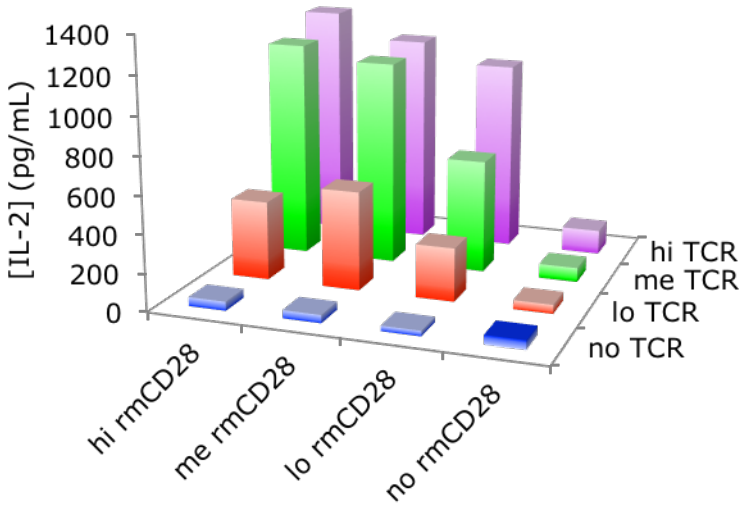

Figure 4-10: Superagonism is partially independent of CD28 signalling on EIA plastic, but not on glass, and dependent on the presence of the TCR on both EIA plastic and glass. $TCR^-$ BW5147 (BW) cells were transfected with CD3 δ and ζ chains to establish TCR expression. $TCR^+$ or $TCR^-$ BW cells were subsequently transfected with either a signalling-competent (rmCD28) or signalling-disabled (truncCD28) CD28 construct. Cell lines, whose identity is indicated in the right-hand legend, were stimulated with a titration of JJ316 indirectly immobilised on **A** glass or **B** EIA plastic *via* DAM secondary antibody. IL-2 secretion was assessed.

Table 4-2: Surface expression of CD3 and CD28 in BW5147 cells.

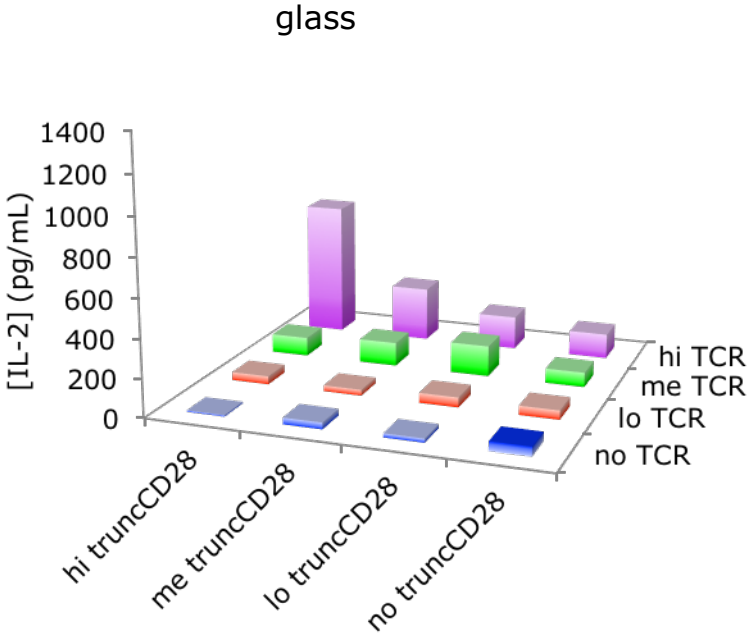
| Cell line | MFI* CD28 | MFI* CD3 |
|---|---|---|
| BW | 1 | 5 |
| BW $TCR^{lo}$ | 1 | 115 |
| BW $TCR^{me}$ | 1 | 334 |
| BW $TCR^{hi}$ | 0 | 817 |
| BW $rmCD28^{lo}$ | 422 | 6 |
| BW $rmCD28^{me}$ | 2161 | 3 |
| BW $rmCD28^{hi}$ | 3081 | 1 |
| BW $TCR^{lo}$ $rmCD28^{lo}$ | 384 | 106 |
| BW $TCR^{lo}$ $rmCD28^{me}$ | 927 | 117 |
| BW $TCR^{lo}$ $rmCD28^{hi}$ | 3926 | 64 |
| BW $TCR^{me}$ $rmCD28^{lo}$ | 488 | 331 |
| BW $TCR^{me}$ $rmCD28^{me}$** | 1129** | 291** |
| BW $TCR^{me}$ $rmCD28^{hi}$ | 1714 | 181 |
| BW $TCR^{hi}$ $rmCD28^{lo}$ | 321 | 694 |
| BW $TCR^{hi}$ $rmCD28^{me}$ | 678 | 1007 |
| BW $TCR^{hi}$ $rmCD28^{hi}$ | 2367 | 896 |
| BW $truncCD28^{lo}$ | 269 | 6 |
| BW $truncCD28^{me}$ | 1313 | 2 |
| BW $truncCD28^{hi}$ | 2328 | 4 |
| BW $TCR^{lo}$ $truncCD28^{lo}$ | 314 | 99 |
| BW $TCR^{lo}$ $truncCD28^{me}$ | 1145 | 124 |
| BW $TCR^{lo}$ $truncCD28^{hi}$ | 3534 | 80 |
| BW $TCR^{me}$ $truncCD28^{lo}$ | 372 | 283 |
| BW $TCR^{me}$ $truncCD28^{me}$** | 1379** | 329** |
| BW $TCR^{me}$ $truncCD28^{hi}$ | 2691 | 261 |
| BW $TCR^{hi}$ $truncCD28^{lo}$ | 187 | 586 |
| BW $TCR^{hi}$ $trucCD28^{me}$ | 1085 | 977 |
| BW $TCR^{hi}$ $truncCD28^{hi}$ | 1247 | 602 |

* Mean fluorescence intensity as assessed by flow cytometry, in relative units.
** Expression levels that lead to superagonistic signalling when rmCD28, but not truncCD28 is ligated with JJ316. In subsequent experiments, CD3 and CD28 expression was matched to these levels.

A


glass
[IL-2] (pg/mL)
1400
1200
1000
800
600
400
200
0
hi rmCD28
me rmCD28
lo rmCD28
no rmCD28
hi TCR
me TCR
lo TCR
no TCR

B


glass
[IL-2] (pg/mL)
1400
1200
1000
800
600
400
200
0
hi truncCD28
me truncCD28
lo truncCD28
no truncCD28
hi TCR
me TCR
lo TCR
no TCR

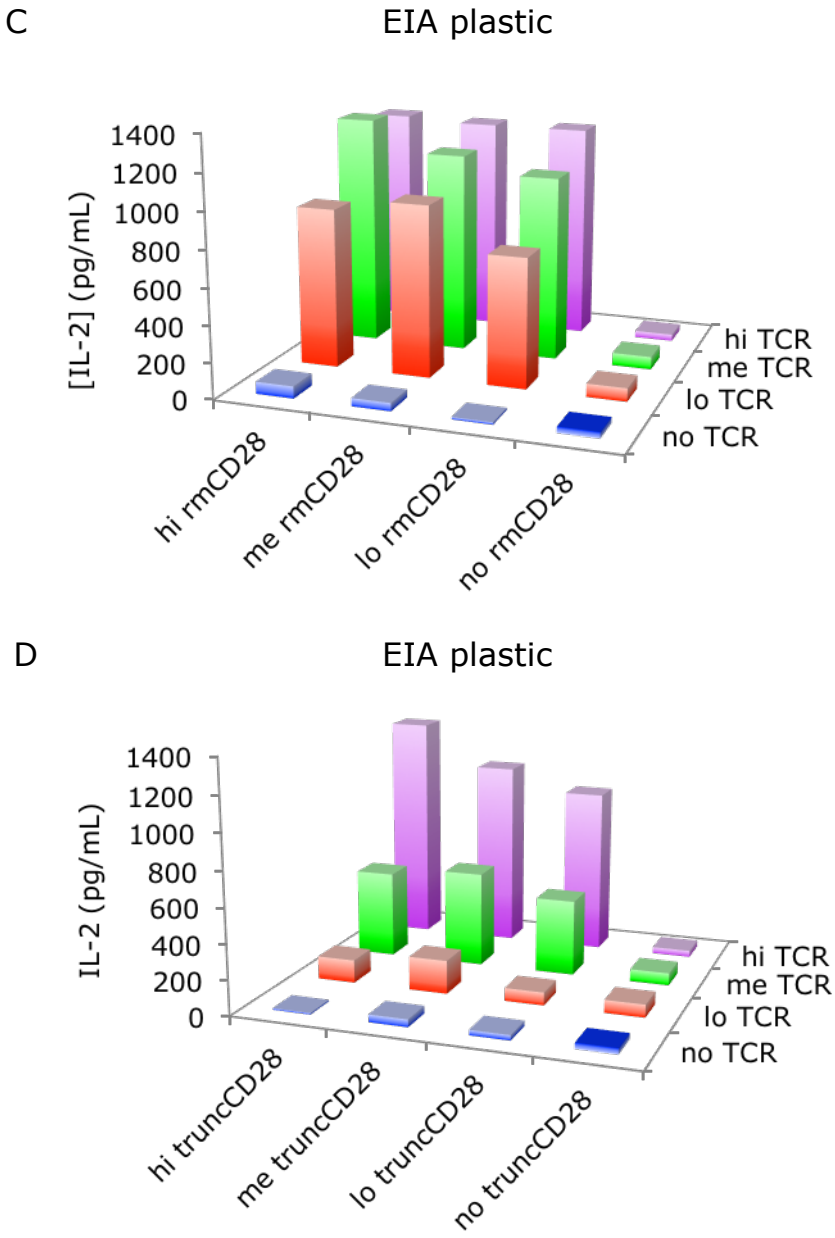



Figure 4-11: Superagonism is dependent on both TCR and CD28 expression levels. BW5147 cells expressing varying levels of TCR and either signalling-competent rmCD28 (**A**, **C**) or signalling-disabled truncCD28 (**B**, **D**) were stimulated with JJ316 indirectly immobilised on either glass (**A**, **B**) or EIA plastic (**C**, **D**). IL-2 production was assessed. Columns represent mean values of four (**A**, **B**) or two (**C**, **D**) independent repeats.

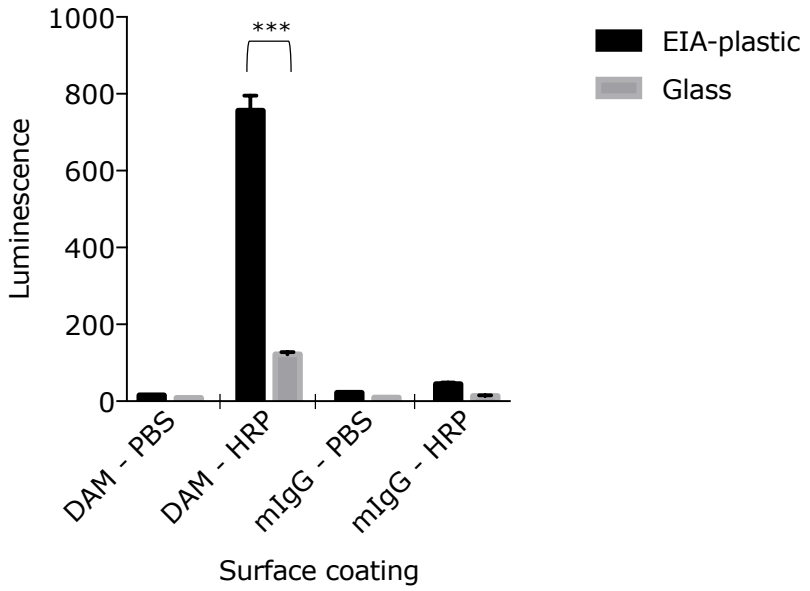



Figure 4-12: EIA plastic immobilises 5-fold more antibody as compared to glass. Glass or EIA plastic surfaces, as indicated in the right-hand legend, were coated with either DAM secondary antibody, or with an unspecific mouse IgG1 as a negative control. After blocking and washing, a mouse antibody (anti-penta-His, Qiagen) coupled to horse radish peroxidase (HRP), or PBS was added. After washing, Pierce ECL Western blotting substrate (Thermo Fisher Scientific) was added, and luminescence was measured. A student's t-test was performed to determine statistical significance ($p<0.0001$).

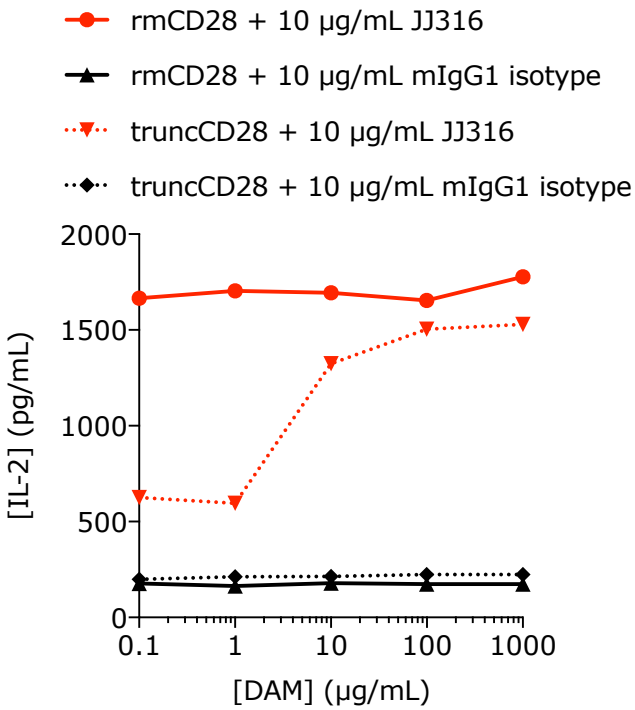



Figure 4-13: Superagonising truncCD28, but not rmCD28 is sensitive to the amount of antibody immobilisation. TCR$^+$ BW5147 cells were transfected with either signalling-competent rmCD28 or signalling-disabled truncCD28, and stimulated with either JJ316 or isotype control indirectly immobilised on EIA plastic. IL-2 secretion in response to a titration of DAM secondary antibody was assessed.

## 4.4. Discussion

Work described in this chapter established an *in vitro* stimulation assay to study antibody superagonism on glass surfaces suitable for fluorescence imaging. It confirmed that antibodies are active when indirectly immobilised on glass surfaces. A quantitative analysis based on curve fitting with a binding model formally showed that JJ316 induces superagonistic signalling whereas JJ319 is costimulatory. Fitting dose-response curves with a multivariable binding model has several advantages over alternative analyses. First, in contrast to visual comparison of curves, it is quantitative, and statistics can be applied to determine if two curves differ from each other significantly. Second, compared to single-concentration measurements that are performed repeatedly and evaluated with statistics such as a t-test, statistical information can be obtained from a single experiment. Third, it can be determined whether differences between two conditions, such as activation with different antibodies, are of a qualitative or of a quantitative nature. When only a single concentration is examined, differences may appear binary; *e.g.* one antibody may induce a full response and the second antibody may induce no response. Such analysis could mask quantitative effects; *e.g.* the second antibody may in fact require a higher dose to induce a response. Examining dose-response curves that cover a range of concentrations over four orders of magnitude, as was done here, minimises the chance of missing a result that occurs only above or below a certain threshold. Fourth, when a binding model based on the Hill equation is chosen, meaningful biochemical parameters are determined as best-fit values. This offers mechanistic insight, because a statement can be made with statistical confidence based on which parameter is altered by a certain condition, and in which way it is altered. Here, JJ319 lowered the median effective concentration of KT3 needed to induce signalling, fulfilling the definition of costimulation, and JJ316 increased the response at zero co-activation with KT3 from background to near-maximal levels, fulfilling the definition of superagonism. This added to prior studies on plastic surfaces, which were of a somewhat semi-quantitative nature [228, 229, 249].

By comparing superagonistic signalling on glass *versus* EIA plastic, an important difference was revealed. Whereas on glass, superagonist-induced signalling was largely dependent on CD28 signalling, CD28-independent signalling contributed to the response on EIA plastic, which is likely mediated by some level of TCR triggering. This means that the setting on EIA plastic is not suitable for studying CD28-dependent signalling *per se*. The most likely explanation for the discrepancy between glass and plastic results is that they differ in their efficiency to bind protein, as shown in this chapter. Lowering the amount of secondary antibody on EIA plastic imitated the results obtained on glass. However, glass and plastic differ in other properties as well, such as surface charge, stiffness, rigidity, and roughness. It has been reported that cells behave differently when interacting with surfaces varying in those characteristics; proliferation, differentiation, and signalling may be affected [254, 255]. T-cell activation and proliferation have been shown specifically to be affected by the rigidity of the activating surface in *in vitro* assays [256]. Therefore, to correlate functional data with imaging results, it was necessary to re-visit the properties of superagonistic signalling on glass, and test the molecular requirements, as has previously been done on EIA plastic [249].

As defined, anti-CD28 superagonism achieves full T-cell activation in the absence of direct TCR stimulation (*i.e.* ligation). However, as has been shown before [231] and confirmed in this chapter, the presence of the TCR is required for superagonist-induced signalling, even on glass where it is strictly CD28-dependent.

IL-2 production was chosen as the read-out for superagonistic signalling because it is indicative of full T-cell activation rather than sub-threshold signalling, and superagonism as defined is a phenomenon that induces full activation. IL-2 production is suitable for evaluating CD28 signalling in particular because it is known to be the main downstream effect amplified by CD28 costimulation [135]. However, calcium signalling was evaluated to characterise the response to the anti-CD28 antibodies within a time frame of minutes. Yae5b3k and DO11.10 hybridoma lines showed a strong calcium response within 2-3 minutes when they were stimulated with plate-

bound KT3, as did primary $CD4^+$ murine splenocytes. BW5147 cells, whose TCR expression was reconstituted by stable transfection with CD3 δ and ζ genes, showed no calcium response to KT3. Some uncertainty remains as to why the BW5147 hybridoma exhibited this type of behaviour. A transcriptome analysis could be undertaken to characterise the three hybridoma cell lines and to determine whether BW5147 cells differ in expression of a gene involved in early TCR-dependent calcium signalling, or early T-cell activation in general. Clearly, all three cell lines produced similar, robust IL-2 responses in response to direct CD3 ligation with KT3. Stimulating all three T-cell hybridoma lines with indirectly immobilised JJ316 failed to induce an early calcium flux; however, this lead to a strong IL-2 response within 24 hours. These results show that an IL-2 response can be elicited without a preceding early calcium flux. The analysis chosen here identifies calcium fluxes, characterised by a strong peak in cytoplasmic calcium levels; it is not suitable to detect tonic fluctuations in intracellular calcium levels. It is thus possible that such calcium oscillations occurred during stimulation with the anti-CD28 antibodies, which may result in T-cell activation over a period of time [257]. It would be interesting to address in future studies how low-level tonic signalling is integrated to result in full activation. Finally, while the indirectly immobilised JJ316 superagonist does not induce any detectable calcium fluxing, it would be interesting to determine whether any detectable PI3K activation takes place. A microscopy-based assay on fixed cells has been described that quantifies the accumulation of PI3K at the T-cell plasma membrane during activation, and it may be a suitable approach to characterise the PI3K response to JJ316 stimulation [258].

*In toto,* this chapter established an assay for CD28-dependent, superagonist-induced signalling on glass surfaces suitable for fluorescence imaging. In the next chapter, key predictions of the KS model will be re-visited in this setting, because antibodies immobilised on glass *versus* plastic surfaces differentially activate T-cells, perhaps *via* distinct mechanisms. A microscopy-based assay showed the absence of an early calcium response to superagonistic stimulation, whereas identical stimulation conditions induced a strong IL-2 response. Therefore, superagonism is likely the result of low-level tonic signalling taking place over an extended time period.

# Chapter 5 The requirements for antibody superagonism are compatible with a "kinetic-segregation" based theory of signalling

## 5.1. Introduction

Work described in the previous chapter established an *in vitro* stimulation assay in which antibody superagonism can be studied on glass surface suitable for imaging studies, and revealed qualitative differences in superagonist-induced signalling on glass *versus* on EIA plastic. To correlate with imaging experiments performed on glass, it was therefore necessary to revisit experiments done on EIA plastic that examined the molecular requirements for superagonism, as they might differ on glass.

Prior work on EIA plastic had confirmed some of the key predictions made by a KS based model of antibody superagonism. It had been shown that JJ316-induced superagonism is sensitive to both receptor and phosphatase dimensions on EIA plastic [249]. In addition, a dependence on CD28 crosslinking on EIA plastic was established [249]. In work described in this chapter, these experiments were repeated on glass. Building on the work, the interplay between TCR- and CD28-mediated signalling in anti-CD28 superagonism was further characterised: the dependence of signalling on receptor and phosphatase dimensions and crosslinking was studied in the presence and absence of the TCR, and using signalling-competent and signalling-disabled CD28 constructs. Work presented in the previous chapter and by others [249] also showed that JJ316 is active in solution, but its activity is increased when it is immobilised. Therefore, whether or not superagonistic and costimulatory signalling mediated by antibodies is enhanced by improving immobilisation efficiency was tested. For this purpose, a His-tagged Fc receptor was produced that can immobilise antibodies very

densely on "nickelated" surfaces. Finally, antibody engineering was employed to examine whether and how changes to the antibody itself affect superagonistic signalling. It was examined whether changes introduced to the JJ316 Fc region abrogate its activity in solution, based on the hypothesis that cells may cross-present JJ316 to each other on Fc receptors. Adding to the experiments that tested dimensional dependence, JJ316 was extended with an insertion in the hinge region to characterise the effect of antibody dimensions on signalling.

## 5.2. Materials and methods

### 5.2.1. Immobilisation of His-tagged mFcγRIIb on Ni-NTA-coated plastic

For comparing the amount of available binding sites on antibody-coated glass (Thermo Scientific™ Nunc™ MicroWell™ 96-well optical-bottom plate with coverglass base) or EIA plastic (Costar® flat-botttomed 96-well EIA-RIA plate) *versus* Ni-NTA-coated plastic (Qiagen Ltd Ni-NTA HisSorb 96-well plate, 35061), His-tagged mFcγRIIb-Alexa647® was incubated on the respective surface for one hour at room temperature in 100 μL PBS at a concentration titrated from 0.0065 to 6.4 μg/mL, after the surface was blocked for one hour RT in 1x blocking buffer (Ready-SET-Go! ELISA kit, eBioscience). For negative controls, wells were coated with PBS. The coated 96-well plates were washed with 200 μL PBS three times. Fluorescence readings were performed in 100 μL PBS, on a CLARIOstar microplate plate reader (BMG Labtech). The gain was set to 4000. A well-scan was performed using top optics.

For the IL-2 stimulation assay, His-tagged mFcγRIIb was incubated on the Ni-NTA surface at a concentration titrated from 0.05 to 6.4 μg/mL in PBS, for one hour at room temperature. The plate was washed three times in PBS. Cells were pre-incubated in antibody and then added to the mFcγRIIb-coated plate, and IL-2 levels were determined after 24 hours; the protocol outlined in Section 2.11 was followed.

## 5.3. Results

### 5.3.1. The activity of soluble JJ316 is not abrogated by "silencing" its Fc region

In the previous chapter, it was shown that JJ316 was superagonistic when used soluble, but indirect immobilisation *via* a secondary antibody induced a larger response (see Section 4.3.2.). It was of interest to further examine the immobilisation dependence of antibody superagonism. Since JJ316 is a mouse antibody and mouse cell lines were used in the stimulation assay, it is possible that the antibody was immobilised on the surface of a cell *via* an Fc receptor (FcR), and cross-presented to a second cell, functioning in an immobilisation-dependent way. To abolish the interaction between the JJ316 Fc region and an FcR, the antibody was deglycosylated by digestion with PNGase F, an enzyme that removes high mannose, hybrid, and complex N-glycans from glycoproteins (New England BioLabs® Inc.)[15]. The digested antibody migrated at a reduced size on SDS-PAGE, indicating that the digest was successful (Figure 5-1)[15]. It was hypothesized that removing the N-linked oligosaccharides from its Fc region may suffice to prevent the antibody from binding to an FcR. PNGase F-digested and undigested JJ316 were compared in a stimulation assay where they were either used in solution, or indirectly immobilised *via* an anti-$\varkappa$ light chain secondary antibody (Figure 5-3A). Both antibodies induced high levels of IL-2 production at relatively low concentrations when immobilised, whereas higher concentrations were required to induce a similar response when they were used in solution (Figure 5-3A). Therefore, PNGase-F digested JJ316 was still active in solution, although the IL-2 response to soluble PNGase-F digested as compared to undigested JJ316 was slightly reduced (Figure 5-3A). The question remained whether deglycosylation of JJ316 was perhaps incomplete, or whether the deglycosylated antibody was still able to bind to an FcR. To overcome these potential problems, a custom-engineered "Fc-silent$^{TM}$" JJ316 form was used (kind gift of Absolute Antibody Ltd). Here, residues in the lower

[15] The digest and purification of the digested antibody was performed by Janet Fennelly, Davis laboratory, University of Oxford.

hinge region which are crucial for binding CD16/CD32 [259], were mutated[16]. Similarly to PNGase-F digested and unmodified JJ316, soluble Fc-silent JJ316 was active, but immobilised Fc-silent JJ316 induced higher levels of IL-2 (Figure 5-3B). Therefore, Fc-silencing JJ316 did not abolish its activity in solution, although the IL-2 response to soluble Fc-silent as compared to soluble unmodified JJ316 was once again reduced (Figure 5-3B).

### 5.3.2. JJ316-induced superagonism is Fc-dependent

Having shown that antibody superagonism is enhanced by, but perhaps not strictly dependent on immobilisation *via* secondary antibody, it was of interest whether the presence of the Fc region in the antibody was required. To test this, JJ316 was digested with ficin (Sigma-Aldrich, F4165) to produce an $F(ab')_2$ fragment[17], which lacks the Fc domain but retains the disulphide bonds in the hinge region. It is thus a bivalent protein and is predicted to retain the ability to crosslink CD28. SDS-PAGE analysis of the digest indicated that a small amount of antibody (~ 10 %) remained undigested (Figure 5-2)[17]. $F(ab')_2$ was separated from Fc with affinity chromatography *via* protein A-coupled Sepharose and purified with size exclusion chromatography, where some contaminant undigested antibody remained (data not shown)[17]. When used at 6.45 nM, the $F(ab')_2$ fragment was active when immobilised *via* anti-$\kappa$ light chain antibody, but inactive when used in solution, whereas undigested JJ316 was active both immobilised and soluble at an equivalent molar concentration (Figure 5-4). At higher concentrations, some activity was observed for the soluble $F(ab')_2$ fragment (Figure 5-4). It is possible that the ~ 10 % contaminant undigested antibody was responsible for this activity. Alternatively, it is also possible that a large amount of stimulation overcomes the requirement for the Fc region. In conclusion, the effect of removing

[16] Surface plasmon resonance and direct competitive inhibition ELISA experiments showed that Fc-silent mouse antibodies no longer bind to CD16, CD16-2, CD32, and CD64 (Stephen Beers, University of Southhampton; [64])

[17] The digest and purification was performed by Janet Fennelly, Davis laboratory, University of Oxford.

the Fc region was much greater than that of Fc-silencing or deglycosylating it, and at concentrations of up to 6.45 nM superagonism is dependent on the antibody Fc region.

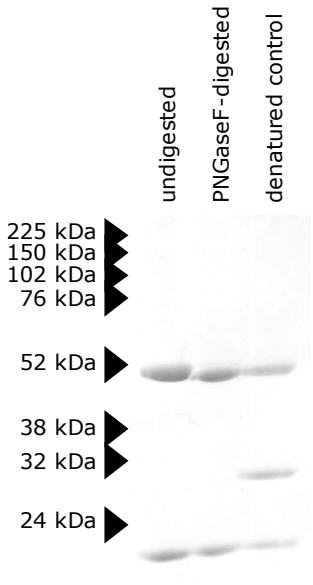



Figure 5-1: SDS-PAGE analysis of a PNGaseF-digest of JJ316[18]. Undigested JJ316, PNGaseF digested JJ316, and JJ316 digested with PNGaseF under denaturing conditions were analysed. 5 μg of each sample was loaded under reducing conditions and separated on a 15 % acrylamide gel.

[18] Performed by Jan Fennelly, Davis laboratory, University of Oxford.

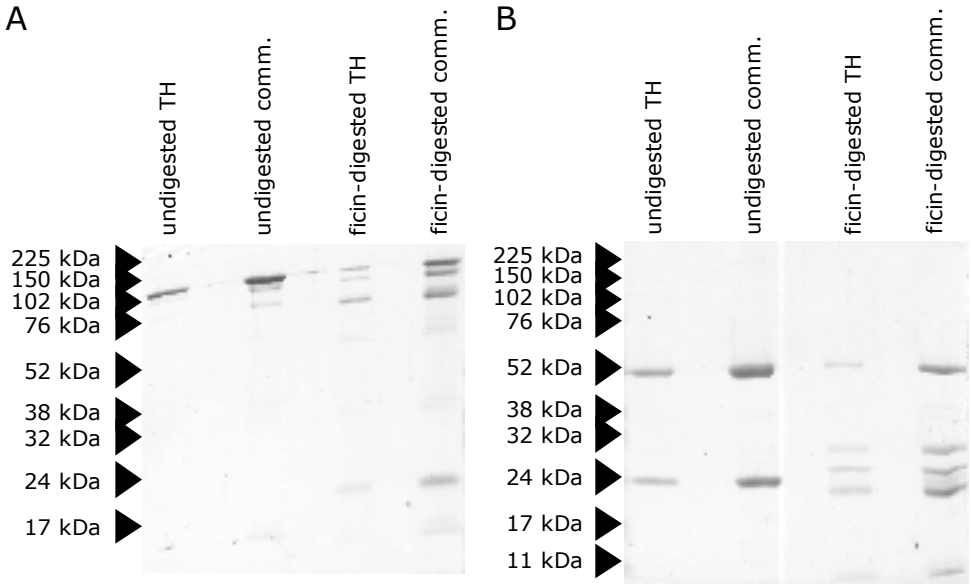



Figure 5-2: SDS-PAGE analysis of a ficin digest of JJ316[19]. Undigested and ficin-digested JJ316, either from a commercial (comm.) source or a kind gift from Thomas Hünig (TH)[20] were analysed. 5 μg of each sample was loaded under **A** non-reducing or **B** reducing conditions and separated on a 10 % acrylamide gel.

[19] Performed by Jan Fennelly, Davis laboratory, University of Oxford.
[20] University of Würzburg

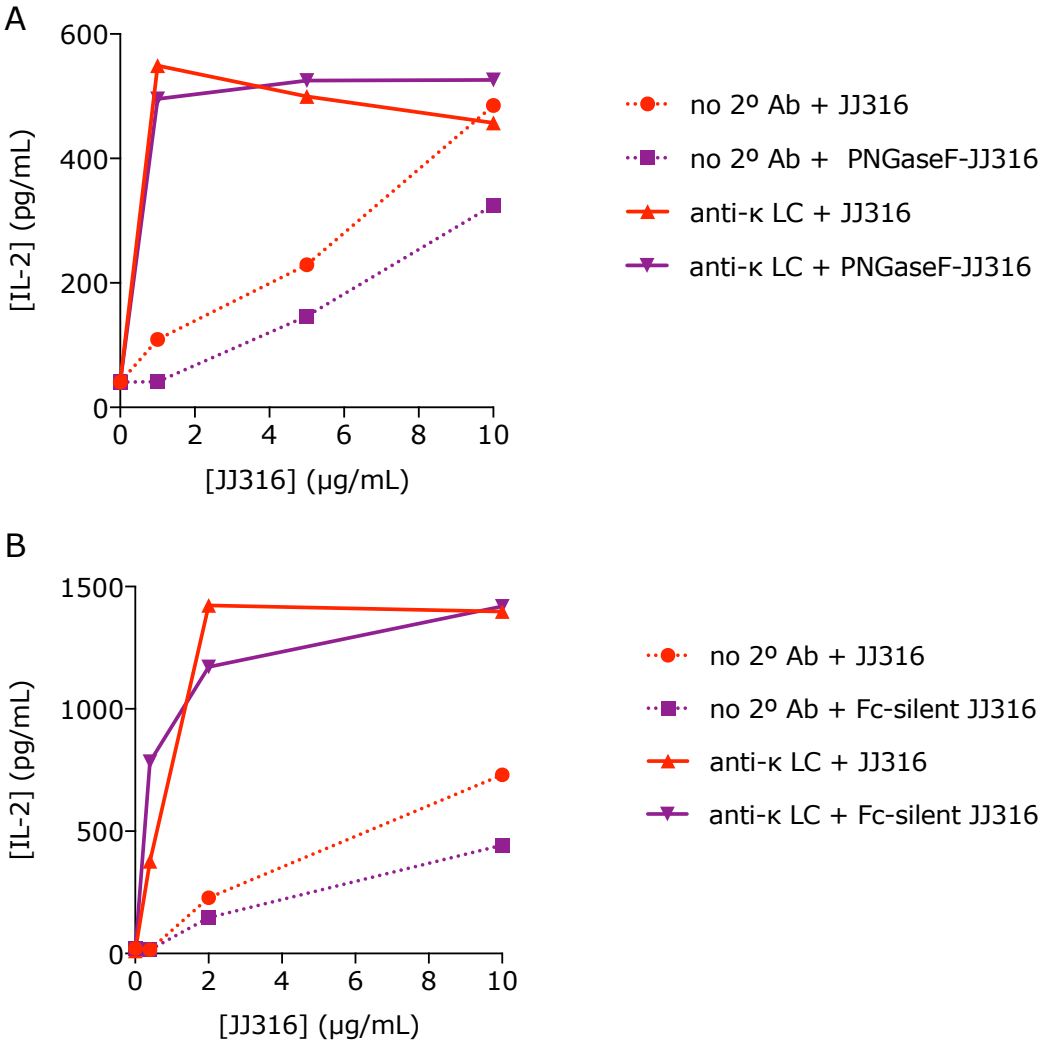



Figure 5-3: Deglycosylated and "Fc-silent™"[21] JJ316-derivatives are active in solution. A glass surface was coated with 100 µg/mL anti-IgG kappa light chain secondary antibody, or coating buffer only (no 2º Ab). In **A**, $TCR^+$ rmCD28-transfected BW5147 cells were incubated with undigested or PNGaseF digested JJ316 antibody, and then allowed to interact with the coated glass surface. In **B**, the cells were incubated with a mutated "Fc-silent™" form of JJ316. IL-2 production was assessed after 24 hours. The results of one out of two independent repeats are displayed.

[21] Fc silent™ JJ316 is a custom-engineered antibody kindly provided by Absolute Antibody Ltd, making use of their technology to disrupt Fc receptor/Fc region interactions.

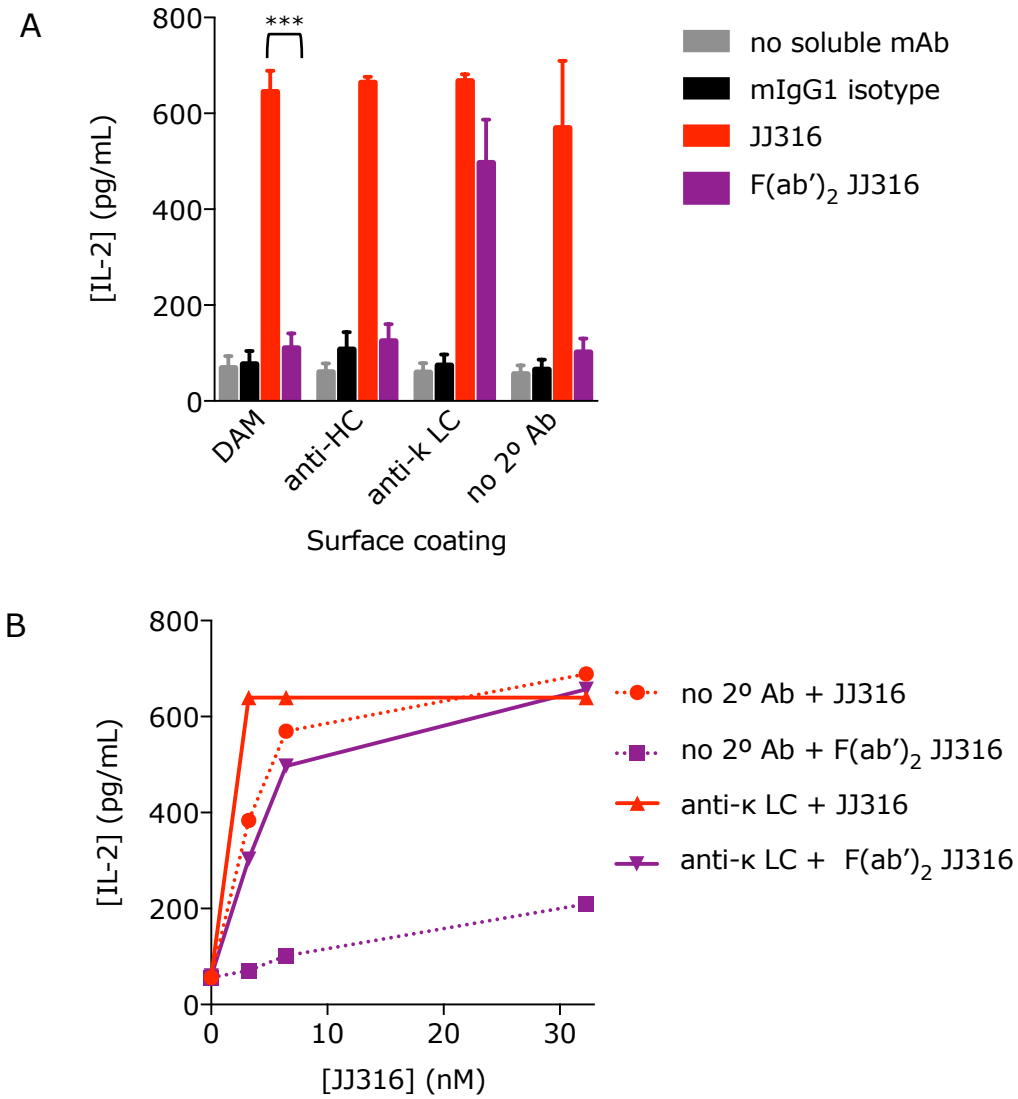



Figure 5-4: The F(ab')$_2$ fragment of JJ316 is only active when immobilised. A glass surface was coated with 100 µg/mL DAM, anti-heavy chain, or anti-IgG kappa light chain secondary antibody, or coating buffer only (no 2º Ab). BW5147 cells expressing high levels of the TCR and CD28 were incubated with undigested JJ316 antibody, or its F(ab')$_2$ fragment, and then allowed to interact with the coated glass surface. IL-2 production was assessed after 24 hours. **A** The mean values of four independent repeats are displayed. 1 µg/mL JJ316 or 0.66 µg/mL of its F(ab')$_2$ fragment, which corresponds to 6.45 nM, was used to compare equal molar concentrations. **B** The results of one representative out of four independent repeat are displayed, for anti-IgG kappa light chain and no immobilisation conditions only. The concentration of JJ316 or its F(ab')$_2$ fragment was titrated, and values are displayed in nM on the x-axis to be able to compare equal molar concentrations.

### 5.3.3. Superagonism is crosslinking-dependent

Because CD28 is a homodimer, it can be crosslinked with bivalent antibodies, and potentially form large crosslinked arrays. It had been suggested that particularly efficient crosslinking may be responsible for the potency of superagonistic anti-CD28 antibodies [132, 229]. It was therefore important to examine whether crosslinking is required for superagonistic signalling on glass, as had been observed on EIA plastic [249]. To test this, a monomeric form of CD28 was designed that could not be crosslinked: the transmembrane and cytoplasmic domains of mouse CD28 were fused to the extracellular domain of human PD1, a monomeric immunoglobulin-family immunoreceptor, giving PDCD28 (Figure 5-5; [249]). CD28 dimerises *via* a disulphide bond in the stalk region of its extracellular domain (see Figure 4-1); thus, replacing its extracellular domain with that of a monomeric receptor renders it monomeric. Two anti-hPD1 antibodies were used to ligate PDCD28: clone 2, which binds an epitope at the "top" of PD1 close to the ligand binding site (*i.e.* analogous to JJ319 binding to CD28), and clone 19, which binds close to the membrane (*i.e.* analogous to JJ316 binding to CD28) [249]. Clone 19 had been shown to induce particularly strong, superagonistic hPD1 signalling that was able to suppress anti-CD3 induced proliferation [260]. As previously observed on EIA plastic [249], both clone 19 and clone 2 were inactive on glass when used on their own to stimulate PDCD28-transfected cells, but induced a strong IL-2 response when they were used in combination (Figure 5-7A). This indicated that a monomeric form of CD28 is not superagonisable on glass, but crosslinking *via* two antibodies enables superagonist-induced signalling. It was necessary to express larger amounts (~ 2-fold) of PDCD28 on the cell surface to observe signalling by the clone 2-clone 19 combination as compared to the amounts of CD28 needed to observe JJ316-induced signalling (Mai Vuong, Davis laboratory, University of Oxford; unpublished work). It was of interest to investigate whether the signalling induced by crosslinking PDCD28 was mediated by the CD28 cytoplasmic domain. A second construct was designed that lacked the CD28 cytoplasmic signalling motifs (Figure 5-5), truncPDCD28, that was analogous to truncCD28 (see Section 4.3.4). Very similar levels of IL-2 production were observed

for ligating truncPDCD28 with a clone 2-clone 19 combination on glass, when surface expression matched PDCD28 levels (Figure 5-7B). Corresponding observations were made on EIA plastic (data not shown). It was hypothesized that the CD28-independent signalling may be TCR-mediated, and to test this, $TCR^-$ BW5147 cells were transfected with either PDCD28 or truncPDCD28, matching expression in the $TCR^+$ cell lines. No signalling was observed when the $TCR^-$ cell lines were stimulated with a combination of clone 2 and clone 19 on glass (Figure 5-7) or on EIA plastic (data not shown), indicating that TCR signalling may indeed be responsible for the IL-2 response observed when truncPDCD28 is crosslinked, and it may contribute a large part of, or even be entirely responsible for the IL-2 response that is observed when PDCD28 is crosslinked.

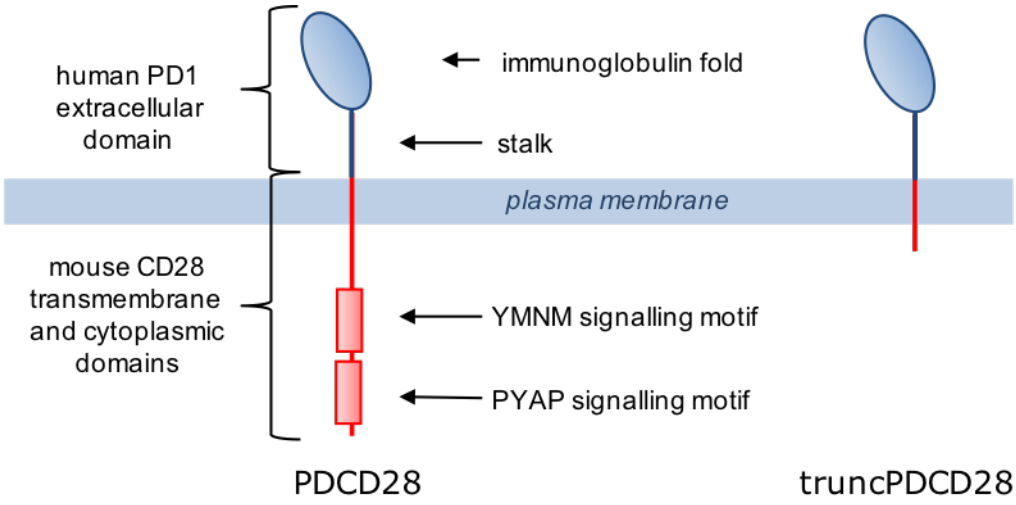



Figure 5-5: Design of a monomeric PDCD28 chimera[22]. The CD28 extracellular domain, which induces formation of the CD28 homodimer *via* a disulphide bond in the stalk region, was replaced with that of PD1, a monomeric receptor, giving the monomeric PDCD28 chimera.

[22] The full-length construct was designed by Sara Morgan, Davis laboratory, University of Oxford. Constructs were cloned by Rachel Knox, Davis laboratory, University of Oxford.

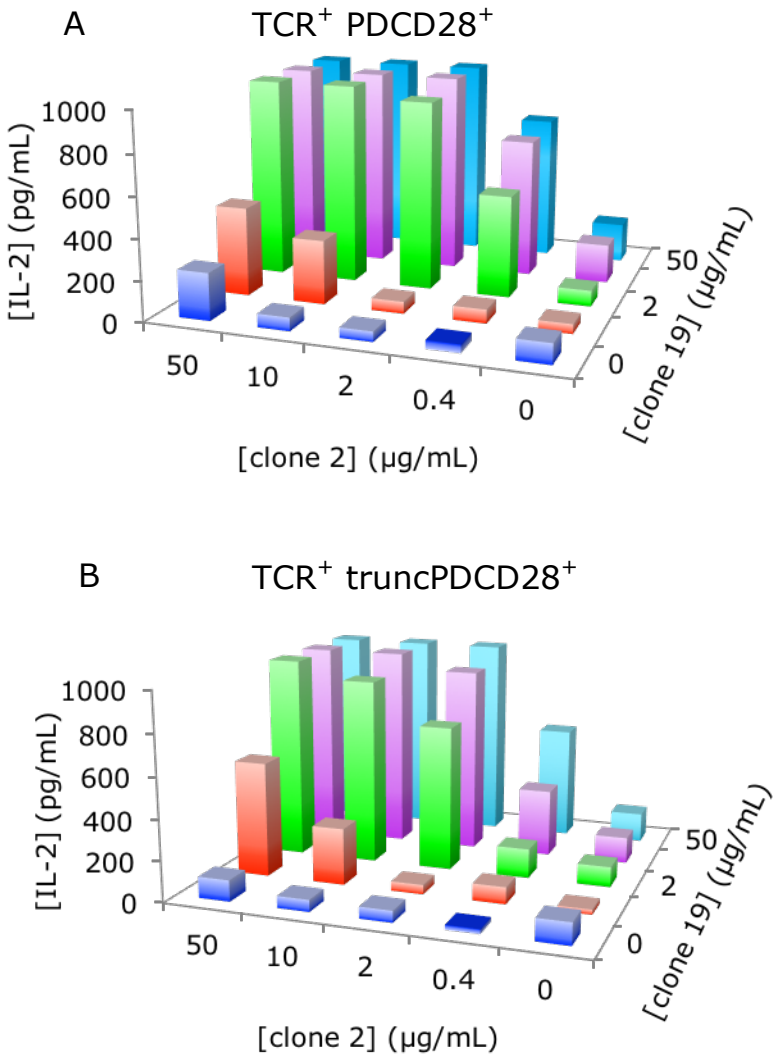



Figure 5-6: Crosslinking CD28 is required for superagonistic signalling. TCR$^+$ BW5147 cells were transfected with high levels of **A** PDCD28, or **B** truncPDCD28. Cells were incubated with a combination of clone 2 and clone 19 anti-PD1 antibodies, and then allowed to interact with DAM-coated glass surfaces. Clone 2 and clone 19 concentrations were titrated from 0 to 50 µg/mL. IL-2 production was assessed after 24 hours.

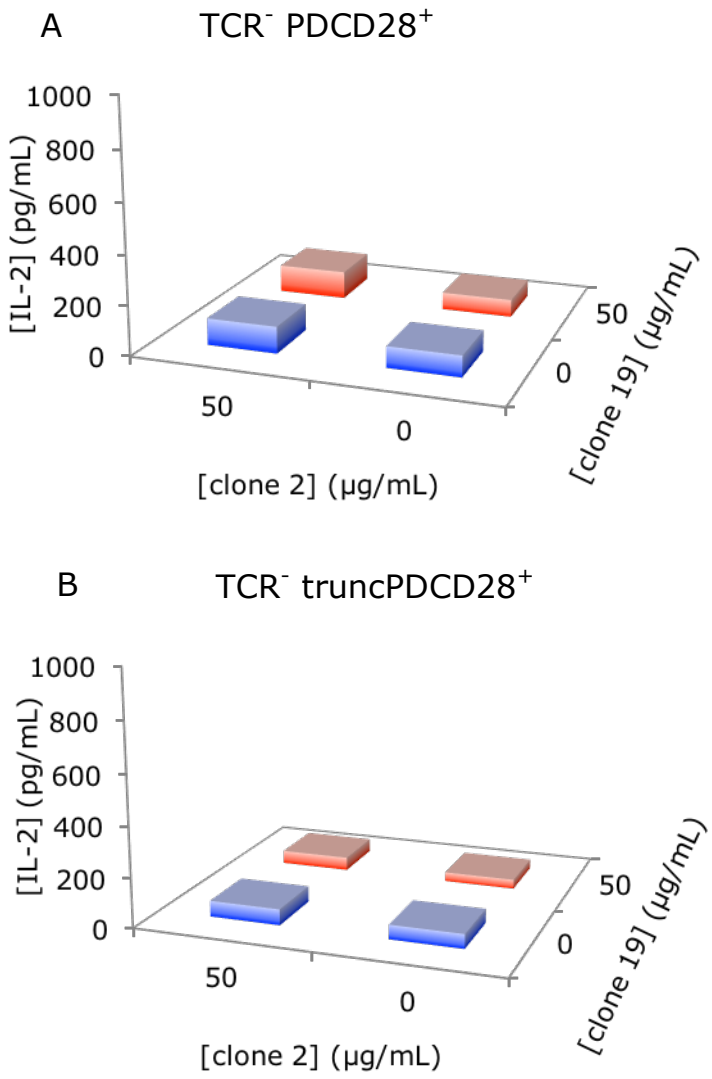



Figure 5-7: PDCD28 signalling induced by crosslinking is TCR-dependent. TCR$^-$ BW5147 cells were transfected with high levels of **A** PDCD28, or **B** truncPDCD28. Cells were incubated with a combination of clone 2 and clone 19 anti-PD1 antibodies, and then allowed to interact with DAM-coated glass surfaces. Clone 2 and clone 19 concentrations were titrated from 0 to 50 µg/mL. IL-2 production was assessed after 24 hours.

### 5.3.4. Superagonism is dependent on receptor dimensions

Previous work on anti-CD28 superagonism had established that it is sensitive to the receptor dimensions on EIA plastic [249]. A chimeric extended CD28 construct was designed, with a human IgG1 Fc-domain insertion in the CD28 stalk region that is expected increase the dimensions by ~ 75 Å (Figure 5-8; [249]). Matching the observations made on EIA plastic [249], ligating FcCD28 with JJ316 induced costimulatory, but not superagonistic signalling on glass*; i.e.* an IL-2 response was not observed when JJ316 was used on its own, but when it was used in combination with KT3, it reduced the minimal concentration of KT3 needed to induce IL-2 production (Figure 5-9B). Two antibodies against the Fc-domain insertion, HP6091 and IC10, that had previously been characterised [249] were used to stimulate FcCD28-expressing cells on glass. HP6091 binds membrane-distally whereas IC10 binds a membrane-proximal epitope on FcCD28 [249]. Observations made on EIA plastic [249] were reproduced on glass: whereas HP6091 was costimulatory, IC10 induced superagonistic signalling, generating an IL-2 response in the absence of co-activation with KT3 (Figure 5-9B). It was, however, necessary to express higher levels of FcCD28 to observe IC10-induced superagonistic signalling on glass (Table 5-1). At "medium" (see Section 4.3.4) levels of expression of FcCD28, IC10 by itself did not induce activation (Figure 5-9C), whereas "medium" rmCD28 expression allowed JJ316-induced superagonistic signalling (Figure 5-9A). IC10-induced superagonistic signalling on glass is FcCD28-rather than TCR mediated, since removing the cytoplasmic domain, giving truncFcCD28 (Figure 5-8), abrogated the IL-2 response (Figure 5-9C). In conclusion, anti-CD28 superagonistic signalling on glass is sensitive to the receptor dimensions, and a membrane-proximal epitope position is predictive of superagonism on glass, as on EIA plastic [249].

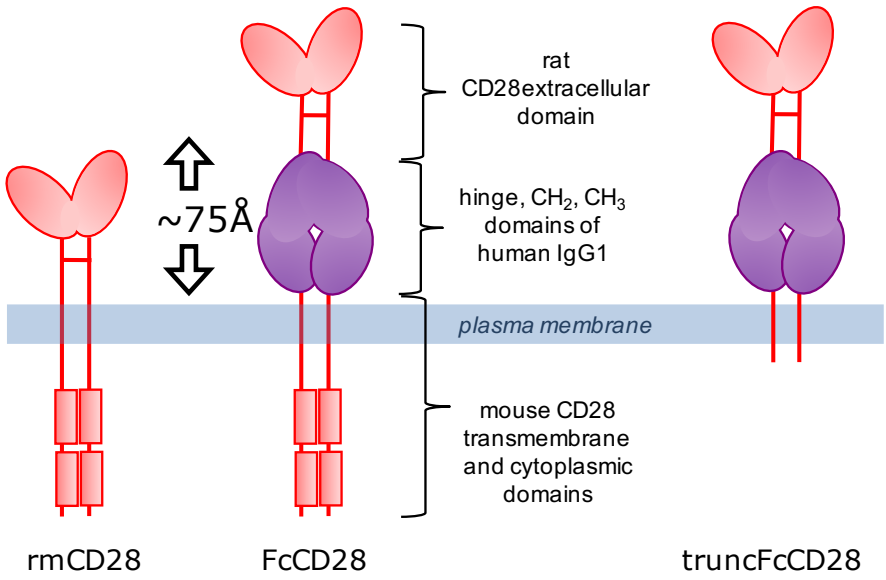



Figure 5-8: Design of an extended FcCD28 chimera[23]. CD28 was extended by ~ 75 Å with an IgG1 Fc-insertion in its stalk region. Signalling-competent (FcCD28) and signalling-disabled (truncFcCD28) forms were made, either including or omitting the CD28 cytoplasmic signalling motifs.

[23] The full-length construct was designed by Sara Morgan, Davis laboratory, University of Oxford; constructs were cloned by Rachel Knox, Davis laboratory, University of Oxford.

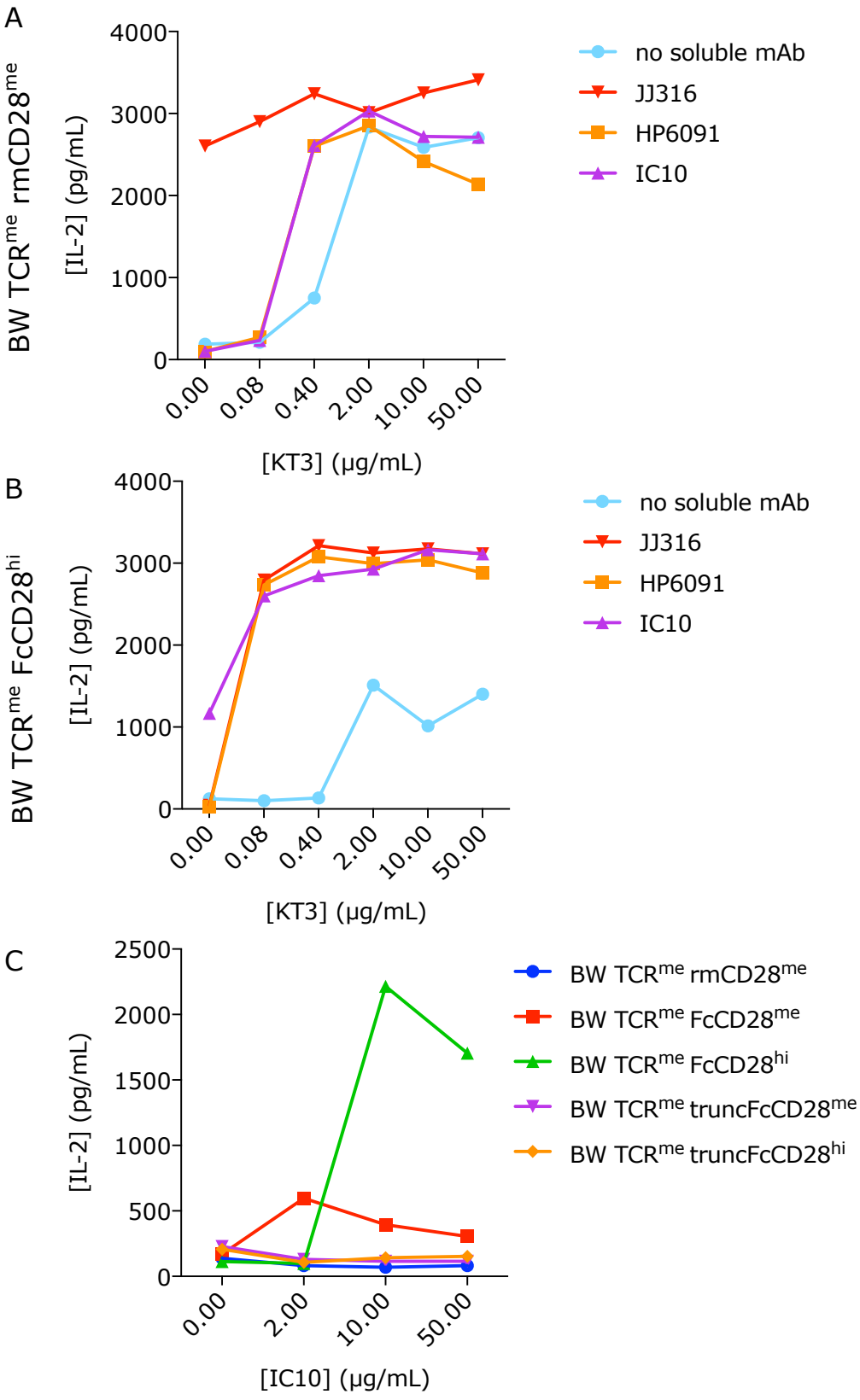

A
BW TCRme rmCD28me
[IL-2] (pg/mL)
4000
3000
2000
1000
0
0.00
0.08
0.40
2.00
10.00
50.00
[KT3] (µg/mL)
no soluble mAb
JJ316
HP6091
IC10
B
BW TCRme FcCD28hi
[IL-2] (pg/mL)
4000
3000
2000
1000
0
0.00
0.08
0.40
2.00
10.00
50.00
[KT3] (µg/mL)
no soluble mAb
JJ316
HP6091
IC10
C
[IL-2] (pg/mL)
2500
2000
1500
1000
500
0
0.00
2.00
10.00
50.00
[IC10] (µg/mL)
BW TCRme rmCD28me
BW TCRme FcCD28me
BW TCRme FcCD28hi
BW TCRme truncFcCD28me
BW TCRme truncFcCD28hi

Figure 5-9: Extending the CD28 extracellular domain abrogates superagonism. In **A** and **B,** $TCR^+$ BW5147 cells were transfected with rmCD28 (A) or FcCD28 (B) at high expression, and stimulated with a titration of KT3 that was directly coated on glass together with DAM secondary antibody. Cells were incubated with 10 μg/mL JJ316, or anti-Fc antibodies HP6091 or IC10, as indicated in the right-hand legends, and then allowed to interact with the coated glass surface. IL-2 secretion was assessed after 24 hours. In **C** $TCR^+$ BW5147 cells were transfected with rmCD28 at medium expression, FcCD28 at medium or high expression, or truncFcCD28 at medium or high expression, as indicated in the right-hand legend. Cells were incubated with a titration of IC10 and then allowed to interact with DAM-coated glass. IL-2 secretion was assessed after 24 hours. The A, B, and C data is plotted on a non-linear scale x-axis. Results for one out of two independent repeats are shown.

Table 5-1: Surface expression of CD3 and CD28 in BW5147 cells.

| Cell line | MFI* CD28 | MFI* CD3 |
|---|---|---|
| BW $TCR^{me}$ $rmCD28^{me}$** | 216** | 137** |
| BW $TCR^{me}$ $FcCD28^{me}$ | 189 | 152 |
| BW $TCR^{me}$ $FcCD28^{hi}$ | 1204 | 88 |
| BW $TCR^{me}$ $truncFcCD28^{me}$ | 209 | 119 |
| BW $TCR^{me}$ $truncFcCD28^{hi}$ | 757 | 147 |

* Mean fluorescence intensity as assessed by flow cytometry, in relative units.
** Expression levels that lead to superagonistic signalling when rmCD28, but not truncCD28 is ligated with JJ316; see Section 4.3.4.

### 5.3.5. Superagonism is sensitive to phosphatase dimensions

Confirming that antibody superagonism depends on the receptor dimensions supported the hypothesis that the superagonist is particularly potent because it sterically excludes phosphatases more efficiently. Testing this hypothesis further, it was important to investigate whether superagonistic signalling is sensitive to the phosphatase dimensions. The receptor-type protein-tyrosine phosphatases CD45 and CD148 both consist of a large, heavily glycosylated extracellular region that is made up of several fibronectin type-3 domains and an N-terminal mucin-like domain, a transmembrane domain, and two intracellular phosphatase domains (Figure 5-10). HA-tagged chimeric forms comprising the rat extracellular and mouse

intracellular and transmembrane domains were designed[24], either spanning the entire sequence of the phosphatases (rmCD45 and rmCD148), or truncated forms (LAT-CD45 and LAT-CD148) wherein the extracellular and transmembrane domains were replaced with those of mouse LAT, a transmembrane protein with a small extracellular domain comprising only four amino acids (Figure 5-10). rmCD28-expressing, $TCR^+$ BW5147 cells were transfected with either rmCD45, LAT-CD45, rmCD148, or LAT-CD148, and the levels of expression of the full-length (rm) and truncated (LAT) proteins were matched, as confirmed by flow cytometry using an antibody against the HA-tag[25] (Table 5-2). Because in preliminary experiments both CD148 and CD45 expressed poorly, the DNA construct sequences were codon-optimised to improve expression.

Co-expression of LAT-CD148, but not rmCD148, completely abrogated JJ316-indued superagonistic signalling on glass, even at high antibody concentrations (Figure 5-11B). For CD45, the effect was less pronounced; LAT-CD45 significantly decreased the IL-2 response induced by high concentrations of JJ316 ($p=0.0143$), but did not completely abrogate JJ316-induced superagonistic signalling on glass (Figure 5-11A, Table 5-3). Expression of the chimeric CD45 forms was relatively low (Table 5-2), and cells started to down-regulate expression after several days; it is thus possible that higher and more stable expression of LAT-CD45 would completely abolish the IL-2 response. These results match observations made on EIA plastic (Sara Morgan, Davis laboratory, University of Oxford; unpublished work). In conclusion, antibody superagonism is sensitive to the dimensions of receptor-type protein-tyrosine phosphatases.

[24] Designed by Sara Morgan and cloned by Rachel Knox and Mai Vuong, Davis laboratory, University of Oxford.
[25] Transfection of cell lines and flow cytometry analysis was performed by Mai Vuong, Davis laboratory, University of Oxford.

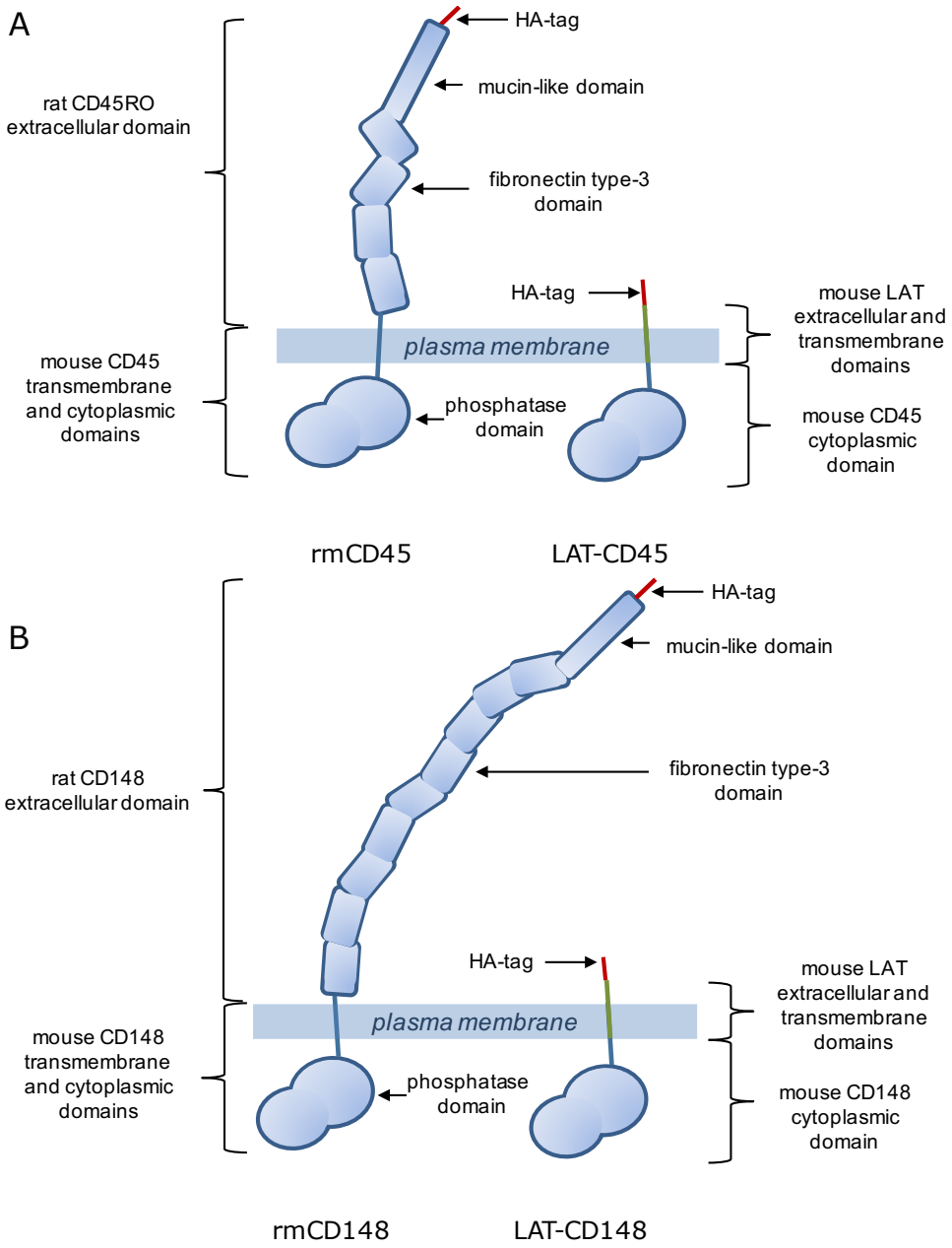



Figure 5-10: Design of chimeric full-length and truncated phosphatases[26]. HA-tagged **A** CD45 and **B** CD148 constructs were designed that either span the full-length phosphatase sequence (rmCD45, rmCD148), or that are truncated in the extracellular region (LAT-CD45, LAT-CD148), expressing the very short LAT extracellular region in place of the large phosphatase extracellular region.

[26] Designed by Sara Morgan and cloned by Mai Vuong, Davis laboratory, Oxford.

The requirements for antibody superagonism are compatible with a "kinetic-segregation" based theory of signalling

Table 5-2: Surface expression of CD45 and CD148 in BW5147 cells[27].

| Cell line | MFI* CD148 | MFI* CD45 |
|---|---|---|
| BW CD3δζ rmCD28 | 3 | 1.5 |
| BW CD3δζ rmCD28 rmCD45** | n.a. | 25.5 |
| BW CD3δζ rmCD28 LAT-CD45** | n.a. | 27 |
| BW CD3δζ rmCD28 rmCD148*** | 32 | n.a. |
| BW CD3δζ rmCD28 LAT-CD148*** | 32 | n.a. |

* Mean fluorescence intensity as assessed by flow cytometry, in relative units.
** The TCR was expressed at "low" levels (see Section 4.3.4)
*** The TCR was expressed at "medium" levels (see Section 4.3.4)

Table 5-3: Non-linear regression with a binding model† quantifies suppression of superagonistic signalling by truncated phosphatases

| Stimulation with a JJ316 titration | | | |
|---|---|---|---|
| | no phosphatase | rmCD45 | LAT-CD45 |
| Maximum | 104 | 108 | 61* |
| n | 1.68 | 0.85 | 1.51 |
| EC50 | 15.41 | 25.19 | 7.10 |
| Minimum | 11 | 4 | 13 |
| | no phosphatase | rmCD148 | LAT-CD148 |
| Maximum | 995 | 1098 | not converged |
| n | 1.45 | 1.39 | not converged |
| EC50 | 5.21 | 5 | not converged |
| Minimum | =0 | =0 | not converged |

* different from no phosphatase p=0.0143; different from rmCD45 p =0.0167
† [IL-2] = Maximum * $[JJ316]^n/(EC50^n + [JJ316]^n)$ + Minimum, where Maximum = [IL2] at maximal [JJ316]; EC50 = [JJ316] that gives half-maximal [IL-2]; n = Hill-slope, Minimum = [IL-2] for [JJ316] = 0

### 5.3.6. Superagonism is sensitive to antibody dimensions

#### Design of extended JJ316 antibodies

Having shown that antibody superagonism is sensitive to both the receptor and the phosphatase dimensions prompted the question of whether extending the JJ316 dimensions would affect signalling. In collaboration with Absolute Antibody Ltd., a JJ316-derived antibody was engineered that was extended with an insertion in the

[27] Transfection of cell lines and flow cytometry analysis was performed by Mai Vuong.

hinge domain (Figure 5-12). A heavily glycosylated sequence originating from the human CD43 N-terminal mucin-like domain was selected to create a rigid, inflexible insertion that would extend the overall dimensions of the antibody. Two different forms were made, with either a 30 amino acid[28] or a 50 amino acid[29] insertion. A 30 amino acids extension was expected to increase the size of the antibody (along an axis parallel with the long axis of the Fc domain) by 75 Å, based on the prediction that each amino acid adds 2.5 Å. The 30 amino acid insertion is thus predicted to correspond to the 75 Å extension of CD28 by insertion of an Fc region (FcCD28; see Section 0), and to the 75 Å difference in height between the JJ316/CD28 and the JJ319/CD28 complexes [251]. In case a more significant extension may be necessary to observe an effect on signalling, a more extreme extension of 50 amino acids was also inserted. To ensure that the chains of the engineered antibody would dimerise and fold correctly, it was important not to hinder the formation of the interchain disulphide bonds [261]. There are four cysteines in the heavy chain linker region that are involved in interchain disulphide bond formation (Figure 5-13; [262]). Whereas three disulphide bonds stabilise the interaction between the two heavy chains, only the N-terminal most of the four (*i.e.* C2; Figure 5-13) pairs with a cysteine of the light chain [262] and is thus particularly important for the stability of the antibody quaternary structure. The insertion was made immediately downstream of this cysteine, starting with a very short glycine-serine linker giving enough flexibility such that formation of the disulphide and the O-linked glycosylation of the CD43 insertion were each unhindered. A second glycine-serine linker was added to connect the CD43 insertion to the downstream Fc sequence, including the remaining three cysteines involved in inter-chain disulphide bond formation (Figure 5-13). Constructs encoding the two extended JJ316 forms were expressed, and the resulting antibodies purified by Absolute Antibody Ltd.

[28] Amino acid sequence: RTTMLPSTPHITAPSTSEAQNASPSVSVGS
[29] Amino acid sequence:
RTTMLPSTPHITAPSTSEAQNASPSVSVGSGTVDSKETISPWGQTTIPVS

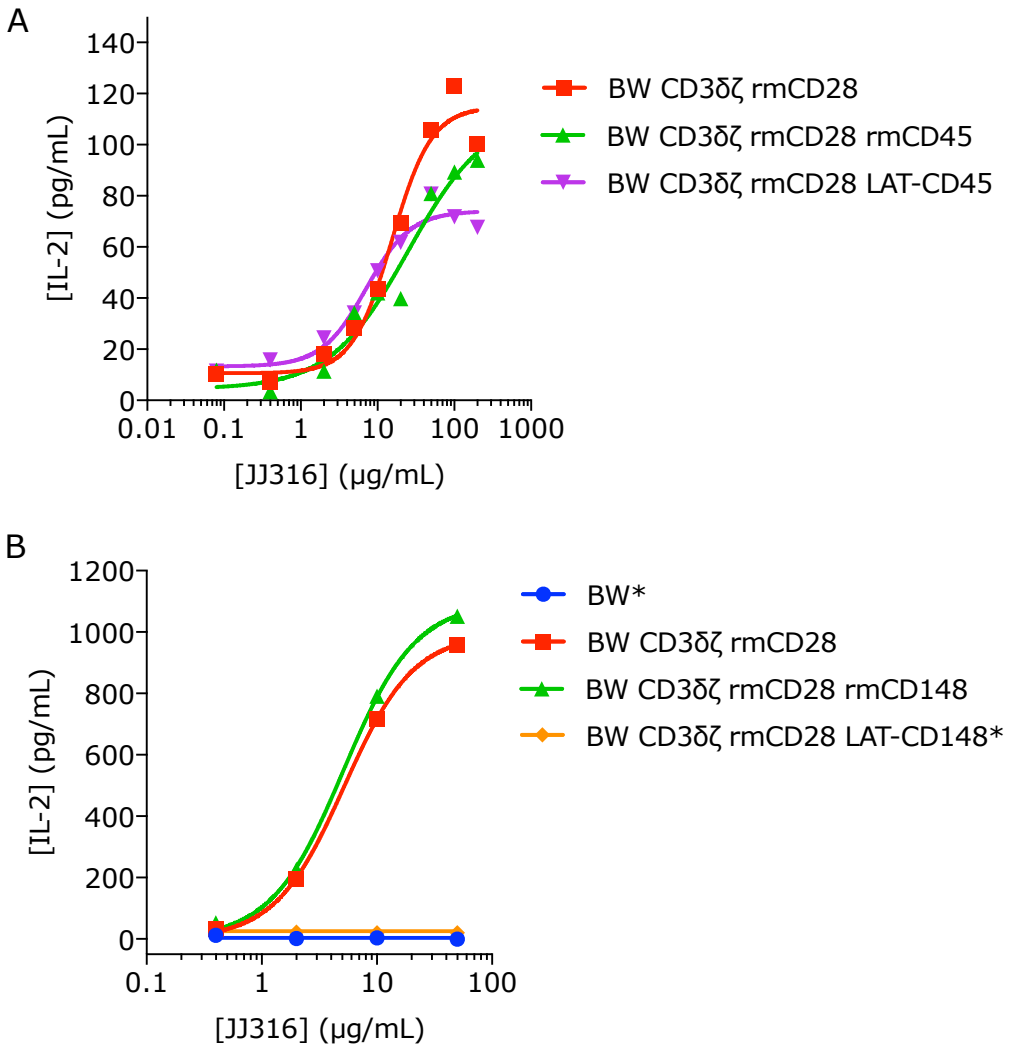



Figure 5-11: JJ316-induced superagonistic signalling is sensitive to the CD148 and CD45 phosphatase dimensions. In **A** $TCR^+$ BW5147 cells were transfected with rmCD28 and with either rmCD45 or LAT-CD45. In **B** $TCR^+$ BW5147 cells were transfected with rmCD28 and with either rmCD148 or LAT-CD148. In A and B untransfected $TCR^-$ BW5147 cells were included as a negative control. Cells were incubated with a titration of JJ316, and then allowed to interact with DAM-coated glass. IL-2 production was measured after 24 hours. Data were fitted with a binding model†, or, where indicated with an asterisk, with a horizontal line because it was the preferred fit as determined by an F-test.

† $[IL\text{-}2] = Maximum * [JJ316]^n/(EC50^n + [JJ316]^n)$; where Maximum = [IL2] at maximal [JJ316]; EC50 = [JJ316] that gives half-maximal [IL-2]; n = Hill-slope

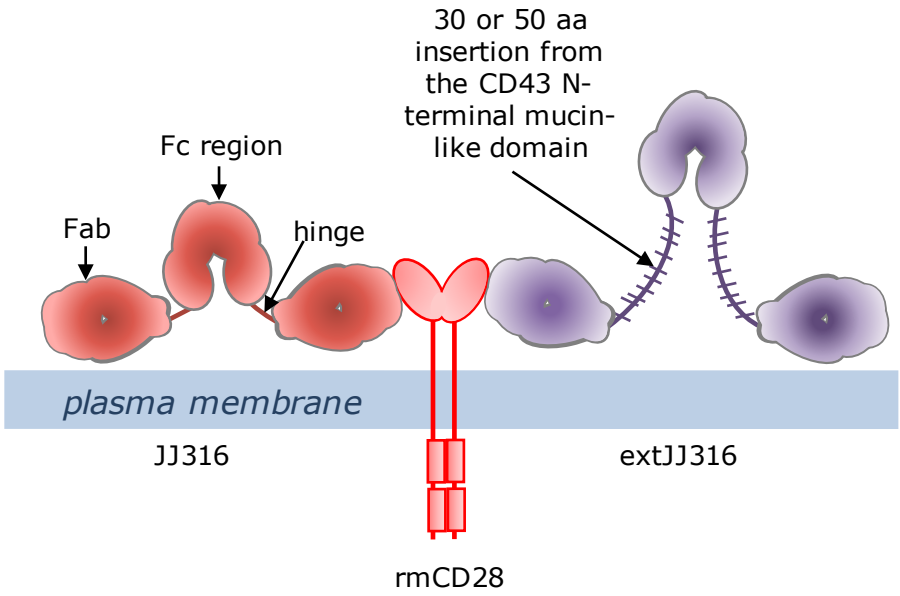



Figure 5-12: Schematic depiction of an extended JJ316 form. A 30 or 50 amino acid sequence derived from the CD43 N-terminal mucin-like domain is inserted in the hinge region of JJ316, which connects the Fc region to the Fab fragments. A 30 amino acid insertion is predicted to extend the antibody by 75 Å.

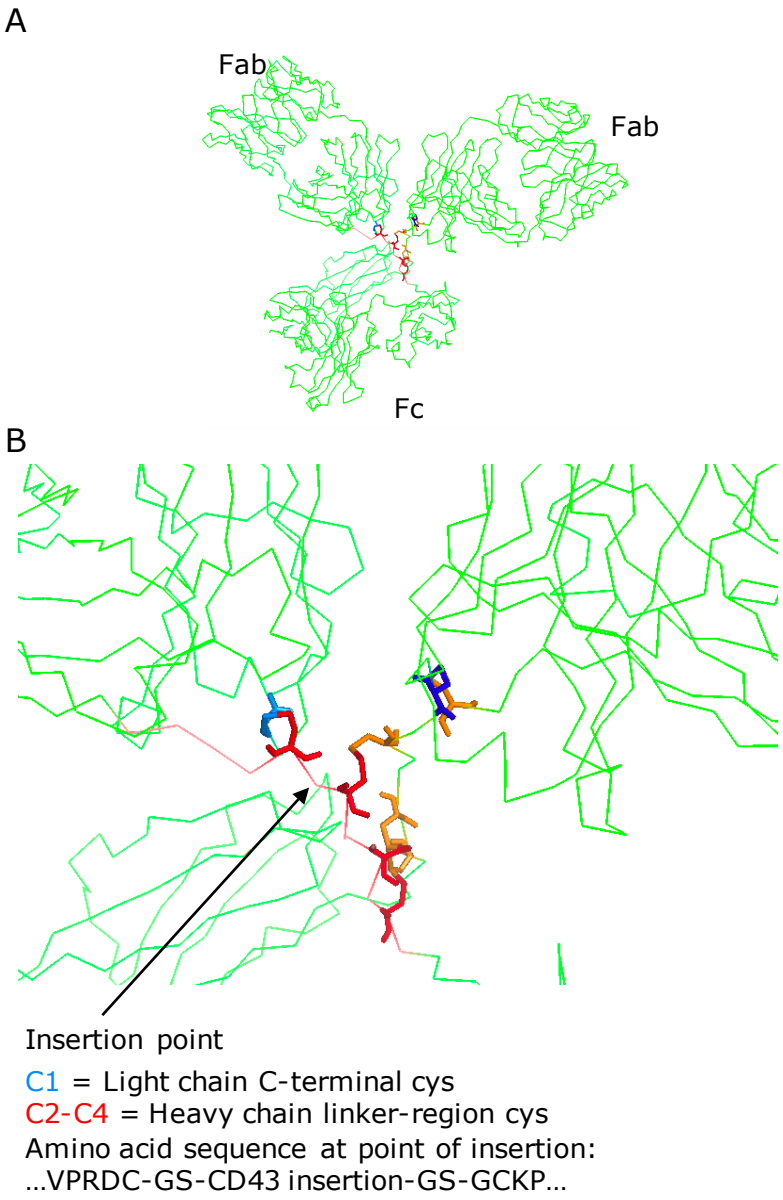



Figure 5-13: Design of a JJ316 antibody extended in the hinge region[30]. **A** Overview of the quaternary structure of an IgG antibody. **B** Detailed view of the IgG hinge region, annotating the insertion point of a 30 or 50 amino acid CD43 sequence to extend the antibody.

[30] Designed by Meike Aßmann and Simon Davis, University of Oxford, in collaboration with Michael Fiebig and Ian Wilkinson, Absolute Antibody Ltd.

### 5.3.7. The extended JJ316 antibodies are demonstrably larger

It was important to confirm that the extended forms with the 30 amino acid (extJJ316+30) and 50 amino acid (extJJ316+50) insertions were larger than JJ316. The three antibodies were subjected to size exclusion chromatography, both separately and as a mixture. Size exclusion chromatography separates biomolecules *via* a porous Sepharaose matrix. Smaller molecules are retained as they are able to enter small pores, whereas larger molecules pass through more quickly as they are excluded from the pores. Size is thus inversely correlated with elution volume. The chromatograms corresponding to the three separate antibodies were overlaid, revealing that extJJ316+50 eluted first, followed by extJJ316+30 and unmodified JJ316 (Figure 5-14). When the antibodies were pooled and re-run, two separate peaks eluted,

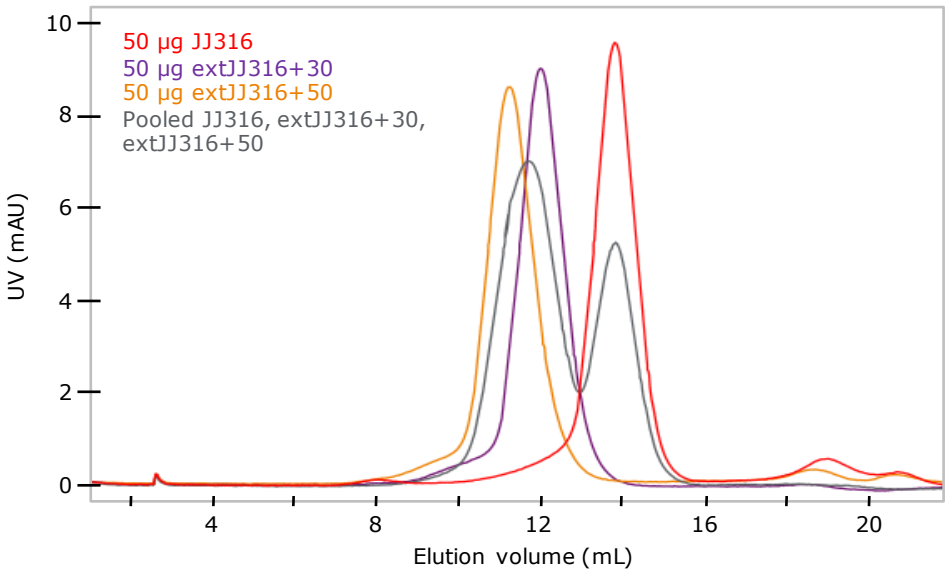



Figure 5-14: Custom-engineered extended JJ316 antibodies[31] are demonstrably larger. 50 µg unmodified JJ316, extJJ316+30, and extJJ316+50 were subjected to size exclusion chromatography. Elution of the antibodies was detected by the absorbance of ultraviolet light. Chromatograms are displayed for injecting the different antibodies separately (blue, orange and green curves), or as a mixture of ~ 20 µg of each antibody (purple curve). An Äkta FPLC system was used, fitted with a Sepharaose 200 column of size 10/300. The antibody was injected and eluted in PBS.

the first corresponding to the extended antibodies, which appeared to co-elute in a broad peak, and to unmodified JJ316, respectively (Figure 5-14). Therefore, extension with a CD43 insertion was successful and the extended antibodies were demonstrably larger than unmodified JJ316.

**Extending JJ316 dimensions does not prevent it from binding cell-expressed CD28 and plate-bound secondary antibody**

Before extJJ316+30 and extJJ316+50 were compared to unmodified JJ316 in a stimulation assay, it was important to confirm that they were able to bind both CD28 and secondary antibody. A flow-cytometry experiment confirmed that the extended antibodies bound cell-surface expressed rmCD28 to the same extent as unmodified JJ316 (Figure 5-15, Table 5-4), and in an ELISA with plate-bound secondary antibody no significant differences (student's t-test) in binding were detected (Figure 5-16).

**The extended JJ316 antibodies act costimulatory, but not superagonistic**

When the extended JJ316 antibodies were used to stimulate $TCR^+$, rmCD28-expressing BW5147 cells in combination with KT3, they significantly lowered the concentration of KT3 required to induce half-maximal signalling ($p<0.0001$), fulfilling the definition of costimulatory activity ( Figure 5-17A, Table 5-5). However, in contrast to unmodified JJ316, they failed to induce an IL-2 response when used in the absence of KT3 co-activation ( Figure 5-17B). Extending JJ316 with either a 30 or a 50 amino acid insertion therefore abrogated its superagonistic activity and transformed it into a conventional (*i.e.* costimulatory) antibody. In conclusion, antibody superagonism is sensitive not only to the receptor- and phosphatase-, but also the antibody dimensions, with the potency of the antibody correlating with its dimensions.

[31] Cloned, produced and purified by Absolute Antibody Ltd.

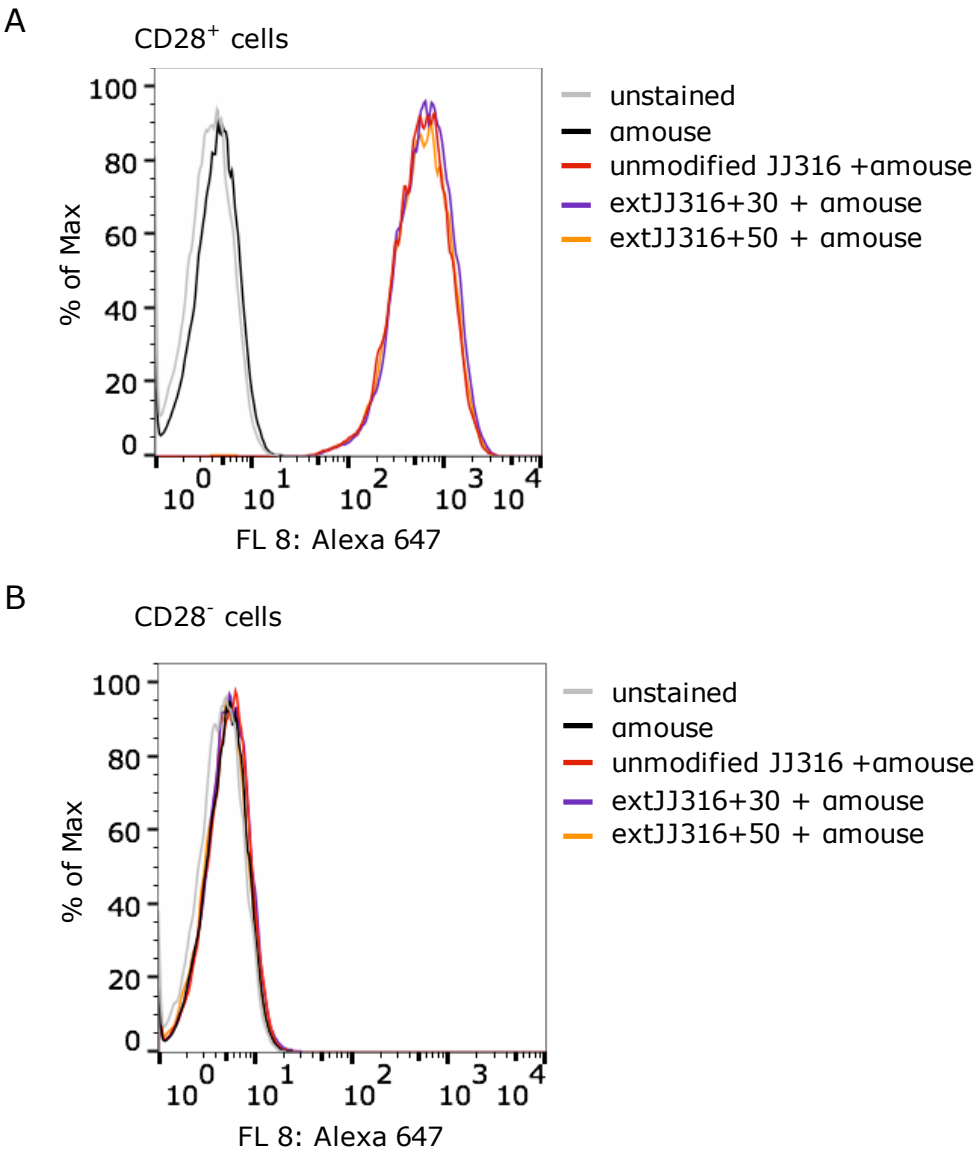



Figure 5-15: Extended JJ316 forms bind cells-surface expressed rmCD28. **A** rmCD28-transfected or **B** untransfected BW5147 cells were coated with unmodified or extended JJ316 antibody, or no antibody, followed by incubation with Alexa647®-coupled anti-mouse secondary antibody, as indicated in the right-hand legend. The fluorescence of single cells was measured by flow cytometry, indicating the amount of anti-mouse-Alexa647® bound per cell.

Table 5-4: Flow cytometry quantifies the binding of unmodified *versus* extended JJ316 to cells-surface expressed rmCD28.

| Cell line | BW | BW CD3δζ rmCD28 |
|---|---|---|
| unstained | 4.13 | 3.54 |
| αmouse | 4.89 | 4.24 |
| extJJ316+50 + αmouse | 4.81 | 541 |
| extJJ316+30 + αmouse | 5.18 | 590 |
| unmodified JJ316 +αmouse | 5.07 | 544 |

Values state mean fluorescence intensity as assessed by flow cytometry, in relative units.

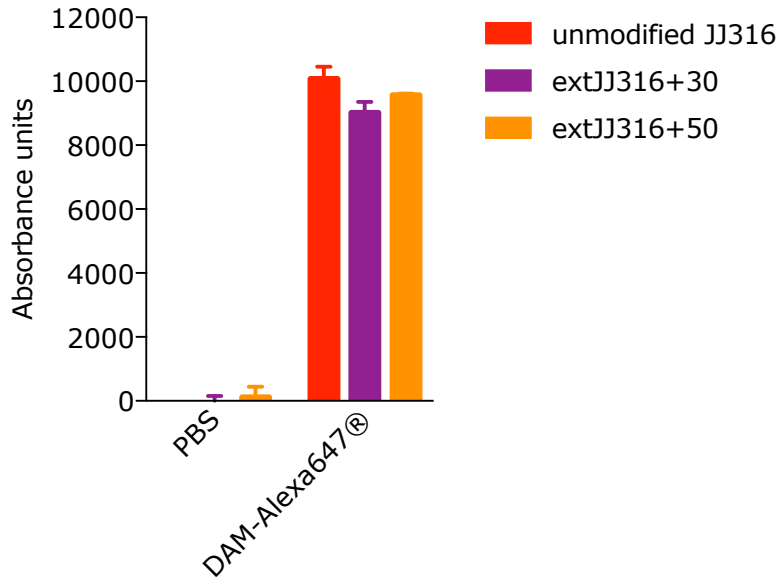



Figure 5-16: Extended JJ316 antibodies bind to plate-bound secondary antibody. An EIA-plastic surface was coated with 500 μg/mL DAM secondary antibody and washed. 10 μL unmodified or extended JJ316, as indicated in the right-hand legend, was incubated for one hour at room temperature, and washed. To detect bound antibody, 25 μg/mL Alexa647®-coupled DAM secondary antibody, or PBS, was incubated for one hour at room temperature, and washed. Fluorescence at 647 nm was detected with a Clariostar fluorescence microplate reader.

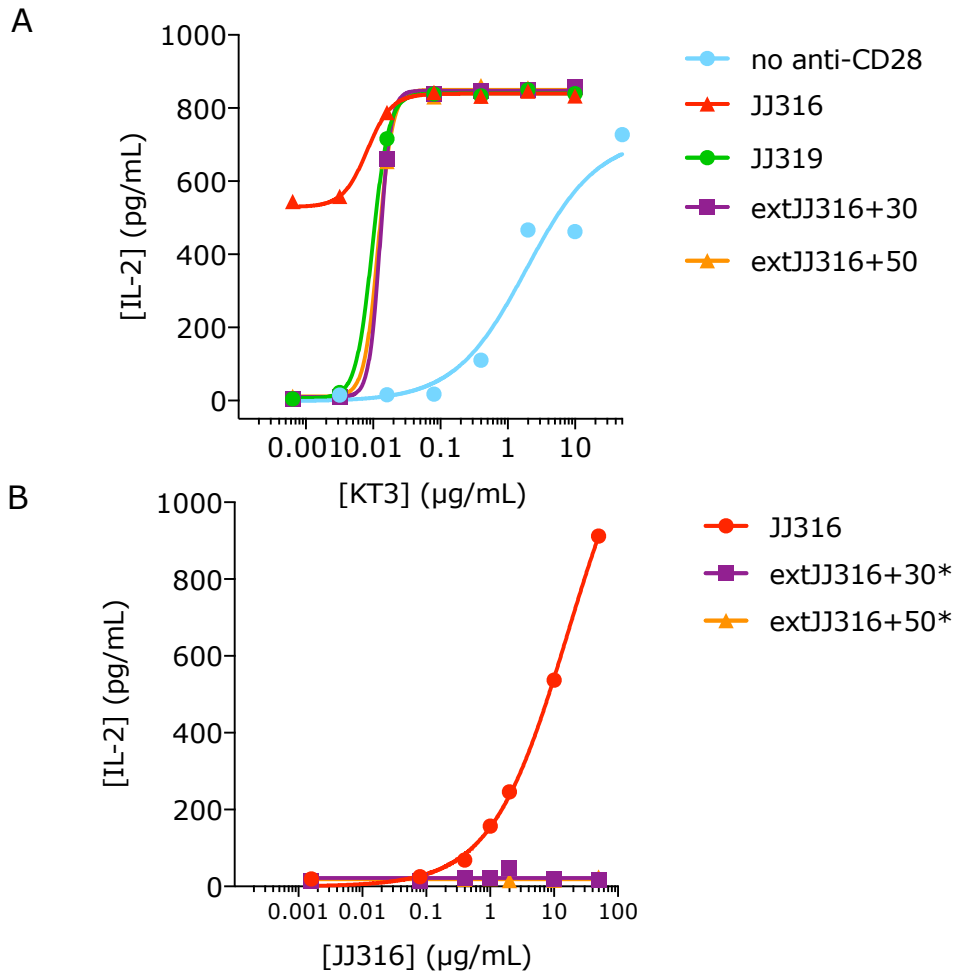



Figure 5-17: Extended JJ316 antibodies are costimulatory, but not superagonistic. In **A** $TCR^+$ BW5147 cells were transfected with rmCD28, and stimulated with a titration of KT3 that was directly coated on glass together with DAM. Cells were incubated with 10 µg/mL JJ316, JJ319, extJJ316+30, or extJJ316+50, as indicated in the right-hand legend, and then allowed to interact with the coated glass surface. In **B** $TCR^+$ BW5147 cells were transfected with rmCD28. Cells were incubated with a titration of unmodified JJ316, extJJ316+30 or extJJ316+50, as indicated in the right-hand legend, and then allowed to interact with DAM-coated glass. In A and B, IL-2 secretion was assessed after 24 hours. Data were fitted with a binding model†, or, where indicated with an asterisk, with a horizontal line because it was the preferred fit as determined by an F-test. For more convenient visualisation data are shown on a logarithmic scale, thus not showing zero on the x-axis. The zero values were, however, included in the fitting and analysis.

† for A $[IL\text{-}2] = Maximum * [KT3]^n/(EC50^n + [KT3]^n) + Minimum$; where Maximum = [IL2] at maximal [KT3]; EC50 = [KT3] that gives half-maximal [IL-2]; n = Hill-slope, Minimum = [IL-2] for [KT3] = 0;
for B $[IL\text{-}2] = Maximum * [JJ316]^n/(EC50^n + [JJ316]^n)$; where Maximum = [IL2] at maximal [JJ316]; EC50 = [JJ316] that gives half-maximal [IL-2]; n = Hill-slope

Table 5-5: Non-linear regression with a binding model† quantifies the costimulatory activities of the extended JJ316 antibodies.

| Co-activation with KT3 | | | | | |
|---|---|---|---|---|---|
| | no anti-CD28 | JJ316 | JJ319 | extJJ316+30 | extJJ316+50 |
| n | 0.815 | 2.398 | 3.553 | 5.305 | 4.142 |
| EC50 | 1.888 | 0.008 | 0.010* | 0.013** | 0.012*** |
| Minimum | -2 | 529**** | 7 | 10 | 11 |

* different from no anti-CD28 p<0.0001
** different from no anti-CD28 p<0.0001
*** different from no anti-CD28 p<0.0001
**** different from no anti-CD28 p<0.0001
† [IL-2] = Maximum * $[KT3]^n/(EC50^n + [KT3]^n)$ + Minimum; where Maximum = [IL2] at maximal [KT3]; EC50 = [KT3] that gives half-maximal [IL-2]; n = Hill-slope, Minimum = [IL-2] for [KT3] = 0

### 5.3.8. Superagonism may be a quantitative phenomenon

It was also of interest whether the observed differences in potency between JJ316 and JJ319 are of a qualitative or a quantitative nature; that is, whether JJ319 could ever induce superagonistic signalling. Under the conditions used in Section 4.3.1, superagonistic signalling by JJ319 was not observed even when it was used at very high concentrations. Section 4.3.2 showed that the threshold antibody concentration needed to observe JJ316-induced superagonistic signalling was decreased when it was indirectly immobilised on glass *via* DAM. In that case, DAM was directly coated on the glass surface at high pH; however, immobilisation in this approach could still be limiting. First, the native confirmation of the secondary antibody may be affected by the coating conditions. Second, the antibody is coated at random orientation, and therefore only a small fraction will be in an "upright" orientation capable of binding its ligand (*i.e.* JJ316 or JJ319). Therefore, the question arose of whether more efficient indirect immobilisation of the antibodies would result in further lowering the threshold for superagonistic signalling such that full T-cell activation could be induced by ligating CD28 even with JJ319. This idea prompted a search for a more efficient way to indirectly immobilise antibodies. Proteins can be immobilised on "nickelated" surfaces specifically, and in the desired orientation, *via* a His-tag interaction. A His-tagged soluble Fc receptor was therefore used as a replacement for the secondary antibody to

immobilise JJ316 or JJ319 *via* their Fc regions. Among the Fc receptors expressed by murine cells, only FcγRIIb is reported to bind to mouse IgG1 antibodies [61].

**Design and production of a soluble mFcγRIIb-His construct**

A soluble mFcγRIIb construct was designed, comprising of: the native signal peptide to ensure secretion of the protein, the extracellular domain of the receptor including the ligand binding site, and a C-terminal tag with two hexahistidine sequences interspaced with a short linker (Figure 5-18; [153]). The His-tag was constructed in such a way as to ensure an "upright" orientation of the receptor, resembling the native conformation when inserted in the plasma membrane of a cell to allow binding of its antibody ligand; a tag comprised of two sets of six histidines separated by a short spacer optimised for attaching soluble protein to nickelated lipids in supported lipid bilayers in an "upright" orientation was used [153]. In terms of length, the extracellular domain sequence was homologous to that of a soluble human FcγRIIb protein that had been successfully produced for the determination of its crystal structure [263].

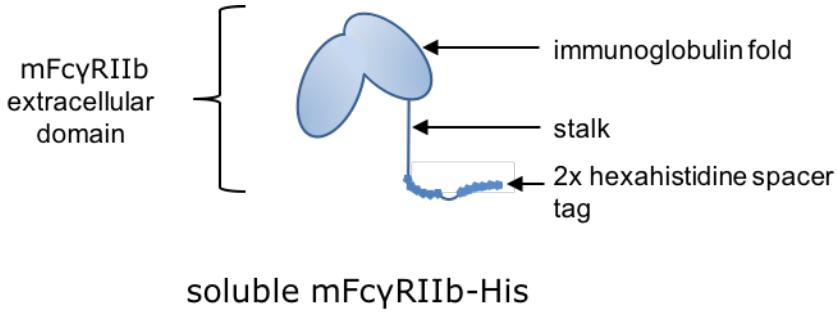



Figure 5-18: Design of a His-tagged soluble mFcγRIIb construct.

Primers were designed that introduce a MluI restriction site at the 5' end preceding the start codon, and a NotI restriction site at the 3' end following the His-tag and the stop codon. The MluI and NotI restriction sites were used to insert the sequence into the pHR vector (see Figure 2-1)[32]. A mammalian expression system (Chinese hamster ovary cells) was chosen to facilitate correct folding and glycosylation of the Fc receptor

[32] Performed by Shirley Yang, Princeton University, under the author's supervision.

construct. A lentiviral transfection system was chosen because good yields can be achieved in a much shorter time period than when a clonal selection approach is chosen. For virus production, a HEK-293T cell line was transfected with the pHR vector containing the gene of interest, and the packaging vectors pMDG and p8.91 (see Section 2.6)[33]. After 48 hours the virus was harvested and used to transduce a CHO-K1 cell line for protein production[33].

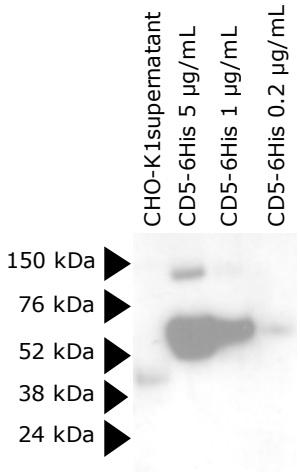



Figure 5-19: Western blot confirms expression of mFcγRIIb-His[33]. Samples were separated on a 12 % acrylamide gel. 7.5 µL cell culture supernatant, or His-tagged CD5 as a positive control, was loaded, under non-reducing conditions. The protein was transferred onto a nitrocellulose membrane and probed with an anti-penta-His antibody (Qiagen, 34660) and an HRP-conjugated secondary antibody (Sigma-Aldrich, A1063), and then incubated with Pierce ECL Western blotting substrate. Luminescence was detected on an x-ray film.

The transduced cell line was expanded, and ten days post-transduction the cellular supernatant was analysed by Western blot to confirm expression of the Fc receptor (Figure 5-19)[33]. Based on the amino-acid sequence, the unglycosylated construct is expected to have a molecular mass of 27.5 kDa. The band observed between 38 and 52 kDa (Figure 5-19) likely represents glycosylated mFcγRIIb-His. Comparing the

[33] Performed by Shirley Yang, Princeton University, under the author's supervision.

intensity of the band to the positive control, approximately 0.2 mg/mL mFcγRIIb-His was present in the supernatant (Figure 5-19).

A 500 mL culture was inoculated with the transduced CHO-K1 cells[34]. The soluble Fc receptor was purified from the cell culture supernatant by affinity chromatography, using NiNTA-coupled Sepharaose that binds to the hexahistidine-tagged protein, and the protein was eluted with imidazole[34]. Elution fractions were characterised by SDS-PAGE (data not shown)[34].

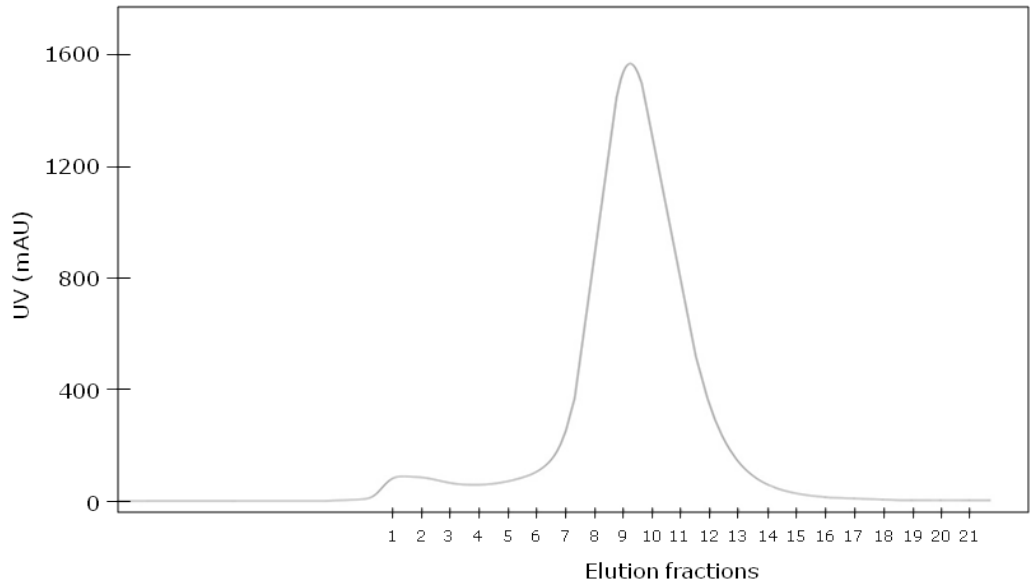



Figure 5-20: Purification of soluble mFcγRIIb-His with size exclusion chromatography[34]. An Äkta FPLC system was used, fitted with a Sepharaose 200 column of size 10/300. The protein was eluted with HBS-azide 0.05 %, and 500 μL fractions were collected.

The fractions were pooled and subjected to size exclusion chromatography[34]. A single peak eluting in fractions 6-12 indicated pure protein free from aggregates (Figure 5-20). The purity of the protein was confirmed by SDS-PAGE (Figure 5-21)[34]. A size of ~ 30-50 kDa as seen on the non-reducing and reducing gels is as expected for glycosylated soluble mFcγRIIb-His (Figure 5-21). The size shift across the peak likely correlates

[34] Performed by Shirley Yang, Princeton University, under the author's supervision.

with the presence of different glycosylation forms of the receptor (Figure 5-21). Fractions 6-12 were pooled and stored at -20 ºC. ~ 6 mg protein was purified from the 500 mL culture.

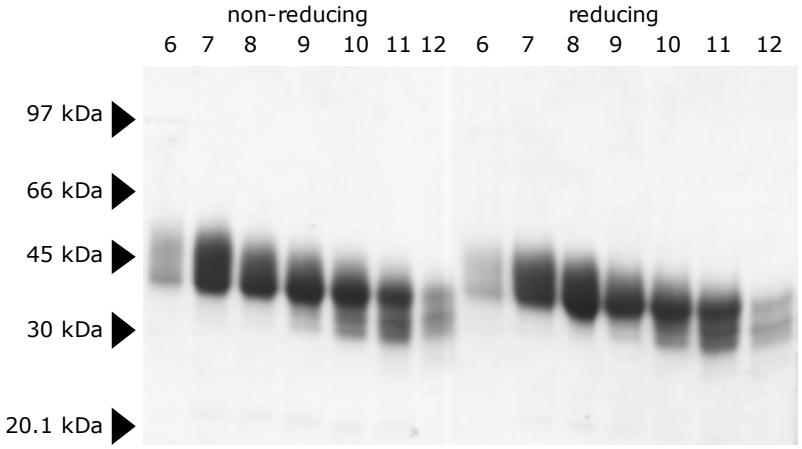



Figure 5-21: SDS-PAGE of purified soluble mFcγRIIb-His[35]. Samples were separated on a 12 % acrylamide gel. 10 μL of each FPLC elution fraction was loaded, under either non-reducing or reducing conditions.

[35] Performed by Shirley Yang, Princeton University, under the author's supervision.

**Purified mFcγRIIb binds mIgG1 and rIgG2a with intermediate affintiy**

To confirm that the purified Fc receptor was in the native conformation and able to bind antibody, its affinity for mIgG1 (*i.e.* JJ316 and JJ319) and rIgG2a (*i.e.* KT3) was measured on the BIAcore, using equilibrium analysis. mFcγRIIb-His was injected into the flow cell at increasing concentrations, allowing it to bind to mIgG1 or rIgG2a, which had been directly immobilised on the BIAcore chip, until saturation was reached. A dissociation constant $K_D$ of 0.70 μM for mIgG1 and 1.2 μM for rIgG2a was measured in this way (Figure 5-22) and this low to intermediate affinity is in agreement with the description of mFcγRIIb as a low-affinity Fc receptor [61]. The experiment confirmed that the purified soluble mFcγRIIb receptor was correctly folded and able to bind both JJ316, JJ319 and KT3. Therefore, it was suitable for replacing secondary antibody for immobilising antibodies in the IL-2 stimulation assay.

**Antibody immobilisation is more efficient *via* Ni-NTA-immobilised FcR *versus* secondary antibody-coated glass or EIA plastic**

It was necessary to test whether a higher antibody immobilisation efficiency could be achieved with the purified Fc receptor. For this purpose, Ni-NTA-coated 96-well plastic plates were obtained from Qiagen Ltd (Ni-NTA HisSorb plates, 35061). The plates are pre-blocked, and specifically immobilise hexahistidine-tagged protein. Proteins are immobilised in a constant orientation, and retain their native conformation. To compare immobilisation efficiency between the different approaches, glass and EIA plastic were coated with an antibody against the Fc receptor (BioLegend, 101302) and blocked, and then a titration of Alexa647®-conjugated mFcγRIIb-His was added to the antibody-coated surfaces, or to the pre-blocked Ni-NTA-coated plastic surface. The amount of fluorescence was measured to determine how much FcR was immobilised with either approach (Figure 5-23). This way, the number of available binding sites for JJ316 or JJ319 could be compared. Each fluorescent FcR immobilised *via* Ni-NTA in this experiment is

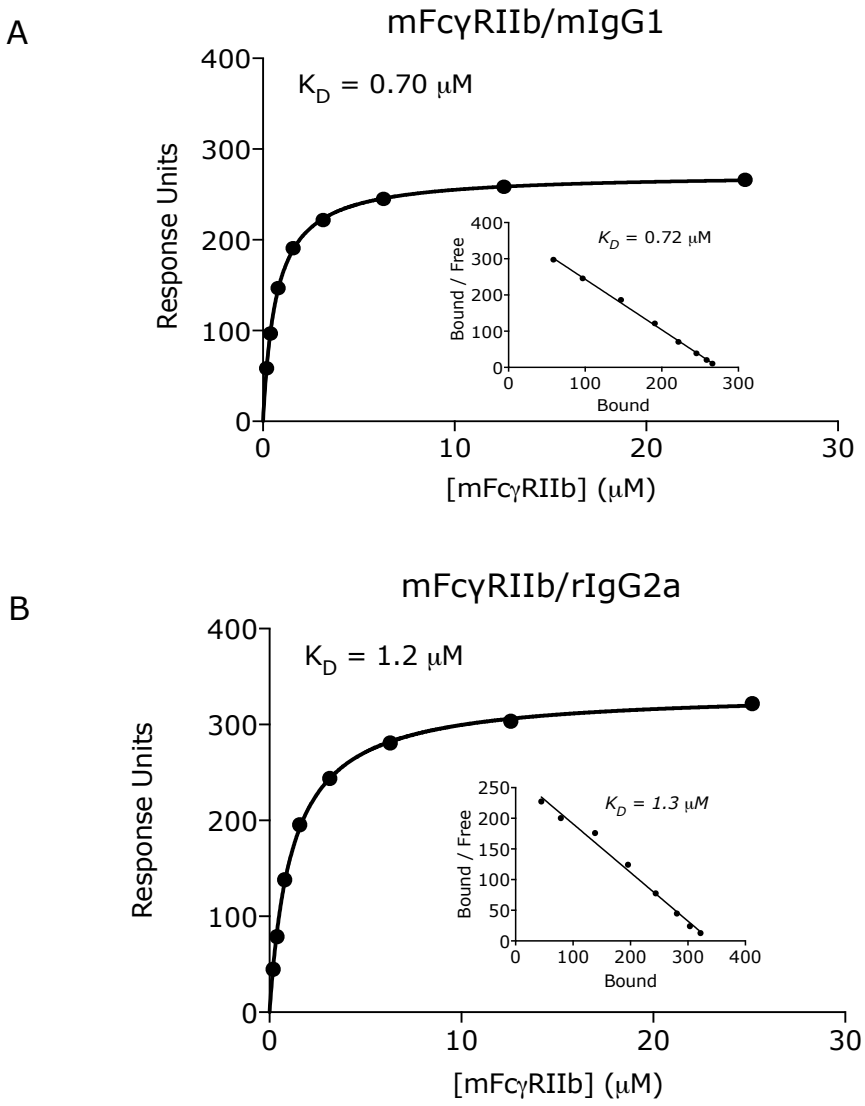



Figure 5-22: mFcγRIIb binds mIgG1 and rIgG2a with low to intermediate affinity. Equilibrium measurements of mouse FcγRIIb affinity for **A** mouse IgG1 or **B** rat IgG2a were carried out on the BIAcore at 37 ºC. One out of two repeats is displayed. Nonlinear regression analysis with a 1:1 Langmuir binding model as well as a Scatchard plot (inlay) are shown. The derived $K_D$ values are displayed.

expected to be capable of binding one antibody, thus corresponding to one binding site. The FcR binds to antibody-coated glass or EIA plastic as JJ316 or JJ319 would bind to DAM-coated surfaces, and thus each fluorescent FcR likewise corresponds to one binding site. The experiment revealed that a higher immobilisation level is reached on FcR-functionalised Ni-NTA as compared to antibody-coated glass or EIA-plastic (Figure 5-23). The immobilisation observed for saturating amounts of ligand in the case of antibody-coated glass or plastic corresponds to that observed for ~ 0.2 μg/mL mFcγRIIb coated on Ni-NTA plastic (Figure 5-23).

**JJ319 induces superagonistic signalling at high FcR immobilisation**

It was now possible to test whether an increased immobilisation level would affect JJ316- or JJ319-induced CD28-signalling. mFcγRIIb was titrated on Ni-NTA plastic, and JJ316- or JJ319-coated cells were allowed to interact with the surface. The antibodies were used at a concentration at which an IL-2 response is only induced when they are immobilised, and not when they are used in solution (data not shown). Strikingly, FcR-immobilised JJ319 induced an IL-2 response in the absence of any additional stimulus, meeting the definition of antibody-induced superagonistic signalling (Figure 5-24A). At immobilisation levels corresponding to < 4 μg/mL FcR, signalling was only induced by JJ316 and not JJ319, replicating results on antibody-coated glass or EIA plastic. Statistical analysis confirmed that a higher degree of FcR immobilisation was needed to generate a half-maximal response for JJ319 *versus* JJ316 (EC50 value; $p<0.0001$; Table 5-6). Strikingly, the response induced by JJ319 plateaus at a lower IL-2 level ("Maximum" value; $p=0.0014$; Table 5-6), and a higher response cannot be generated by increasing the amount of stimulation. Figure 5-23A confirms that the FcR-binding capacity of Ni-NTA plastic is not saturated at the amount of added FcR that saturates the JJ319-induced response (2 μg/mL). Finally, when truncCD28 was ligated on the FcR-coated surface, only JJ316 and not JJ319 induced IL-2 production (Figure 5-23B). Therefore, on the FcR-coated NiNTA plastic only JJ319-induced superagonistic signalling is strictly CD28-dependent, whereas ligand-independent triggering of a bystander receptor contributes to JJ316-induced signalling.

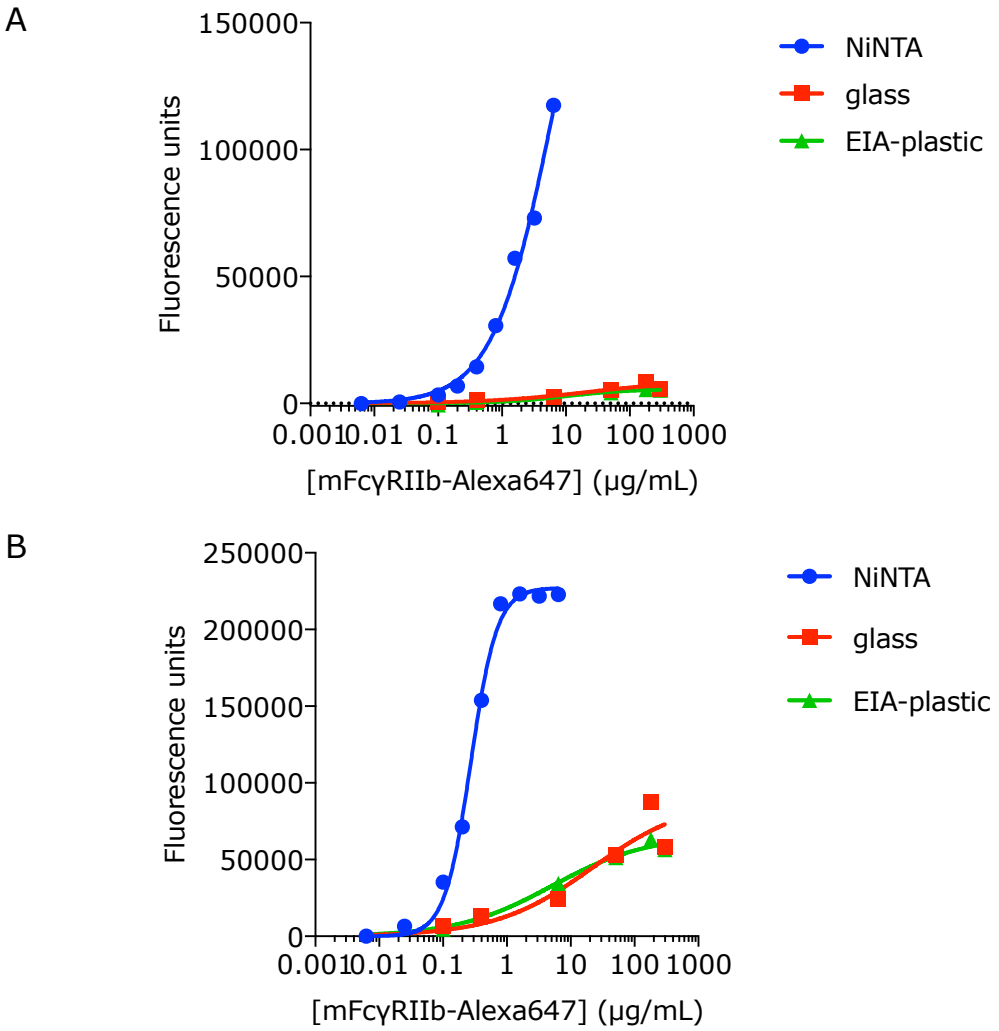



Figure 5-23: Ni-NTA plastic immobilises His-tagged protein more efficiently than antibody-coated glass or EIA plastic. His-tagged mFcγRIIb was coupled to Alexa647® and then allowed to bind to Ni-NTA-coated plastic, or anti-FcR antibody-coated EIA plastic or glass. Fluorescence at 647 nm was measured to determine the amount of binding. A gain of **A** 3000 or **B** 4000 was applied.

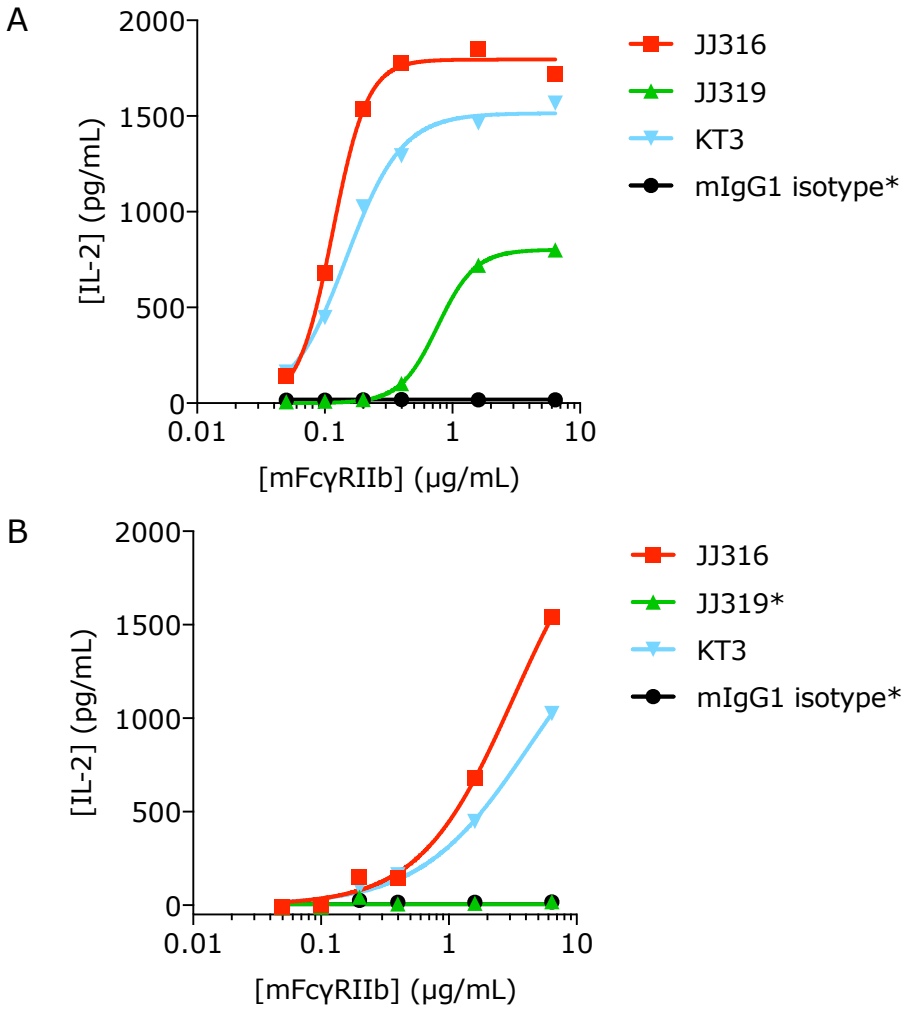



Figure 5-24: JJ319 is superagonistic when immobilised densely *via* a His-tagged Fc receptor on Ni-NTA-coated plastic. $TCR^+$ BW5147 cells were transfected with **A** rmCD28, or **B** truncCD28, and incubated with 1.5 μg/mL JJ316, JJ319, KT3, or mIgG1 isotype, as indicated in the right-hand legends. Cells were then allowed to interact with a Ni-NTA-coated plastic surface that was functionalised with a titration of His-tagged mFcγRIIb. IL-2 levels were measured after 24 hours. Data were fitted with a binding model†, or, where indicated with an asterisk, with a horizontal line because it was the preferred fit as determined by an F-test. For more convenient visualisation data are shown on a logarithmic scale, thus not showing zero on the x-axis. The zero values were, however, included in the fitting and analysis.

Table 5-6: Non-linear regression with a binding model† confirms superagonistic signalling induced by JJ319 when immobilised at high density.

| | JJ316 | JJ319 | KT3 | isotype |
|---|---|---|---|---|
| Maximum | 1795 | 802.1* | 1515 | not converged |
| n | 3.2 | 2.949 | 1.998 | not converged |
| EC50 | 0.1157 | 0.7655** | 0.1475 | not converged |

* different from JJ316 p=0.0014
** different from JJ316 p<0.0001
† [IL-2] = Maximum * $[JJ316]^n/(EC50^n + [JJ316]^n)$; where Maximum = [IL2] at maximal [JJ316]; EC50 = [JJ316] that gives half-maximal [IL-2]; n = Hill-slope

## 5.4. Discussion

A key objective of this chapter was to test several of the predictions of the KS-based model of antibody signalling on glass. The KS model is based on the steric exclusion of phosphatases based on their large size, and thus predicts that antibody-induced signalling will be sensitive to the dimensions of the receptor-antibody complex and the co-expressed receptor-type protein-tyrosine phosphatases relative to each other. Three experiments tested and confirmed this hypothesis in this chapter. First, the CD28 dimensions were extended with an IgG1 Fc domain insertion [249]. As had been observed on EIA plastic [249], ligating extended CD28 with JJ316 no longer allowed superagonistic signalling, but costimulatory signalling was possible on glass. However, superagonistic signalling on glass was restored with another antibody, IC10 (kind gift of John Young, Compton), that binds to the inserted Fc domain closer to the membrane, as had been reported for EIA plastic [249]. Epitope positioning close to the membrane thus correlates with superagonistic signalling, as predicted by the KS model [131]. It was also confirmed that IC10-mediated superagonistic signalling was dependent on the CD28 cytoplasmic domain. The dimensions of the antibody-receptor complex were altered in a second way, by extending the JJ316 antibody with an insertion in the hinge region. Extending the antibody by 30 amino acids, predicted to correspond to ~ 75 Å, transformed it from a superagonistic to a conventional antibody, without affecting its binding to cell-surface expressed CD28. Third, the dimensions of the receptor-type protein-tyrosine phosphatases CD45 and CD148 were varied. Truncated CD148 completely abrogated JJ316-induced superagonistic

signalling, whereas the full-length construct had no effect. Truncated, but not full-length, CD45 had a relatively small, but statistically significant dampening effect on JJ316 superagonistic activity. Antibody-mediated superagonistic signalling is thus sensitive to the phosphatase dimensions, consistent with a KS-based explanation for signalling. The CD148 phosphatase domain appears to have a higher enzymatic activity as compared to CD45, because a much larger inhibitory effects were observed with truncated CD148. Both phosphatases expressed relatively poorly, and expression was downregulated in cells after ~ one week post transduction, likely because it is essential for cellular homeostasis to closely maintain the kinase/phosphatase balance [264]. It is possible that truncated CD45 may completely abrogate superagonistic signalling at higher and more stable expression. In addition, it was shown here that it is necessary to crosslink CD28 to observe superagonistic signalling on glass, as it is on EIA plastic [249]. Overall, CD28 superagonism is explained by a model combining crosslinking and phosphatase segregation.

The KS model predicts that receptor signalling is dependent on the immobilisation of its ligand, or for the experiments described in this thesis, the antibody. JJ316, however, showed activity in solution. It was hypothesised that it may function in an immobilisation-dependent way by binding to Fc receptors expressed by the murine cell lines used in the stimulation assay, such that cells cross-present JJ316 to each other. Several strategies were used to disrupt the hypothetical interaction with Fc receptors. First, JJ316 was co-incubated with an excess of isotype control antibody, aiming to occupy all receptors that may interact with the Fc region of JJ316 (see Section 4.3.2). This attempt was unsuccessful, possibly because the interaction with JJ316 is favoured because it binds to cell-surface expressed CD28 with high avidity, whereas the isotype control antibody does not have a ligand. Second, JJ316 was deglycosylated, on the basis that the glycans in the Fc region are important for recognition by a receptor [265-270], but only a small dampening effect on the activity of soluble JJ316 was observed. Third, CD16/CD32 blocking antibodies were co-incubated with JJ316, but its activity in solution remained (Sara Morgan, Davis laboratory, University of Oxford; unpublished work). Fourth, the residues in the Fc region known to interact with CD16/CD32 were

mutated in an effort to "Fc-silence" the antibody[36]. Again, only a small dampening effect on the activity of soluble JJ316 was observed. It is possible, however, that either a very low affinity for CD16/CD32 remained allowing cross-presentation between cells, or that another, thus far undescribed Fc receptor was responsible for cross-presentation. Therefore, a more radical approach for disrupting the potential JJ316/FcR interaction was chosen, and the JJ316 Fc region was completely removed. An $F(ab')_2$ fragment was generated, and this was largely inactive in solution but active when immobilised *via* an anti-light chain antibody, indicating that immobilisation is required for superagonism.

A striking result was that even JJ319 showed superagonistic activity following high levels of immobilisation *via* an Fc receptor. Another curious observation is that the IL-2 response to JJ319 stimulation saturated at a lower level (~ 50 %) than that for JJ316-induced signalling. Saturation of the response cannot be explained by saturation of FcR immobilisation on the nickelated surface. This suggests that the signalling pathways induced by the two antibodies are qualitatively different.

Having shown that signalling depends on the dimensions of the antibody/CD28 complex relative to those of the phosphatase strengthened the hypothesis that JJ316 more efficiently segregates CD45. It was now possible to test this idea directly in an imaging approach, and to further explore how crosslinking and steric segregation each contribute to antibody signalling.

[36] Performed by Absolute Antibody Ltd. Fc-silent™ JJ316 was a kind gift.

# Chapter 6 Imaging-based analysis of the effects of antibodies on receptor diffusion and phosphatase segregation[37]

## 6.1. Introduction

Work described in the preceding chapters established an assay for studying antibody superagonism on a glass surface, and defined the requirements for signalling in that setting. This was done to facilitate subsequent imaging-based analysis of antibody superagonism. Three observations stood out in particular: one, that signalling depends on the dimensions of the receptor, antibody, and phosphatase; two, that signalling depends on receptor crosslinking, and three, that a bystander receptor, most likely the TCR, can be triggered under certain conditions and contribute to signalling. A plausible explanation for superagonistic antibody signalling would need to account for these observations.

Fluorescence imaging promised to be a suitable method for further investigating how size-dependent phosphatase segregation, receptor crosslinking, and ligand-independent triggering of bystander receptors may each contribute to signalling. Thus far, the experiments support the idea that the superagonist sterically excludes CD45 more efficiently than "conventional" antibodies, which might be observable using a microscopy-based approach if such receptor rearrangements occur [153]. However, it is also possible the diffusion of "bystander" receptors is hindered by the antibodies, to the extent that this favours receptor phosphorylation and signalling. The questions would then be: (1) What is the underlying mechanism of the diffusion effects, e.g. the

[37] This chapter is a result of a collaboration with the Klenerman and Lee groups at the University of Cambridge. Contributions of collaborators are indicated in footnotes.

formation of crosslinked arrays of CD28, or the steric hindering of receptor diffusion when the cell is in close proximity to the glass surface; and (2) to what extent do diffusional effects contribute to the overall signal if at all?

Because antibody-induced changes may take place on a very small spatial or temporal scale, and differences in receptor distribution or diffusion induced by superagonistic *versus* conventional antibodies may be small, an imaging approach with sufficiently high resolution was needed. A combination of total internal reflection fluorescence microscopy, super-resolution microscopy and single-molecule imaging was used in the experiments described in this chapter, each tailored to the spatial and temporal resolution needed for each experiment, as part of a collaboration with the laboratories of Professor David Klenerman and Dr. Steven Lee in Cambridge. In order to image the different receptors, they were labelled either as chimeric molecules with a fluorescent protein tag, or *via* fluorophore-coupled Fab fragments. Work described in this chapter therefore included the molecular cloning of chimeric receptors, and purification of antibodies from hybridoma cultures and their digestion to Fab fragments. Finally, in order to draw conclusions from the imaging data, a complex data analysis was undertaken, involving novel approaches developed in collaboration with the Klenerman/Lee laboratories.

## 6.2. Materials and methods

### 6.2.1. Culturing of the YW62.3.20 hybridoma for anti-mCD45-Fab production

The hybridoma was received growing in IMDM medium supplemented with 5% IgG-stripped foetal calf serum and ampicillin and streptomycin antibiotics. The cells were then subcultured in RPMI medium supplemented with 10% IgG-stripped foetal calf serum, MEM Non-Essential Amino Acids (Gibco), HT Media Supplement Hybri-Max (SigmaAldrich), 10 mM HEPES, 1 mM sodium pyruvate, 2 mM L-glutamine and antibiotics [50 units penicillin, 50 μg streptomycin and 100 μg neomycin per mL]).

### 6.2.2. Photoactivated localization microscopy (PALM) imaging [271]

For PALM imaging, collimated 561 nm (Cobolt, Jive 500) and 405 nm (Cobolt, MLD 405) laser beams were aligned and focussed at the back aperture of an Olympus 1.49 NA 60x oil objective mounted on an IX73 Olympus inverted microscope frame. The power of the collimated beams at the back aperture of the microscope was 4 mW and <10 μW, respectively. The fluorescent signal was filtered with a four-band dichroic (Semrock, Di01-R405/488/561/635) and a combination of a 561 long-pass (Semrock, BLP02-561R) and a band-pass filter (Semrock, FF01-587/35), expanded through a 2.5x achromatic beam expander (Olympus, PE 2.5x 125), and finally projected onto an EMCCD camera (Photometrics, Evolve Delta).

For imaging T cells, 3,000 frames were imaged with a 50 ms exposure under constant 561 nm and 405 nm illumination, using the MicroManager control software. In the super-resolved images, each localization is plotted as a sub-pixel with a specific intensity convolved with a 2D-Gaussian point-spread function. The amplitudes of all rebuilt localizations are equal, and their widths correspond to the average precision of all localizations.

For single-molecule experiments, single-particle tracking (spt) was combined with PALM, as explained above, when CD28-mEos was imaged. For imaging CD45, spt was carried out labelling CD45 with fluorophore-conjugated Fab at single-molecule concentrations, and trajectories where imaged until photobleaching. In Section 6.3.5 dual-colour single-molecule experiments were carried out, imaging CD28-mEos (with spt-PALM) and CD45-Fab (with spt) simultaneously.

### 6.2.3. Diffusion analysis

Diffusion data were analysed with a published code, calculating mean square displacement and jump distance-derived diffusion coefficients, that had been characterised with Monte-Carlo simulations [272] (Sections 6.3.6 and 6.3.7), or with a "home-made" published code [271] based on previous works [194, 272], calculating the "cumulative jump distance" (Section 6.3.3). Localizations appearing in consecutive

frames and closer than 300 nm were grouped in trajectories, using a nearest-neighbours-approach with a memory of one for CD28 and three for CD45 (Sections 6.3.6 and 6.3.7) or four frames for CD28 (Section 6.3.3). For each trajectory counting more than five localizations, a mean square displacement (MSD) analysis was performed with regression on the first five points (Sections 6.3.6 and 6.3.7). Jump distance (JD) analysis was performed for all trajectories counting more than five localisations (Sections 6.3.6 and 6.3.7), or a "cumulative jump distance" analysis. was performed for all trajectories counting more than ten localisations (Section 6.3.3). Two (Sections 6.3.6 and 6.3.7) or three (Section 6.3.3) populations of diffusing membrane proteins were fitted.

### 6.2.4. Bulk-labelling experiments

For dual-colour imaging of CD45 and CD28 in bulk, 488 and 640 nm lasers (Semrock, US) were used. Filter sets for excitation were Di0 405 488 562 635 (Semrock, US), and for emission they were FF605-Di02 (dichroic, Dual-View mounted, Photometrics, Roper Scientific US), FF03-525/50-25 (filter, 488 emission), BLP01-635R-25 (filter, 640 emission). Exposure time was 50 ms, An EmCCD camera (512 Delta Evolve, Photometrics) was used. Laser power was at 0.01 - 0.1 kW/cm$^2$.

Images were averaged over no more than 100 frames to avoid artefacts from bleaching. To overlay the images of the two channels, a convolution function was used to shift the images relative to each other.

In order to create differential amplitude vector intensity signal (DAVIS) plots, a Sobel edge detector vector was applied to the overlaid images to calculate the intensity gradient in x (*i.e.* from left to right) and y (*i.e.* from top to bottom) for each pixel:

$$\underset{G_x}{\begin{pmatrix} -1 & 0 & +1 \\ -2 & 0 & +2 \\ -1 & 0 & +1 \end{pmatrix}} \quad \underset{G_y}{\begin{pmatrix} +1 & +2 & +1 \\ 0 & 0 & 0 \\ -1 & -2 & -1 \end{pmatrix}}$$

One gradient vector was calculated for each of the two channels per pixel. The two vectors were then subtracted from each other to create a difference vector for each

pixel. The amplitude of the difference vector was plotted as brightness value in the DAVIS plot.

## 6.3. Results

### 6.3.1. Principles of PALM and TIRFM imaging

An imaging approach was chosen to study whether and how the superagonistic and conventional antibodies alter CD28 behaviour. It seemed possible that changes occurred on such a small scale that they would not be detectable by conventional, diffraction-limited light microscopy. Therefore, a method was sought that was able to characterise CD28 behaviour on the super-resolution level. One such approach makes use of photoswitchable fluorophores. Resolution is defined as the ability to discriminate between two separate entities that are a certain distance apart. When two fluorophores are in close proximity, *i.e.* < 200 nm in the visible wavelength domain, diffraction-limited techniques are not able to detect them as separate entities. However, when they are separated temporally, *i.e.* when they fluoresce one at a time, they can be resolved as separate entities and their positions determined with a high degree of precision (*i.e.* within ~ 20 nm; Figure 6-1). Photoswitchable fluorophores are typically designed such that their fluorescence can be controlled with two lasers, an activation and an excitation laser. In the absence of the activation laser, they are in a dark state and thus not excitable. The activation laser brings the fluorophores into an excitable state, *i.e.* the ground state, and when both lasers are used in combination, the electrons in the activated fluorophores can be excited to a higher energy state after which they return to their ground state, producing fluorescence. The power of the activation laser can be fine-tuned to control the density of fluorescing entities independently of the actual density of the fluorophores. When the activation laser is used at low power, few fluorophores are switched on, in a stochastic process (Figure 6-1A,B). Collecting images over time, the position of the few fluorescing fluorophores can be determined precisely for each frame before they are photobleached or return to their dark state (Figure 6-1C), and a super-resolved image can be based on localizations collected over many (hundreds to thousands of) frames (Figure 6-1D,E).

One draw-back is that some temporal resolution is lost in the final super-resolved image. This imaging method is called "PALM" (photoactivated localization microscopy), and relies on photoswitchable fluorescent proteins, typically expressed in the form of fusion proteins. "STORM" (stochastic optical reconstruction microscopy) is a related method that makes use of the stochastic blinking of certain fluorescent dyes under specific buffer conditions [273], which are typically conjugated to antibodies or Fabs for immunolabelling of a biological specimen.

The present study is concerned with very first molecular events that lead to signalling rather than downstream processes, *i.e.* with potential changes imposed by the antibodies on the organisation and behaviour of their target- and bystander receptors, and therefore the interest in the present experiments was on processes that occur at the cell surface. That is, for the stimulation assay developed in Chapter 4, at the interface between the antibody-coated glass slide and the T cell. Total internal reflection fluorescence microscopy (TIRFM) is a very well-suited excitation method for imaging such processes at reasonably high resolution. The main advantage is that background fluorescence from beyond the plane of focus is virtually completely removed, facilitating the detection of single molecules [274]. The physical phenomenon that allows very shallow (*i.e.* ~ 100-200 nm deep) illumination of the sample involves surface plasmon resonance, which is explained in Section 3.3.3. When light is internally reflected at the interface between media differing in their refractive index, such as the glass-buffer interface of a coverslip, a non-propagating evanescent wave is established that decays exponentially with distance to the interface. Only fluorophores in immediate proximity to the interface, *i.e.* within the effective reach of the evanescent field, become excited (Figure 6-2). TIRFM can be combined with super-resolution techniques such as PALM/STORM when resolution beyond the diffraction limit is needed, to dramatically increase the detection and localisation of single emitters, and thus the final resolution of the image.

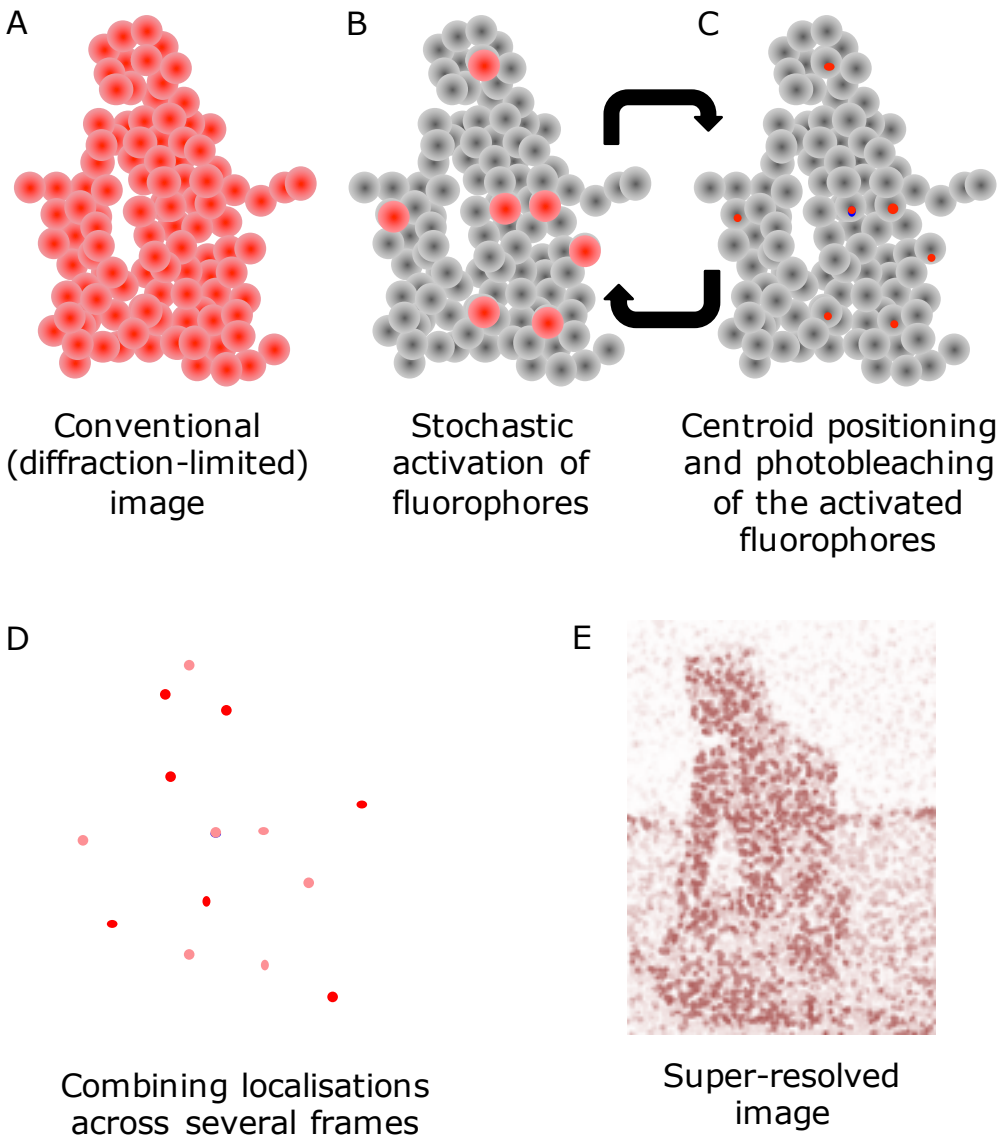



Figure 6-1: Schematic explanation of the principle behind PALM/STORM super-resolution imaging. **A** shows that point-spread functions (PSFs) of neighbouring fluorophores overlap, such that they cannot be resolved in the diffraction-limited image. **B-D** show how the localization of each fluorophore is determined precisely by switching on fluorescence stochastically and fitting the PSFs. **E** depicts the super-resolved image built up from localizations collected over many frames.

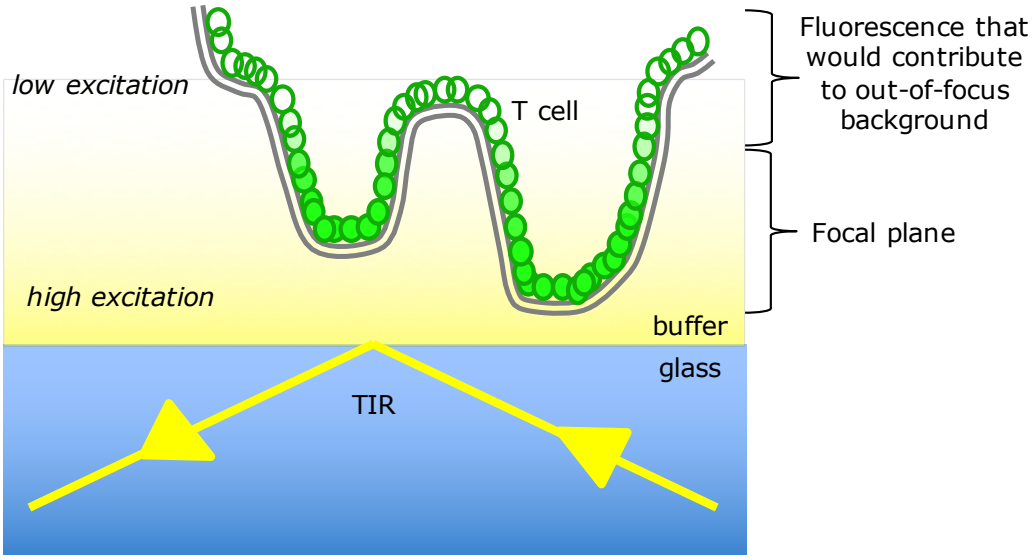



Figure 6-2: Schematic depiction of the principle behind TIRFM. An evanescent wave emerges at the glass-buffer interface when it is illuminated with light at an angle of total internal reflection. The energy of the wave decays exponentially with distance, such that the sample is selectively illuminated where it is in close proximity (< 200 nm) to the interface. Only fluorophores within this distance are sufficiently excited and observed (bright green circles).

### 6.3.2. Super-resolved images indicate that CD28 distribution or diffusion is altered by the superagonist

#### Molecular cloning of a CD28-mEos fusion protein

Eos is a photoswitchable fluorescent protein that can be expressed as a chimera with a protein of interest. mEos3.2 is a derivative that was engineered to have improved photoproperties, such a brightness, and to be monomeric even at very high concentrations [275]. It is important to choose a strictly monomeric fluorescent fusion protein to study the behaviour of a protein of interest in the plasma membrane to prevent artefacts such as induced dimerization or aggregation. Two CD28-mEos3.2 constructs were designed: a signalling-competent one, containing the CD28 signalling motifs (rmCD28-mEos3.2), and a signalling-disabled one, lacking these motifs (truncCD28-mEos3.2; Figure 6-3). In a first attempt, mEos3.2 was directly fused to the C-terminus of the full-length CD28 sequence without a linker. However, an IL-2

stimulation assay revealed that this construct was incapable of signalling (data not shown). It was hypothesized that the mEos protein sterically hindered downstream signalling proteins from binding to the CD28 cytoplasmic tail. A 10 amino acid glycine-proline linker was therefore inserted between the CD28 cytoplasmic tail and mEos, and signalling was restored, albeit reduced to about 25 % as compared to the untagged rmCD28 construct (data not shown). Signalling was restored to 100 % when the linker was extended to a 30 amino acid glycine-proline-serine sequence (data not shown). Thus, the 30 amino acid linker, attached to mEos3.2 N-terminally, was used to generate the final rmCD28-mEos3.2 and truncCD28-mEos3.2 constructs (Figure 6-3).

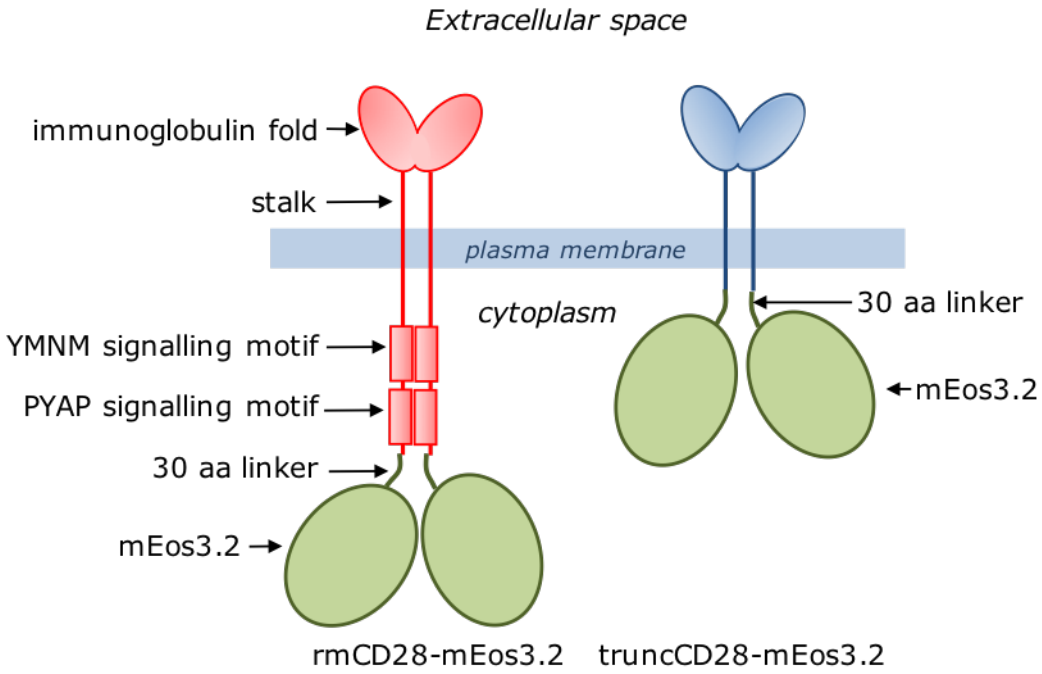



Figure 6-3: Design of chimeric CD28-mEos3.2 fusion proteins. The photoswitchable fluorescent protein mEos3.2 was fused to the C-terminus of either signalling-competent (rmCD28-mEos3.2) or signalling-disabled (truncCD28-mEos3.2) CD28. A 30 amino acid linker was inserted to enable downstream signalling proteins to interact with the CD28 cytoplasmic tail.

## Super-resolved imaging suggests that the superagonist induces changes in the organisation of CD28

When exploring whether the antibodies induce changes in CD28 distribution or diffusion in live cells, it was important to distinguish changes directly imposed by the antibodies, occurring as part of the mechanism, from changes that result from signalling. In other words, changes that occur as a consequence of receptor triggering, such as the formation of an immunological synapse, could mask the subtle changes preceding signalling that were the focus of interest here. In order to observe processes leading to signalling in isolation, therefore, the aim was to image under non-signalling conditions. Others had shown that the presence of the TCR leads to changes in cell organisation and calcium signalling in the absence of any TCR ligand when a cell makes contact with a surface [153]. To avoid any artefacts resulting from ligand-independent triggering of the TCR, TCR-deficient BW5147 cells were used for imaging here. Because antibody-induced changes potentially take place on a very small spatial scale, PALM microscopy was performed to generate images with a very high (~ 20 nm) precision. A TIRFM set-up was used to specifically image the T-cell/glass contact and to minimise background fluorescence. rmCD28-mEos3.2 transfected T-cells were treated as they were for the IL-2 stimulation assay (see Section 4.3.1). They were incubated with JJ316, JJ319 or no antibody in medium at 37 ºC for 15 minutes, and then were imaged live as they interacted with DAM-coated glass. Images were collected at 20 ºC. Super-resolved images were generated, plotting localizations from all frames (Figure 6-4). The data for JJ319 stimulation closely resemble those for the no antibody (*i.e.* DAM only) control, with CD28 localizations largely dispersed throughout the cell/glass contact (Figure 6-4A,C). Under JJ316 stimulation, however, localizations appear to be highly concentrated (Figure 6-4B). Two different explanations are possible: either CD28 is aggregated following JJ316 stimulation, or its diffusion is constrained. In order to determine whether concentrated localizations results from several distinct CD28 molecules clustering, or from single CD28 molecules whose diffusion is constrained to a small area or slowed down, single-particle tracking [276, 277] was undertaken.

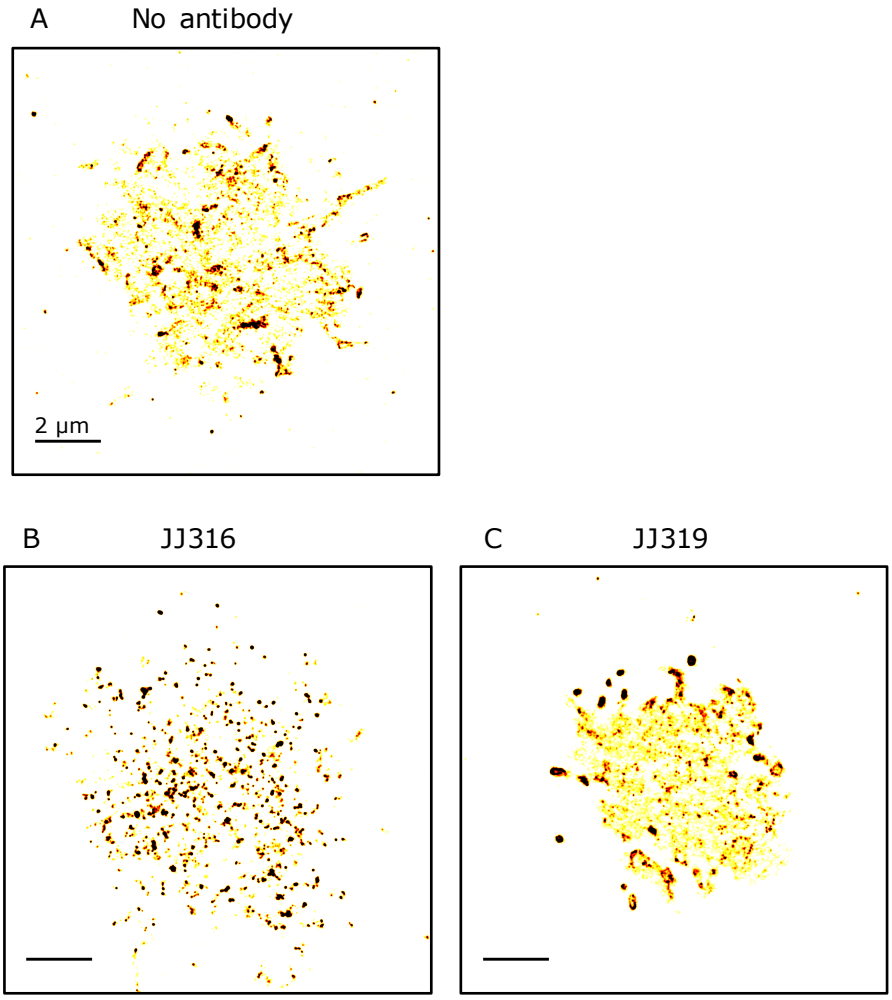



Figure 6-4: Super-resolved images of truncCD28-mEos3.2 stimulated with JJ316 or JJ319[38]. TCR$^-$ BW5147 cells were stably transfected with a rmCD28-mEos3.2 fusion protein. Cells were stimulated with **A** no antibody or **B** 50 µg/mL JJ316 or **C** 50 µg/mL JJ319 for 15 minutes and then applied to a cover slip coated with DAM secondary antibody. PALM images of live cells at 20 °C were collected on a TIRF microscope. Images display single representative cells.

[38] Cell lines were transfected by the author, and data were collected in collaboration by the author and Matthieu Palayret, Klenerman group, University of Cambridge. Data were analysed and visualised by Matthieu Palayret.

### 6.3.3. Single-particle tracking reveals that the superagonist constrains CD28 diffusion

In single-particle tracking combined with PALM (spt-PALM), localizations are grouped into trajectories. A nearest-neighbour approach was chosen, grouping localizations in consecutive frames into trajectories based on spatial proximity (300 nm). A memory of four frames was included to allow for short blinking events. Figure 6-5 displays CD28 trajectories for exemplary cells stimulated with either JJ316, JJ319, or no anti-CD28 antibody. The approach is able to reliably detect diffusion coefficients between 0.01 and 0.1 $\mu m^2/s$. In order to derive diffusion coefficients, and to be able to detect several populations with distinct diffusion coefficients, a "cumulative jump-distance distribution" approach [194] was chosen [271]. In brief, the distribution of the probability that a particle is located within a circle of a certain radius from its origin after a certain lag time is calculated [271]. Models of $n$ diffusing populations with diffusion constants $D_i$ can be fitted [271]. The simplest model that fitted the data well assumed three distinct populations, the slowest of which was likely the result of an artefact, because it was present in all data sets including those where no anti-CD28 antibody was used, and its calculated diffusion coefficient was below the precision of the experiment, such that it would be considered null [271]. Two populations thus remained, the faster of which is referred to as the "mobile fraction" here, and the slower of which has a diffusion coefficient < 0.01 $\mu m^2/s$ and is referred to as the "immobilised fraction" here. A more detailed description of the analysis can be found in [271]. The slower-diffusing entities very likely represent CD28 receptors that are immobilised on the glass surface *via* DAM, but this has yet to be confirmed. The more-quickly diffusing receptors may be antibody-bound but not immobilised *via* DAM.

**Both signalling-competent and signalling-disabled CD28 slow down**

Comparing the diffusion coefficient of the "mobile fraction" of rmCD28-mEos3.2 at 37 ºC in the presence or absence of antibodies, it was highest in the absence of anti-CD28 antibody, and decreased to ~ 60 % with JJ319, and it further decreased to ~ 30 % following ligation with JJ316 (Figure 6-6). From these measurements it was unclear whether CD28 slows down as part of the mechanism leading to triggering, or whether it is triggered by some other mechanism and then slows down as the result of becoming phosphorylated, *e.g.* because downstream signalling proteins are recruited it its cytoplasmic tail, constraining its diffusion. To differentiate between these two possibilities, the diffusional behaviour of truncCD28-mEos3.2 was characterised under the different antibody treatments. Any changes observed in this setting would be expected to precede CD28 signalling, and can thus be interpreted to be directly imposed by the antibodies. At 37 ºC the "mobile" fraction of truncCD28-mEos3.2 slowed its diffusion to ~ 35 % in the presence of JJ316, but no effect was observed for JJ319 (Figure 6-6). At 20 ºC constraining effects on CD28 diffusion were observed for both antibodies, with JJ316 having a greater effect than JJ319, but the effects were smaller (Figure 6-6). Table 6-1 lists the fractions (*i.e.* proportions) of CD28 receptors that were grouped into the "mobile fraction" by mathematical fitting. Whilst overall, the fractions of mobile receptors are not substantially different at 37 ºC, this fraction appears to be slightly larger for JJ319 (Table 6-1). At 20 ºC more of the receptors are mobile in the absence of the antibodies (Table 6-1). Overall, the superagonist constrains CD28 diffusion under both signalling and non-signalling conditions. The conventional antibody constrains CD28 diffusion to a smaller extent, and this effect does not appear to be completely independent of downstream signalling events.

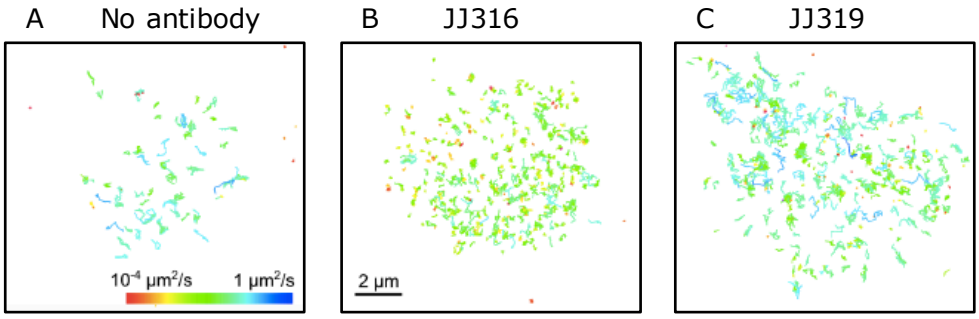



Figure 6-5: Single-particle tracking of CD28 in live cells[39]. TCR⁻ BW5147 cells were transfected with rmCD28-mEos3.2 Cells were incubated with **A** buffer only, or **B** 50 µg/mL JJ316 or **C** 50 µg/mL JJ319, and then imaged live at 20 ºC on a TIRF microscope as they contacted DAM-coated glass. Single-particle tracking was applied, grouping localizations in consecutive frames within 300 nm of each other into trajectories. A memory of four frames was allowed. Trajectories are displayed for single representative cells, colour-coded for the mean square displacement (MSD)-derived diffusion coefficient (see inset legend).

Table 6-1: Quantification of the fraction of CD28 receptors that are grouped into the faster, "mobile" population.

| Fraction of mobile receptors at 37 ºC | | |
|---|---|---|
| | rmCD28-mEos3.2 | truncCD28-mEos3.2 |
| No antibody | 0.35 | 0.34 |
| JJ316 | 0.33 | 0.38 |
| JJ319 | 0.51 | 0.46 |
| **Fraction of mobile receptors at 20 ºC** | | |
| | rmCD28-mEos3.2 | truncCD28-mEos3.2 |
| No antibody | 0.63 | 0.71 |
| JJ316 | 0.25 | 0.24 |
| JJ319 | 0.48 | 0.49 |

[39] Modified from [271], Figure 7.4B,E,H. Cell lines were transfected by the author, and data were collected in collaboration by the author and Matthieu Palayret, Klenerman group, University of Cambridge. Data were analysed and visualised by Matthieu Palayret

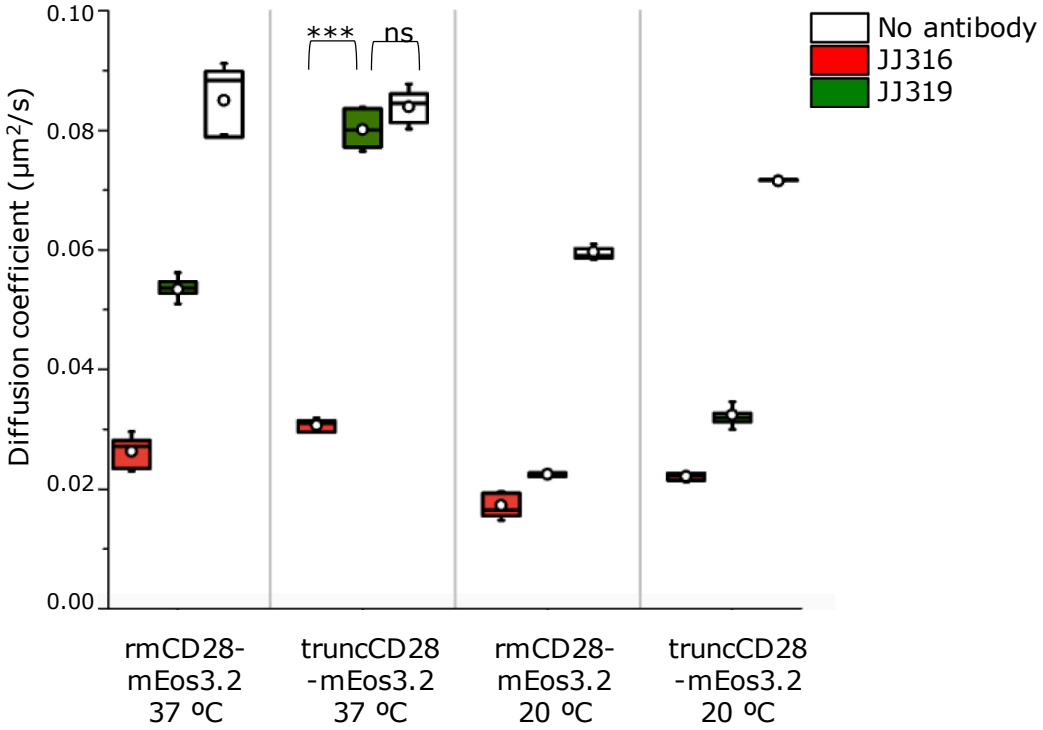



Figure 6-6: JJ316 constrains CD28 diffusion under both signalling and non-signalling conditions[40]. TCR$^-$ BW5147 cells were transfected with either rmCD28-mEos3.2 or truncCD28-mEos3.2. Cells were incubated with 50 μg/mL JJ316 or JJ319, or with buffer only, as indicated in the right-hand legend. They were then imaged live at 37 or 20 ºC on a TIRF microscope as they contacted DAM-coated glass. Single-particle tracking was applied, grouping localizations in consecutive frames that are located within 300 nm of each other into trajectories. A memory of four frames was allowed. Data were fitted with a three-population model. The diffusion coefficients of the fastest, "mobile" fraction are displayed. *** here corresponds to $p<0.0001$.

[40] Modified from [271], Figure 7.6C. Cell lines were transfected by the author, and data were collected in collaboration by the author and Matthieu Palayret, Klenerman group, University of Cambridge. Data were analysed and visualised by Matthieu Palayret.

**Transmembrane proteins do not slow down globally and unspecifically**

The question emerged of what phenomenon caused the constraining effect on CD28 diffusion. Several hypotheses were possible. One hypothesis is that the antibodies may cause CD28 aggregation or the formation of crosslinked arrays that generally hinder the diffusion of transmembrane proteins. In this setting, the very slow, "immobilised" CD28 fraction could represent aggregated or crosslinked CD28, and the "mobile" fraction could represent CD28 receptors that are diffusing but hindered by the aggregates. If this idea was correct, any transmembrane protein would be expected to be constrained in its diffusion, even if it was not antibody-ligated. To test this, a truncCD86-mEos3.2 construct was designed and used to transduce TCR-deficient, truncCD28-transfected BW5147 cells. CD86 is a monomeric transmembrane protein whose extracellular domain has similar dimensions to CD28. Its cytoplasmic domain was truncated, as in the case of truncCD28, to prevent artefacts from downstream signalling events, and fused to mEos3.2 *via* a 30 amino acid glycine-proline-serine linker, similarly to truncCD28-mEos3.2. In contrast to truncCD28-mEos3.2, the diffusion of its "mobile fraction" was not affected by either JJ316 or JJ319 (Figure 6-7), and the size of the "mobile fraction" was equally unaffected (Table 6-2). Therefore, the antibodies do not globally slow down the diffusion of bystander transmembrane proteins, and the constraining effect on CD28 diffusion cannot be explained by CD28 clusters that hinder the diffusion of unclustered CD28.

Table 6-2: Quantification of the fraction of CD28 or CD86 receptors that are grouped into the faster, "mobile" population.

| Fraction of mobile receptors | | |
|---|---|---|
| | truncCD28-mEos3.2 | truncCD86-mEos3.2 |
| No activation | 0.35 | 0.31 |
| JJ316 | 0.38 | 0.33 |
| JJ319 | 0.45 | 0.27 |

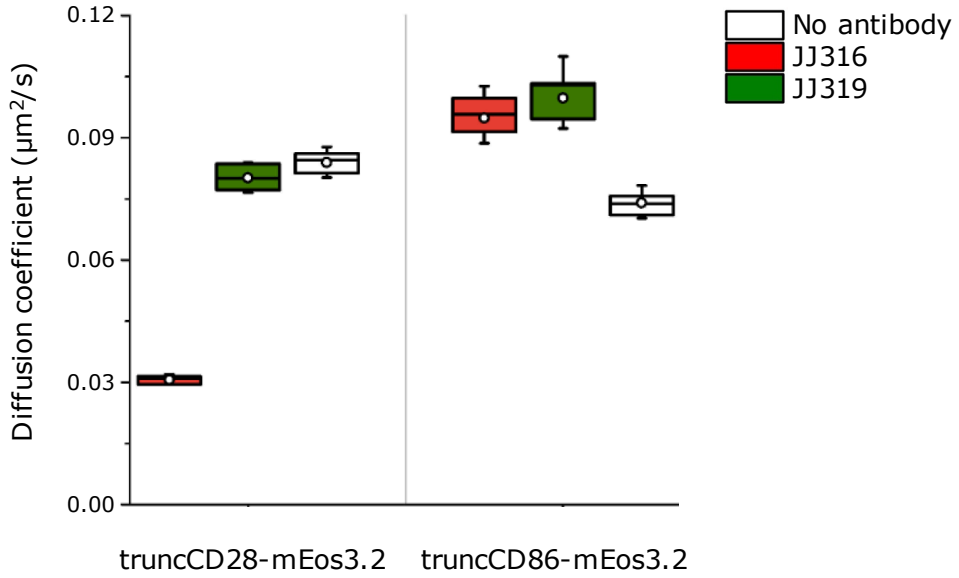



Figure 6-7: JJ316 does not affect CD86 diffusion[41]. TCR⁻ BW5147 cells were transfected with either truncCD28-mEos3.2, or truncCD28 and truncCD86-mEos3.2. Cells were incubated with 50 μg/mL JJ316 or JJ319, or with buffer only, as indicated in the right-hand legend. They were then imaged live at 37 °C on a TIRF microscope as they contacted DAM-coated glass. Single-particle tracking was applied, grouping localizations in consecutive frames that are located within 300 nm of each other into trajectories. A memory of four frames was allowed. Data were fitted with a three-population model. The diffusion coefficients of the fastest, "mobile" fraction are displayed.

**Crosslinking enhances the constraining effect on CD28 diffusion**

A second hypothesis focused on the crosslinking properties of the antibodies. Section 5.3.3 confirmed a crosslinking dependence of JJ316 superagonism on glass, and others had suggested that an improved ability to crosslink CD28 may underpin the potency of superagonistic antibodies [132, 229]. Crosslinking a number of receptors would be expected to have a constraining effect on receptor diffusion. To explore the role of crosslinking in CD28 diffusion, the monovalent chimeric truncPDCD28 construct (see Section 5.3.3) was fused to mEos3.2 *via* a 30 amino acid glycine-proline-serine linker for spt-PALM. The diffusion of its "mobile fraction" was measured in the

[41] Modified from [271], Figure 7.8A. Cell lines were transfected by the author, and data were collected in collaboration by the author and Matthieu Palayret, Klenerman group, University of Cambridge. Data were analysed and visualised by Matthieu Palayret.

presence of either clone 19 or clone 2 (see Section 5.3.3), or with a combination of the two antibodies. Both antibodies constrained the diffusion of the truncPDCD28 construct (Figure 6-8). Interestingly, the effect was larger for clone 19 (Figure 6-8), which binds a membrane-proximal epitope and is thus comparable to JJ316, whereas clone 2, like JJ319, binds a membrane-distal epitope. The diffusion coefficient in the presence of clone 19 was comparable to that of JJ316-stimulated CD28. Thus, a correlation between epitope position and diffusional constraint was observed, which was independent of crosslinking. When clone 2 and clone 19 were used in combination, the constraining effect on PDCD28 diffusion was further enhanced: the diffusion coefficient of the "mobile fraction" was reduced to ~ 30 % of that for clone 19 stimulation only, and was essentially immobile at < 0.01 $\mu m^2/s$ (Figure 6-8). Thus, clone 19 and clone 2 in combination had a larger effect on receptor diffusion than JJ316. Perhaps crosslinking with two different antibodies that bind distinct epitopes is more efficient than crosslinking of a homodimeric receptor with one bivalent antibody. Considering the size of the "mobile fraction", the trend is similar: both antibodies decreased the fraction of "mobile" PDCD28, but in combination the size of the fraction was further decreased (Table 6-3). In conclusion, constraining effects on receptor diffusion were observed independently of crosslinking, and efficient crosslinking with two antibodies enhanced these effects.

Table 6-3: Quantification of the fraction of PDCD28 receptors that are grouped into the faster, "mobile" population.

| Fraction of mobile receptors | |
|---|---|
| | truncPDCD28-mEos3.2 |
| No activation | 0.64 |
| Clone 19 | 0.45 |
| Clone 2 | 0.48 |
| Clone 19 + Clone 2 | 0.20 |

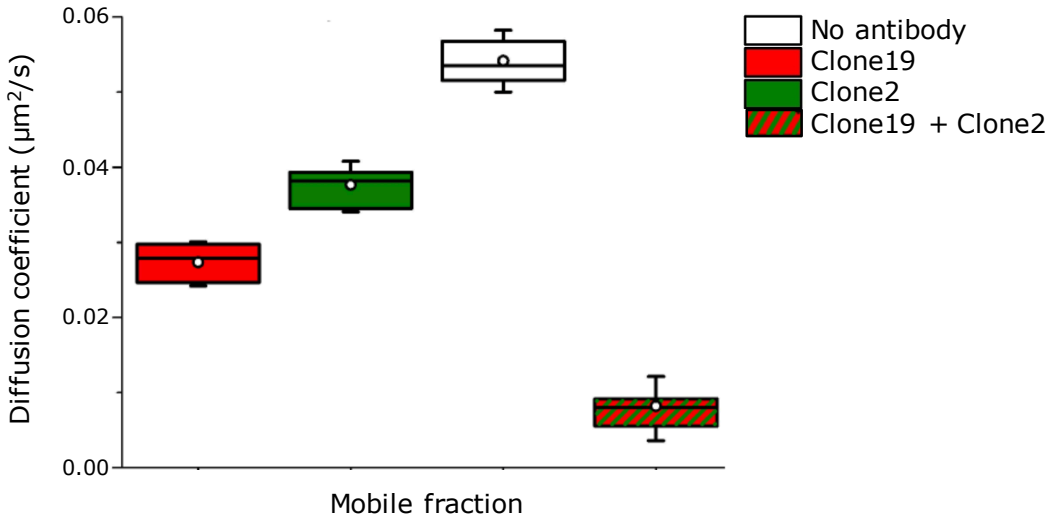



Figure 6-8: Anti-PD1 antibodies constrain truncPDCD28-mEos3.2 diffusion[42]. TCR⁻ BW5147 cells were transfected with truncPDCD28-mEos3.2. Cells were incubated with 50 μg/mL clone 19 or clone 2, or with a combination of 50 μg/mL clone 19 and 50 μg/mL clone 2, or with buffer only, as indicated in the right-hand legend. They were then imaged live at 37 ºC on a TIRF microscope as they contacted DAM-coated glass. Single-particle tracking was applied, grouping localizations in consecutive frames that are located within 300 nm of each other into trajectories. A memory of four frames was allowed. Data were fitted with a three-population model. The diffusion coefficients of the fastest, "mobile" fraction are displayed.

**Constraining effects on CD28 diffusion are dependent on antibody concentration**

Thus far antibodies were used at a fixed concentration in the imaging experiments. The question emerged whether the differences between JJ316- and JJ319-induced changes in CD28 behaviour would be robustly observed independently of the concentration of the antibodies. To test this, the antibodies were titrated from 0.1 to 50 μg/mL, and their effect on CD28 diffusion was measured. The range of concentrations was chosen to vary the molar ratio of antibody to CD28 such that conditions were included in which the antibody was in excess, and others in which

[42] Modified from [271], Figure 7.9C. Cell lines were transfected by the author, and data were collected in collaboration by the author and Matthieu Palayret, Klenerman group, University of Cambridge. Data were analysed and visualised by Matthieu Palayret.

CD28 was in excess. Maximal CD28 crosslinking is expected for a molar ratio of antibody : CD28 homodimer of ~ 1. Table 6-4 lists the molar ratios of antibodies to CD28 homodimers that were estimated for each antibody concentration.

For JJ316 stimulation, the diffusion coefficient of the CD28 "mobile fraction" consistently decreased as the antibody concentration increased (Figure 6-9A). In contrast, for JJ319, the constraining effect on CD28 diffusion was maximal for an intermediate concentration of 1 µg/mL (Figure 6-9B). Interestingly, this concentration comes closest to a molar ratio of 1 (Table 6-4), which is optimal for CD28 crosslinking. Therefore, the small constraining effect that JJ319 has on CD28 diffusion appears to depend on optimal receptor crosslinking, whereas no such correlation was observed for JJ316.

Table 6-4: Estimation of the molar ratio of antibodies to CD28 homodimers for varying the antibody concentration.

| Antibody/homodimer molar ratio for varying concentrations of antibody* | | | | |
|---|---|---|---|---|
| [antibody] (µg/mL) | 0.1 | 1 | 5 | 50 |
| molar ratio | ~ 0.16 | ~ 1.6 | ~ 8 | ~ 80 |

* assumed $1*10^6$ CD28 homodimers per cell, $2.5*10^5$ cells in 0.1 mL antibody-containing buffer, mIgG1 molar mass of 155,000 g/mol. $1*10^6 * 2.5*10^5 = 2.5*10^{11}$ homodimers in 0.1 mL. 1 µg/mL antibody * 0.1mL * $1g/1*10^6µg$ * 1 mol/155,000g * $6.022*10^{23}$ antibodies per mol = $3.885*10^{11}$ antibodies for 1 µg/mL in 0.1 mL. Molar ratio = $2.5*10^{11}$ homodimers/[antibody](µg/mL)$*3.885*10^{11}$.

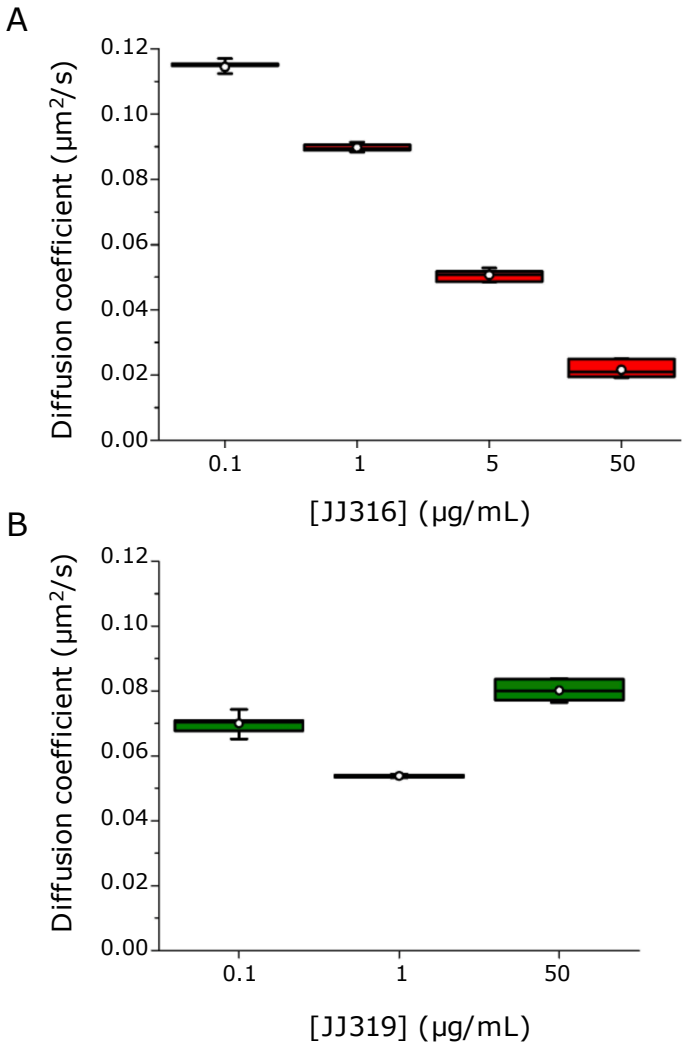



Figure 6-9: Diffusional effects of antibodies are dependent on their concentration[43]. TCR⁻ BW5147 cells were transfected with truncCD28-mEos3.2. Cells were incubated with a titration of **A** JJ316 or **B** JJ319, as indicated on the x-axis. They were then imaged live at 37 ºC on a TIRF microscope as they contacted DAM-coated glass. Single-particle tracking was applied, grouping localizations in consecutive frames that are located within 300 nm of each other into trajectories. A memory of four frames was allowed. Data were fitted with a three-population model. The diffusion coefficients of the fastest, "mobile" fraction are displayed.

[43] Modified from [271], Figure 7.10B,E. Cell lines were transfected by the author, and data were collected in collaboration by the author and Matthieu Palayret, Klenerman group, University of Cambridge. Data were analysed and visualised by Matthieu Palayret.

Table 6-5: Quantification of the fraction of CD28 receptors that are grouped into the faster, "mobile" population.

| Fraction of mobile truncCD28-mEos3.2 receptors | | |
|---|---|---|
| | JJ316 | JJ319 |
| 0.1 µg/mL | 0.54 | 0.28 |
| 1 µg/mL | 0.62 | 0.29 |
| 5 µg/mL | 0.49 | n.a. |
| 50 µg/mL | 0.28 | 0.46 |

### 6.3.4. Production of labelled anti-mCD45-Fab

Given that the experiments described in Chapter 5 indicated that the size-dependent exclusion of CD45 from superagonist-engaged CD28 may play a role in the mechanism, it was of interest to characterise how the spatial distribution and diffusional behaviour of CD45 is affected by the presence of JJ316 and JJ319 antibodies. In order to label CD45 for fluorescence imaging, it was first attempted to express CD45 as a fusion protein with a SNAP-tag, which could be covalently labelled with a fluorescent dye. However, stable expression of a CD45 construct was unsuccessful, as discussed elsewhere in this thesis (see Section 5.3.5): cells appear to downregulate expression several days after transduction until it is not detectable. It was therefore necessary to label endogenously expressed CD45, using Fab fragments rather than antibodies to prevent artefacts by inducing dimerization or aggregation, and to limit artefacts induced by increasing the dimensions of CD45 with a label. Because very large quantities of antibody are generally needed to prepare sufficient amounts of high-quality Fab fragments[44], using a commercial antibody was not feasible. Instead, a hybridoma was sought from which large quantities of antibody could be purified.

[44] The reaction is very inefficient when small quantities are digested; see Section 3.3.3.

**Papain digest of anti-mouse CD45 antibody to generate Fab fragments**

Pan-reactive anti-mouse CD45 rat IgG2b antibody was purified from the YW62.3.20 hybridoma [278, 279], a kind gift of H. Waldmann and S. Cobbold, University of Oxford. A total of 30 mg antibody was purified from a 2 L culture, and this was used to prepare Fab fragments.

The peptidase papain digests antibodies in the hinge region, yielding two Fab fragments and one Fc fragment. It is active at neutral pH at 37 ºC in the presence of cysteine. Because the Fc and Fab fragments are similar in size, it is not possible to separate them by size-exclusion chromatography. Instead, affinity chromatography with protein G-coupled Sepharose was used, and this produced high-quality Fab fragments (Figure 6-10).

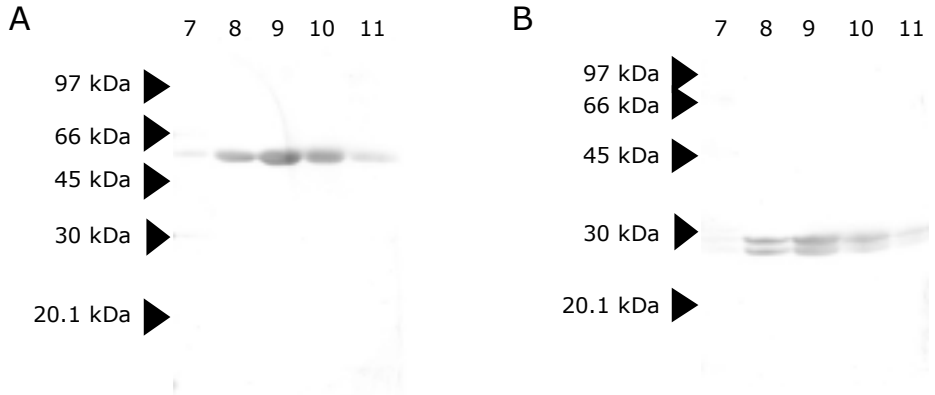



Figure 6-10: SDS-PAGE analysis of protein G-purified anti-mouse CD45 Fab after size exclusion chromatography. Samples were separated on a 12 % acrylamide gel. 7.5 µL of each sample was loaded, under either **A** non-reducing or **B** reducing conditions.

For imaging, Fab fragments were labelled with Atto655 or Alexa647® or Alexa488®. Good and specific binding of Atto655-labelled YW62.3.20-Fab to cell-surface expressed mouse CD45 was confirmed by flow cytometry (Figure 6-11, Table 6-6).

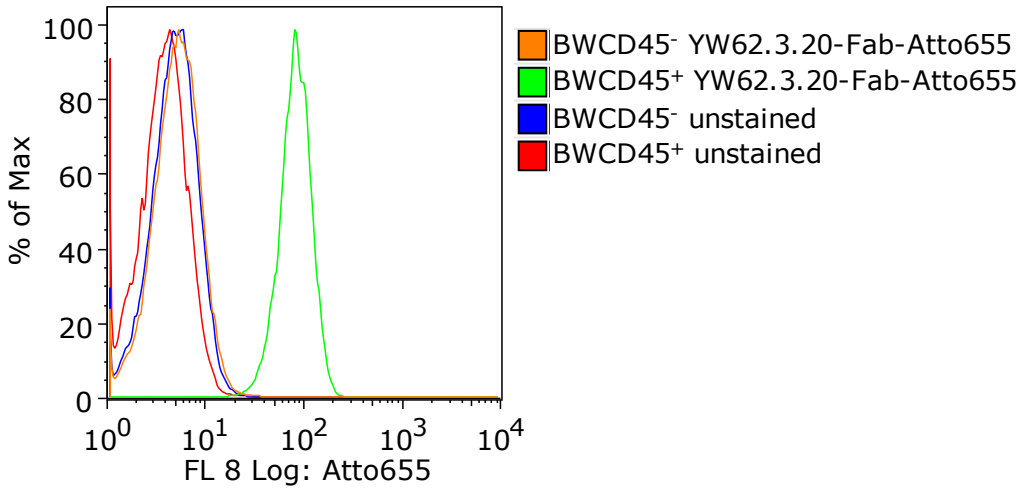



Figure 6-11: YW62.3.20-Fab specifically binds to CD45 endogenously expressed in BW5147 cells. Wild-type BW5147 cells (BWCD45$^+$) or their CD45-deficient variant (BWCD45$^-$) were incubated with Atto655-coupled YW62.3.20 Fab fragments in PBS-azide, or PBS-azide only, as indicated in the right-hand legend. The fluorescence of single cells was measured by flow cytometry.

Table 6-6: Quantification of YW62.3.20-Fab binding to CD45 endogenously expressed in BW5147 cells.

| Cell line | MFI* unstained | MFI* YW62.320-Fab-Atto655 |
|---|---|---|
| BW5147 CD45+ | 5 | 82 |
| BW5147 CD45- | 4 | 5 |

* Mean fluorescence intensity as assessed by flow cytometry, in relative units.

### 6.3.5. Single-molecule imaging reveals that CD28 and CD45 do not colocalize

Since it was anticipated that the potential segregation of CD45 from CD28 would occur, if at all, on a very small spatial scale, a single-molecule approach was chosen to image the two receptors simultaneously in live cells at 37 °C. TCR-deficient, truncCD28-mEos3.2 transfected BW5147 cells were labelled with anti-CD45-Fab-Atto655 at a low density in order to distinguish and track single CD45 receptors. Spt-PALM was simultaneously used to track single truncCD28-mEos3.2 receptors. In the presence of either JJ316 or JJ319 and DAM, CD45 and CD28 exhibited anti-correlated behaviour, as their trajectories rarely intersected (Figure 6-12). Indeed, CD28 and

CD45 diffusion appeared to be confined to small, largely separate regions (Figure 6-12). To quantify whether there was any difference in the spatial segregation of CD45 *versus* CD28 between the stimulation conditions, a quantitative coordinate-based colocalization (CBC) analysis [280] was performed [271]. Here, coordinates derived from single-particle localizations are used to determine how two entities labelled in different colours behave relative to each other rather than comparing intensity values of two channels, and this analysis is well-suited for simultaneous dual-colour microscopy experiments as performed in this chapter [280]. CD45 and CD28 localizations were anti-correlated for each stimulation condition, even when no anti-CD28 antibody was used (Figure 6-13). However, a significant difference between the effects of the two antibodies was not detected (Figure 6-13). Nonetheless, anti-correlation appeared to be larger under JJ316 stimulation, and it is possible that the large error, *i.e.* the large variation between repeats of the experiment, masks real differences (Figure 6-13).

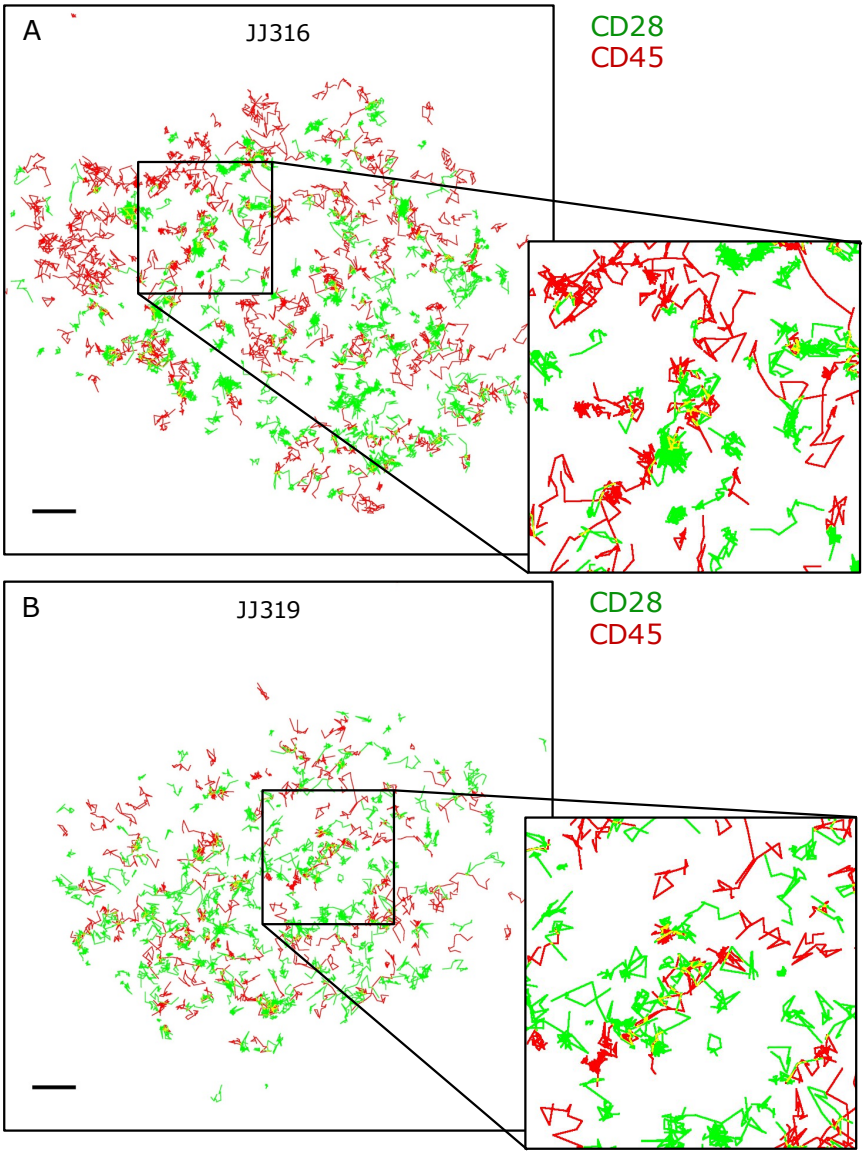



Figure 6-12: Simultaneous dual-colour single-particle tracking of Fab-labelled CD45 and CD28-mEos.[45] TCR$^-$ truncCD28-mEos3.2-transfected BW5147 cells were incubated with anti-CD45 Fab-Atto655 and **A** 50 μg/mL JJ316 or **B** 50 μg/mL JJ319. They were then imaged live at 37 ºC on a TIRF microscope as they contacted DAM-coated glass. Single-particle tracking was applied, grouping localizations in consecutive frames that are located within 300 nm of each other into trajectories. A memory of four frames was allowed. Images show the trajectories of single molecules in a single representative cell. A size bar of 1 μm is displayed.

[45] Cell lines were transfected by the author, and data were collected in collaboration by the author and Matthieu Palayret, Klenerman group, University of Cambridge. Data were analysed and visualised by Matthieu Palayret.

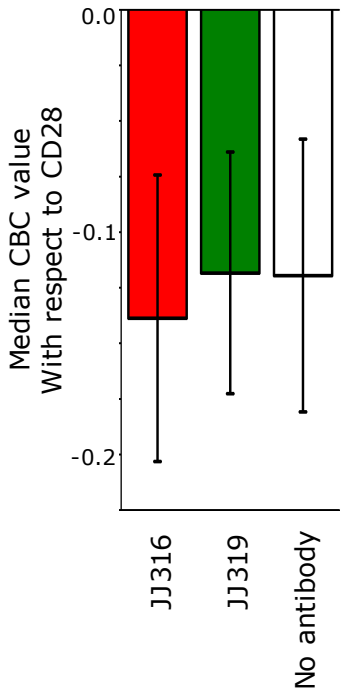



Figure 6-13: CD45 and CD28 localizations are anti-correlated for all stimulation conditions[46]. TCR$^-$ truncCD28-mEos3.2-transfected BW5147 cells were incubated with anti-CD45 Fab-Atto655 and 50 μg/mL JJ316 or 50 μg/mL JJ319 or no anti-CD28 antibody, as indicated on the y-axis. They were then imaged at 37 ºC on a TIRF microscope as they contacted DAM-coated glass. Quantitative coordinate-based colocalization (CBC) analysis was performed to assess the correlation between CD28 and CD45 localizations. For each cell, the CBC values of the localizations of each channel were calculated with respect to the other channel. The mean CBC values of five cells are plotted with respect to CD28. Error bars display one standard deviation in each direction.

[46] Modified from [271], Figure 7.16. Cell lines were transfected by the author, and data were collected in collaboration by the author and Matthieu Palayret, Klenerman group, University of Cambridge. Data were analysed and visualised by Matthieu Palayret.

### 6.3.6. JJ316, but not JJ319 constrains CD45 diffusion

It was of interest to determine whether CD45 diffusion was affected by ligating truncCD28 with JJ316 or JJ319. For tracking purposes, single CD45 molecules were labelled with anti-mCD45-Fab-Alex488® at low density. To exclude signalling artefacts, imaging was performed under non-signalling conditions, using TCR-deficient BW5147 cells expressing truncCD28. A mean square displacement (MSD) analysis was applied to derive diffusion coefficients. For reference, MSD-derived diffusion coefficients for truncCD28-mEos3.2 were also included in the analysis, confirming the differential effect that JJ316 and JJ319 had on constraining its diffusion (Figure 6-14). In the presence of JJ316, the diffusion coefficient of CD45 was reduced to ~ 75 % as compared to the "no antibody" control, whereas for JJ319, it was slightly increased (Figure 6-14). Therefore, the superagonistic and conventional antibodies differentially affect CD45 diffusion, and only the superagonist constrains it. The superagonist appears to affect the diffusion of some (*e.g.* CD45), but not all (*e.g.* CD86) bystander receptors in the cell/glass contact. This prompted the hypothesis that only receptors with certain dimensions, *i.e.* exceeding those of CD86 and CD28, are slowed down unspecifically.

### 6.3.7. The superagonist constrains CD28 diffusion partially by steric effects

Testing whether steric effects were sufficient to constrain the diffusion of antibody-bound CD28, a close cell/glass contact was created independently of JJ316: a humanised anti-PD1 antibody, either clone 19 binding a membrane-proximal or clone 10 binding a membrane-distal epitope [260], was indirectly immobilised *via* surface-bound goat anti-human secondary antibody (GAH), and used to ligate co-transfected, signalling-disabled PDCD28 (Figure 6-15). Both JJ316- and JJ319-bound CD28 slowed its diffusion when a contact was created *via* either clone 19 or clone 10 *versus* no anti-PD1 antibody, but the effect was relatively small (Figure 6-16). JJ319-bound CD28 slowed down to a greater extent for the clone 19 *versus* clone 10-defined contact, whereas no such effect was observed for JJ316-bound CD28 (Figure 6-16). Crosslinking PDCD28 with two antibodies did not enhance the constraining effect on

antibody-bound CD28 (Figure 6-16). Overall, this shows that while steric effects contribute to the constraining effect on receptor diffusion by antibodies, they cannot fully account for it.

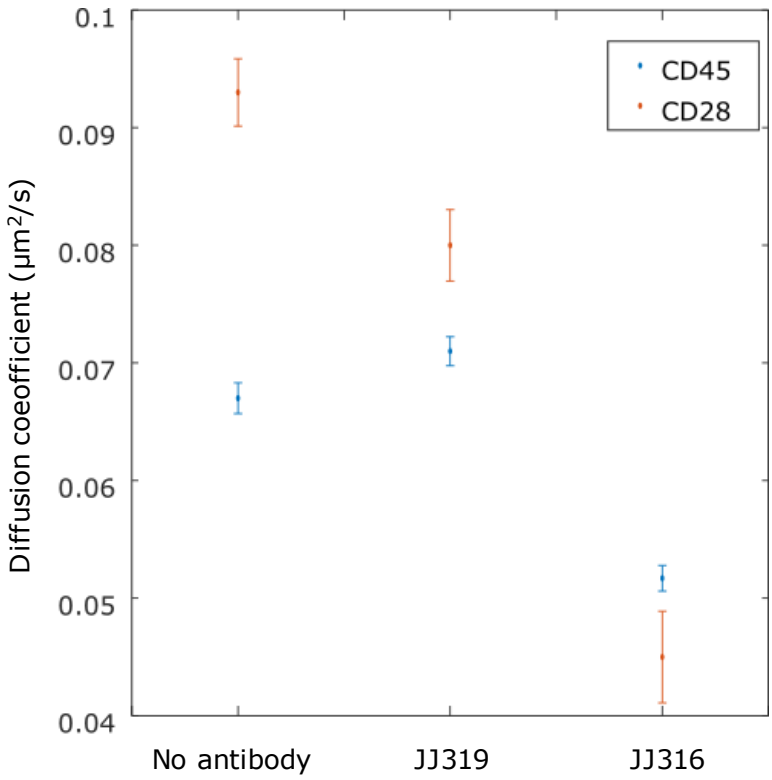



Figure 6-14: JJ316 constrains both CD28 and CD45 diffusion[47]. TCR⁻ truncCD28-mEos3.2 expressing BW5147 cells were labelled with anti-mCD45-Fab-Alexa488® at low density. Cells were incubated with either no antibody, or 50 μg/mL JJ319, or 50 μg/mL JJ316, as indicated on the x-axis, and then imaged live on a TIRF microscope at 37 ºC as they interacted with DAM-coated glass. Single-particle tracking of either truncCD28-mEos3.2 or of CD45 was performed. An MSD analysis was used to determine the diffusion coefficient for each trajectory. The mean diffusion coefficients are displayed. Error bars display the standard error of the mean.

[47] Cell lines were transfected by the author, and data were collected in collaboration by the author and Anna Lippert, Klenerman group, University of Cambridge. Data were analysed and visualised by Anna Lippert.

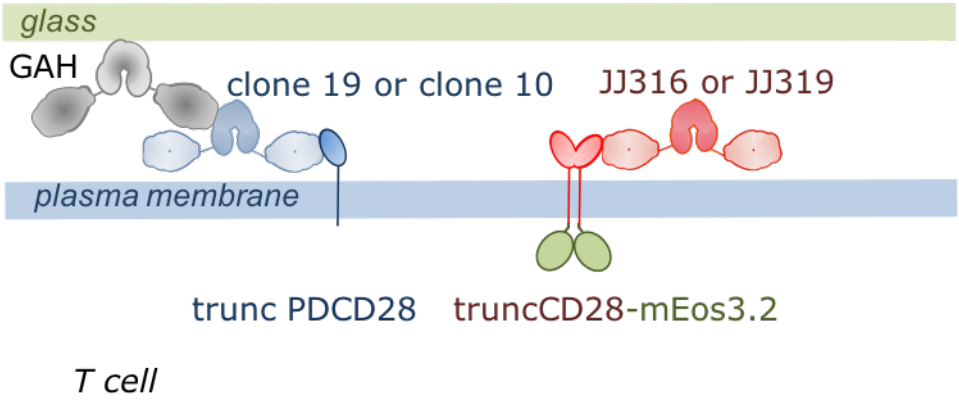



Figure 6-15: Experimental set-up for measuring the diffusion of non-immobilised, antibody-bound CD28. A cell/glass contact was defined *via* a PD1/antibody interaction, and the distance was varied by using either humanised clone 19, binding membrane-proximally, or humanised clone 10, binding membrane-distally. The glass surface was coated with goat anti-human secondary antibody (GAH) to immobilise the antibody/PD1 but not the antibody/CD28 complexes. The diffusion of antibody-bound, mEos-tagged truncCD28 is measured.

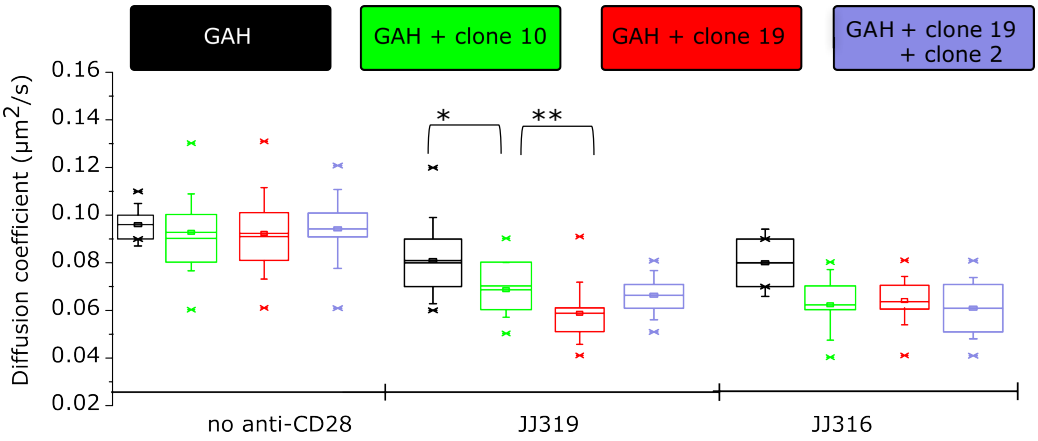



Figure 6-16: Non-immobilised, antibody-bound CD28 slows its diffusion when a close cell/glass contact is created[48]. TCR⁻ BW5147 cells were co-transfected with truncPDCD28 and truncCD28-mEos3.2. Cells were incubated with or without anti-CD28 antibody, in combination with or without humanised anti-PD1 antibody. They were then imaged live at 37 ºC as they contacted GAH-coated glass. The JD-derived diffusion coefficients of the faster, "mobile" fraction are displayed. * here corresponds to p=0.03 and ** here corresponds to p=0.01.

[48] Cell lines were transfected by the author, and data were collected in collaboration by the author and Anna Lippert, Klenerman group, University of Cambridge. Data were analysed and visualised by Anna Lippert.

### 6.3.8. Bulk-labelling experiments reveals that JJ316 induces the local segregation of CD45 more efficiently than JJ319

Single-molecule imaging generated very high-resolution images that showed an anti-correlated behaviour for CD45 *versus* CD28 localization. However, significant differences between the effects of JJ316 and JJ319 were not detected using this approach. Possibly, differences were masked because all CD28 receptors were included in the analysis, and some may not have been antibody-ligated. It is also possible that the temporal resolution of this approach was not high enough to detect CD45-depleted segregation zones as observed by Chang *et al* [153], because they are dynamic, or that the labelling density was not high enough to detect such zones. Therefore, a diffraction-limited bulk-labelling analysis was undertaken. CD45 was labelled at a higher density with Alexa488®-labelled anti-mCD45-Fab. Rather than labelling CD28 with a fusion protein, the JJ316 and JJ319 antibodies were labelled with Alexa647® and used at a dilution of 1/5 in unlabelled antibody because previously the cells were treated with 50 μg/mL antibody, but labelling was too dense at this level. In order to improve temporal resolution, images were collected at 20 ºC. Receptors diffuse more slowly at this temperature and CD45 segregation zones evolve more slowly [153]. Areas depleted in CD45 were observed for both antibodies (Figure 6-17), although they were not as clearly defined as those observed by Chang *et al* [153].

It was of interest to analyse how CD45 behaves in relation to the antibody on a spatial scale to address the hypothesis that the superagonist sterically excluded CD45 more efficiently. In the presence of JJ316, the pixel-based CD45 intensity was decreased across the cell/glass contact to ~ 70 %, which was defined by considering intensities twice as high as the background (Figure 6-18A). The effect was even larger when only the antibody-enriched areas, defined by considering intensities > 30 % of the maximum pixel in that channel, were analysed, with the mean CD45 staining intensity value for JJ316 being ~ 55 % of that for JJ319 (Figure 6-18B). The extent of CD45 exclusion (*i.e.* reduction in its intensity) from antibody-enriched area was independent of the size of the area (data not shown). A difference between JJ316 and JJ319

stimulation was also observed when CD45 intensities exclusively outside of antibody-enriched regions were compared (data not shown), indicating that CD45 was globally excluded in the cell/glass.

Finally, it was of interest to identify areas in the cell-glass contact in which antibody *versus* CD45 behaviour was particularly anti-correlated. Differential Amplitude Vector Intensity Signal (DAVIS) plots were used to visualise such areas. For each pixel two vectors were calculated, one for the antibody and one for the CD45 channel, that quantified the intensity gradient; *i.e.* in whether intensity increased or decreased with respect to the neighbouring pixels from left to right and from top to bottom. The two vectors were subtracted from each other, yielding one difference vector for each pixel. In Figure 6-19 the amplitude of the difference vector is plotted as an intensity for each pixel, highlighting areas in yellow that show anti-correlated intensity changes for the CD45 and antibody channels. Fourteen representative images are shown for each antibody treatment (Figure 6-19). More and brighter highlighted areas are observed for JJ316 stimulation, confirming that it increases anti-correlated behaviour and heterogeneity in receptor distribution (Figure 6-19). The many ring-like structures that are seen are of particular interest. Because CD45 and CD28 dynamics around the ring are anti-correlated, but less different in the centre, areas inside the ring are either low in CD45 and high in CD28 or *vice versa*. Overall, the bulk-level dual-colour imaging showed that JJ316 alters CD45 spatial distribution more so than JJ319.

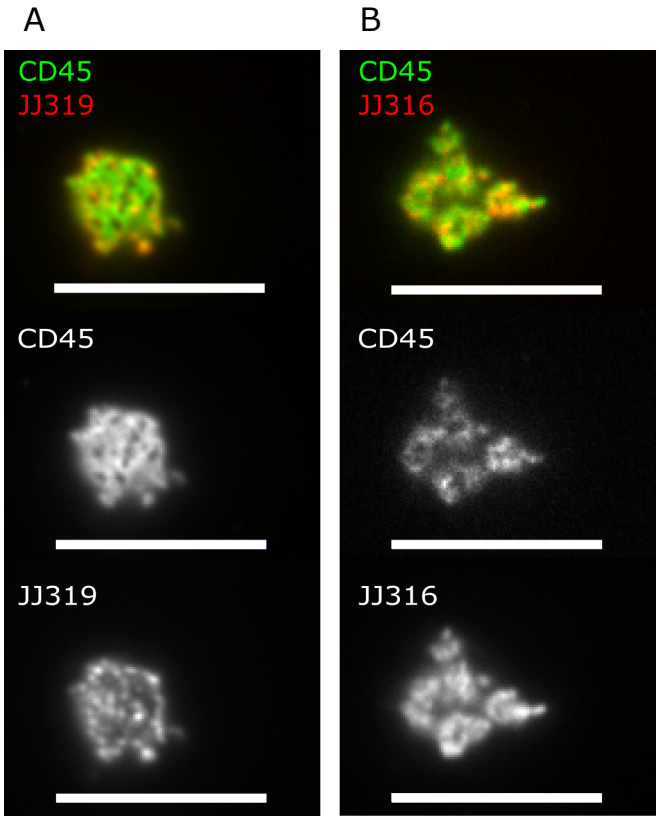



Figure 6-17: Areas depleted of CD45 are observed under both JJ316 and JJ319 treatment[49]. TCR$^-$ truncCD28-expressing BW5147 cells were incubated with 20 μg/mL anti-mCD45-Fab-Alexa488® and either **A** 10 μg/mL JJ316-Alexa647® in 40 μg/mL unlabelled JJ316, or **B** 10 μg/mL JJ319-Alexa647® in 40 μg/mL unlabelled JJ319, and then imaged at 20 ºC on a TIRF microscope as they interacted with DAM-coated glass. Images display averages of up to 100 frames. Images in the top panel display an overlay of the CD45 and antibody channels, and images in the middle and bottom panel display the CD45 or antibody channel, respectively. Size bars of 10 μm are displayed.

[49] Cell lines were transfected by the author, and data were collected in collaboration by the author and Anna Lippert, Klenerman group, University of Cambridge. Data were analysed and visualised by Anna Lippert.

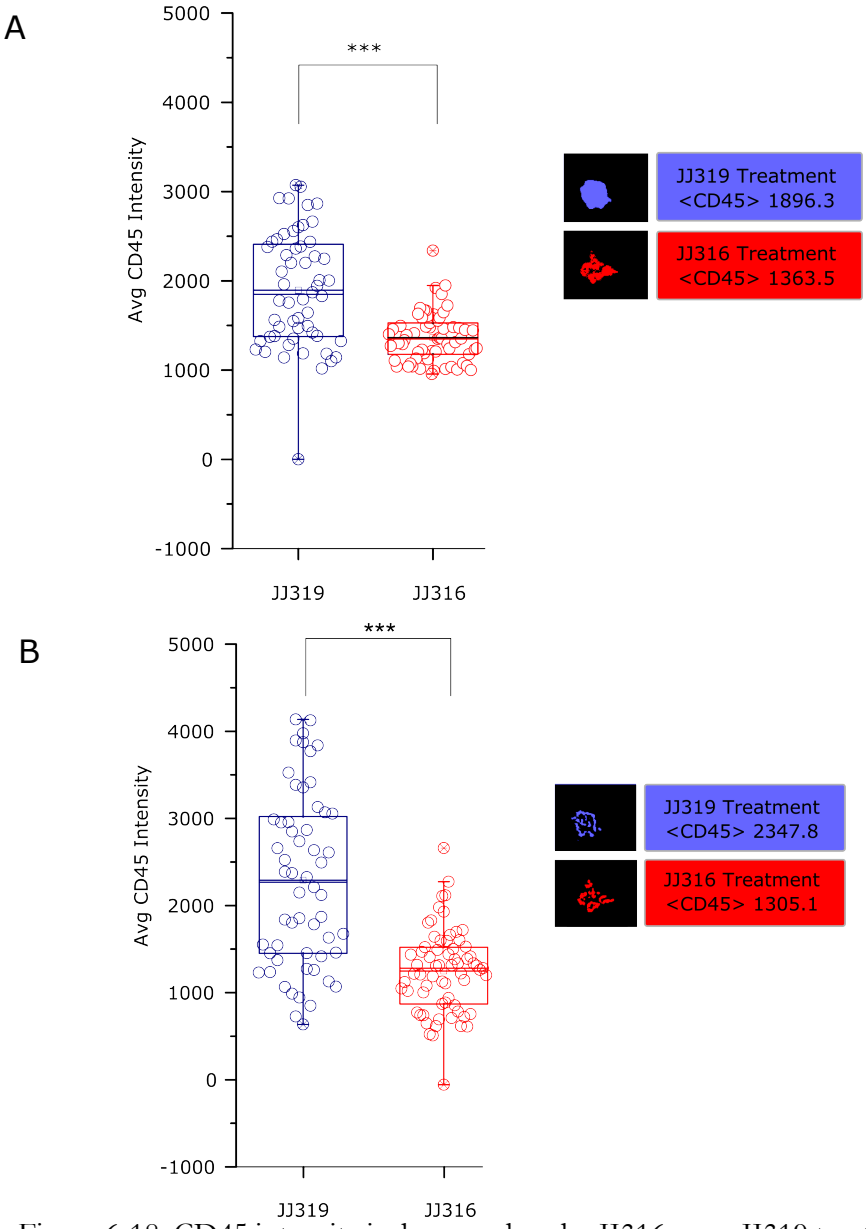



Figure 6-18: CD45 intensity is decreased under JJ316 *versus* JJ319 treatment across the cell-glass contact as well as in antibody-enriched areas[50]. Box plots of the average CD45 intensity per cell are displayed for either **A** the entire cell-glass contact or **B** antibody-enriched regions, under either JJ316 (n = 62 cells) or JJ319 (n = 53 cells) treatment. Inlays display the masks applied to define the respective regions. *** here corresponds to $p < 0.0001$ (two-sample t-test).

[50] Cell lines were transfected by the author, and data were collected in collaboration by the author and Anna Lippert, Klenerman group, University of Cambridge. Data were analysed and visualised by Anna Lippert.

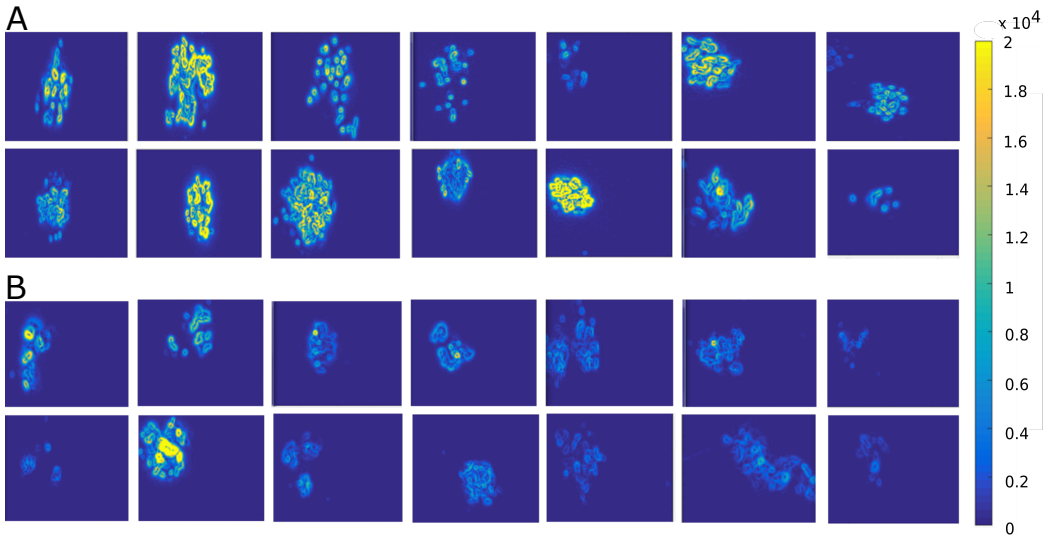



Figure 6-19: Differential Amplitude Vector Intensity Signal (DAVIS) plots visualise the increased anti-correlated receptor distribution under **A** JJ316 *versus* **B** JJ319 treatment[51]. Areas of anti-correlated intensity changes between the CD45 and antibody channels are highlighted. The intensity gradient in x and y was calculated for each pixel, resulting in one gradient vector per pixel for each channel. The two gradient vectors were then subtracted from each other, and the amplitude of the difference vector was plotted as a brightness value in the DAVIS plot (see right-hand legend; a high-amplitude difference vector is plotted as a yellow pixel).

## 6.4. Discussion

A key objective of this chapter was to test the hypothesis that CD28 is spatially segregated from CD45 to a greater extent under stimulation with a superagonistic as compared to a conventional antibody. An imaging approach thus needed to be chosen that can quantify the "spatial segregation" of two molecular entities. In a first approach simultaneous dual-colour single-particle tracking was employed to generate images of single-molecule resolution, and a quantitative coordinate-based colocalisation analysis was performed to test whether CD28 and CD45 showed anti-correlated behaviour. However, this analysis did not reveal a significant difference for JJ316 *versus* JJ319

[51] Cell lines were transfected by the author, and data were collected in collaboration by the author and Anna Lippert, Klenerman group, University of Cambridge. Data were analysed and visualised by Anna Lippert.

treatment, perhaps because it is not the ideal approach to detect spatial segregation. Whereas the dual-colour images generated with this approach have a very high spatial resolution, temporal information is very limited. Trajectories that are displayed as intersecting (see Figure 6-12) may in fact represent two particles that were always separated through time; *i.e.* they were likely never in the same space at the same time. Furthermore, the temporal resolution here may be insufficient to visualize areas in which CD28 and CD45 are spatially segregated [153], because such zones may be dynamic, since live cells are imaged; *i.e.* they may change over time. Other technical factors that may be limiting, and therefore potentially masking real differences, are insufficient labelling densities, photobleaching, and imprecise sub-nm alignment and superposition of the two channels [271].

Next, a bulk-labelling experiment was undertaken to overcome the limitations of the single-molecule approach. The superagonistic antibody excluded CD45, in terms of a reduction in the pixel-based CD45 intensity, to a greater extent (~ 2-fold) than the non-superagonist. The differences were robust using two different masks (*i.e.* either intensities 2-fold larger than the background, or intensities > 30 % of the maximum) for defining the area of analysis. It was also excluded that the observed differences were an effect of differential labelling of the cells with anti-mCD45-Fab: the labelling intensity measured in "epi" (*i.e.* outside of the TIRF field) was equal for JJ316 and JJ319 stimulation (data not shown).

To overcome any limitations resulting from a potential labelling bias, or from using pixel intensity as a proxy for estimating the density of proteins, a new type of analysis was developed in collaboration with the Klenerman/Lee groups that contrasts the intensity gradients of the two channels. Anti-correlated behaviour for CD45 *versus* the antibody in terms of spatial dynamics was highlighted in the DAVIS plots. The DAVIS analysis is less prone to bias because it is mask-free and robust to potential variations in illumination and labelling. Whereas it was very clear by eye that the spatial dynamics of CD45 and CD28 were more anti-correlated under treatment with the superagonistic *versus* the conventional antibody, the analysis did not produce a

numerical value that could quantify this difference precisely. Furthermore, it would be of interest to exclude that membrane perturbations were responsible for the "segregation" (in terms of anti-correlated spatial dynamics) by testing whether a labelled membrane lipid was differentially segregated.

A striking observation was that CD28 diffusion is slowed down by the antibodies, and more so (by a factor of ~ 2.5) by the superagonistic antibody. This effect was independent of CD28 phosphorylation, and was robust to different ways of analysing the data, such as grouping receptors into one, two, or three populations with distinct diffusion coefficients. Some differences were observed in diffusion at 20 *versus* 37 ºC, particularly in the size of the "mobile" fraction of CD28 receptors. This variation could be explained either by non-linear temperature-dependent diffusion effects, or by limits of the population mathematical fitting method. However, the results were quantitatively very reproducible, and surprisingly robust to slightly different conditions, such as the period of time for which the cells were incubated with soluble antibody, the incubation temperature, and the batch of transfected T-cell lines (data not shown). The grouping of receptors into distinct populations with different diffusion coefficients is somewhat artificial and should be considered an aid to statistical analysis rather than necessarily an accurate reflection of distinct biological entities. Heterogeneity exists within populations, and a continuous distribution of diffusion coefficients may represent the data more accurately. A conservative approach was taken here, fitting the data with the smallest number of populations that could approximate the data well. However, it can be stated with certainty that there is heterogeneity within the sample; some receptors are approximately stationary whereas others diffuse moderately quickly. More experimental evidence may be needed to identify the molecular entities corresponding to the different populations, and based on the available data, a number of interpretations are possible. The very slowly diffusing entities very likely represent CD28 receptors that are immobilised on the glass surface *via* DAM. The more quickly diffusing receptors may be antibody-bound but not immobilised *via* DAM. Alternatively, they may be part of an array of crosslinked receptors, with a distant "anchoring" receptor immobilised *via* DAM. In

understanding the mechanism that leads to the slowing down of CD28 under JJ316 stimulation, it would be important to define the nature of the receptors diffusing at different speeds.

A bystander receptor of a similar size to CD28 (or the TCR), CD86, was not affected in its diffusion when co-expressed truncCD28 was ligated with JJ316 or JJ319, whereas CD45, spanning a larger dimension [153], was constrained. Two conclusions can be drawn from this. First, the formation of large CD28 clusters hindering the diffusion of non-clustered proteins cannot explain the diffusional constraint on CD28; and second, transmembrane proteins may be constrained in their diffusion dependent on their dimensions; *i.e.* a diffusing antibody/CD28 complex and CD45 may both be sufficiently large to be slowed down whereas CD86, and by inference the TCR and unligated CD28, may be too short to be affected. Testing this idea, the distance of the cell/glass contact was established *via* an antibody/PD1 complex, and the diffusion of JJ316-, JJ319- or unligated CD28 was measured. Antibody-bound but not unbound CD28 was slowed down when either a membrane-proximally or a membrane-distally binding anti-PD1 antibody was used to create the cell/glass distance, but the effect was smaller than when antibody-bound CD28 was immobilised itself *via* DAM. In a future experiment, it would be of interest to test whether the diffusion of CD43 constructs differing in the length of the extracellular domain would be affected differentially in this setting. Overall, whatever the mechanism, it appears that diffusing CD28 receptors are slowed down by the creation of a close cell/glass contact *via* surface-immobilised CD28 receptors. Mathematical modelling of receptor signalling could be used to determine whether a ~2.5-fold difference in CD28 diffusion makes a significant contribution to signalling, and how much the diffusional effects and the effects on spatial segregation of CD45 (~2-fold difference) each contribute to signalling by the superagonistic *versus* non-superagonistic antibodies.

# Chapter 7 General discussion

Work described in this thesis investigated the molecular mechanism underlying antibody-induced lymphocyte signalling with a focus on "superagonists", which comprise a particularly potent class of antibody. The new work contributes to elucidating the "triggering problem", *i.e.* the mechanism by which immunoreceptors become phosphorylated by extrinsic kinases. This is because any plausible explanation for receptor triggering needs to satisfy the different means by which receptors are triggered, and those include their ligation with antibodies in addition to native ligands, and even ligand-independent pathways of signalling [153]. Furthermore, it is crucial to understand the signalling mechanism when designing therapeutic antibodies to be used to treat cancer or autoimmune patients. First, mechanistic insight is needed to successfully switch on or off immune responses, and to understand the full potential of this type of therapeutic approach, and second, perhaps more importantly, so that serious adverse effects are to be avoided that might otherwise occur unexpectedly [237-240, 281].

## 7.1. Results from this thesis

### Characterising the anti-CD28 model antibodies JJ316 and JJ319

The experiments described herein addressed the molecular mechanism of superagonistic antibodies using JJ316 as a model, an anti-rat CD28 antibody shown to induce full T-cell activation in the absence of a second stimulus [228]. JJ319, a "conventional" anti-rat CD28 antibody, is costimulatory: while it is inactive on its own, it reduces the amount of anti-TCR stimulus required to induce activation [228]. While the two antibodies had been characterised functionally by others *in vitro* and *in vivo* [131, 228, 229, 231, 249], information on their thermodynamic properties and binding kinetics was limited. To address the hypothesis that an increased affinity for CD28 underpins the greater potency of JJ316, work in Chapter 3 compared the binding kinetics and affinities of JJ316 and JJ319 using two approaches. A flow-cytometry

based assay confirmed that bivalent JJ319 had a larger apparent on-rate for cell-bound CD28 than JJ316 (as also observed in [228]), while no difference in the apparent off-rate was observed. A surface plasmon resonance-based analysis showed that the monovalent affinities of JJ316- and JJ319 Fab fragments for CD28 were identical, and therefore it was formally excluded that JJ316 is more potent because it has a higher affinity. Indeed, its affective affinity is slightly lower because of its smaller on-rate for cell-bound CD28.

**Antibody superagonism can be studied on glass surfaces suitable for imaging**

Having excluded affinity as the defining factor underpinning antibody superagonism, the structural differences between the antibodies were considered: whereas superagonists bind membrane-proximally, forming flat complexes with CD28, conventional antibodies bind membrane-distally and form V-shaped complexes that are extended by ~ 75 Å [131, 229]. This prompted the hypothesis that superagonists more efficiently exclude large receptor-type protein-tyrosine phosphatases from CD28, as proposed for the TCR [86, 214], leading to receptor phosphorylation and signalling. Previous work tested this hypothesis by stimulating T-cell lines with antibodies immobilised on EIA plastic surfaces, and found that superagonism depends on the dimensions of both CD28 and the phosphatase [249]. This thesis aimed to further investigate the hypothesis using imaging, testing whether segregation of the phosphatase CD45 can be directly observed in the vicinity of antibody-ligated CD28, and whether any differences in the extent of segregation are measurable for the two antibodies. However, imaging is typically performed on glass surfaces, and it was therefore necessary to test whether the antibodies were active on glass. Work in Chapter 4 established a stimulation assay on glass, and formally confirmed that JJ316 is also superagonistic on glass whereas JJ319 is costimulatory on glass using mathematical fitting with a biochemical binding model. Others had previously reported that JJ316-induced signalling requires the presence of the TCR [231], and this requirement was re-confirmed for signalling on glass in Chapter 4. A possible explanation for this is that low level, sub-threshold TCR triggering occurs, although

TCR phosphorylation in response to JJ316 was not detectable [229]. It is conceivable that tonic TCR signalling is required to recruit signalling partners to the plasma membrane, facilitating the induction of a signalling cascade. This would be consistent with the observation that active ZAP-70 is required for superagonistic signalling [19]. It has been shown previously that low-level TCR triggering occurs when cells form contacts with glass surfaces in the absence of any TCR ligand [153]. Importantly, signalling differed on glass *versus* EIA plastic: whereas on glass JJ316-induced signalling was CD28-mediated, another receptor, most likely the TCR, was in large part responsible for the signalling observed on EIA plastic. It was therefore helpful to characterise antibody superagonism on glass because CD28 superagonism could be studied in isolation.

Although JJ316 induces IL-2 production when indirectly immobilised on glass, early calcium fluxes were not detected in this setting, suggesting that antibody superagonism is characterised by low-level tonic signalling that leads to activation. This distinguishes CD28- from TCR-signalling, which typically involves early calcium fluxes. Of note, two separate processes lead to calcium signalling [282]. First, calcium channels in the membrane surrounding the endoplasmic reticulum are opened, resulting in a calcium flux into the cytoplasm. Second, calcium is transported from the extracellular space *via* channels in the plasma membrane [232], a process prevented in the present experiments by suspension of the cells in a buffer with negligible calcium. The CD28 cytoplasmic tail encodes several signalling motifs, including the membrane-proximal YNMN and the membrane-distal PYAP motifs, which have been well-studied [118]. There is evidence that other, thus far uncharacterised motifs may also contribute to CD28-dependent signalling [130]. Distinct signalling pathways are triggered by the separate motifs, suggesting an explanation for how an IL-2 response is triggered in the absence of strong calcium signalling: YNMN is known to recruit PI3K, inducing calcium signalling, whereas PYAP recruits Src-family kinases that initiate a cascade resulting in activation of the transcription factor NFκB, and IL-2 production [130, 219]. It is conceivable that the superagonist induces PYAP-mediated rather than YNMN-mediated signalling. Alternatively, the superagonist may induce signalling *via*

both motifs, and while PYAP-mediated signalling is sufficiently strong to induce NF𝜅B activation, the YNMN-based signalling may be sub-threshold for inducing a calcium flux in the absence of an additional, overt TCR-mediated signal. These explanations are compatible with the observation that soluble anti-human CD28 superagonist ANC28.1 efficiently induces NF-𝜅B, but not NFAT, which is dependent on calcium signalling [283]. ANC28.1, however, is reported to induce calcium fluxing when used in solution in a flow cytometry-based assay [231, 284]. Whether calcium signalling is induced may either depend on the specific superagonistic antibody, or it may be a species-specific phenomenon. Functional differences between human and mouse CD28 signalling have previously been reported: a one amino acid difference in the membrane-distal PYAP motif has been suggested to uniquely enable the human motif to recruit and activate VAV-1, and this could be responsible for inducing calcium signalling when human CD28 is superagonised [135].

In future experiments, it would be of interest to further investigate the signalling pathways triggered by JJ316, using, for example, a phosphorylation-sensitive Western blot of key downstream signalling proteins. Mutant forms of CD28 could be used where either of the two motifs, or both, are disrupted (Jiandong Huo, Davis laboratory, University of Oxford; unpublished work).

**Superagonist-induced signalling is explainable by a combination of kinetic segregation and crosslinking**

Experiments in Chapter 5 defined the molecular requirements for superagonist-induced signalling on glass, using conditions for which signalling is strictly CD28-dependent. In addition to confirming that signalling is sensitive to the dimensions of CD28 [249] and the phosphatases CD45 and CD148 as previously observed on EIA plastic ([249]; Sara Morgan, Davis laboratory, University of Oxford; unpublished work), it was shown here that extending the dimensions of JJ316 itself by ~ 75 Å transforms it from a superagonistic into a conventional antibody. These findings confirm a key prediction of the KS model, *i.e.* that signalling depends on the

dimensions of the CD28-antibody complex and the phosphatase relative to each other. Another important prediction is that signalling depends on the immobilisation of the antibody. Work in Chapter 5 showed that while JJ316 was active in solution, the $F(ab')_2$ form of the antibody was only active when immobilised, suggesting that immobilisation *via* an Fc receptor other than CD16/CD32 may be responsible for the activity of "soluble" JJ316.

A dependence on CD28 crosslinking was also confirmed on glass, matching previous results obtained on EIA plastic [249]. The question then arises of whether it is sufficient. Others reporting that $F(ab')_2$ fragments of superagonists are inactive have argued that the Fc region decreases hinge flexibility thereby promoting an antibody conformation that is more active because it crosslinks CD28 more efficiently [230]. However, the $F(ab')_2$ fragments appear to be stable and in an active conformation following immobilisation *via* anti-light chain antibody, and it seems unlikely that the antibody would stabilise the hinge region in the same fashion as the Fc region would, creating the same "parallel" antibody conformation that was suggested to be essential by Ball *et al* [230]. These considerations suggest that cross-linking alone is not sufficient. It would be of interest to test whether signalling induced by "soluble" JJ316 was affected by the dimensions of the phosphatases. If very efficient crosslinking of CD28 by non-immobilised JJ316 was really sufficient to induce superagonistic signalling without immobilisation, extending the CD28-antibody complex or truncating the phosphatase ought not to affect signalling. If, on the other hand, "soluble" JJ316 was sensitive to phosphatase dimensions, one could conclude that JJ316 is likely immobilised on a cell surface, and signalling arises due to cross-presentation of the antibody. Consistent with this conclusion, it has previously been reported that expression of Fc receptors is necessary for antibody-mediated superagonism [281, 285], and it seems more likely that JJ316 is active in solution because it is cross-presented by an undescribed Fc receptor. The hypothesis that JJ316 is more potent because it is a more efficient crosslinker [132] is also inconsistent with cryo-EM images showing that both conventional and superagonistic antibodies can crosslink CD28 efficiently and form large arrays [131]. It appears that the crosslinking

is a requirement in the case of CD28 because a monomeric form of CD28, *i.e.* a PD1/CD28 chimera, is inactive unless it is crosslinked by a second antibody. Crosslinking appears, however, to be a special requirement of anti-CD28 superagonism, since PD1 itself is agonisable despite being a monomeric receptor [260]. It is possible that CD28 evolved to be a particularly weak signaller in order that it complements, rather than overwhelms signalling by the TCR. The natural, cell-bound ligands, CD80 and CD86, both interact monovalently with CD28 [132]. Therefore, CD28 crosslinking and superagonistic signalling likely does not occur naturally and is a phenomenon associated only with artificial bivalent ligands, such as antibodies.

The effects of efficient crosslinking of CD28 could explain why particularly dense immobilisation of JJ316 produced unexpected results. Firstly, at high levels of immobilisation, JJ316-induced signalling is observed even when cells express a signalling-disabled form of CD28, as seen on EIA plastic and on FcR-coated, nickelated plastic. The observed signalling likely results from the triggering of another receptor for which no ligand is present, most probably the TCR since its presence is required for CD28 superagonism. Possibly, crosslinked arrays of CD28 trap the TCR in phosphatase-depleted regions, causing it to trigger. This hypothesis could be tested using imaging, measuring the diffusion rate of the TCR and determining whether it is affected when cells are stimulated with highly crosslinked JJ316 or JJ319. A problem with this approach, however, is that it would not be possible to determine whether the TCR changes its diffusion because of steric effects and triggers signalling as a consequence, or whether the TCR triggers signalling *via* some other mechanism and then slows down as a consequence, *e.g.* due to downstream signalling molecules binding to its phosphorylated signalling motifs. As a proxy, the diffusion of CD86, which roughly matches the TCR with respect to its dimensions, was measured. Since its diffusion was unaffected by the anti-CD28 antibodies, it appears unlikely that the TCR would be significantly constrained by CD28 crosslinking.

A second surprising result was that, at high levels of immobilisation *via* a densely coated FcR, superagonistic signalling was induced even by JJ319. However, in this case, higher

levels of immobilisation were required than for JJ316. A possible explanation is that JJ319 and JJ316 induce signalling by the same mechanism, but JJ319 does this less efficiently, and thus a larger amount of ligation is needed to overcome the threshold for a superagonistic response. This explanation is compatible with a KS-based signalling model, in which both antibodies exclude large phosphatases by size, but JJ316 does so more efficiently because it creates a closer contact. Interestingly, however, JJ319-induced signalling plateaued at a lower level (*i.e.* a lower amount of released IL-2) than did JJ316-induced signalling. This suggests that JJ319-induced signalling differs qualitatively from JJ316-induced signalling. It is possible the difference in response for JJ316 *versus* JJ319 at saturating amounts of stimulation results from a larger contribution by the TCR to signalling, and this interpretation is compatible with the fact that JJ316, but not JJ319 induces IL-2 production at high FcR immobilisation in cells that express signalling-disabled CD28. Another explanation is that weak *versus* strong signalling by the two antibodies leads to the recruitment of different effectors to the signalling motifs. In addition to the levels of immobilisation possible, antibody presentation using immobilised FcRs differs in two more ways from presentation *via* secondary antibody. Firstly, the FcR forms a more compact complex with the antibody; it binds to the lower hinge region of the antibody, and forces it into a configuration in which the Fc region faces downward [63, 64], as illustrated in Figure 7-1. Since the KS model predicts signalling to correlate with the receptor-antibody dimensions, it is possible that not only high levels of immobilisation, but also the more compact binding of JJ319 to the FcR versus its immobilisation *via* secondary antibody on glass now result in superagonistic activity. Secondly, the affinity of the mFcγRIIb/mIgG1 interaction is low at 0.70 μM, due to a relatively high off-rate. Effectively, this decreases the affinity of the FcR/antibody-CD28 complex ~ 10 fold[52]. The high off-rate resembles that of natural ligands, and could perhaps allow the antibodies to serially engage and trigger a lot more receptors. Mathematical modelling of signalling could indicate in which way and to what extent these factors (high

[52] JJ316 and JJ319 bind CD28 with an affinity of ~ 0.095 μM (see Section 3.3.4).

immobilisation of the antibody, a TCR contribution, compact complex formation with the FcR, low affinity of the FcR/antibody interaction) contribute.

Because JJ319, which binds at the top of CD28 near the ligand-binding site and is likely a blocker, can be turned into a superagonist, it suggests that for small proteins like PD1 there will be no such thing as a blocking-only antibody (*i.e.* all blockers will have some agonistic activity). It would be interesting to test whether residual agonistic activity of blocking antibodies could be reduced or completely removed by extending their hinge region with a rigid insertion, since this abrogated the superagonistic activity in the case of JJ316.

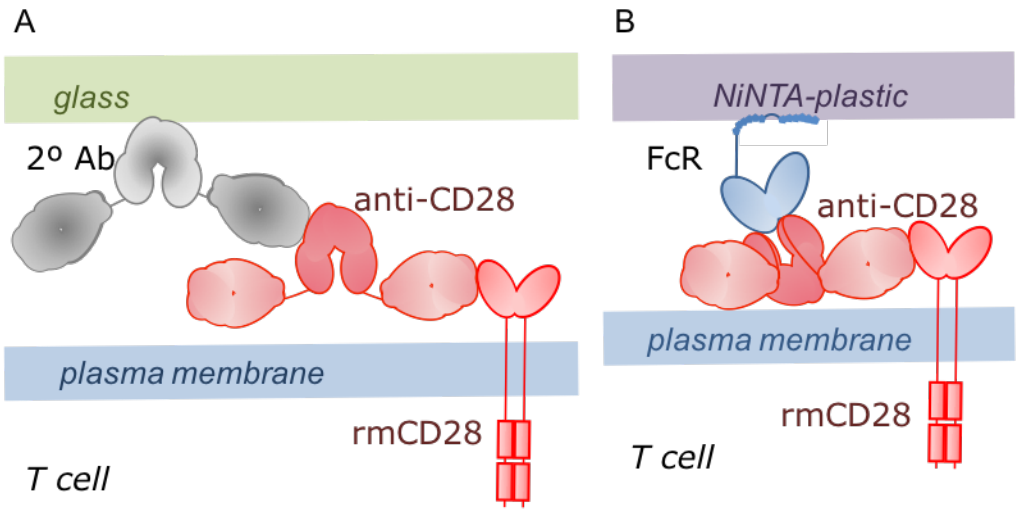



Figure 7-1: Antibody immobilisation *via* secondary antibody or Fc receptor. A cartoon illustrates the configuration thought to be adopted by an IgG antibody when immobilised via **A** secondary antibody (2º Ab) *versus* **B** an Fc receptor. (FcR)

**The superagonist excludes CD45 more efficiently and constrains the diffusion of sufficiently large transmembrane proteins**

Finally, in Chapter 6, imaging experiments were undertaken to investigate whether (1) differences in the extent of CD45 segregation by the two antibodies could be directly observed, and (2) the diffusion of CD28 and bystander receptors is affected, potentially also contributing to their phosphorylation and signalling. It was found first of all that

segregation of CD45 was more pronounced in case of the superagonistic versus the conventional antibody (~2-fold), and was apparent across the entire cell/glass contact and not confined to areas enriched in antibody, although it was more pronounced in those areas. It is possible that the ligand-independent triggering of the TCR under superagonistic stimulation, as observed in the IL-2 experiments, is caused by such a global exclusion of CD45. This differs from observations made by Chang *et al* who studied the signalling consequences of ligand-independent segregation of CD45 from the TCR (*i.e.* without antibody ligation). In that case, clear-cut "close contacts" were observed from which CD45 was very efficiently excluded, and whose formation correlated with signalling [153]. In the present experiments, similar ring-like regions of enhanced "segregation" in terms of anti-correlated spatial dynamics could only be visualised in DAVIS plots, implying that subtler changes in CD45 distribution were occurring. A possible interpretation is that these areas are the hotspots of antibody-induced signalling, accommodating antibody-bound CD28 and protecting it from CD45 dephosphorylation by steric exclusion of the phosphatase. Another possibility is that these are regions where the antibody "catches" the DAM as initial contacts grow. A difference between the two studies is that here, the cell was held away from the glass by a distance defined by the receptor/antibody complex, whereas Chang *et al* imaged cells directly interacting with protein-coated glass, possibly creating closer cell/glass contacts. It is also possible that the formation of such clear-cut "close contacts" is cell line-dependent, and may occur to a smaller extent with the BW5147 cells used here.

Chang *et al* reported that a ~2.2-fold increase in the Lck/CD45 ratio within "close contacts" sufficed to induce ligand-independent receptor triggering that resulted in calcium signalling [153], indicating that the increased segregation of CD45 by JJ316 may well be enough to explain its superagonistic activity. A more efficient segregation of phosphatases from superagonist-ligated CD28 had been predicted based on the compact dimensions of the complex [86, 131]. The explanation that the expected ~ 75 Å difference in height for JJ316/CD28 *versus* JJ319/CD28 is responsible for the observed differences in spatial segregation of CD45 is supported by several studies

reporting that dimensional differences in the range of 40-60 Å suffice to drive the passive segregation of unbound proteins [217, 286-288]. In a GUV system, where factors such as cytoskeleton-driven protein rearrangements and lipid raft formations are eliminated, a 40 Å difference in height between a ligated protein, defining the gap size between two GUVs, and an unbound bystander protein proved to be sufficient for complete segregation [217]. The TCR-pMHC interaction, spanning ~ 13 nm, was also shown to effect the steric exclusion of CD45, which is thermodyamically driven by membrane rigidity [286]. In the immunulogical synapse, particles [287] and transmembrane proteins [288] exceeding a threshold length by ~ 60 Å are excluded, again by a factor of ~ 2. Another possible explanation for CD45 segregation is efficient crosslinking of CD28 by the superagonist, analogous to the observation that lateral crowding of ligand-engaged protein excludes unbound bystander proteins [217]. It would therefore be of interest to test whether CD45 segregation is crosslinking-dependent, *e.g.* whether ligating truncPDCD28 with clone 19 alone suffices to exclude CD45 from the cell/glass contact or whether a combination of clone 19 and clone 2 is required, and whether bystander receptors with smaller dimensions (*e.g.* CD86, or LAT-CD45) are segregated independently of size due to crowding effects.

Single-particle tracking showed that the antibodies constrain the diffusion of antibody-bound CD28, with JJ316 having a larger (~2.5-fold) effect than JJ319. Co-expressed CD86, a receptor that matches unligated CD28 and the TCR in size, but that is expected to be smaller than antibody-bound CD28, was unaffected in its diffusion, whereas the larger CD45 slowed its diffusion, prompting the hypothesis that the diffusion of only bystander receptors exceeding a certain length is constrained, possible because JJ316 creates a close contact between cell and glass. The clone 19/PD1 interaction, which is predicted to span similar dimensions as CD28/JJ316, was used to create such a contact, and the antibody-ligated CD28 slowed down its diffusion, although the effect was smaller. This indicates that creating a close gap as well as immobilisation of the receptor both contribute to slowing its diffusion. It was noteworthy that crosslinking of PDCD28 was not required to constrain the diffusion of bystander receptors (*i.e.* antibody-ligated CD28).

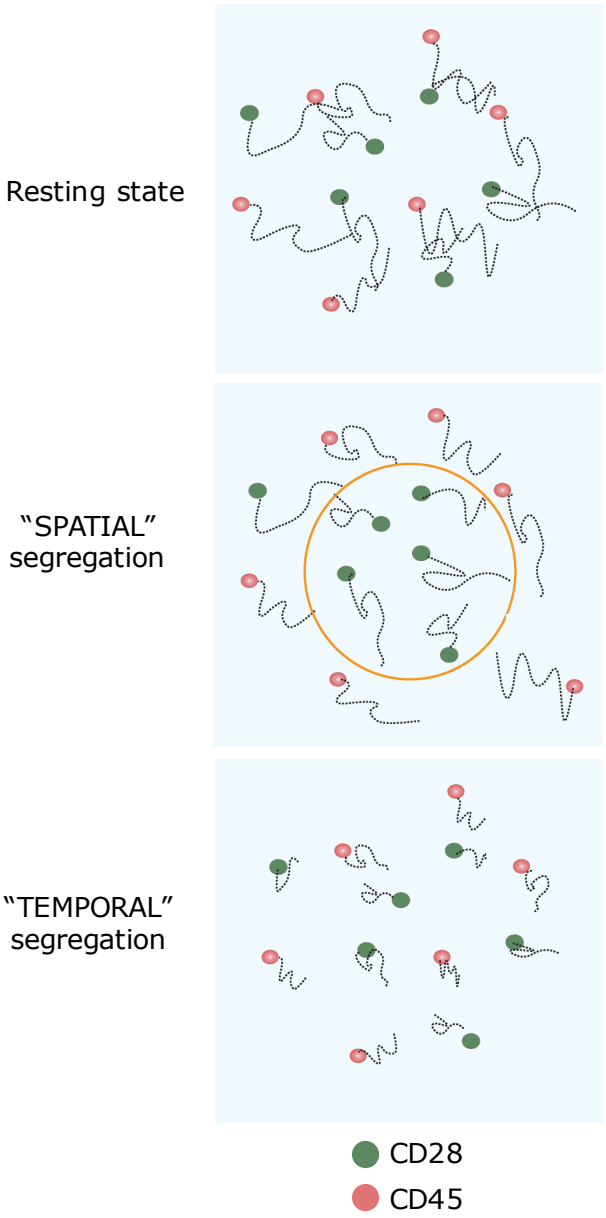



Figure 7-2: Segregation on a spatial or a temporal scale can lead to signalling. **A** At resting state, both CD28 and CD45 diffuse quickly and undergo frequent encounters that keep CD28 phosphorylation levels very low. **B** Stimulation with immobilised anti-CD28 antibodies creates a close contact from which CD45 is sterically excluded. CD28 receptors are held in the contact *via* their interaction with the antibodies, and are thereby protected from dephosphorylation, resulting in signalling. **C** Both CD28 and CD45 show a decreased diffusion during antibody stimulation. This results in a decreases their encounter rate, which in turn increases the probability of CD28 being phosphorylated, and results in signalling.

Further investigation, perhaps in the form of mathematical modelling, is needed to determine if and in what way the diffusional effects contribute to superagonist-induced signalling. It is conceivable that non-immobilised but superagonist antibody-bound CD28 resides in phosphatase-depleted areas for longer periods of time because it slows down in its diffusion, sufficiently increasing the half-life of its phosphorylation to induce downstream signalling. Another possibility is that CD45 and non-immobilised CD28 are separated on a temporal rather than a spatial scale. Because they both experience reduced diffusion (in contrast to Lck), the probability of their encounter is decreased, which could result in signalling by increasing the half-life of Lck-mediated CD28 phosphorylation (see Figure 7-2).

## 7.2. Future work

The work presented in this thesis focused on the role of receptor-type protein tyrosine phosphatases in antibody-mediated signalling, and showed that (1) signalling depends on the dimensions of the phosphatases relative to the antibody-receptor complex, and (2) that the more potent superagonistic antibody spatially excludes CD45 from the cell/glass contact to a greater extent than the non-superagonist. However, the role of kinases has not yet been addressed. According to the KS model, receptors become triggered because the kinase/phosphatase balance is locally shifted to favour phosphorylation when large phosphatases are excluded from "close contacts" where the receptor is held, whereas kinases continue to diffuse unperturbed [86]. The prediction is that, if the phosphatases and kinases (*e.g.* Lck, which is required for superagonist-mediated signalling [231, 289, 290]) were to be equally excluded by the antibodies, the kinase/phosphatase balance would be unchanged, and there would be no signalling. This question could be addressed by expressing a chimeric form of Lck in Lck-negative cells (*e.g.* JCAM) that is fused to either (A) a transmembrane domain and a truncated (*e.g.* four amino acids) extracellular domain, or (B) a transmembrane domain and the full-length extracellular domain of CD45. One could test whether the (A) and (B) forms of Lck would differentially (1) restore anti-CD28 mediated IL-2 production in JCAM cells and (2) segregate from CD28 in imaging experiments.

Similar experiments were done by Chang *et al* to show that ligand-independent TCR triggering is strictly dependent on the local segregation of CD45 and Lck at close contacts [153].

In the stimulation assay developed in this thesis, T cells were stimulated with antibodies indirectly immobilised on glass surfaces, and the same arrangement was used to image the T-cell surface. This particular arrangement was chosen (1) because it most closely resembles the *in vitro* setting in which antibody superagonism had been characterised before, *i.e.* on plastic surfaces [228, 229, 249], and (2) because it is well-suited to TIRFM-based imaging of the T-cell surface [153, 291, 292]. It is, however, rather unphysiological. *In vivo*, antibodies are most likely immobilised on the surface of a second cell *via* FcRs [281, 285]. Considering that the distribution of surface proteins relative to each other appears to be rearranged by the antibodies, leading to signalling, such processes may well be influenced by the proteins and lipid environment in the membrane of the FcR-bearing cell [111, 217]. Also, the glass surface may induce artefacts. Contact with a glass surface alone suffices to induce receptor rearrangements, including the segregation of phosphatases, leading to calcium signalling [153], although signalling-dependent effects were minimised in the imaging experiments here by using non-signalling conditions. For the signalling experiments, the glass surface alone was never able to induce IL-2 production. Lymphocyte motility is greatly reduced on two-dimensional substrates [257], and the glass substrate is much more rigid than lymphoid tissue, which has been reported to affect cellular signalling, differentiation and proliferation [254-256]. It would be ideal, of course, to image antibody-mediated changes in the context of a cell/cell contact, and this has recently become possible with the advent of 3D light-sheet microscopy [293]. A T cell could be brought into contact with an FcR-bearing cell that was coated with antibody, for instance with a micropipette [294] or with the help of low-energy lasers ("optical tweezers"; [295]). In the case that it may not be possible to achieve sufficient resolution in this setting, T cells could be imaged in contact with superagonistic antibody-coated supported lipid bilayers (SLBs) that are functionalised with proteins [153, 296]. The mFcγRIIb-His construct that was produced (see Section 5.3.8) is well-suited to insertion into an SLB

*via* a "nickelated" lipid, allowing presentation of the anti-CD28 antibodies. More proteins could be included in the SLB to build up a proper physiological context for signalling, such as adhesion molecules like CD2 [297, 298], or glycocalyx proteins such as CD45 that would potentially constrain the formation of close contacts that lead to ligand-independent signalling [153] (*i.e.* under the "no antibody" negative control condition). It would be important to confirm that the antibodies can diffuse freely on the bilayers, since the interactions with PLL-coated glass are reported to decrease receptor mobility and to promote clustering [107]. Studies on receptor distribution and diffusion could be complemented with a calcium flux assay (as discussed in Section 4.3.3) to better characterise antibody-induced signalling on SLBs.

The work in this thesis has shown that superagonistic signalling on glass is sensitive to receptor and phosphatase dimensions, and that large proteins (*i.e.* CD45) are spatially segregated and constrained in their diffusion. This, together with the observation that superagonists bind membrane-proximally [229] and form compact complexes [131], has prompted the hypothesis that superagonistic antibodies create a cell/glass contact that spans a smaller distance than the contact created by conventional antibodies. It would be of interest to measure the membrane/glass distance by imaging, *i.e.* to generate an image that displays a "height map" of the cell/glass contact. One might be able to overlay such a "height map" with a DAVIS plot to test whether areas in which CD45 is particularly segregated from antibody-bound CD28 correlate with areas in which the cell is particularly close to the glass. Several techniques may be suitable to detect the expected ~ 75 Å height difference for the superagonistic *versus* the conventional antibody, such as reflection interference contrast microscopy (RICM; resolution ~ 50 Å; [217, 299], metal-induced energy transfer (resolution ~ 50 Å; [300]), or variable-angle TIRFM (resolution ~ 100 Å; [301]). Alternatively, fluorescent particles of different sizes could be used to probe the cell/glass distance since they would be sterically excluded from contacts that are smaller than their diameter [288, 302].

## 7.3. Concluding remarks

The work embodied in this thesis provides new evidence that not only signalling by native ligands, but also by antibodies, is accountable according to the KS model, broadening its explanatory range. An important corollary of these findings is that the simple mechanism of antibody-induced signalling uncovered here ought to apply to any receptor likely to be triggered by the interplay of Src kinases and large tyrosine phosphatases, offering important opportunities to agonise receptors in therapeutic settings.

An anti-hCD28 superagonist, TGN1412, was used in a "first-in-humans" trial with the aim of selectively activating regulatory T cells, but all six healthy volunteers experienced an unexpected cytokine storm [237-239, 248, 303]. Pre-clinical *in vitro* experiments did not predict the adverse effects, possibly because the antibodies were not immobilised as they likely are *in vivo* [230, 238, 281], and because species-specific differences in CD28 signalling [135] and the expression levels of CD28 in effector memory T-cell subsets [304] likely masked potentially serious adverse effects in pre-clinical *in vivo* experiments. This episode partially motivating the research into the mechanism of antibody superagonism as presented in this thesis. Although later *in vitro* and first-in-humans studies showed that lowering the TGN1412 dose effected the desired selective expansion of regulatory T-cells without inducing inflammation [240], the possible clinical use of superagonistic antibodies against CD28, or other costimulators, remains highly controversial. Targeting negative regulators of immunity, however, offers a potentially safer way of tuning immune responses with the help of superagonistic antibodies, *i.e.* to supress TCR-mediated signalling in autoimmune disease. The experiments described in this thesis offer a sound foundation for developing a new class of potentially therapeutic antibodies, the inhibitory superagonists.

# Appendix

## Sequence of a soluble rat CD28 – mouse Fc – hexahistidine fusion protein (rCD28-mFc-His)

XbaI Kozak START rCD28 ECD thrombin cleavage site XmaI mFc 6His-tag STOP BamHI

```
tctagactcaagcaggccaccatgacgctcaggctgctattcttggctctcagcttcttc
 -  -  -  -  -  -  -  M  T  L  R  L  L  F  L  A  L  S  F  F
tcagttcaagtaacagaaaacaagattttggtgaagcagtccccgctgcttgtggtagat
 S  V  Q  V  T  E  N  K  I  L  V  K  Q  S  P  L  L  V  V  D
aacaatgaggtcagcctcagctgcaggtattcctacaaccttcttgcaaaggagttccgg
 N  N  E  V  S  L  S  C  R  Y  S  Y  N  L  L  A  K  E  F  R
gcatccctttacaagggcgtgaacagtgacgtggaagtctgtgtcgggaatgggaatttt
 A  S  L  Y  K  G  V  N  S  D  V  E  V  C  V  G  N  G  N  F
acctatcagccccagttccgcccaaacgtggggttcaactgtgatgggaatttcgacaat
 T  Y  Q  P  Q  F  R  P  N  V  G  F  N  C  D  G  N  F  D  N
gaaacagtgacgttccgtctctggaatctgcatgttaatcacacagatatttacttctgc
 E  T  V  T  F  R  L  W  N  L  H  V  N  H  T  D  I  Y  F  C
aaaatcgaggtcatgtatcctccgccatacctggacaacgagaagagcaacggaactatt
 K  I  E  V  M  Y  P  P  P  Y  L  D  N  E  K  S  N  G  T  I
attcacataaaagagaaacatctttgtcatgctcagacgtctcctaagctgctggtaccc
 I  H  I  K  E  K  H  L  C  H  A  Q  T  S  P  K  L  L  V  P
cggggtagtggtagtaagcctagcataagtacagtcccagaagtatcatctgtcttcatc
 R  G  S  G  S  K  P  S  I  S  T  V  P  E  V  S  S  V  F  I
ttccccccaaagcccaaggatgtgctcaccattactctgactcctaaggtcacgtgtgtt
 F  P  P  K  P  K  D  V  L  T  I  T  L  T  P  K  V  T  C  V
gtggtagacatcagcaaggatgatcccgaggtccagttcagctggtttgtagatgatgtg
 V  V  D  I  S  K  D  D  P  E  V  Q  F  S  W  F  V  D  D  V
gaggtgcacacagctcagacgcaacccagggaggagcagttcaacagcactttccgctca
 E  V  H  T  A  Q  T  Q  P  R  E  E  Q  F  N  S  T  F  R  S
gtcagtgaacttcccatcatgcaccaggactggctcaatggcaaggagttcaaatgcagg
 V  S  E  L  P  I  M  H  Q  D  W  L  N  G  K  E  F  K  C  R
gtcaacagtgcagctttccctgcccccatcgagaaaaccatctccaaaaccaaaggcaga
 V  N  S  A  A  F  P  A  P  I  E  K  T  I  S  K  T  K  G  R
ccgaaggctccacaggtgtacaccattccacctcccaaggagcagatggccaaggataaa
 P  K  A  P  Q  V  Y  T  I  P  P  P  K  E  Q  M  A  K  D  K
gtcagtctgacctgcatgataacagacttcttccctgaagacattactgtggagtggcag
 V  S  L  T  C  M  I  T  D  F  F  P  E  D  I  T  V  E  W  Q
tggaatgggcagccagcggagaactacaagaacactcagcccatcatggacacagatggc
 W  N  G  Q  P  A  E  N  Y  K  N  T  Q  P  I  M  D  T  D  G
tcttacttcgtctacagcaagctcaatgtgcagaagagcaactgggaggcaggaaatact
 S  Y  F  V  Y  S  K  L  N  V  Q  K  S  N  W  E  A  G  N  T
ttcacctgctctgtgttacatgagggcctgcacaaccaccatactgagaagagcctctcc
 F  T  C  S  V  L  H  E  G  L  H  N  H  H  T  E  K  S  L  S
cactctcctggtaaacatcaccatcaccatcactaaggatcc
 H  S  P  G  K  H  H  H  H  H  H  -  -  -
```

**Sequence of a chimeric rat-mouse CD28 gene (rmCD28)**[53]

MluI Kozak START rCD28 ECD mCD28 TMD mCD28 ICD STOP NotHI

```
acgcgtctcaagcaggccaccatgacgctcaggctgctattcttggctctcagcttcttc
 T  R  L  K  Q  A  T  M  T  L  R  L  L  F  L  A  L  S  F  F
tcagttcaagtaacagaaaacaagattttggtgaagcagtccccgctgcttgtggtagat
 S  V  Q  V  T  E  N  K  I  L  V  K  Q  S  P  L  L  V  V  D
aacaatgaggtcagcctcagctgcaggtattcctacaaccttcttgcaaaggagttccgg
 N  N  E  V  S  L  S  C  R  Y  S  Y  N  L  L  A  K  E  F  R
gcatccctttacaagggcgtgaacagtgacgtggaagtctgtgtcgggaatgggaatttt
 A  S  L  Y  K  G  V  N  S  D  V  E  V  C  V  G  N  G  N  F
acctatcagccccagttccgcccaaacgtggggttcaactgtgatgggaatttcgacaat
 T  Y  Q  P  Q  F  R  P  N  V  G  F  N  C  D  G  N  F  D  N
gaaacagtgacgttccgtctctggaatctgcatgttaatcacacagatatttacttctgc
 E  T  V  T  F  R  L  W  N  L  H  V  N  H  T  D  I  Y  F  C
aaaatcgaggtcatgtatcctccgccatacctggacaacgagaagagcaacggaactatt
 K  I  E  V  M  Y  P  P  P  Y  L  D  N  E  K  S  N  G  T  I
attcacataaaagagaaacatctttgtcatgctcagacgtctcctaagctgttttgggca
 I  H  I  K  E  K  H  L  C  H  A  Q  T  S  P  K  L  F  W  A
ctggtcgtggttgctggagtcctgttttgttatggcttgctagtgacagtggctctttgt
 L  V  V  V  A  G  V  L  F  C  Y  G  L  L  V  T  V  A  L  C
gttatctggacaaatagtagaaggaacagactccttcaaagtgactacatgaacatgact
 V  I  W  T  N  S  R  R  N  R  L  L  Q  S  D  Y  M  N  M  T
ccccggaggcctgggctcactcgaaagccttaccagccctacgcccctgccagagacttt
 P  R  R  P  G  L  T  R  K  P  Y  Q  P  Y  A  P  A  R  D  F
gcagcgtaccgcccctagtaggcggccgc
 A  A  Y  R  P  -
```

[53] Cloned by Sara Morgan, D.Phil. OXON, Simon Davis laboratory, University of Oxford.

**Sequence of a non-signalling chimeric rat-mouse CD28 gene truncated in the cytosolic domain (truncCD28)**[54]

MluI Kozak START rCD28 ECD mCD28 TMD truncated mCD28 ICD STOP NotHI

```
acgcgtgccaccatgacactcagactgctattcttggctctcagcttcttctcagttcaa
 -  -  -  -  M  T  L  R  L  L  F  L  A  L  S  F  F  S  V  Q
gtaacagaaaacaagattttggtgaagcagtccccgctgcttgtggtagataacaatgag
 V  T  E  N  K  I  L  V  K  Q  S  P  L  L  V  V  D  N  N  E
gtcagcctcagctgcaggtattcctacaaccttcttgcaaaggagttccgggcatccctt
 V  S  L  S  C  R  Y  S  Y  N  L  L  A  K  E  F  R  A  S  L
tacaagggcgtgaacagtgacgtggaagtctgtgtcgggaatgggaattttacctatcag
 Y  K  G  V  N  S  D  V  E  V  C  V  G  N  G  N  F  T  Y  Q
ccccagttccgcccaaacgtggggttcaactgtgatgggaatttcgacaatgaaacagtg
 P  Q  F  R  P  N  V  G  F  N  C  D  G  N  F  D  N  E  T  V
acgttccgtctctggaatctgcatgttaatcacacagatatttacttctgcaaaatcgag
 T  F  R  L  W  N  L  H  V  N  H  T  D  I  Y  F  C  K  I  E
gtcatgtatcctccgccatacctggacaacgagaagagcaacggaactattattcacata
 V  M  Y  P  P  P  Y  L  D  N  E  K  S  N  G  T  I  I  H  I
aaagagaaacatctttgtcatgctcagacgtctcctaagctgttttgggcactggtcgtg
 K  E  K  H  L  C  H  A  Q  T  S  P  K  L  F  W  A  L  V  V
gttgctggagtcctgttttgttatggcttgctagtgacagtggctctttgtgttatctgg
 V  A  G  V  L  F  C  Y  G  L  L  V  T  V  A  L  C  V  I  W
acaaatagtagaaggaacagataggcggccgc
 T  N  S  R  R  N  R  -  -  -
```

[54] Cloned by Rachel Knox, B.Sc., Simon Davis laboratory, University of Oxford.

**Sequence of a chimeric human PD1 – mouse CD28 gene (PDCD28)**[55]

BglII Kozak START hPD1 ECD mCD28 TMD mCD28 ICD STOP XhoI

```
agatctctcaagcaggccaccatgcagatcccacaggcgccctggccagtcgtctgggcg
 -  -  -  -  -  -  -  M  Q  I  P  Q  A  P  W  P  V  V  W  A
gtgctacaactgggctggcggccaggatggttcttagactccccagacaggccctggaac
 V  L  Q  L  G  W  R  P  G  W  F  L  D  S  P  D  R  P  W  N
ccccccaccttctccccagccctgctcgtggtgaccgaaggggacaacgccaccttcacc
 P  P  T  F  S  P  A  L  L  V  V  T  E  G  D  N  A  T  F  T
tgcagcttctccaacacatcggagagcttcgtgctaaactggtaccgcatgagccccagc
 C  S  F  S  N  T  S  E  S  F  V  L  N  W  Y  R  M  S  P  S
aaccagacggacaagctggccgccttccccgaggaccgcagccagcccggccaggactgc
 N  Q  T  D  K  L  A  A  F  P  E  D  R  S  Q  P  G  Q  D  C
cgcttccgtgtcacacaactgcccaacgggcgtgacttccacatgagcgtggtcagggcc
 R  F  R  V  T  Q  L  P  N  G  R  D  F  H  M  S  V  V  R  A
cggcgcaatgacagcggcacctacctctgtggggccatctccctggcccccaaggcgcag
 R  R  N  D  S  G  T  Y  L  C  G  A  I  S  L  A  P  K  A  Q
atcaaagagagcctgcgggcagagctcagggtgacagagagaagggcagaagtgcccaca
 I  K  E  S  L  R  A  E  L  R  V  T  E  R  R  A  E  V  P  T
gcccaccccagcccctcacccaggtcagccggccagttccaaacctttgggcactggtc
 A  H  P  S  P  S  P  R  S  A  G  Q  F  Q  T  F  W  A  L  V
gtggttgctggagtcctgttttgttatggcttgctagtgacagtggctctttgtgttatc
 V  V  A  G  V  L  F  C  Y  G  L  L  V  T  V  A  L  C  V  I
tggacaaatagtagaaggaacagactccttcaaagtgactacatgaacatgactccccgg
 W  T  N  S  R  R  N  R  L  L  Q  S  D  Y  M  N  M  T  P  R
aggcctgggctcactcgaaagccttaccagccctacgcccctgccagagactttgcagcg
 R  P  G  L  T  R  K  P  Y  Q  P  Y  A  P  A  R  D  F  A  A
taccgcccctagctcgag
 Y  R  P  -  -  -
```

[55] Cloned by Rachel Knox, B.Sc., Simon Davis laboratory, University of Oxford.

**Sequence of a non-signalling chimeric human PD1 – mouse CD28 gene truncated in the cytosolic domain (truncPDCD28)**[56]

BglII Kozak START hPD1 ECD mCD28 TMD truncated mCD28 ICD STOP XhoI

```
agatctctcaagcaggccaccatgcaaatcccacaggcgccctggccagtcgtctgggcg
 R  S  L  K  Q  A  T  M  Q  I  P  Q  A  P  W  P  V  V  W  A
gtgctacaactgggctggcggccaggatggttcttagactccccagacaggccctggaac
 V  L  Q  L  G  W  R  P  G  W  F  L  D  S  P  D  R  P  W  N
ccccccaccttctccccagccctgctcgtggtgaccgaaggggacaacgccaccttcacc
 P  P  T  F  S  P  A  L  L  V  V  T  E  G  D  N  A  T  F  T
tgcagcttctccaacacatcggagagcttcgtgctaaactggtaccgcatgagccccagc
 C  S  F  S  N  T  S  E  S  F  V  L  N  W  Y  R  M  S  P  S
aaccagacggacaagctggccgccttccccgaggaccgcagccagcccggccaggactgc
 N  Q  T  D  K  L  A  A  F  P  E  D  R  S  Q  P  G  Q  D  C
cgcttccgtgtcacacaactgcccaacgggcgtgacttccacatgagcgtggtcagggcc
 R  F  R  V  T  Q  L  P  N  G  R  D  F  H  M  S  V  V  R  A
cggcgcaatgacagcggcacctacctctgtggggccatctccctggcccccaaggcgcag
 R  R  N  D  S  G  T  Y  L  C  G  A  I  S  L  A  P  K  A  Q
atcaaagagagcctgcgggcagagctcagggtgacagagagaagggcagaagtgcccaca
 I  K  E  S  L  R  A  E  L  R  V  T  E  R  R  A  E  V  P  T
gcccaccccagcccctcacccaggccagccggccagttccaaacctttgggcactggtc
 A  H  P  S  P  S  P  R  P  A  G  Q  F  Q  T  F  W  A  L  V
gtggttgctggagtcctgttttgttatggcttgctagtgacagtggctctttgtgttatc
 V  V  A  G  V  L  F  C  Y  G  L  L  V  T  V  A  L  C  V  I
tggacaaatagtagaaggaacagatagctcgag
 W  T  N  S  R  R  N  R  -  -  -
```

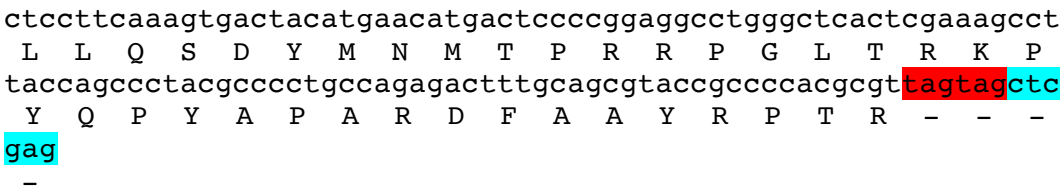
[56] Cloned by Rachel Knox, B.Sc., Simon Davis laboratory, University of Oxford.

**Sequence of a chimeric human Fc – rat-mouse CD28 gene (FcCD28)**[57]

BamHI Kozak START rCD28 ECD hFc mCD28 TMD mCD28 ICD STOP XhoI

```
ggatccgccaccatgacactcagactgctattcttggctctcagcttcttctcagttcaa
 -  -  -  -  M  T  L  R  L  L  F  L  A  L  S  F  F  S  V  Q
gtaacagaaaacaagattttggtgaagcagtccccgctgcttgtggtagataacaatgag
 V  T  E  N  K  I  L  V  K  Q  S  P  L  L  V  V  D  N  N  E
gtcagcctcagctgcaggtattcctacaaccttcttgcaaaggagttccgggcatccctt
 V  S  L  S  C  R  Y  S  Y  N  L  L  A  K  E  F  R  A  S  L
tacaagggcgtgaacagtgacgtggaagtctgtgtcgggaatgggaattttacctatcag
 Y  K  G  V  N  S  D  V  E  V  C  V  G  N  G  N  F  T  Y  Q
ccccagttccgcccaaacgtggggttcaactgtgatgggaatttcgacaatgaaacagtg
 P  Q  F  R  P  N  V  G  F  N  C  D  G  N  F  D  N  E  T  V
acgttccgtctctggaatctgcatgttaatcacacagatatttacttctgcaaaatcgag
 T  F  R  L  W  N  L  H  V  N  H  T  D  I  Y  F  C  K  I  E
gtcatgtatcctccgccatacctggacaacgagaagagcaacggaactattattcacata
 V  M  Y  P  P  P  Y  L  D  N  E  K  S  N  G  T  I  I  H  I
aaagagaaacatctttgtcatgctcagacgtctcctaagctggagcccaaatctagtgac
 K  E  K  H  L  C  H  A  Q  T  S  P  K  L  E  P  K  S  S  D
aaaactcacacatcgccaccgtcgccagcacctgaattcgagggtgcaccgtcagtcttc
 K  T  H  T  S  P  P  S  P  A  P  E  F  E  G  A  P  S  V  F
ctcttcccccaaaacccaaggacaccctcatgatctcccggactcctgaggtcacatgc
 L  F  P  P  K  P  K  D  T  L  M  I  S  R  T  P  E  V  T  C
gtggtggtggacgtaagccacgaagaccctgaggtcaagttcaactggtacgtggacggc
 V  V  V  D  V  S  H  E  D  P  E  V  K  F  N  W  Y  V  D  G
gtggaggtgcataatgccaagacaaagccgcgggaggagcagtacaacagcacgtaccgt
 V  E  V  H  N  A  K  T  K  P  R  E  E  Q  Y  N  S  T  Y  R
gtggtcagcgtcctcaccgtcctgcaccaggactggctgaatggcaaggagtacaagtgc
 V  V  S  V  L  T  V  L  H  Q  D  W  L  N  G  K  E  Y  K  C
aaggtctccaacaaagccctcccaacccccatcgagaaaaccatctccaaagccaaaggg
 K  V  S  N  K  A  L  P  T  P  I  E  K  T  I  S  K  A  K  G
cagccccgagaaccacaggtgtacaccctgcccccatcccgggatgagctgaccaagaac
 Q  P  R  E  P  Q  V  Y  T  L  P  P  S  R  D  E  L  T  K  N
caggtcagcctgacctgcctggtcaaaggcttctatccaagcgacatcgccgtggagtgg
 Q  V  S  L  T  C  L  V  K  G  F  Y  P  S  D  I  A  V  E  W
gagagcaatgggcagccggagaacaactacaagaccacgcctcccgtgctggactccgac
 E  S  N  G  Q  P  E  N  N  Y  K  T  T  P  P  V  L  D  S  D
ggctccttcttcctctacagcaagctcaccgtggacaagagcaggtggcagcaggggaac
 G  S  F  F  L  Y  S  K  L  T  V  D  K  S  R  W  Q  Q  G  N
gtcttctcatgctccgtgatgcatgaggctctgcacaaccactacacgcagaagagcctc
 V  F  S  C  S  V  M  H  E  A  L  H  N  H  Y  T  Q  K  S  L
tccctgtctccgggtaaactgttttgggcactggtcgtggttgctggagtcctgttttgt
 S  L  S  P  G  K  L  F  W  A  L  V  V  V  A  G  V  L  F  C
tatggcttgctagtgacagtggctctttgtgttatctggacaaatagtagaaggaacaga
 Y  G  L  L  V  T  V  A  L  C  V  I  W  T  N  S  R  R  N  R
```

[57] Cloned by Rachel Knox, B.Sc., Simon Davis laboratory, University of Oxford.

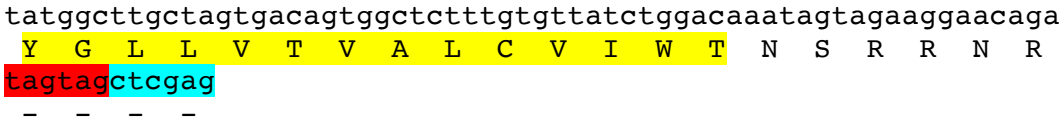

ctccttcaaagtgactacatgaacatgactccccggaggcctgggctcactcgaaagcct
L L Q S D Y M N M T P R R P G L T R K P
taccagccctacgcccctgccagagactttgcagcgtaccgccccacgcgttagtagctc
Y Q P Y A P A R D F A A Y R P T R - - -
gag
-

**Sequence of a non-signalling chimeric human Fc – rat-mouse CD28 gene truncated in the cytosolic domain (truncFcCD28)**[58]

BamHI Kozak START rCD28 ECD hFc mCD28 TMD truncated mCD28 ICD STOP XhoI

```
ggatccgccaccatgacactcagactgctattcttggctctcagcttcttctcagttcaa
 -  -  -  -  M  T  L  R  L  L  F  L  A  L  S  F  F  S  V  Q
gtaacagaaaacaagattttggtgaagcagtccccgctgcttgtggtagataacaatgag
 V  T  E  N  K  I  L  V  K  Q  S  P  L  L  V  V  D  N  N  E
gtcagcctcagctgcaggtattcctacaaccttcttgcaaaggagttccgggcatccctt
 V  S  L  S  C  R  Y  S  Y  N  L  L  A  K  E  F  R  A  S  L
tacaagggcgtgaacagtgacgtggaagtctgtgtcgggaatgggaattttacctatcag
 Y  K  G  V  N  S  D  V  E  V  C  V  G  N  G  N  F  T  Y  Q
ccccagttccgcccaaacgtggggttcaactgtgatgggaatttcgacaatgaaacagtg
 P  Q  F  R  P  N  V  G  F  N  C  D  G  N  F  D  N  E  T  V
acgttccgtctctggaatctgcatgttaatcacacagatatttacttctgcaaaatcgag
 T  F  R  L  W  N  L  H  V  N  H  T  D  I  Y  F  C  K  I  E
gtcatgtatcctccgccatacctggacaacgagaagagcaacggaactattattcacata
 V  M  Y  P  P  P  Y  L  D  N  E  K  S  N  G  T  I  I  H  I
aaagagaaacatctttgtcatgctcagacgtctcctaagctggagcccaaatctagtgac
 K  E  K  H  L  C  H  A  Q  T  S  P  K  L  E  P  K  S  S  D
aaaactcacacatcgccaccgtcgccagcacctgaattcgagggtgcaccgtcagtcttc
 K  T  H  T  S  P  P  S  P  A  P  E  F  E  G  A  P  S  V  F
ctcttcccccaaaacccaaggacaccctcatgatctcccggactcctgaggtcacatgc
 L  F  P  P  K  P  K  D  T  L  M  I  S  R  T  P  E  V  T  C
gtggtggtggacgtaagccacgaagaccctgaggtcaagttcaactggtacgtggacggc
 V  V  V  D  V  S  H  E  D  P  E  V  K  F  N  W  Y  V  D  G
gtggaggtgcataatgccaagacaaagccgcgggaggagcagtacaacagcacgtaccgt
 V  E  V  H  N  A  K  T  K  P  R  E  E  Q  Y  N  S  T  Y  R
gtggtcagcgtcctcaccgtcctgcaccaggactggctgaatggcaaggagtacaagtgc
 V  V  S  V  L  T  V  L  H  Q  D  W  L  N  G  K  E  Y  K  C
aaggtctccaacaaagccctcccaacccccatcgagaaaaccatctccaaagccaaaggg
 K  V  S  N  K  A  L  P  T  P  I  E  K  T  I  S  K  A  K  G
cagccccgagaaccacaggtgtacaccctgcccccatcccgggatgagctgaccaagaac
 Q  P  R  E  P  Q  V  Y  T  L  P  P  S  R  D  E  L  T  K  N
caggtcagcctgacctgcctggtcaaaggcttctatccaagcgacatcgccgtggagtgg
 Q  V  S  L  T  C  L  V  K  G  F  Y  P  S  D  I  A  V  E  W
gagagcaatgggcagccggagaacaactacaagaccacgcctcccgtgctggactccgac
 E  S  N  G  Q  P  E  N  N  Y  K  T  T  P  P  V  L  D  S  D
ggctccttcttcctctacagcaagctcaccgtggacaagagcaggtggcagcaggggaac
 G  S  F  F  L  Y  S  K  L  T  V  D  K  S  R  W  Q  Q  G  N
gtcttctcatgctccgtgatgcatgaggctctgcacaaccactacacgcagaagagcctc
 V  F  S  C  S  V  M  H  E  A  L  H  N  H  Y  T  Q  K  S  L
tccctgtctccgggtaaactgttttgggcactggtcgtggttgctggagtcctgttttgt
 S  L  S  P  G  K  L  F  W  A  L  V  V  V  A  G  V  L  F  C
```

[58] Cloned by Rachel Knox, B.Sc., Simon Davis laboratory, University of Oxford.


tatggcttgctagtgacagtggctctttgtgttatctggacaaatagtagaaggaacaga
Y G L L V T V A L C V I W T N S R R N R
tagtagctcgag
- - - -

**Sequence of a HA-tagged chimeric rat-mouse CD45 gene (rmCD45)**[59]

BglII Kozak START signal peptide chick PTPRS HA tag linker
rCD45 ECD mature peptide BamHI mCD45 TMD mCD45 ICD STOP XhoI

```
agatctgccaccatgggcatccttcccagccctgggatgcctgcgctg
 -   -   -   -   M   G   I   L   P   S   P   G   M   P   A   L
ctctccctcgtgagccttctctccgtgctgctgatgggttgcgtagctgaatacccatac
 L   S   L   V   S   L   L   S   V   L   L   M   G   C   V   A   E   Y   P   Y
gacgtcccagactacgctggatctcaaggaacaaccgacgatggtgccaacctcacaacc
 D   V   P   D   Y   A   G   S   Q   G   T   T   D   D   G   A   N   L   T   T
cctgcaccatccactctgggctttgcaagcaataccaccacaagcacagaaatagctacc
 P   A   P   S   T   L   G   F   A   S   N   T   T   S   T   E   I   A   T
cctcaaacgaagccatcatgtgatgaaaaatttgggaacgttactgtgcgttacatctat
 P   Q   T   K   P   S   C   D   E   K   F   G   N   V   T   V   R   Y   I   Y
gatgacagtagtaagaattttaacgcaaacctagaaggtgacaaaaaacctaagtgtgaa
 D   D   S   S   K   N   F   N   A   N   L   E   G   D   K   K   P   K   C   E
tatacggattgtgaaaaagagttaaaaaatctaccagaatgctcacagaaaaacgtcact
 Y   T   D   C   E   K   E   L   K   N   L   P   E   C   S   Q   K   N   V   T
ctctccaatggctcatgtactccagataaaattataaatttagatgtaccaccagggact
 L   S   N   G   S   C   T   P   D   K   I   I   N   L   D   V   P   P   G   T
cacaactttaacttaacaaactgcacaccagacatagaagctaatacctcaatttgtttg
 H   N   F   N   L   T   N   C   T   P   D   I   E   A   N   T   S   I   C   L
gagtggaaaataaaaaacaaatttacctgcgacattcaaaagatttcatacaatttccgt
 E   W   K   I   K   N   K   F   T   C   D   I   Q   K   I   S   Y   N   F   R
tgtacaccagagatgaaaacatttgctttggacaaacacggaacactttggttacacaac
 C   T   P   E   M   K   T   F   A   L   D   K   H   G   T   L   W   L   H   N
cttacagtccgaacaaattacacatgtgctgcggaagtcctctacaataacgtaatactt
 L   T   V   R   T   N   Y   T   C   A   A   E   V   L   Y   N   N   V   I   L
ttaaaacaagacagaagggtgcagactgattttgggactccagaaatgcttccccatgtt
 L   K   Q   D   R   R   V   Q   T   D   F   G   T   P   E   M   L   P   H   V
caatgtaagaattcaactaacagcacaacattagtctcctgggctgagcccgcatctaaa
 Q   C   K   N   S   T   N   S   T   T   L   V   S   W   A   E   P   A   S   K
caccatggatacattttatgctataaaaagacccttcagaaaaatgtgaaaatttggct
 H   H   G   Y   I   L   C   Y   K   K   T   P   S   E   K   C   E   N   L   A
aatgatgtgaacagttttgaggtgaaaaacctgaggccttatacagagtacacagtgtct
 N   D   V   N   S   F   E   V   K   N   L   R   P   Y   T   E   Y   T   V   S
ctatttgcctatgttattgggagggtgcaacgaaatggccctgctaaggattgcaacttt
 L   F   A   Y   V   I   G   R   V   Q   R   N   G   P   A   K   D   C   N   F
cggacaaaagcagctcgtccaggcaaagtcaatggtatgaaaacctcccgggcgtcagac
 R   T   K   A   A   R   P   G   K   V   N   G   M   K   T   S   R   A   S   D
aatagtataaatgtcacgtgtaattctccttatgaaattaatggccctgaagcgcgttac
 N   S   I   N   V   T   C   N   S   P   Y   E   I   N   G   P   E   A   R   Y
attttggaagtcaaaagtggaggttctttagttaaaactttcaaccaatccacatgtaaa
 I   L   E   V   K   S   G   G   S   L   V   K   T   F   N   Q   S   T   C   K
tttgttgtagacaatctctattattcaactgactatgagtttctggtctatttttacaat
 F   V   V   D   N   L   Y   Y   S   T   D   Y   E   F   L   V   Y   F   Y   N
```

[59] Cloned by Rachel Knox, B.Sc., Simon Davis laboratory, University of Oxford.

```
ggagagtacctgggagacccagaaataaaacctcaatcaacatcttataattctaaagga
 G  E  Y  L  G  D  P  E  I  K  P  Q  S  T  S  Y  N  S  K  G
tccaaagcactgattatattcctggtgtttctgattattgtgacatcaatagccttgctt
 S  K  A  L  I  I  F  L  V  F  L  I  I  V  T  S  I  A  L  L
gttgttttgtataaaatctatgatctgcgcaagaaaagatccagcaatttagatgaacaa
 V  V  L  Y  K  I  Y  D  L  R  K  K  R  S  S  N  L  D  E  Q
caggaactcgttgaaagggatgatgaaaagcagctgatggatgtggagccaatccattct
 Q  E  L  V  E  R  D  D  E  K  Q  L  M  D  V  E  P  I  H  S
gacattttgttggaaacatacaaaaggaagattgctgatgagggcaggctgttcctggct
 D  I  L  L  E  T  Y  K  R  K  I  A  D  E  G  R  L  F  L  A
gaatttcagagcattccacgggtattcagcaagtttcccatcaaagatgcccgaaagccc
 E  F  Q  S  I  P  R  V  F  S  K  F  P  I  K  D  A  R  K  P
cacaatcagaataaaaaccgttatgttgacattcttccctatgattataaccgtgtggaa
 H  N  Q  N  K  N  R  Y  V  D  I  L  P  Y  D  Y  N  R  V  E
ctctctgaaataaatggagatgcagggtccacctacataaatgccagctacattgatggc
 L  S  E  I  N  G  D  A  G  S  T  Y  I  N  A  S  Y  I  D  G
ttcaaggaacccaggaaatacattgctgcacaagggccccgggatgagacagttgatgac
 F  K  E  P  R  K  Y  I  A  A  Q  G  P  R  D  E  T  V  D  D
ttctggaggatgatctgggagcaaaaggccacagttattgtcatggtcacacgatgtgaa
 F  W  R  M  I  W  E  Q  K  A  T  V  I  V  M  V  T  R  C  E
gaaggaaacaggaacaagtgcgcagaatactggccaagcatggaggaaggcactcgggct
 E  G  N  R  N  K  C  A  E  Y  W  P  S  M  E  E  G  T  R  A
ttcaaagatattgttgtgacaatcaatgaccacaaacgatgtcctgattacatcattcag
 F  K  D  I  V  V  T  I  N  D  H  K  R  C  P  D  Y  I  I  Q
aagctgaacgttgcacataaaaaagaaaaagcaactggaagagaagtgactcatatccaa
 K  L  N  V  A  H  K  K  E  K  A  T  G  R  E  V  T  H  I  Q
ttcaccagctggccagaccatggggttcctgaagaccctcacctgctcctcaaacttcga
 F  T  S  W  P  D  H  G  V  P  E  D  P  H  L  L  L  K  L  R
cggagagttaatgcttttagcaacttcttcagtggtcccattgtggtgcactgcagtgct
 R  R  V  N  A  F  S  N  F  F  S  G  P  I  V  V  H  C  S  A
ggtgttgggcgtacaggtacctacattggaattgatgccatgctggaaggcctggaagca
 G  V  G  R  T  G  T  Y  I  G  I  D  A  M  L  E  G  L  E  A
gagggcaaagtggatgtctatggttatgttgtcaagctaaggcgacagaggtgtctgatg
 E  G  K  V  D  V  Y  G  Y  V  V  K  L  R  R  Q  R  C  L  M
gtgcaagtggaggcacagtatatcctgattcatcaggctttagtggaatacaatcagttt
 V  Q  V  E  A  Q  Y  I  L  I  H  Q  A  L  V  E  Y  N  Q  F
ggagaaacagaagtgaacttgtctgagttacattcatgcctacacaacatgaagaagaga
 G  E  T  E  V  N  L  S  E  L  H  S  C  L  H  N  M  K  K  R
gatccacccagtgacccctcccctcgtgaggctgaataccagagacttccttcatacagg
 D  P  P  S  D  P  S  P  R  E  A  E  Y  Q  R  L  P  S  Y  R
agttggaggacacagcacattggaaatcaaggagagaataagaagaagaacaggaattct
 S  W  R  T  Q  H  I  G  N  Q  G  E  N  K  K  K  N  R  N  S
aatgttgttccatatgactttaacagagtgccacttaagcatgaactggagatgagcaaa
 N  V  V  P  Y  D  F  N  R  V  P  L  K  H  E  L  E  M  S  K
gagagtgagcctgaatcagatgagtcttcagatgatgacagtgactcagaagaaaccagc
 E  S  E  P  E  S  D  E  S  S  D  D  D  S  D  S  E  E  T  S
aaatacattaatgcatcctttgtgatgagttactggaaaccagaaatgatgattgctgct
 K  Y  I  N  A  S  F  V  M  S  Y  W  K  P  E  M  M  I  A  A
caggggccactaaaagaaacgatcggtgacttttggcagatgatattccaaagaaaagtc
 Q  G  P  L  K  E  T  I  G  D  F  W  Q  M  I  F  Q  R  K  V
```

```
aaagttattgtgatgttgacagagttagtgaatggagaccaggaagtctgtgctcagtac
 K  V  I  V  M  L  T  E  L  V  N  G  D  Q  E  V  C  A  Q  Y
tggggcgaaggaaagcagacttatggagacatggaagtggagatgaaagacacaaacaga
 W  G  E  G  K  Q  T  Y  G  D  M  E  V  E  M  K  D  T  N  R
gcctcagcctacactctccgaacttttgagctgagacattccaagaggaaggagcccaga
 A  S  A  Y  T  L  R  T  F  E  L  R  H  S  K  R  K  E  P  R
actgtgtaccagtaccagtgtaccacatggaaaggggaagagctgcctgcagaacccaaa
 T  V  Y  Q  Y  Q  C  T  T  W  K  G  E  E  L  P  A  E  P  K
gacctggtgtctatgattcaggacctcaaacagaagcttcccaaggcttccccagaaggg
 D  L  V  S  M  I  Q  D  L  K  Q  K  L  P  K  A  S  P  E  G
atgaagtatcacaagcatgcatccatcctcgtccactgcagagatggctcccagcagaca
 M  K  Y  H  K  H  A  S  I  L  V  H  C  R  D  G  S  Q  Q  T
gggttgttctgtgccttgttcaatctcttggaaagtgcagaaacagaagatgtggttgat
 G  L  F  C  A  L  F  N  L  L  E  S  A  E  T  E  D  V  V  D
gttttccaagtggtaaagtctctacgcaaagcacggcctggggtggtgtgcagctatgag
 V  F  Q  V  V  K  S  L  R  K  A  R  P  G  V  V  C  S  Y  E
caataccagttcctctatgacatcatcgccagcatctatcccgcccagaatggacaagtc
 Q  Y  Q  F  L  Y  D  I  I  A  S  I  Y  P  A  Q  N  G  Q  V
aagaaaacaaacagccaagacaaaattgaatttcataatgaagtggatggaggcaagcag
 K  K  T  N  S  Q  D  K  I  E  F  H  N  E  V  D  G  G  K  Q
gatgctaactgtgtccgtccagatggtcctctgaataaagcccaggaagacagcagaggg
 D  A  N  C  V  R  P  D  G  P  L  N  K  A  Q  E  D  S  R  G
gtgggaaccccggagcctaccaatagtgctgaggaaccagaacatgctgccaatggttct
 V  G  T  P  E  P  T  N  S  A  E  E  P  E  H  A  A  N  G  S
gcgagcccagctccaacccagagttcatagtagctcgag
 A  S  P  A  P  T  Q  S  S  -  -  -  -
```

**Sequence of a codon-optimised, HA-tagged chimeric mouse LAT – mouse CD45 gene with a short ectodomain (LAT-CD45)**[60]

BamHI Kozak START HA tag mLAT ECD and TM mCD45 ICD STOP NotI

```
ggatccttgaagcaggccactatgtacccttacgacgtgcctgactacgctgaagccgat
  -  -  -  -  -  -  -  -  M  Y  P  Y  D  V  P  D  Y  A  E  A  D
gctctgtcccctgtggggctgggcctgctcctgctgccattcctcgtgacactccttgct
 A  L  S  P  V  G  L  G  L  L  L  L  P  F  L  V  T  L  L  A
gccttgtgtgtaaggtgccgggaactcccatcatacgacctgcgaaagaaaaggagctct
 A  L  C  V  R  C  R  E  L  P  S  Y  D  L  R  K  K  R  S  S
aacctggatgagcagcaggaactggtggagagagatgacgagaaacagttgatggatgtg
 N  L  D  E  Q  Q  E  L  V  E  R  D  D  E  K  Q  L  M  D  V
gagcccatccacagcgacatcctgctcgaaacatataaacgcaaaatcgccgatgaagga
 E  P  I  H  S  D  I  L  L  E  T  Y  K  R  K  I  A  D  E  G
agactgttcctggcagaattccagtcaattccacgggtattcagcaaatttcccattaag
 R  L  F  L  A  E  F  Q  S  I  P  R  V  F  S  K  F  P  I  K
gacgctcggaagcctcacaaccagaataagaacagatatgtggatattcttccatatgat
 D  A  R  K  P  H  N  Q  N  K  N  R  Y  V  D  I  L  P  Y  D
tataacagagtggagctctccgaaattaacggtgacgccggcagcacctacatcaatgct
 Y  N  R  V  E  L  S  E  I  N  G  D  A  G  S  T  Y  I  N  A
tcttacatcgatggatttaaggaaccaagaaaatacatcgccgctcagggtcctagggac
 S  Y  I  D  G  F  K  E  P  R  K  Y  I  A  A  Q  G  P  R  D
gagaccgtagatgatttttggaggatgatctgggagcagaaggcaactgttatcgtcatg
 E  T  V  D  D  F  W  R  M  I  W  E  Q  K  A  T  V  I  V  M
gttaccagatgcgaagaggggaatcgaaataaatgcgccgagtactggccctctatggag
 V  T  R  C  E  E  G  N  R  N  K  C  A  E  Y  W  P  S  M  E
gaaggcacaagggcattcaaggacatcgtggtcacgattaacgatcacaaaaggtgccct
 E  G  T  R  A  F  K  D  I  V  V  T  I  N  D  H  K  R  C  P
gactatattattcagaaactcaacgtggctcataaaaaggagaaggccacggggcgcgag
 D  Y  I  I  Q  K  L  N  V  A  H  K  K  E  K  A  T  G  R  E
gtgactcatatccagttcacatcatggccagaccacggggtgccggaggaccctcatctg
 V  T  H  I  Q  F  T  S  W  P  D  H  G  V  P  E  D  P  H  L
ctcctgaaattgagacgacgcgttaacgccttttcaaacttttctccggcccgatcgtg
 L  L  K  L  R  R  R  V  N  A  F  S  N  F  F  S  G  P  I  V
gtgcactgctctgccggagttggccgcaccggaacctatatcggcatcgatgcaatgctg
 V  H  C  S  A  G  V  G  R  T  G  T  Y  I  G  I  D  A  M  L
gaggggctggaagccgagggcaaagttgacgtgtacgggtacgtcgttaaacttcgacgg
 E  G  L  E  A  E  G  K  V  D  V  Y  G  Y  V  V  K  L  R  R
cagcgatgcctgatggttcaagtggaggctcaatacatcctgatccatcaagctctggtc
 Q  R  C  L  M  V  Q  V  E  A  Q  Y  I  L  I  H  Q  A  L  V
gagtacaatcaattcggggagacccaggttaacctgtccgaactccacagctgccttcac
 E  Y  N  Q  F  G  E  T  Q  V  N  L  S  E  L  H  S  C  L  H
aacatgaaaaagcgagacccgcccagtgatccgagcccacgagaagccgagtaccagagg
 N  M  K  K  R  D  P  P  S  D  P  S  P  R  E  A  E  Y  Q  R
cttcccagctaccggtcctggagaacccaacacataggtaaccaggggaaaacaagaag
 L  P  S  Y  R  S  W  R  T  Q  H  I  G  N  Q  G  E  N  K  K
```

[60] Cloned by Mai Vuong, M.Sc., Simon Davis laboratory, University of Oxford.

```
aagaaacgcaattccaatgttgtaccatacgattttaatagagtgccacttaaacatgag
 K  K  R  N  S  N  V  V  P  Y  D  F  N  R  V  P  L  K  H  E
cttgaaatgtcaaaggaatctgagcctgagtctgatgaatcctctgatgacgatagcgac
 L  E  M  S  K  E  S  E  P  E  S  D  E  S  S  D  D  D  S  D
tctgaggaaaccagcaagtacataaacgcctcctttgtgatgagttattggaaacctgag
 S  E  E  T  S  K  Y  I  N  A  S  F  V  M  S  Y  W  K  P  E
atgatgatcgcagcccaaggacctctgaaagagaccattggcgacttctggcaaatgatc
 M  M  I  A  A  Q  G  P  L  K  E  T  I  G  D  F  W  Q  M  I
tttcagcgaaaggttaaggtgattgtgatgctcacagagctggtcaacggcgaccaggaa
 F  Q  R  K  V  K  V  I  V  M  L  T  E  L  V  N  G  D  Q  E
gtctgcgcccaatactgggggggaaggcaaacagacctacggtgacatggaagtggagatg
 V  C  A  Q  Y  W  G  E  G  K  Q  T  Y  G  D  M  E  V  E  M
aaggataccaacagggcctccgcttacaccctgcggacattcgagctgagacatagcaaa
 K  D  T  N  R  A  S  A  Y  T  L  R  T  F  E  L  R  H  S  K
cgcaaggagccaagaaccgtgtatcagtaccagtgtacaacctggaagggagaagagttg
 R  K  E  P  R  T  V  Y  Q  Y  Q  C  T  T  W  K  G  E  E  L
cctgctgagcctaaagatcttgtgtcaatgattcaggacctgaagcagaagctccccaag
 P  A  E  P  K  D  L  V  S  M  I  Q  D  L  K  Q  K  L  P  K
gctagtcctgaaggaatgaaataccacaaacacgcaagcattctcgtgcactgcagagac
 A  S  P  E  G  M  K  Y  H  K  H  A  S  I  L  V  H  C  R  D
ggcagtcagcagacaggactgttttgcgcactgtttaacctgcttgaatcagccgaaaca
 G  S  Q  Q  T  G  L  F  C  A  L  F  N  L  L  E  S  A  E  T
gaggacgtggtggatgtctttcaggttgtaaagtccctccgcaaagctaggccgggcgtg
 E  D  V  V  D  V  F  Q  V  V  K  S  L  R  K  A  R  P  G  V
gtgtgctcatatgaacagtaccagttcctgtacgatatcatagcatctatttatccagct
 V  C  S  Y  E  Q  Y  Q  F  L  Y  D  I  I  A  S  I  Y  P  A
cagaatggccaggtgaagaaaacaaactcccaggacaagatcgagttccataacgaggtc
 Q  N  G  Q  V  K  K  T  N  S  Q  D  K  I  E  F  H  N  E  V
gacggcggcaaacaagacgcaaactgcgtgcgaccagacggtccgttgaacaaggctcag
 D  G  G  K  Q  D  A  N  C  V  R  P  D  G  P  L  N  K  A  Q
gaagatagtaggggagttggtacacccgaacccactaattctgctgaggaacctgaacat
 E  D  S  R  G  V  G  T  P  E  P  T  N  S  A  E  E  P  E  H
gctgctaatggttccgccagtccagctcctacgcagtcttcttaggcggccgc
 A  A  N  G  S  A  S  P  A  P  T  Q  S  S  -  -  -
```

**Sequence of a codon-optimised, HA-tagged chimeric mouse LAT – rat- mouse CD148 gene (rmCD148)**[61]

BamHI Kozak START signal peptide chick PTPRS HA tag linker rCD148 ECD mature peptide BamHI mLAT ECD and TMD mCD148 ICD STOP XhoI

```
ggatccctcaagcaagccaccatggcattttgccttctcctggcatgccggctctgttg
 -  -  -  -  -  -  -  M  G  I  L  P  S  P  G  M  P  A  L  L
tctcttgtatcactgctcagcgttctcctgatgggttgcgttgctgagtacccctatgat
 S  L  V  S  L  L  S  V  L  L  M  G  C  V  A  E  Y  P  Y  D
gtgccagattatgccggcagccgccagggccaagtcgtgtgtgcaggagctgccccgtca
 V  P  D  Y  A  G  S  R  Q  G  Q  V  V  C  A  G  A  A  P  S
cccgtctttgatgtcgaagccgtcaccagcccaacgtctgtggtgctgacatggaagcat
 P  V  F  D  V  E  A  V  T  S  P  T  S  V  V  L  T  W  K  H
aacgactcagccactagtgagtacaagattaatgagggcaacaccttgcggtataccgtc
 N  D  S  A  T  S  E  Y  K  I  N  E  G  N  T  L  R  Y  T  V
aagaaccagacatcttttaatatcaccggactgagtccagccacttcttacaaattcagc
 K  N  Q  T  S  F  N  I  T  G  L  S  P  A  T  S  Y  K  F  S
attactctgggaacagtgaacgagacctcaggcaagccaacctataaaaacatcaccacc
 I  T  L  G  T  V  N  E  T  S  G  K  P  T  Y  K  N  I  T  T
gagccatggcctgtgagcgatctgcaggttgcttacataggcgtaacacaggccctgctg
 E  P  W  P  V  S  D  L  Q  V  A  Y  I  G  V  T  Q  A  L  L
gcctggtctaatgccaacggcacggcttcttacaggatgcaaatagttgagctcaccacc
 A  W  S  N  A  N  G  T  A  S  Y  R  M  Q  I  V  E  L  T  T
aattcaagtggagggatttccgacctgaagccaggtactcacaagtccctggcagttcaa
 N  S  S  G  G  I  S  D  L  K  P  G  T  H  K  S  L  A  V  Q
gggtccaacgagacacaacatgatctgtgggtgactgagggcgtgagcgacgccaatggc
 G  S  N  E  T  Q  H  D  L  W  V  T  E  G  V  S  D  A  N  G
accgagggaagcccagtggccaacatatcccaactacataagaattctcttgcctctgca
 T  E  G  S  P  V  A  N  I  S  Q  L  H  K  N  S  L  A  S  A
gaccctcctagcgcccgagacccttccctgaccgaagtactgctgactgagctgaaaccg
 D  P  P  S  A  R  D  P  S  L  T  E  V  L  L  T  E  L  K  P
gacacgcaatacaaggtcacaatctatagtcaggctgccgacggaactgaggggcaacca
 D  T  Q  Y  K  V  T  I  Y  S  Q  A  A  D  G  T  E  G  Q  P
ggaaacaaagttttcaagacgaatccgatccaggtctcagacatcagagcagtcaatatc
 G  N  K  V  F  K  T  N  P  I  Q  V  S  D  I  R  A  V  N  I
agtgatagcaatatgacactcacgtggaagagtaacaataatgagagtcatgccagcttc
 S  D  S  N  M  T  L  T  W  K  S  N  N  N  E  S  H  A  S  F
acttataaaatctacgtggctggtggcagcgattcaattaacgagactgttaacgagaca
 T  Y  K  I  Y  V  A  G  G  S  D  S  I  N  E  T  V  N  E  T
caggccgtgatccgcggattgagctcttcaacccttacaatattaccgtactcccttc
 Q  A  V  I  R  G  L  S  S  S  T  L  Y  N  I  T  V  L  P  F
ctggggcagaccgccggtattcccggtttcctccaagtctacacatccccacggccggtg
 L  G  Q  T  A  G  I  P  G  F  L  Q  V  Y  T  S  P  R  P  V
agcgacttcagggttaccaatgtgtctctcagagaaattggacttgcctggaggtccaac
 S  D  F  R  V  T  N  V  S  L  R  E  I  G  L  A  W  R  S  N
```

[61] Cloned by Mai Vuong, M.Sc., Simon Davis laboratory, University of Oxford.

```
gacagcgagagctttgagatattcattacccaggagggaagcgaaaaaagatggaacgca
 D  S  E  S  F  E  I  F  I  T  Q  E  G  S  E  K  R  W  N  A
agcaccggcgacctttcctatatagtggaaaacctcaagcccggcacatcatatcagttc
 S  T  G  D  L  S  Y  I  V  E  N  L  K  P  G  T  S  Y  Q  F
gaaattttcccaagaggaccaaatggcactgagggacctagccagacagtggtaggacgc
 E  I  F  P  R  G  P  N  G  T  E  G  P  S  Q  T  V  V  G  R
actgactgtagcgccgtgactgacattcgagtcgtctccgtttctacaacagaaatccag
 T  D  C  S  A  V  T  D  I  R  V  V  S  V  S  T  T  E  I  Q
ctggaatggcaaaacacagacagcgcctccggctacacctaccatctggtgctggaatcc
 L  E  W  Q  N  T  D  S  A  S  G  Y  T  Y  H  L  V  L  E  S
gagaacgggtccattaaaaccaacagctctcagaagtggatcaccgtgggcgggctgacc
 E  N  G  S  I  K  T  N  S  S  Q  K  W  I  T  V  G  G  L  T
ccaggaaccctgtacaacgtgacaatatttcctgaggtggaccaaatggaaggtaactca
 P  G  T  L  Y  N  V  T  I  F  P  E  V  D  Q  M  E  G  N  S
tccagcattactcagtacacaaggccttcaaatgtgtcttatatcgaggttaacaccaat
 S  S  I  T  Q  Y  T  R  P  S  N  V  S  Y  I  E  V  N  T  N
actaccgtggcagccattcaatggaaaaatctggacgctgcttccgctagttactcctac
 T  T  V  A  A  I  Q  W  K  N  L  D  A  A  S  A  S  Y  S  Y
tctgtattgatcttgaaggccggagatggtagtaacgttacctctagagtcagagacatt
 S  V  L  I  L  K  A  G  D  G  S  N  V  T  S  R  V  R  D  I
ccttctgtgactatccctggacttatccctggggtgagttacgaggtcaagattttcact
 P  S  V  T  I  P  G  L  I  P  G  V  S  Y  E  V  K  I  F  T
aagatcaggaacactgaagtcgggaatgaagtccctgggcagaaacttttttgcatggaa
 K  I  R  N  T  E  V  G  N  E  V  P  G  Q  K  L  F  C  M  E
cctgcacaggtcgattccctgcattgcgaggtggtgcccaaggaacccgccttggttctc
 P  A  Q  V  D  S  L  H  C  E  V  V  P  K  E  P  A  L  V  L
aagtgggcctgccccccaggcatgaactctgggtttgaactgggggtgagaagcgacgct
 K  W  A  C  P  P  G  M  N  S  G  F  E  L  G  V  R  S  D  A
tgggacaatatgactcacctcgagaactgtacccttgataacgatactgaatgtcggaca
 W  D  N  M  T  H  L  E  N  C  T  L  D  N  D  T  E  C  R  T
gaagttacttatctgaacttctcaacgagctataacatctctatcgccactctctcttgt
 E  V  T  Y  L  N  F  S  T  S  Y  N  I  S  I  A  T  L  S  C
gggaaaatggccctccccacccagagtacatgcacgacaggtatcacagacccgcccccg
 G  K  M  A  L  P  T  Q  S  T  C  T  T  G  I  T  D  P  P  P
cctgatgggagccctaacattacctcagtgtcccacaatagcgtcaaggtgaagttctct
 P  D  G  S  P  N  I  T  S  V  S  H  N  S  V  K  V  K  F  S
gggttcgaggccagccacggccctatcaaagcctatgccgtgcttctgaccacaggcgaa
 G  F  E  A  S  H  G  P  I  K  A  Y  A  V  L  L  T  T  G  E
gccgggcagccctccactgacgtgcttaaatacacatacgaggacttcaagaaaggggcc
 A  G  Q  P  S  T  D  V  L  K  Y  T  Y  E  D  F  K  K  G  A
agcgatacatatgtgacttacctgatacgcatcgaggagaaaggacagagccagggattg
 S  D  T  Y  V  T  Y  L  I  R  I  E  E  K  G  Q  S  Q  G  L
agcgaggctctgaattatgaaatcgacgtgggcaaccagtccacaaccctggggtattat
 S  E  A  L  N  Y  E  I  D  V  G  N  Q  S  T  T  L  G  Y  Y
aacggtcggctggagcctctgggcagttaccgggcatgtgtggctggttttacgaatatt
 N  G  R  L  E  P  L  G  S  Y  R  A  C  V  A  G  F  T  N  I
acgtacaacctccagaacgatggcctcattaacggcgatgagtcctatgtatcattctct
 T  Y  N  L  Q  N  D  G  L  I  N  G  D  E  S  Y  V  S  F  S
ccttatagcgaggctgtgtctctgccccaagatcctggagaagctgatgctctgtccccc
 P  Y  S  E  A  V  S  L  P  Q  D  P  G  E  A  D  A  L  S  P
```

```
gtgggacttggattgcttcttctccccttcctggtcaccctcttggctgcactctgcgtc
 V  G  L  G  L  L  L  L  P  F  L  V  T  L  L  A  A  L  C  V
agatgtagagagctgccccggaagaagcggaccgacgccaagaacaatgaggtgagcttc
 R  C  R  E  L  P  R  K  K  R  T  D  A  K  N  N  E  V  S  F
tcacagatcaaaccaaagaaatcaaagcttatccgcgtcgaaaacttcgaagcctacttc
 S  Q  I  K  P  K  K  S  K  L  I  R  V  E  N  F  E  A  Y  F
aagaagcaacaggcagactctaactgcggtttcgcagaagagtatgaggatttgaagttg
 K  K  Q  Q  A  D  S  N  C  G  F  A  E  E  Y  E  D  L  K  L
atcggcatcagtcttcctaaatacaccgccgagatcgcagagaataggggcaaaaacaga
 I  G  I  S  L  P  K  Y  T  A  E  I  A  E  N  R  G  K  N  R
tacaacaatgtcctgccctatgacattagcagagtgaagttgtctgtacaaacccatagc
 Y  N  N  V  L  P  Y  D  I  S  R  V  K  L  S  V  Q  T  H  S
acagacgattacattaatgctaattacatgccaggctaccactccaaaaaggacttcatt
 T  D  D  Y  I  N  A  N  Y  M  P  G  Y  H  S  K  K  D  F  I
gccacccagggccctctgcccaatactctgaaagacttctggagaatggtgtgggaaaaa
 A  T  Q  G  P  L  P  N  T  L  K  D  F  W  R  M  V  W  E  K
aacgtttacgccattgtgatgctgacaaagtgcgtggagcagggtaggactaagtgcgag
 N  V  Y  A  I  V  M  L  T  K  C  V  E  Q  G  R  T  K  C  E
gagtactggcccagcaagcaggctcaggactacggtgatataaccgtggccatgacctca
 E  Y  W  P  S  K  Q  A  Q  D  Y  G  D  I  T  V  A  M  T  S
gaggttgtgctgcccgaatggacaattcgagatttcgtggtgaagaatatgcaaaatagc
 E  V  V  L  P  E  W  T  I  R  D  F  V  V  K  N  M  Q  N  S
gagtcccaccctctgagacaatttcatttcacctcttggccagatcacggtgtgcctgat
 E  S  H  P  L  R  Q  F  H  F  T  S  W  P  D  H  G  V  P  D
accacggacctgctgataaacttcagataccttgtcagggactatatgaagcagatcccg
 T  T  D  L  L  I  N  F  R  Y  L  V  R  D  Y  M  K  Q  I  P
cccgagtcccccatcctggtacactgtagtgcaggcgttggccggaccggcacattcatt
 P  E  S  P  I  L  V  H  C  S  A  G  V  G  R  T  G  T  F  I
gccattgaccggctgatttaccaaatagagaatgagaataccgttgacgtgtacggaatc
 A  I  D  R  L  I  Y  Q  I  E  N  E  N  T  V  D  V  Y  G  I
gtttacgatttgagaatgcacaggccactcatggtacagaccgaggaccagtacgtgttt
 V  Y  D  L  R  M  H  R  P  L  M  V  Q  T  E  D  Q  Y  V  F
ctgaatcagtgtgtgctcgacatcatccgagcacaaaaagactcaaaagtggatctgatc
 L  N  Q  C  V  L  D  I  I  R  A  Q  K  D  S  K  V  D  L  I
taccagaatactacagctatgaccatttacgaaaatctggaaccggtaagcatgtttggg
 Y  Q  N  T  T  A  M  T  I  Y  E  N  L  E  P  V  S  M  F  G
aagacaaatggctatatcgcttaggcggccgc
 K  T  N  G  Y  I  A  -  -  -
```

**Sequence of a codon-optimised, chimeric mouse LAT – mouse CD148 gene with a short ectodomain (LAT-CD148)**[62]

BamHI Kozak START HA tag mLAT ECD and TM mCD148 ICD STOP NotI

```
ggatccctcaagcaagccaccatgtatccctacgatgtaccagactacgccgaagctgat
 -  -  -  -  -  -  -  -  M  Y  P  Y  D  V  P  D  Y  A  E  A  D
gctctgtcccccgtgggacttggattgcttcttctccccttcctggtcaccctcttggct
 A  L  S  P  V  G  L  G  L  L  L  L  P  F  L  V  T  L  L  A
gcactctgcgtcagatgtagagagctgccccggaagaagcggaccgacgccaagaacaat
 A  L  C  V  R  C  R  E  L  P  R  K  K  R  T  D  A  K  N  N
gaggtgagcttctcacagatcaaaccaaagaaatcaaagcttatccgcgtcgaaaacttc
 E  V  S  F  S  Q  I  K  P  K  K  S  K  L  I  R  V  E  N  F
gaagcctacttcaagaagcaacaggcagactctaactgcggtttcgcagaagagtatgag
 E  A  Y  F  K  K  Q  Q  A  D  S  N  C  G  F  A  E  E  Y  E
gatttgaagttgatcggcatcagtcttcctaaatacaccgccgagatcgcagagaatagg
 D  L  K  L  I  G  I  S  L  P  K  Y  T  A  E  I  A  E  N  R
ggcaaaaacagatacaacaatgtcctgccctatgacattagcagagtgaagttgtctgta
 G  K  N  R  Y  N  N  V  L  P  Y  D  I  S  R  V  K  L  S  V
caaacccatagcacagacgattacattaatgctaattacatgccaggctaccactccaaa
 Q  T  H  S  T  D  D  Y  I  N  A  N  Y  M  P  G  Y  H  S  K
aaggacttcattgccacccagggccctctgcccaatactctgaaagacttctggagaatg
 K  D  F  I  A  T  Q  G  P  L  P  N  T  L  K  D  F  W  R  M
gtgtgggaaaaaaacgtttacgccattgtgatgctgacaaagtgcgtggagcagggtagg
 V  W  E  K  N  V  Y  A  I  V  M  L  T  K  C  V  E  Q  G  R
actaagtgcgaggagtactggcccagcaagcaggctcaggactacggtgatataaccgtg
 T  K  C  E  E  Y  W  P  S  K  Q  A  Q  D  Y  G  D  I  T  V
gccatgacctcagaggttgtgctgcccgaatggacaattcgagatttcgtggtgaagaat
 A  M  T  S  E  V  V  L  P  E  W  T  I  R  D  F  V  V  K  N
atgcaaaatagcgagtcccaccctctgagacaatttcatttcacctcttggccagatcac
 M  Q  N  S  E  S  H  P  L  R  Q  F  H  F  T  S  W  P  D  H
ggtgtgcctgataccacggacctgctgataaacttcagataccttgtcagggactatatg
 G  V  P  D  T  T  D  L  L  I  N  F  R  Y  L  V  R  D  Y  M
aagcagatcccgcccgagtcccccatcctggtacactgtagtgcaggcgttggccggacc
 K  Q  I  P  P  E  S  P  I  L  V  H  C  S  A  G  V  G  R  T
ggcacattcattgccattgaccggctgatttaccaaatagagaatgagaataccgttgac
 G  T  F  I  A  I  D  R  L  I  Y  Q  I  E  N  E  N  T  V  D
gtgtacggaatcgtttacgatttgagaatgcacaggccactcatggtacagaccgaggac
 V  Y  G  I  V  Y  D  L  R  M  H  R  P  L  M  V  Q  T  E  D
cagtacgtgtttctgaatcagtgtgtgctcgacatcatccgagcacaaaaagactcaaaa
 Q  Y  V  F  L  N  Q  C  V  L  D  I  I  R  A  Q  K  D  S  K
gtggatctgatctaccagaatactacagctatgaccatttacgaaaatctggaaccggta
 V  D  L  I  Y  Q  N  T  T  A  M  T  I  Y  E  N  L  E  P  V
agcatgtttgggaagacaaatggctatatcgcttaggcggccgc
 S  M  F  G  K  T  N  G  Y  I  A  -  -  -
```

[62] Cloned by Mai Vuong, M.Sc., Simon Davis laboratory, University of Oxford.

**Sequence of a soluble, polyhistidine-tagged mouse FcγRIIb gene**[63]

MluI Kozak START mFcγRIIb ECD His-tag STOP NotI

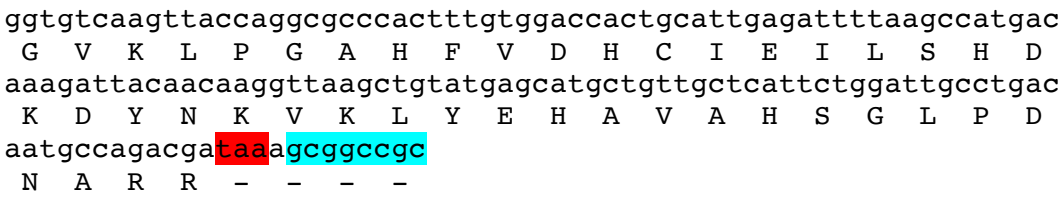
```
acgcgtgccaccatgggaatcctgccgttcctactgatccccatggagagcaactggact
 -  -  -  -  M  G  I  L  P  F  L  L  I  P  M  E  S  N  W  T
gtccatgtgttctcacggactttgtgccatatgctactgtggacagccgtgctaaatctt
 V  H  V  F  S  R  T  L  C  H  M  L  L  W  T  A  V  L  N  L
gctgctgggactcatgatcttccaaaggctgtggtcaaactcgagcccccgtggatccag
 A  A  G  T  H  D  L  P  K  A  V  V  K  L  E  P  P  W  I  Q
gtgctcaaggaagacacggtgacactgacatgcgaagggacccacaaccctgggaactct
 V  L  K  E  D  T  V  T  L  T  C  E  G  T  H  N  P  G  N  S
tctacccagtggttccacaatgggaggtccatccggagccaggtccaagccagctacacg
 S  T  Q  W  F  H  N  G  R  S  I  R  S  Q  V  Q  A  S  Y  T
tttaaggccacagtcaatgacagtggagaatatcggtgtcaaatggagcagacccgcctc
 F  K  A  T  V  N  D  S  G  E  Y  R  C  Q  M  E  Q  T  R  L
agcgaccctgtagatctgggagtgatttctgactggctgctgctccagacccctcagctg
 S  D  P  V  D  L  G  V  I  S  D  W  L  L  L  Q  T  P  Q  L
gtgtttctggaaggggaaaccatcacgctaaggtgccatagctggaggaacaaactactg
 V  F  L  E  G  E  T  I  T  L  R  C  H  S  W  R  N  K  L  L
aacaggatctcgttcttccataatgaaaaatccgtgaggtatcatcactacagtagtaat
 N  R  I  S  F  F  H  N  E  K  S  V  R  Y  H  H  Y  S  S  N
ttctctatcccaaaagccaaccacagtcacagtggggactactactgcaaaggaagtcta
 F  S  I  P  K  A  N  H  S  H  S  G  D  Y  Y  C  K  G  S  L
ggaaggacactgcaccagtccaagcctgtcaccatcactgtccaagggcccaagtccagc
 G  R  T  L  H  Q  S  K  P  V  T  I  T  V  Q  G  P  K  S  S
gggcaccatcaccatcaccatagccgagcatggagacaccctcaattcggaggtcaccac
 G  H  H  H  H  H  H  S  R  A  W  R  H  P  Q  F  G  G  H  H
catcaccatcactaggcggccgcg
 H  H  H  H  -  -  -  -
```

[63] Cloning and protein production was performed by Shirley Yang, B.Sc., Princeton University, under the supervision of Meike Aßmann, B.Sc., Simon Davis laboratory, University of Oxford.

**Sequence of a chimeric rat-mouse CD28 – mEos3.2 gene (rmCD28-mEos)**

MluI Kozak START rCD28 ECD mCD28 TM mCD28 ICD BamHI flexible linker mEOS3.2 STOP NotI

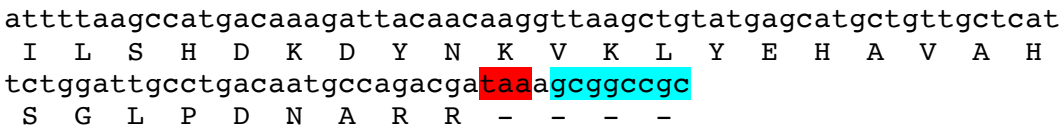
```
acgcgtctcaagcaggccaccatgacgctcaggctgctattcttggctctcagcttcttc
 -  -  -  -  -  -  -  -  M  T  L  R  L  L  F  L  A  L  S  F  F
tcagttcaagtaacagaaaacaagattttggtgaagcagtccccgctgcttgtggtagat
 S  V  Q  V  T  E  N  K  I  L  V  K  Q  S  P  L  L  V  V  D
aacaatgaggtcagcctcagctgcaggtattcctacaaccttcttgcaaaggagttccgg
 N  N  E  V  S  L  S  C  R  Y  S  Y  N  L  L  A  K  E  F  R
gcatccctttacaagggcgtgaacagtgacgtggaagtctgtgtcgggaatgggaatttt
 A  S  L  Y  K  G  V  N  S  D  V  E  V  C  V  G  N  G  N  F
acctatcagccccagttccgcccaaacgtggggttcaactgtgatgggaatttcgacaat
 T  Y  Q  P  Q  F  R  P  N  V  G  F  N  C  D  G  N  F  D  N
gaaacagtgacgttccgtctctggaatctgcatgttaatcacacagatatttacttctgc
 E  T  V  T  F  R  L  W  N  L  H  V  N  H  T  D  I  Y  F  C
aaaatcgaggtcatgtatcctccgccatacctggacaacgagaagagcaacggaactatt
 K  I  E  V  M  Y  P  P  P  Y  L  D  N  E  K  S  N  G  T  I
attcacataaaagagaaacatctttgtcatgctcagacgtctcctaagctgttttgggca
 I  H  I  K  E  K  H  L  C  H  A  Q  T  S  P  K  L  F  W  A
ctggtcgtggttgctggagtcctgttttgttatggcttgctagtgacagtggctctttgt
 L  V  V  V  A  G  V  L  F  C  Y  G  L  L  V  T  V  A  L  C
gttatctggacaaatagtagaaggaacagactccttcaaagtgactacatgaacatgact
 V  I  W  T  N  S  R  R  N  R  L  L  Q  S  D  Y  M  N  M  T
ccccggaggcctgggctcactcgaaagccttaccagccctacgcccctgccagagacttt
 P  R  R  P  G  L  T  R  K  P  Y  Q  P  Y  A  P  A  R  D  F
gcagcgtaccgccccgggatccaggcagtggaagtgggagcggttctggctccggatca
 A  A  Y  R  P  G  D  P  G  S  G  S  G  S  G  S  G  S  G  S
gggtcgggtagtggcagcggatctggtcctggccccgggccgggaccaggtcctatgagt
 G  S  G  S  G  S  G  S  G  P  G  P  G  P  G  P  G  P  M  S
gcgattaagccagacatgaagatcaaactccgtatggaaggcaacgtaaacgggcaccac
 A  I  K  P  D  M  K  I  K  L  R  M  E  G  N  V  N  G  H  H
tttgtgatcgacggagatggtacaggcaagccttttgagggaaaacagagtatggatctt
 F  V  I  D  G  D  G  T  G  K  P  F  E  G  K  Q  S  M  D  L
gaagtcaaagagggcggacctctgcctttgcctttgatatcctgaccactgcattccat
 E  V  K  E  G  G  P  L  P  F  A  F  D  I  L  T  T  A  F  H
tacggcaacagggtattcgccaaatatccagacaacatacaagactattttaagcagtcg
 Y  G  N  R  V  F  A  K  Y  P  D  N  I  Q  D  Y  F  K  Q  S
tttcctaaggggtattcgtgggaacgaagcttgactttcgaagacgggggcatttgcaac
 F  P  K  G  Y  S  W  E  R  S  L  T  F  E  D  G  G  I  C  N
gccagaaacgacataacaatggaaggggacactttctataataaagttcgattttatggt
 A  R  N  D  I  T  M  E  G  D  T  F  Y  N  K  V  R  F  Y  G
accaactttcccgccaatggtccagttatgcagaagaagacgctgaaatgggagccctcc
 T  N  F  P  A  N  G  P  V  M  Q  K  K  T  L  K  W  E  P  S
actgagaaaatgtatgtgcgtgatggagtgctgacgggtgatattgagatggctttgttg
 T  E  K  M  Y  V  R  D  G  V  L  T  G  D  I  E  M  A  L  L
cttgaaggaaatgcccattaccgatgtgacttcagaactacttacaaagctaaggagaag
 L  E  G  N  A  H  Y  R  C  D  F  R  T  T  Y  K  A  K  E  K
```


ggtgtcaagttaccaggcgcccactttgtggaccactgcattgagattttaagccatgac
G V K L P G A H F V D H C I E I L S H D
aaagattacaacaaggttaagctgtatgagcatgctgttgctcattctggattgcctgac
K D Y N K V K L Y E H A V A H S G L P D
aatgccagacgataaagcggccgc
N A R R - - - -

**Sequence of a non-signalling chimeric rat-mouse CD28 – mEos3.2 gene truncated in the cytosolic domain (truncCD28-mEos)**

MluI Kozak START rCD28 ECD mCD28 TM truncated mCD28 ICD BamHI flexible linker mEOS3.2 STOP NotI

```
acgcgtctcaagcaggccaccatgacgctcaggctgctattcttggctctcagcttcttc
 -  -  -  -  -  -  -  -  M  T  L  R  L  L  F  L  A  L  S  F  F
tcagttcaagtaacagaaaacaagattttggtgaagcagtccccgctgcttgtggtagat
 S  V  Q  V  T  E  N  K  I  L  V  K  Q  S  P  L  L  V  V  D
aacaatgaggtcagcctcagctgcaggtattcctacaaccttcttgcaaaggagttccgg
 N  N  E  V  S  L  S  C  R  Y  S  Y  N  L  L  A  K  E  F  R
gcatccctttacaagggcgtgaacagtgacgtggaagtctgtgtcgggaatgggaatttt
 A  S  L  Y  K  G  V  N  S  D  V  E  V  C  V  G  N  G  N  F
acctatcagccccagttccgcccaaacgtggggttcaactgtgatgggaatttcgacaat
 T  Y  Q  P  Q  F  R  P  N  V  G  F  N  C  D  G  N  F  D  N
gaaacagtgacgttccgtctctggaatctgcatgttaatcacacagatatttacttctgc
 E  T  V  T  F  R  L  W  N  L  H  V  N  H  T  D  I  Y  F  C
aaaatcgaggtcatgtatcctccgccatacctggacaacgagaagagcaacggaactatt
 K  I  E  V  M  Y  P  P  P  Y  L  D  N  E  K  S  N  G  T  I
attcacataaaagagaaacatctttgtcatgctcagacgtctcctaagctgttttgggca
 I  H  I  K  E  K  H  L  C  H  A  Q  T  S  P  K  L  F  W  A
ctggtcgtggttgctggagtcctgttttgttatggcttgctagtgacagtggctctttgt
 L  V  V  V  A  G  V  L  F  C  Y  G  L  L  V  T  V  A  L  C
gttatctggacaaatagtagaaggaacagactggatccaggcagtggaagtgggagcggt
 V  I  W  T  N  S  R  R  N  R  L  D  P  G  S  G  S  G  S  G
tctggctccggatcagggtcgggtagtggcagcggatctggtcctggccccgggccggga
 S  G  S  G  S  G  S  G  S  G  S  G  S  G  P  G  P  G  P  G
ccaggtcctatgagtgcgattaagccagacatgaagatcaaactccgtatggaaagcaac
 P  G  P  M  S  A  I  K  P  D  M  K  I  K  L  R  M  E  S  N
gtaaacgggcaccactttgtgatcgacggagatggtacaggcaagccttttgagggaaaa
 V  N  G  H  H  F  V  I  D  G  D  G  T  G  K  P  F  E  G  K
cagagtatggatcttgaagtcaaagagggcggacctctgcctttgcctttgatatcctg
 Q  S  M  D  L  E  V  K  E  G  G  P  L  P  F  A  F  D  I  L
accactgcattccattacggcaacagggtattcgccaaatatccagacaacatacaagac
 T  T  A  F  H  Y  G  N  R  V  F  A  K  Y  P  D  N  I  Q  D
tattttaagcagtcgtttcctaaggggtattcgtgggaacgaagcttgactttcgaagac
 Y  F  K  Q  S  F  P  K  G  Y  S  W  E  R  S  L  T  F  E  D
gggggcatttgcaacgccagaaacgacataacaatggaaggggacactttctataataaa
 G  G  I  C  N  A  R  N  D  I  T  M  E  G  D  T  F  Y  N  K
gttcgattttatggtaccaactttcccgccaatggtccagttatgcagaagaagacgctg
 V  R  F  Y  G  T  N  F  P  A  N  G  P  V  M  Q  K  K  T  L
aaatgggagccctccactgagaaaatgtatgtgcgtgatggagtgctgacgggtgatatt
 K  W  E  P  S  T  E  K  M  Y  V  R  D  G  V  L  T  G  D  I
gagatggctttgttgcttgaaggaaatgcccattaccgatgtgacttcagaactacttac
 E  M  A  L  L  L  E  G  N  A  H  Y  R  C  D  F  R  T  T  Y
aaagctaaggagaagggtgtcaagttaccaggcgcccactttgtggaccactgcattgag
 K  A  K  E  K  G  V  K  L  P  G  A  H  F  V  D  H  C  I  E
```


attttaagccatgacaaagattacaacaaggttaagctgtatgagcatgctgttgctcat
I L S H D K D Y N K V K L Y E H A V A H
tctggattgcctgacaatgccagacgataaagcggccgc
S G L P D N A R R - - - -

**Sequence of a chimeric human CD86– mEos3.2 gene truncated in the cytosolic domain (truncCD86-mEos)**

MluI Kozak START hCD86 ECD hCD86 TM truncated hCD86 ICD BamHI flexible linker mEOS3.2 STOP NotI

```
acgcgtgccaccatggagccccagtgcactatggggctgagtaacattctctttgtgatg
 -  -  -  -  M  E  P  Q  C  T  M  G  L  S  N  I  L  F  V  M
gccttcctgctctctggtgctgctcctctgaagattcaagcttatttcaatgagactgca
 A  F  L  L  S  G  A  A  P  L  K  I  Q  A  Y  F  N  E  T  A
gacctgccatgccaatttgcaaactctcaaaaccaaagcctgagtgagctagtagtattt
 D  L  P  C  Q  F  A  N  S  Q  N  Q  S  L  S  E  L  V  V  F
tggcaggaccaggaaaacttggttctgaatgaggtatacttaggcaaagagaaatttgac
 W  Q  D  Q  E  N  L  V  L  N  E  V  Y  L  G  K  E  K  F  D
agtgttcattccaagtatatgggccgcacaagttttgattcggacagttggaccctgaga
 S  V  H  S  K  Y  M  G  R  T  S  F  D  S  D  S  W  T  L  R
cttcacaatcttcagatcaaggacaagggcttgtatcaatgtatcatccatcacaaaaag
 L  H  N  L  Q  I  K  D  K  G  L  Y  Q  C  I  I  H  H  K  K
cccacaggaatgattcgcatccaccagatgaattctgaactgtcagtgcttgctaacttc
 P  T  G  M  I  R  I  H  Q  M  N  S  E  L  S  V  L  A  N  F
agtcaacctgaaatagtaccaatttctaatataacagaaaatgtgtacataaatttgacc
 S  Q  P  E  I  V  P  I  S  N  I  T  E  N  V  Y  I  N  L  T
tgctcatctatacacggttacccagaacctaagaagatgagtgttttgctaagaaccaag
 C  S  S  I  H  G  Y  P  E  P  K  K  M  S  V  L  L  R  T  K
aattcaactatcgagtatgatggtattatgcagaaatctcaagataatgtcacagaactg
 N  S  T  I  E  Y  D  G  I  M  Q  K  S  Q  D  N  V  T  E  L
tacgacgtttccatcagcttgtctgtttcattccctgatgttacgagcaatatgaccatc
 Y  D  V  S  I  S  L  S  V  S  F  P  D  V  T  S  N  M  T  I
ttctgtattctggaaactgacaagacgcggcttttatcttcacctttctctatagagctt
 F  C  I  L  E  T  D  K  T  R  L  L  S  S  P  F  S  I  E  L
gaggaccctcagcctcccccagaccacattccttggattacagctgtacttccaacagtt
 E  D  P  Q  P  P  P  D  H  I  P  W  I  T  A  V  L  P  T  V
attatatgtgtgatggttttctgtctaattctatggaaatggaagaagaagaagcggcct
 I  I  C  V  M  V  F  C  L  I  L  W  K  W  K  K  K  K  R  P
cgggatccaggcagtggaagtgggagcggttctggctccggatcagggtcgggtagtggc
 R  D  P  G  S  G  S  G  S  G  S  G  S  G  S  G  S  G  S  G
agcggatctggtcctggccccgggccgggaccaggtcctatgagtgcgattaagccagac
 S  G  S  G  P  G  P  G  P  G  P  G  P  M  S  A  I  K  P  D
atgaagatcaaactccgtatggaaggcaacgtaaacgggcaccactttgtgatcgacgga
 M  K  I  K  L  R  M  E  G  N  V  N  G  H  H  F  V  I  D  G
gatggtacaggcaagccttttgagggaaaacagagtatggatcttgaagtcaaagagggc
 D  G  T  G  K  P  F  E  G  K  Q  S  M  D  L  E  V  K  E  G
ggacctctgccttttgccttgatatcctgaccactgcattccattacggcaacagggta
 G  P  L  P  F  A  F  D  I  L  T  T  A  F  H  Y  G  N  R  V
ttcgccaaatatccagacaacatacaagactattttaagcagtcgtttcctaaggggtat
 F  A  K  Y  P  D  N  I  Q  D  Y  F  K  Q  S  F  P  K  G  Y
tcgtgggaacgaagcttgactttcgaagacgggggcatttgcaacgccagaaacgacata
 S  W  E  R  S  L  T  F  E  D  G  G  I  C  N  A  R  N  D  I
```

acaatggaaggggacactttctataataaagttcgattttatggtaccaactttcccgcc
 T  M  E  G  D  T  F  Y  N  K  V  R  F  Y  G  T  N  F  P  A
aatggtccagttatgcagaagaagacgctgaaatgggagccctccactgagaaaatgtat
 N  G  P  V  M  Q  K  K  T  L  K  W  E  P  S  T  E  K  M  Y
gtgcgtgatggagtgctgacgggtgatattgagatggctttgttgcttgaaggaaatgcc
 V  R  D  G  V  L  T  G  D  I  E  M  A  L  L  L  E  G  N  A
cattaccgatgtgacttcagaactacttacaaagctaaggagaagggtgtcaagttacca
 H  Y  R  C  D  F  R  T  T  Y  K  A  K  E  K  G  V  K  L  P
ggcgcccactttgtggaccactgcattgagattttaagccatgacaaagattacaacaag
 G  A  H  F  V  D  H  C  I  E  I  L  S  H  D  K  D  Y  N  K
gttaagctgtatgagcatgctgttgctcattctggattgcctgacaatgccagacgataa
 V  K  L  Y  E  H  A  V  A  H  S  G  L  P  D  N  A  R  R  -
agcggccgc
 -  -  -

## Bibliography


1. Hedrick, S. M., *The acquired immune system: a vantage from beneath.* Immunity, 2004. **21**(5): p. 607-15.
2. Dunne, D. W. and Cooke, A., *A worm's eye view of the immune system: consequences for evolution of human autoimmune disease.* Nat Rev Immunol, 2005. **5**(5): p. 420-6.
3. Muraille, E., *Redefining the immune system as a social interface for cooperative processes.* PLoS Pathog, 2013. **9**(3): p. e1003203.
4. van Valen, L., *A new evolutionary law.* Evol Theor, 1973. **1**: p. 1-30.
5. Linn, S. and Arber, W., *Host specificity of DNA produced by Escherichia coli, X. In vitro restriction of phage fd replicative form.* Proc Natl Acad Sci U S A, 1968. **59**(4): p. 1300-6.
6. Kelly, T. J., Jr. and Smith, H. O., *A restriction enzyme from Hemophilus influenzae: II. Base sequence of the recognition site.* J Mol Biol, 1970. **51**(2): p. 393-409.
7. Smith, H. O. and Wilcox, K. W., *A restriction enzyme from Hemophilus influenzae: I. Purification and general properties.* J Mol Biol, 1970. **51**(2): p. 379-91.
8. Danna, K. and Nathans, D., *Specific cleavage of simian virus 40 DNA by restriction endonuclease of Hemophilus influenzae.* Proc Natl Acad Sci U S A, 1971. **68**(12): p. 2913-7.
9. Garneau, J. E., Dupuis, M. E., Villion, M., Romero, D. A., Barrangou, R., Boyaval, P., Fremaux, C., Horvath, P., Magadan, A. H., and Moineau, S., *The CRISPR/Cas bacterial immune system cleaves bacteriophage and plasmid DNA.* Nature, 2010. **468**(7320): p. 67-71.
10. Chan, Y. K. and Gack, M. U., *Viral evasion of intracellular DNA and RNA sensing.* Nat Rev Microbiol, 2016. **14**(6): p. 360-73.
11. Rigby, R. E. and Rehwinkel, J., *RNA degradation in antiviral immunity and autoimmunity.* Trends Immunol, 2015. **36**(3): p. 179-88.
12. Parkin, J. and Cohen, B., *An overview of the immune system.* Lancet, 2001. **357**(9270): p. 1777-89.
13. Chaplin, D. D., *Overview of the immune response.* J Allergy Clin Immunol, 2010. **125**(2): p. S3-S23.
14. James, J. R., *Molecular organisation of the T cell surface*, in *Nuffield Department of Medicine*. 2006, University of Oxford: Oxford.
15. Klenerman, D., Shevchuk, A., Novak, P., Korchev, Y. E., and Davis, S. J., *Imaging the cell surface and its organization down to the level of single molecules.* Philos T Roy Soc B, 2013. **368**(1611): p. 20120027.
16. Klenerman, D., Korchev, Y. E., and Davis, S. J., *Imaging and characterisation of the surface of live cells.* Curr Opin Chem Biol, 2011. **15**(5): p. 696-703.
17. Germain, R. N., Miller, M. J., Dustin, M. L., and Nussenzweig, M. C., *Dynamic imaging of the immune system: progress, pitfalls and promise.* Nat Rev Immunol, 2006. **6**(7): p. 497-507.
18. Akira, S. and Takeda, K., *Toll-like receptor signalling.* Nat Rev Immunol, 2004. **4**(7): p. 499-511.

19. Murphy, K., Travers, P., Walport, M., and Janeway, C., *Janeway's immunobiology*. 8th ed. 2012, New York: Garland Science.
20. Varol, C., Mildner, A., and Jung, S., *Macrophages: development and tissue specialization.* Annu Rev Immunol, 2015. **33**(1): p. 643-75.
21. Sarma, J. V. and Ward, P. A., *The complement system.* Cell Tissue Res, 2011. **343**(1): p. 227-35.
22. Getz, G. S., *Thematic review series: the immune system and atherogenesis. Bridging the innate and adaptive immune systems.* J Lipid Res, 2005. **46**(4): p. 619-22.
23. Zhang, J. M. and An, J., *Cytokines, inflammation, and pain.* Int Anesthesiol Clin, 2007. **45**(2): p. 27-37.
24. Dalai, S. K., Khoruzhenko, S., Drake, C. G., Jie, C. C., and Sadegh-Nasseri, S., *Resolution of infection promotes a state of dormancy and long survival of CD4 memory T cells.* Immunol Cell Biol, 2011. **89**(8): p. 870-81.
25. Farber, D. L., Netea, M. G., Radbruch, A., Rajewsky, K., and Zinkernagel, R. M., *Immunological memory: lessons from the past and a look to the future.* Nat Rev Immunol, 2016. **16**(2): p. 124-8.
26. Neefjes, J., Jongsma, M. L., Paul, P., and Bakke, O., *Towards a systems understanding of MHC class I and MHC class II antigen presentation.* Nat Rev Immunol, 2011. **11**(12): p. 823-36.
27. Marsh, S. G. E., Parham, P., and Barber, L. D., *The HLA factsbook*. Factsbook series. 2000, San Diego: Academic Press.
28. Dalchau, N., Phillips, A., Goldstein, L. D., Howarth, M., Cardelli, L., Emmott, S., Elliott, T., and Werner, J. M., *A peptide filtering relation quantifies MHC class I peptide optimization.* PLoS Computat Biol, 2011. **7**(10).
29. Howe, C., Garstka, M., Al-Balushi, M., Ghanem, E., Antoniou, A. N., Fritzsche, S., Jankevicius, G., Kontouli, N., Schneeweiss, C., Williams, A., Elliott, T., and Springer, S., *Calreticulin-dependent recycling in the early secretory pathway mediates optimal peptide loading of MHC class I molecules.* EMBO J, 2009. **28**(23): p. 3730-44.
30. Yewdell, J. W., *The seven dirty little secrets of major histocompatibility complex class I antigen processing.* Immunol Rev, 2005. **207**(1): p. 8-18.
31. Apcher, S., Prado Martins, R., and Fåhraeus, R., *The source of MHC class I presented peptides and its implications.* Curr Opin Immunol, 2016. **40**: p. 117-22.
32. Yewdell, J. W., Anton, L. C., and Bennink, J. R., *Defective ribosomal products (DRiPs): a major source of antigenic peptides for MHC class I molecules?* J Immunol, 1996. **157**(5): p. 1823-6.
33. Petersen, J. L., Morris, C. R., and Solheim, J. C., *Virus evasion of MHC class I molecule presentation.* J Immunol, 2003. **171**(9): p. 4473-8.
34. Bessoles, S., Grandclement, C., Alari-Pahissa, E., Gehrig, J., Jeevan-Raj, B., and Held, W., *Adaptations of Natural Killer Cells to Self-MHC Class I.* Front Immunol, 2014. **5**: p. 349.
35. Dudley, D. D., Chaudhuri, J., Bassing, C. H., and Alt, F. W., *Mechanism and control of V(D)J recombination versus class switch recombination: similarities and differences.* Adv Immunol, 2005. **86**: p. 43-112.

36. Anderson, M. S., Venanzi, E. S., Klein, L., Chen, Z., Berzins, S. P., Turley, S. J., von Boehmer, H., Bronson, R., Dierich, A., Benoist, C., and Mathis, D., *Projection of an immunological self shadow within the thymus by the aire protein.* Science, 2002. **298**(5597): p. 1395-401.
37. Venanzi, E. S., Melamed, R., Mathis, D., and Benoist, C., *The variable immunological self: genetic variation and nongenetic noise in Aire-regulated transcription.* Proc Natl Acad Sci U S A, 2008. **105**(41): p. 15860-5.
38. Pelanda, R. and Torres, R. M., *Central B-cell tolerance: where selection begins.* Cold Spring Harb Perspect Biol, 2012. **4**(4): p. a007146.
39. Vindigni, S. M., Zisman, T. L., Suskind, D. L., and Damman, C. J., *The intestinal microbiome, barrier function, and immune system in inflammatory bowel disease: a tripartite pathophysiological circuit with implications for new therapeutic directions.* Therap Adv Gastroenterol, 2016. **9**(4): p. 606-25.
40. de Souza, H. S. and Fiocchi, C., *Immunopathogenesis of IBD: current state of the art.* Nat Rev Gastroenterol Hepatol, 2016. **13**(1): p. 13-27.
41. Tscharke, D. C., Croft, N. P., Doherty, P. C., and La Gruta, N. L., *Sizing up the key determinants of the CD8(+) T cell response.* Nat Rev Immunol, 2015. **15**(11): p. 705-16.
42. Dustin, M. L. and Long, E. O., *Cytotoxic immunological synapses.* Immunol Rev, 2010. **235**(1): p. 24-34.
43. Monks, C. R. F., Freiberg, B. A., Kupfer, H., Sciaky, N., and Kupfer, A., *Three-dimensional segregation of supramolecular activation clusters in T cells.* Nature, 1998. **395**(6697): p. 82-6.
44. Luckheeram, R., Zhou, R., Verma, A., and Xia, B., *CD4⁺T cells: differentiation and functions.* Clin Dev Immunol, 2012. **2012**: p. 925135.
45. Crotty, S., *A brief history of T cell help to B cells.* Nat Rev Immunol, 2015. **15**(3): p. 185-9.
46. Schmitt, E. G. and Williams, C. B., *Generation and function of induced regulatory T cells.* Front Immunol, 2013. **4**: p. 152.
47. Burkett, P. R., Meyer zu Horste, G., and Kuchroo, V. K., *Pouring fuel on the fire: Th17 cells, the environment, and autoimmunity.* J Clin Invest, 2015. **125**(6): p. 2211-9.
48. Han, A., Glanville, J., Hansmann, L., and Davis, M. M., *Linking T-cell receptor sequence to functional phenotype at the single-cell level.* Nat Biotechnol, 2014. **32**(7): p. 684.
49. Germain, R. N., *T-cell development and the CD4-CD8 lineage decision.* Nat Rev Immunol, 2002. **2**(5): p. 309-22.
50. Takahama, Y., *Journey through the thymus: stromal guides for T-cell development and selection.* Nat Rev Immunol, 2006. **6**(2): p. 127-35.
51. Hayday, A. C. and Pennington, D. J., *Key factors in the organized chaos of early T cell development.* Nat Immunol, 2007. **8**(2): p. 137-44.
52. Schroeder, H. W., Jr. and Cavacini, L., *Structure and function of immunoglobulins.* J Allergy Clin Immunol, 2010. **125**(2 0 2): p. S41-52.

53. Seidel, U. J., Schlegel, P., and Lang, P., *Natural killer cell mediated antibody-dependent cellular cytotoxicity in tumor immunotherapy with therapeutic antibodies.* Front Immunol, 2013. **4**: p. 76.
54. Miller, J. F. and Mitchell, G. F., *Cell to cell interaction in the immune respons: I. Hemolysin-forming cells in neonatally thymectomized mice reconstituted with thymus or thoracic duct lymphocytes.* J Exp Med, 1968. **128**(4): p. 801-20.
55. Mitchell, G. F. and Miller, J. F., *Cell to cell interaction in the immune response: II. The source of hemolysin-forming cells in irradiated mice given bone marrow and thymus or thoracic duct lymphocytes.* J Exp Med, 1968. **128**(4): p. 821-37.
56. Nossal, G. J., Cunningham, A., Mitchell, G. F., and Miller, J. F., *Cell to cell interaction in the immune response: III. Chromosomal marker analysis of single antibody-forming cells in reconstituted, irradiated, or thymectomized mice.* J Exp Med, 1968. **128**(4): p. 839-53.
57. Aguzzi, A., Kranich, J., and Krautler, N. J., *Follicular dendritic cells: origin, phenotype, and function in health and disease.* Trends Immunol, 2014. **35**(3): p. 105-13.
58. Plomp, R., Dekkers, G., Rombouts, Y., Visser, R., Koeleman, C. A., Kammeijer, G. S., Jansen, B. C., Rispens, T., Hensbergen, P. J., Vidarsson, G., and Wuhrer, M., *Hinge-Region O-Glycosylation of Human Immunoglobulin G3 (IgG3).* Mol Cell Proteomics, 2015. **14**(5): p. 1373-84.
59. Tan, J., Pieper, K., Piccoli, L., Abdi, A., Foglierini, M., Geiger, R., Tully, C. M., Jarrossay, D., Ndungu, F. M., Wambua, J., Bejon, P., Fregni, C. S., Fernandez-Rodriguez, B., Barbieri, S., Bianchi, S., Marsh, K., Thathy, V., Corti, D., Sallusto, F., Bull, P., and Lanzavecchia, A., *A LAIR1 insertion generates broadly reactive antibodies against malaria variant antigens.* Nature, 2016. **529**(7584): p. 105-9.
60. Collin, M., Shannon, O., and Bjorck, L., *IgG glycan hydrolysis by a bacterial enzyme as a therapy against autoimmune conditions.* Proc Natl Acad Sci U S A, 2008. **105**(11): p. 4265-70.
61. Bruhns, P., *Properties of mouse and human IgG receptors and their contribution to disease models.* Blood, 2012. **119**(24): p. 5640-9.
62. Bruhns, P. and Jönsson, F., *Mouse and human FcR effector functions.* Immunol Rev, 2015. **268**(1): p. 25-51.
63. Sondermann, P., Huber, R., Oosthuizen, V., and Jacob, U., *The 3.2-A crystal structure of the human IgG1 Fc fragment-Fc gammaRIII complex.* Nature, 2000. **406**(6793): p. 267-73.
64. Woof, J. M. and Burton, D. R., *Human antibody-Fc receptor interactions illuminated by crystal structures.* Nat Rev Immunol, 2004. **4**(2): p. 89-99.
65. van der Merwe, P. A., Davis, S. J., Shaw, A. S., and Dustin, M. L., *Cytoskeletal polarization and redistribution of cell-surface molecules during T cell antigen recognition.* Semin Immunol, 2000. **12**(1): p. 5-21.
66. Mattila, P. K., Batista, F. D., and Treanor, B., *Dynamics of the actin cytoskeleton mediates receptor cross talk: An emerging concept in tuning receptor signaling.* J Cell Biol, 2016. **212**(3): p. 267-80.

67. Alarcón, B., Mestre, D., and Martínez-Martín, N., *The immunological synapse: a cause or consequence of T-cell receptor triggering?* Immunology, 2011. **133**(4): p. 420-5.
68. Burroughs, N. J., Köhler, K., Miloserdov, V., Dustin, M. L., van der Merwe, P. A., and Davis, D. M., *Boltzmann energy-based image analysis demonstrates that extracellular domain size differences explain protein segregation at immune synapses.* PLoS Comput Biol, 2011. **7**(8): p. e1002076.
69. Dustin, M. L. and Depoil, D., *New insights into the T cell synapse from single molecule techniques.* Nat Rev Immunol, 2011. **11**(10): p. 672-84.
70. Grakoui, A., Bromley, S. K., Sumen, C., Davis, M. M., Shaw, A. S., Allen, P. M., and Dustin, M. L., *The Immunological Synapse: A Molecular Machine Controlling T Cell Activation.* Science, 1999. **285**(6325): p. 221-7.
71. Delon, J. and Germain, R. N., *Information transfer at the immunological synapse.* Curr Biol, 2000. **10**(24): p. R923-R33.
72. Davis, S. J. and van der Merwe, P. A., *The immunological synapse: required for T cell receptor signalling or directing T cell effector function?* Curr Biol, 2001. **11**(8): p. R289-91.
73. Purbhoo, M. A., Irvine, D. J., Huppa, J. B., and Davis, M. M., *T cell killing does not require the formation of a stable mature immunological synapse.* Nat Immunol, 2004. **5**(5): p. 524-30.
74. Brossard, C., Feuillet, V., Schmitt, A., Randriamampita, C., Romao, M., Raposo, G., and Trautmann, A., *Multifocal structure of the T cell - dendritic cell synapse.* Eur J Immunol, 2005. **35**(6): p. 1741–53.
75. Varma, R., Campi, G., Yokosuka, T., Saito, T., and Dustin, M. L., *T cell receptor-proximal signals are sustained in peripheral microclusters and terminated in the central supramolecular activation cluster.* Immunity, 2006. **25**(1): p. 117-27.
76. Choudhuri, K., Llodrá, J., Roth, E. W., Tsai, J., Gordo, S., Wucherpfennig, K. W., Kam, L. C., Stokes, D. L., and Dustin, M. L., *Polarized release of T-cell-receptor-enriched microvesicles at the immunological synapse.* Nature, 2014. **507**(7490): p. 118-23.
77. van Merwe, A. P. and Davis, S. J., *The Immunological Synapse--a Multitasking System.* Science, 2002. **295**(5559): p. 1479-80.
78. de la Roche, M., Asano, Y., and Griffiths, G. M., *Origins of the cytolytic synapse.* Nat Rev Immunol, 2016. **16**(7): p. 421-32.
79. Guedj, C., Abraham, N., Jullie, D., and Randriamampita, C., *T cell adhesion triggers an early signaling pole distal to the immune synapse.* J Cell Sci, 2016. **129**(13): p. 2526-37.
80. Orange, J. S., *Formation and function of the lytic NK-cell immunological synapse.* Nat Rev Immunol, 2008. **8**(9): p. 713-25.
81. Natkanski, E., Lee, W. Y., Mistry, B., Casal, A., Molloy, J. E., and Tolar, P., *B cells use mechanical energy to discriminate antigen affinities.* Science, 2013. **340**(6140): p. 1587-90.
82. Batista, F. D., Iber, D., and Neuberger, M. S., *B cells acquire antigen from target cells after synapse formation.* Nature, 2001. **411**(6836): p. 489-94.

83. Nowosad, C. R., Spillane, K. M., and Tolar, P., *Germinal center B cells recognize antigen through a specialized immune synapse architecture.* Nat Immunol, 2016. **17**(7): p. 870-7.
84. Dushek, O., Goyette, J., and van der Merwe, P. A., *Non-catalytic tyrosine-phosphorylated receptors.* Immunol Rev, 2012. **250**(1): p. 258-76.
85. Merwe, P. A. and Davis, S. J., *Molecular interactions mediating T cell antigen recognition.* Ann Rev Immunol, 2003. **21**: p. 659-84.
86. Davis, S. J. and van der Merwe, P. A., *The kinetic-segregation model: TCR triggering and beyond.* Nat Immunol, 2006. **7**(8): p. 803-9.
87. Allard, J. F., Dushek, O., Coombs, D., and van der Merwe, P. A., *Mechanical modulation of receptor-ligand interactions at cell-cell interfaces.* Biophys J, 2012. **102**(6): p. 1265-73.
88. Daeron, M., Jaeger, S., Du Pasquier, L., and Vivier, E., *Immunoreceptor tyrosine-based inhibition motifs: a quest in the past and future.* Immunol Rev, 2008. **224**: p. 11-43.
89. Reth, M., *Antigen receptor tail clue.* Nature, 1989. **338**(6214): p. 383-4.
90. Shlapatska, L. M., Mikhalap, S. V., Berdova, A. G., Zelensky, O. M., Yun, T. J., Nichols, K. E., Clark, E. A., and Sidorenko, S. P., *CD150 association with either the SH2-containing inositol phosphatase or the SH2-containing protein tyrosine phosphatase is regulated by the adaptor protein SH2D1A.* J Immunol, 2001. **166**(9): p. 5480-7.
91. Okazaki, T., Maeda, A., Nishimura, H., Kurosaki, T., and Honjo, T., *PD-1 immunoreceptor inhibits B cell receptor-mediated signaling by recruiting src homology 2-domain-containing tyrosine phosphatase 2 to phosphotyrosine.* Proc Natl Acad Sci U S A, 2001. **98**(24): p. 13866-71.
92. Billadeau, D. D. and Leibson, P. J., *ITAMs versus ITIMs: striking a balance during cell regulation.* J Clin Invest, 2002. **109**(2): p. 161-8.
93. Rachmilewitz, J. and Lanzavecchia, A., *A temporal and spatial summation model for T-cell activation: signal integration and antigen decoding.* Trends Immunol, 2002. **23**(12): p. 592-5.
94. Gett, A. V. and Hodgkin, P. D., *A cellular calculus for signal integration by T cells.* Nat Immunol, 2000. **1**(3): p. 239-44.
95. Kuhns, M. S., Davis, M. M., and Garcia, C. K., *Deconstructing the Form and Function of the TCR/CD3 Complex.* Immunity, 2006. **24**(2): p. 133-9.
96. Rudolph, M. G. and Wilson, I. A., *The specificity of TCR/pMHC interaction.* Curr Opin Immunol, 2002. **14**(1): p. 52-65.
97. Manning, T. C., Schlueter, C. J., Brodnicki, T. C., Parke, E. A., Speir, J. A., Garcia, K. C., Teyton, L., Wilson, I. A., and Kranz, D. M., *Alanine scanning mutagenesis of an alphabeta T cell receptor: mapping the energy of antigen recognition.* Immunity, 1998. **8**(4): p. 413-25.
98. Lee, P. U., Churchill, H. R., Daniels, M., Jameson, S. C., and Kranz, D. M., *Role of 2CT cell receptor residues in the binding of self- and allo-major histocompatibility complexes.* J Exp Med, 2000. **191**(8): p. 1355-64.
99. Garcia, K. C., Degano, M., Pease, L. R., Huang, M., Peterson, P. A., Teyton, L., and Wilson, I. A., *Structural basis of plasticity in T cell receptor recognition of a self peptide-MHC antigen.* Science, 1998. **279**(5354): p. 1166-72.

100. Reiser, J. B., Gregoire, C., Darnault, C., Mosser, T., Guimezanes, A., Schmitt-Verhulst, A. M., Fontecilla-Camps, J. C., Mazza, G., Malissen, B., and Housset, D., *A T cell receptor CDR3beta loop undergoes conformational changes of unprecedented magnitude upon binding to a peptide/MHC class I complex.* Immunity, 2002. **16**(3): p. 345-54.
101. Ding, Y. H., Baker, B. M., Garboczi, D. N., Biddison, W. E., and Wiley, D. C., *Four A6-TCR/peptide/HLA-A2 structures that generate very different T cell signals are nearly identical.* Immunity, 1999. **11**(1): p. 45-56.
102. Mason, D., *A very high level of crossreactivity is an essential feature of the T-cell receptor.* Immunol Today, 1998. **19**(9): p. 395-404.
103. Hennecke, J. and Wiley, D. C., *T cell receptor-MHC interactions up close.* Cell, 2001. **104**(1): p. 1-4.
104. Manolios, N., Bonifacino, J. S., and Klausner, R. D., *Transmembrane helical interactions and the assembly of the T cell receptor complex.* Science, 1990. **249**(4966): p. 274-7.
105. Teixeiro, E., Daniels, M. A., Hausmann, B., Schrum, A. G., Naeher, D., Luescher, I., Thome, M., Bragado, R., and Palmer, E., *T cell division and death are segregated by mutation of TCRbeta chain constant domains.* Immunity, 2004. **21**(4): p. 515-26.
106. Call, M. E., Pyrdol, J., Wiedmann, M., and Wucherpfennig, K. W., *The organizing principle in the formation of the T cell receptor-CD3 complex.* Cell, 2002. **111**(7): p. 967-79.
107. James, J. R., McColl, J., Oliveira, M. I., Dunne, P. D., Huang, E., Jansson, A., Nilsson, P., Sleep, D. L., Gonçalves, C. M., Morgan, S. H., Felce, J. H., Mahen, R., Fernandes, R. A., Carmo, A. M., Klenerman, D., and Davis, S. J., *The T cell receptor triggering apparatus is composed of monovalent or monomeric proteins.* J Biol Chem, 2011. **286**(37): p. 31993-2001.
108. James, J. R., White, S. S., Clarke, R. W., Johansen, A. M., Dunne, P. D., Sleep, D. L., Fitzgerald, W. J., Davis, S. J., and Klenerman, D., *Single-molecule level analysis of the subunit composition of the T cell receptor on live T cells.* Proc Natl Acad Sci U S A, 2007. **104**(45): p. 17662–7.
109. Schamel, W., Arechaga, I., Risueño, R. M., van Santen, H. M., Cabezas, P., Risco, C., Valpuesta, J. M., and Alarcón, B., *Coexistence of multivalent and monovalent TCRs explains high sensitivity and wide range of response.* J Exp Med, 2005. **202**(4): p. 493-503.
110. Sigalov, A. B., *"Monovalent" ligands that trigger TLR-4 and TCR are not necessarily truly monovalent.* Mol Immunol, 2012. **51**(3-4): p. 356-62.
111. Dillard, P., Pi, F., Lellouch, A. C., Limozin, L., and Sengupta, K., *Nano-clustering of ligands on surrogate antigen presenting cells modulates T cell membrane adhesion and organization.* Integr Biol, 2016. **8**(3): p. 287-301.
112. Acuto, O., Bartolo, V., and Michel, F., *Tailoring T-cell receptor signals by proximal negative feedback mechanisms.* Nat Rev Immunol, 2008. **8**(9): p. 699-712.
113. Wang, H., Kadlecek, T. A., Au-Yeung, B. B., Goodfellow, H. E., Hsu, L.-Y., Freedman, T. S., and Weiss, A., *ZAP-70: An Essential Kinase in T-cell Signaling.* Cold Spring Harb Perspect Biol, 2010. **2**(5): p. a002279.

114. Yokosuka, T. and Saito, T., *The immunological synapse, TCR microclusters, and T cell activation*, in *Immunological Synapse*, Saito, T. and Batista, F.D., Editors. 2010, Springer Berlin Heidelberg: Berlin, Heidelberg. p. 81-107.
115. Moreau, H. D. D., Lemaître, F., Garrod, K. R., Garcia, Z., Lennon-Duménil, A.-M. M., and Bousso, P., *Signal strength regulates antigen-mediated T-cell deceleration by distinct mechanisms to promote local exploration or arrest.* Proc Natl Acad Sci U S A, 2015. **112**(39): p. 12151-6.
116. Quill, H. and Schwartz, R. H., *Stimulation of normal inducer T cell clones with antigen presented by purified Ia molecules in planar lipid membranes: specific induction of a long-lived state of proliferative nonresponsiveness.* J Immunol, 1987. **138**(11): p. 3704-12.
117. June, C. H., Ledbetter, J. A., Linsley, P. S., and Thompson, C. B., *Role of the CD28 receptor in T-cell activation.* Immunol Today, 1990. **11**(6): p. 211-6.
118. Boomer, J. S. and Green, J. M., *An enigmatic tail of CD28 signaling.* Cold Spring Harb Perspect Biol, 2010. **2**(8): p. a002436.
119. Esensten, J. H., Helou, Y. A., Chopra, G., Weiss, A., and Bluestone, J. A., *CD28 Costimulation: From Mechanism to Therapy.* Immunity, 2016. **44**(5): p. 973-88.
120. Camperio, C., Muscolini, M., Volpe, E., Mitri, D., Mechelli, R., Buscarinu, M. C., Ruggieri, S., Piccolella, E., Salvetti, M., Gasperini, C., Battistini, L., and Tuosto, L., *CD28 ligation in the absence of TCR stimulation up-regulates IL-17A and pro-inflammatory cytokines in relapsing-remitting multiple sclerosis T lymphocytes.* Immunol Lett, 2014. **158**(1-2): p. 134-42.
121. de Kouchkovsky, D., Esensten, J. H., Rosenthal, W. L., Morar, M. M., Bluestone, J. A., and Jeker, L. T., *microRNA-17-92 regulates IL-10 production by regulatory T cells and control of experimental autoimmune encephalomyelitis.* J Immunol, 2013. **191**(4): p. 1594-605.
122. Guo, F., Iclozan, C., Suh, W. K., Anasetti, C., and Yu, X. Z., *CD28 controls differentiation of regulatory T cells from naive CD4 T cells.* J Immunol, 2008. **181**(4): p. 2285-91.
123. Lyddane, C., Gajewska, B. U., Santos, E., King, P. D., Furtado, G. C., and Sadelain, M., *Cutting Edge: CD28 controls dominant regulatory T cell activity during active immunization.* J Immunol, 2006. **176**(6): p. 3306-10.
124. Aruffo, A. and Seed, B., *Molecular cloning of a CD28 cDNA by a high-efficiency COS cell expression system.* Proc Natl Acad Sci U S A, 1987. **84**(23): p. 8573-7.
125. Carreno, B. M. and Collins, M., *The B7 family of ligands and its receptors: new pathways for costimulation and inhibition of immune responses.* Annu Rev Immunol, 2002. **20**: p. 29-53.
126. Holdorf, A. D., Green, J. M., Levin, S. D., Denny, M. F., Straus, D. B., Link, V., Changelian, P. S., Allen, P. M., and Shaw, A. S., *Proline residues in CD28 and the Src homology (SH)3 domain of Lck are required for T cell costimulation.* J Exp Med, 1999. **190**(3): p. 375-84.
127. Raab, M., Cai, Y. C., Bunnell, S. C., Heyeck, S. D., Berg, L. J., and Rudd, C. E., *p56Lck and p59Fyn regulate CD28 binding to phosphatidylinositol 3-kinase, growth factor receptor-bound protein GRB-2, and T cell-specific protein-tyrosine kinase ITK: implications for T-cell costimulation.* Proc Natl Acad Sci U S A, 1995. **92**(19): p. 8891-5.

128. Sadra, A., Cinek, T., Arellano, J. L., Shi, J., Truitt, K. E., and Imboden, J. B., *Identification of tyrosine phosphorylation sites in the CD28 cytoplasmic domain and their role in the costimulation of Jurkat T cells.* J Immunol, 1999. **162**(4): p. 1966-73.
129. Kim, H. H., Tharayil, M., and Rudd, C. E., *Growth factor receptor-bound protein 2 SH2/SH3 domain binding to CD28 and its role in co-signaling.* J Biol Chem, 1998. **273**(1): p. 296-301.
130. Boomer, J. S., Deppong, C. M., Shah, D. D., Bricker, T. L., and Green, J. M., *Cutting edge: a double-mutant knockin of the CD28 YMNM and PYAP motifs reveals a critical role for the YMNM motif in regulation of T cell proliferation and Bcl-xL expression.* J Immunol, 2014. **192**(8): p. 3465-9.
131. Evans, E. J., Esnouf, R. M., Manso-Sancho, R., Gilbert, R. J. C., James, J. R., Yu, C., Fennelly, J. A., Vowles, C., Hanke, T., Walse, B., Hünig, T., Sørensen, P., Stuart, D. I., and Davis, S. J., *Crystal structure of a soluble CD28-Fab complex.* Nat Immunol, 2005. **6**(3): p. 271-9.
132. Dennehy, K. M., Elias, F., Zeder-Lutz, G., Ding, X., Altschuh, D., Lühder, F., and Hünig, T., *Cutting edge: monovalency of CD28 maintains the antigen dependence of T cell costimulatory responses.* J Immunol, 2006. **176**(10): p. 5725-9.
133. Bohjanen, P. R., Petryniak, B., June, C. H., Thompson, C. B., and Lindsten, T., *AU RNA-binding factors differ in their binding specificities and affinities.* J Biol Chem, 1992. **267**(9): p. 6302-9.
134. Tian, R., Wang, H., Gish, G. D., Petsalaki, E., Pasculescu, A., Shi, Y., Mollenauer, M., Bagshaw, R. D., Yosef, N., Hunter, T., Gingras, A. C., Weiss, A., and Pawson, T., *Combinatorial proteomic analysis of intercellular signaling applied to the CD28 T-cell costimulatory receptor.* Proc Natl Acad Sci U S A, 2015. **112**(13): p. E1594-603.
135. Porciello, N. and Tuosto, L., *CD28 costimulatory signals in T lymphocyte activation: Emerging functions beyond a qualitative and quantitative support to TCR signalling.* Cytokine Growth Factor Rev, 2016. **28**: p. 11-9.
136. Tavano, R., Contento, R. L., Baranda, S. J., Soligo, M., Tuosto, L., Manes, S., and Viola, A., *CD28 interaction with filamin-A controls lipid raft accumulation at the T-cell immunological synapse.* Nat Cell Biol, 2006. **8**(11): p. 1270-6.
137. Fooksman, D. R., Vardhana, S., Vasiliver-Shamis, G., Liese, J., Blair, D. A., Waite, J., Sacristan, C., Victora, G. D., Zanin-Zhorov, A., and Dustin, M. L., *Functional anatomy of T cell activation and synapse formation.* Annu Rev Immunol, 2010. **28**: p. 79-105.
138. Frauwirth, K. A., Riley, J. L., Harris, M. H., Parry, R. V., Rathmell, J. C., Plas, D. R., Elstrom, R. L., June, C. H., and Thompson, C. B., *The CD28 signaling pathway regulates glucose metabolism.* Immunity, 2002. **16**(6): p. 769-77.
139. Boise, L. H., Minn, A. J., Noel, P. J., June, C. H., Accavitti, M. A., Lindsten, T., and Thompson, C. B., *CD28 costimulation can promote T cell survival by enhancing the expression of Bcl-xL.* Immunity, 1995. **3**(1): p. 87-98.
140. Acuto, O. and Michel, F., *CD28-mediated co-stimulation: a quantitative support for TCR signalling.* Nat Rev Immunol, 2003. **3**: p. 939-51.

141. Michel, F., Attal-Bonnefoy, G., Mangino, G., Mise-Omata, S., and Acuto, O., *CD28 as a molecular amplifier extending TCR ligation and signaling capabilities.* Immunity, 2001. **15**(6): p. 935-45.
142. Yokosuka, T., Kobayashi, W., Sakata-Sogawa, K., Takamatsu, M., Hashimoto-Tane, A., Dustin, M. L., Tokunaga, M., and Saito, T., *Spatiotemporal regulation of T cell costimulation by TCR-CD28 microclusters and protein kinase C theta translocation.* Immunity, 2008. **29**(4): p. 589-601.
143. Lafferty, K. J. and Cunningham, A. J., *A new analysis of allogeneic interactions.* Aust J Exp Biol Med Sci, 1975. **53**(1): p. 27-42.
144. Sanchez-Lockhart, M., Kim, M., and Miller, J., *Cutting edge: A role for inside-out signaling in TCR regulation of CD28 ligand binding.* J Immunol, 2011. **187**(11): p. 5515-9.
145. Bashour, K. T., Tsai, J., Shen, K., Lee, J.-H. H., Sun, E., Milone, M. C., Dustin, M. L., and Kam, L. C., *Cross talk between CD3 and CD28 is spatially modulated by protein lateral mobility.* Mol Cell Biol, 2014. **34**(6): p. 955-64.
146. Sykulev, Y., Joo, M., Vturina, I., Tsomides, T. J., and Eisen, H. N., *Evidence that a single peptide-MHC complex on a target cell can elicit a cytolytic T cell response.* Immunity, 1996. **4**(6): p. 565-71.
147. Irvine, D. J., Purbhoo, M. A., Krogsgaard, M., and Davis, M. M., *Direct observation of ligand recognition by T cells.* Nature, 2002. **419**(6909): p. 845-9.
148. Palmer, E. and Naeher, D., *Affinity threshold for thymic selection through a T-cell receptor-co-receptor zipper.* Nat Rev Immunol, 2009. **9**(3): p. 207-13.
149. van der Merwe, P. A. and Dushek, O., *Mechanisms for T cell receptor triggering.* Nat Rev Immunol, 2011. **11**(1): p. 47-55.
150. Jorissen, R. N., Walker, F., Pouliot, N., Garrett, T. P., Ward, C. W., and Burgess, A. W., *Epidermal growth factor receptor: mechanisms of activation and signalling.* Exp Cell Res, 2003. **284**(1): p. 31-53.
151. Katritch, V., Cherezov, V., and Stevens, R. C., *Structure-function of the G protein-coupled receptor superfamily.* Annu Rev Pharmacol Toxicol, 2013. **53**: p. 531-56.
152. O'Shea, J. J., McVicar, D. W., Bailey, T. L., Burns, C., and Smyth, M. J., *Activation of human peripheral blood T lymphocytes by pharmacological induction of protein-tyrosine phosphorylation.* Proc Natl Acad Sci U S A, 1992. **89**(21): p. 10306-10.
153. Chang, V. T., Fernandes, R. A., Ganzinger, K. A., Lee, S. F., Siebold, C., McColl, J., Jönsson, P., Palayret, M., Harlos, K., Coles, C. H., Jones, E. Y., Lui, Y., Huang, E., Gilbert, R. J., Klenerman, D., Aricescu, A. R., and Davis, S. J., *Initiation of T cell signaling by CD45 segregation at 'close contacts'.* Nat Immunol, 2016. **17**(5): p. 574-82.
154. Garcia, K. C., Teyton, L., and Wilson, I. A., *Structural basis of T cell recognition.* Annu Rev Immunol, 1999. **17**: p. 369-97.
155. Ayres, C. M., Scott, D. R., Corcelli, S. A., and Baker, B. M., *Differential utilization of binding loop flexibility in T cell receptor ligand selection and cross-reactivity.* Sci Rep, 2016. **6**: p. 25070.
156. Kjer-Nielsen, L., Clements, C. S., Purcell, A. W., Brooks, A. G., Whisstock, J. C., Burrows, S. R., McCluskey, J., and Rossjohn, J., *A structural basis for the*

*selection of dominant alphabeta T cell receptors in antiviral immunity.* Immunity, 2003. **18**(1): p. 53-64.
157. Beddoe, T., Chen, Z. J., Clements, C. S., Ely, L. K., Bushell, S. R., Vivian, J. P., Kjer-Nielsen, L., Pang, S. S., Dunstone, M. A., Liu, Y. C., Macdonald, W. A., Perugini, M. A., Wilce, M. C. J., Burrows, S. R., Purcell, A. W., Tiganis, T., Bottomley, S. P., McCluskey, J., and Rossjohn, J., *Antigen Ligation Triggers a Conformational Change within the Constant Domain of the alpha beta T Cell Receptor.* Immunity, 2009. **30**(6): p. 777-88.
158. Hawse, W. F., Champion, M. M., Joyce, M. V., Hellman, L. M., Hossain, M., Ryan, V., Pierce, B. G., Weng, Z., and Baker, B. M., *Cutting edge: Evidence for a dynamically driven T cell signaling mechanism.* J Immunol, 2012. **188**(12): p. 5819-23.
159. Martinez-Martin, N., Risueno, R. M., Morreale, A., Zaldivar, I., Fernandez-Arenas, E., Herranz, F., Ortiz, A. R., and Alarcon, B., *Cooperativity between T cell receptor complexes revealed by conformational mutants of CD3epsilon.* Sci Signal, 2009. **2**(83): p. ra43.
160. Fernandes, R. A., Shore, D. A., Vuong, M. T., Yu, C., Zhu, X., Pereira-Lopes, S., Brouwer, H., Fennelly, J. A., Jessup, C. M., Evans, E. J., Wilson, I. A., and Davis, S. J., *T cell receptors are structures capable of initiating signaling in the absence of large conformational rearrangements.* J Biol Chem, 2012. **287**(16): p. 13324-35.
161. Xu, C., Gagnon, E., Call, M. E., Schnell, J. R., Schwieters, C. D., Carman, C. V., Chou, J. J., and Wucherpfennig, K. W., *Regulation of T cell receptor activation by dynamic membrane binding of the CD3epsilon cytoplasmic tyrosine-based motif.* Cell, 2008. **135**(4): p. 702-13.
162. Zhang, H., Cordoba, S.-P., Dushek, O., and van der Merwe, P. A., *Basic residues in the T-cell receptor ζ cytoplasmic domain mediate membrane association and modulate signaling.* Proc Natl Acad Sci U S A, 2011. **108**(48): p. 19323–8.
163. Dobbins, J., Gagnon, E., Godec, J., Pyrdol, J., Vignali, D. A. A., Sharpe, A. H., and Wucherpfennig, K. W., *Binding of the cytoplasmic domain of CD28 to the plasma membrane inhibits Lck recruitment and signaling.* Sci Signal, 2016. **9**(438): p. ra75.
164. Gagnon, E., Schubert, D. A., Gordo, S., Chu, H. H., and Wucherpfennig, K. W., *Local changes in lipid environment of TCR microclusters regulate membrane binding by the CD3ε cytoplasmic domain.* J Exp Med, 2012. **209**(13): p. 2423-39.
165. Fernandes, R. A., Yu, C., Carmo, A. M., Evans, E. J., van der Merwe, P. A., and Davis, S. J., *What controls T cell receptor phosphorylation?* Cell, 2010. **142**(5): p. 668-9.
166. Sanchez-Lockhart, M., Rojas, A. V., Fettis, M. M., Bauserman, R., Higa, T. R., Miao, H., Waugh, R. E., and Miller, J., *T cell receptor signaling can directly enhance the avidity of CD28 ligand binding.* PLoS One, 2014. **9**(2): p. e89263.
167. Das, D. K., Feng, Y., Mallis, R. J., Li, X., Keskin, D. B., Hussey, R. E., Brady, S. K., Wang, J.-H. H., Wagner, G., Reinherz, E. L., and Lang, M. J., *Force-dependent transition in the T-cell receptor β-subunit allosterically regulates peptide discrimination and pMHC bond lifetime.* Proc Natl Acad Sci U S A, 2015. **112**(5): p. 1517-22.

168. Finkel, T. H., Ma, Z. Y., and Janmey, P. A., *The receptor deformation model - a novel solution to the TCR triggering puzzle.* Arthritis and Rheumatism, 2008. **58**(9): p. S847-S.
169. Husson, J., Chemin, K., Bohineust, A., Hivroz, C., and Henry, N., *Force Generation upon T Cell Receptor Engagement.* PLoS ONE, 2011. **6**(5): p. e19680.
170. Valitutti, S., Dessing, M., Aktories, K., Gallati, H., and Lanzavecchia, A., *Sustained Signaling Leading to T-Cell Activation Results from Prolonged T-Cell Receptor Occupancy - Role of T-Cell Actin Cytoskeleton.* J Exp Med, 1995. **181**(2): p. 577-84.
171. Sun, Z. Y. J., Kim, H. S., Wagner, G., and Reinherz, E. L., *Mechanisms contributing to T cell receptor signaling and assembly revealed by the solution structure of an ectodomain fragment of the CD3 epsilon gamma heterodimer.* Cell, 2001. **105**(7): p. 913-23.
172. Call, M. E., Schnell, J. R., Xu, C. Q., Lutz, R. A., Chou, J. J., and Wucherpfennig, K. W., *The structure of the zeta zeta transmembrane dimer reveals features essential for its assembly with the T cell receptor.* Cell, 2006. **127**(2): p. 355-68.
173. Geppert, T. D. and Lipsky, P. E., *Accessory cell independent proliferation of human T4 cells stimulated by immobilized monoclonal antibodies to CD3.* J Immunol, 1987. **138**(6): p. 1660-6.
174. Ma, Z., Sharp, K. A., Janmey, P. A., and Finkel, T. H., *Surface-anchored monomeric agonist pMHCs alone trigger TCR with high sensitivity.* PLoS Biol, 2008. **6**(2): p. e43.
175. Choudhuri, K., Parker, M., Milicic, A., Cole, D. K., Shaw, M. K., Sewell, A. K., Stewart-Jones, G., Dong, T., Gould, K. G., and van der Merwe, P. A., *Peptide-major histocompatibility complex dimensions control proximal kinase-phosphatase balance during T cell activation.* J Biol Chem, 2009. **284**(38): p. 26096-105.
176. Choudhuri, K., Wiseman, D., Brown, M. H., Gould, K., and van der Merwe, P. A., *T-cell receptor triggering is critically dependent on the dimensions of its peptide-MHC ligand.* Nature, 2005. **436**(7050): p. 578-82.
177. Ma, Z. Y., Janmey, P. A., and Finkel, T. H., *The receptor deformation model of TCR triggering.* Faseb J, 2008. **22**(4): p. 1002-8.
178. Pryshchep, S., Zarnitsyna, V. I., Hong, J., Evavold, B. D., and Zhu, C., *Accumulation of Serial Forces on TCR and CD8 Frequently Applied by Agonist Antigenic Peptides Embedded in MHC Molecules Triggers Calcium in T Cells.* J Immunol, 2014. **193**(1): p. 68-76.
179. Li, Y. C., Chen, B. M., Wu, P. C., Cheng, T. L., Kao, L. S., Tao, M. H., Lieber, A., and Roffler, S. R., *Cutting Edge: Mechanical Forces Acting on T Cells Immobilized via the TCR Complex Can Trigger TCR Signaling.* J Immunol, 2010. **184**(11): p. 5959-63.
180. Kim, S. T., Takeuchi, K., Sun, Z. Y. J., Touma, M., Castro, C. E., Fahmy, A., Lang, M. J., Wagner, G., and Reinherz, E. L., *The alpha beta T Cell Receptor Is an Anisotropic Mechanosensor.* J Biol Chem, 2009. **284**(45): p. 31028-37.
181. Hui, E. and Vale, R. D., *In vitro membrane reconstitution of the T-cell receptor proximal signaling network.* Nat Struct Mol Biol, 2014. **21**(2): p. 133-42.
182. Housden, H. R., Skipp, P. J., Crump, M. P., Broadbridge, R. J., Crabbe, T., Perry, M. J., and Gore, M. G., *Investigation of the kinetics and order of tyrosine*

*phosphorylation in the T-cell receptor zeta chain by the protein tyrosine kinase Lck.* Eur J Biochem, 2003. **270**(11): p. 2369-76.
183. Hashimoto-Tane, A., Sakuma, M., Ike, H., Yokosuka, T., Kimura, Y., Ohara, O., and Saito, T., *Micro-adhesion rings surrounding TCR microclusters are essential for T cell activation.* J Exp Med, 2016. **213**(8): p. 1609-25.
184. Hui, K., Wang, C., Grooman, B., Wayt, J., and Upadhyaya, A., *Membrane dynamics correlate with formation of signaling clusters during cell spreading.* Biophys J, 2012. **102**(7): p. 1524-33.
185. Campi, G., Varma, R., and Dustin, M. L., *Actin and agonist MHC-peptide complex-dependent T cell receptor microclusters as scaffolds for signaling.* J Exp Med, 2005. **202**(8): p. 1031-6.
186. He, H. T. and Marguet, D., *T-cell antigen receptor triggering and lipid rafts: a matter of space and time scales.* EMBO Rep, 2008. **9**(6): p. 525-30.
187. Yokosuka, T., Sakata-Sogawa, K., Kobayashi, W., Hiroshima, M., Hashimoto-Tane, A., Tokunaga, M., Dustin, M. L., and Saito, T., *Newly generated T cell receptor microclusters initiate and sustain T cell activation by recruitment of Zap70 and SLP-76.* Nat Immunol, 2005. **6**(12): p. 1253-62.
188. Manz, B. N., Jackson, B. L., Petit, R. S., Dustin, M. L., and Groves, J., *T-cell triggering thresholds are modulated by the number of antigen within individual T-cell receptor clusters.* Proc Natl Acad Sci U S A, 2011. **108**(22): p. 9089-94.
189. Yokosuka, T. and Saito, T., *Dynamic regulation of T-cell costimulation through TCR–CD28 microclusters.* Immunol Rev, 2009. **229**(1): p. 27-40.
190. Lillemeier, B. F., Mörtelmaier, M. A., Forstner, M. B., Huppa, J. B., Groves, J. T., and Davis, M. M., *TCR and Lat are expressed on separate protein islands on T cell membranes and concatenate during activation.* Nat Immunol, 2010. **11**(1): p. 90-6.
191. Williamson, D. J., Owen, D. M., Rossy, J., Magenau, A., Wehrmann, M., Gooding, J. J., and Gaus, K., *Pre-existing clusters of the adaptor Lat do not participate in early T cell signaling events.* Nat Immunol, 2011. **12**(7): p. 655-62.
192. Crites, T. J., Padhan, K., Muller, J., Krogsgaard, M., Gudla, P. R., Lockett, S. J., and Varma, R., *TCR Microclusters Pre-Exist and Contain Molecules Necessary for TCR Signal Transduction.* J Immunol, 2014. **193**(1): p. 56-67.
193. Rossy, J., Owen, D. M., Williamson, D. J., Yang, Z., and Gaus, K., *Conformational states of the kinase Lck regulate clustering in early T cell signaling.* Nat Immunol, 2013. **14**(1): p. 82-9.
194. Schütz, G. J., Schindler, H., and Schmidt, T., *Single-molecule microscopy on model membranes reveals anomalous diffusion.* Biophys J, 1997. **73**(2): p. 1073-80.
195. Kumar, R., Ferez, M., Swamy, M., Arechaga, I., Rejas, M., Valpuesta, J. M., Schamel, W. W. A., Alarcon, B., and van Santen, H. M., *Increased sensitivity of antigen-experienced T cells through the enrichment of oligomeric T cell receptor complexes.* Immunity, 2011. **35**(3): p. 375-87.
196. Tolar, P. and Pierce, S. K., *A conformation-induced oligomerization model for B cell receptor microclustering and signaling*, in *Immunological Synapse*, Saito, T. and Batista, F.D., Editors. 2010, Springer Berlin Heidelberg: Berlin, Heidelberg. p. 155-69.
197. Metzger, H., *Transmembrane signaling: the joy of aggregation.* J Immunol, 1992. **149**(5): p. 1477-87.

198. Krogsgaard, M., Juang, J., and Davis, M. M., *A role for "self" in T-cell activation.* Semin Immunol, 2007. **19**(4): p. 236-44.
199. Juang, J., Ebert, P. J., Feng, D., Garcia, K. C., Krogsgaard, M., and Davis, M. M., *Peptide-MHC heterodimers show that thymic positive selection requires a more restricted set of self-peptides than negative selection.* J Exp Med, 2010. **207**(6): p. 1223-34.
200. Schilham, M. W., Fung-Leung, W. P., Rahemtulla, A., Kuendig, T., Zhang, L., Potter, J., Miller, R. G., Hengartner, H., and Mak, T. W., *Alloreactive cytotoxic T cells can develop and function in mice lacking both CD4 and CD8*. Eur J Immunol, 1993. **23**(6): p. 1299-304.
201. Locksley, R. M., Reiner, S. L., Hatam, F., Littman, D. R., and Killeen, N., *Helper T cells without CD4: control of leishmaniasis in CD4-deficient mice.* Science, 1993. **261**(5127): p. 1448-51.
202. Jönsson, P., Southcombe, J. H., Santos, A. M., Huo, J., Fernandes, R. A., McColl, J., Lever, M., Evans, E. J., Hudson, A., Chang, V. T., Hanke, T., Godkin, A., Dunne, P. D., Horrocks, M. H., Palayret, M., Screaton, G. R., Petersen, J., Rossjohn, J., Fugger, L., Dushek, O., Xu, X. N., Davis, S. J., and Klenerman, D., *Remarkably low affinity of CD4/peptide-major histocompatibility complex class II protein interactions.* Proc Natl Acad Sci U S A, 2016. **113**(20): p. 5682-7.
203. Tolar, P., Hanna, J., Krueger, P. D., and Pierce, S. K., *The constant region of the membrane immunoglobulin mediates B cell-receptor clustering and signaling in response to membrane antigens.* Immunity, 2009. **30**(1): p. 44-55.
204. Schoenborn, J. R., Tan, Y. X., Zhang, C., Shokat, K. M., and Weiss, A., *Feedback circuits monitor and adjust basal Lck-dependent events in T cell receptor signaling.* Sci Signal, 2011. **4**(190): p. ra59.
205. Tan, Y. X., Zikherman, J., and Weiss, A., *Novel tools to dissect the dynamic regulation of TCR signaling by the kinase Csk and the phosphatase CD45.* Cold Spring Harb Symp Quant Biol, 2013. **78**: p. 131-9.
206. Manz, B. N., Tan, Y. X., Courtney, A. H., Rutaganira, F., Palmer, E., Shokat, K. M., and Weiss, A., *Small molecule inhibition of Csk alters affinity recognition by T cells.* eLife, 2015. **4**: p. e08088.
207. D'Oro, U., Sakaguchi, K., Appella, E., and Ashwell, J. D., *Mutational analysis of Lck in CD45-negative T cells: dominant role of tyrosine 394 phosphorylation in kinase activity.* Mol Cell Biol, 1996. **16**(9): p. 4996-5003.
208. Nika, K., Soldani, C., Salek, M., Paster, W., Gray, A., Etzensperger, R., Fugger, L., Polzella, P., Cerundolo, V., Dushek, O., Höfer, T., Viola, A., and Acuto, O., *Constitutively active Lck kinase in T cells drives antigen receptor signal transduction.* Immunity, 2010. **32**(6): p. 766-77.
209. Secrist, J. P., Burns, L. A., Karnitz, L., Koretzky, G. A., and Abraham, R. T., *Stimulatory effects of the protein tyrosine phosphatase inhibitor, pervanadate, on T-cell activation events.* J Biol Chem, 1993. **268**(8): p. 5886-93.
210. Williams, A. F. and Barclay, A. N., *Glycoprotein antigens of the lymphocyte surface and their purification by antibody affinity chromatography*, in *Handbook of Experimental Immunology, 4th edition*, Weir, D.M. and Herzenberg, L.A., Editors. 1986, Blackwell: Oxford.

211. Fischer, E. H., Charbonneau, H., and Tonks, N. K., *Protein tyrosine phosphatases: a diverse family of intracellular and transmembrane enzymes.* Science, 1991. **253**(5018): p. 401-6.
212. Barr, A. J., Ugochukwu, E., Lee, W. H., King, O. N., Filippakopoulos, P., Alfano, I., Savitsky, P., Burgess-Brown, N. A., Muller, S., and Knapp, S., *Large-scale structural analysis of the classical human protein tyrosine phosphatome.* Cell, 2009. **136**(2): p. 352-63.
213. Hermiston, M. L., Zikherman, J., and Zhu, J. W., *CD45, CD148, and Lyp/Pep: critical phosphatases regulating Src family kinase signaling networks in immune cells.* Immunol Rev, 2009. **228**(1): p. 288-311.
214. Cordoba, S.-P. P., Choudhuri, K., Zhang, H., Bridge, M., Basat, A. B., Dustin, M. L., and van der Merwe, P. A., *The large ectodomains of CD45 and CD148 regulate their segregation from and inhibition of ligated T-cell receptor.* Blood, 2013. **121**(21): p. 4295-302.
215. Roskoski, R., Jr., *Src protein-tyrosine kinase structure and regulation.* Biochem Biophys Res Commun, 2004. **324**(4): p. 1155-64.
216. Lin, J. and Weiss, A., *The tyrosine phosphatase CD148 is excluded from the immunologic synapse and down-regulates prolonged T cell signaling.* J Cell Biol, 2003. **162**(4): p. 673-82.
217. Schmid, E. M., Bakalar, M. H., Choudhuri, K., Weichsel, J., Ann, H. S., Geissler, P. L., Dustin, M. L., and Fletcher, D. A., *Size-dependent protein segregation at membrane interfaces.* Nature Phys, 2016. **12**(7): p. 704-11.
218. Irles, C., Symons, A., Michel, F., Bakker, T. R., van der Merwe, P. A., and Acuto, O., *CD45 ectodomain controls interaction with GEMs and Lck activity for optimal TCR signaling.* Nat Immunol, 2002. **4**(2): p. 189-97.
219. Lim, H. S., Cordoba, S. P., Dushek, O., Goyette, J., Taylor, A., Rudd, C. E., and van der Merwe, P. A., *Costimulation of IL-2 Production through CD28 Is Dependent on the Size of Its Ligand.* J Immunol, 2015. **195**(11): p. 5432-9.
220. Bluemel, C., Hausmann, S., Fluhr, P., Sriskandarajah, M., Stallcup, W. B., Baeuerle, P. A., and Kufer, P., *Epitope distance to the target cell membrane and antigen size determine the potency of T cell-mediated lysis by BiTE antibodies specific for a large melanoma surface antigen.* Cancer Immunol Immunother, 2010. **59**(8): p. 1197-209.
221. James, S. E., Greenberg, P. D., Jensen, M. C., Lin, Y., Wang, J., Till, B. G., Raubitschek, A. A., Forman, S. J., and Press, O. W., *Antigen sensitivity of CD22-specific chimeric TCR is modulated by target epitope distance from the cell membrane.* J Immunol, 2008. **180**(10): p. 7028-38.
222. Sezgin, E., Kaiser, H. J., Baumgart, T., Schwille, P., Simons, K., and Levental, I., *Elucidating membrane structure and protein behavior using giant plasma membrane vesicles.* Nat Protoc, 2012. **7**(6): p. 1042-51.
223. Beck-Garcia, K., Beck-Garcia, E., Bohler, S., Zorzin, C., Sezgin, E., Levental, I., Alarcon, B., and Schamel, W. W., *Nanoclusters of the resting T cell antigen receptor (TCR) localize to non-raft domains.* Biochim Biophys Acta, 2015. **1853**(4): p. 802-9.

224. He, H. T., Lellouch, A., and Marguet, D., *Lipid rafts and the initiation of T cell receptor signaling.* Semin Immunol, 2005. **17**(1): p. 23-33.
225. Davis, S. J. and van der Merwe, P. A., *TCR triggering: co-receptor-dependent or -independent?* Trends Immunol, 2003. **24**(12): p. 624-6.
226. Su, X., Ditlev, J. A., Hui, E., Xing, W., Banjade, S., Okrut, J., King, D. S., Taunton, J., Rosen, M. K., and Vale, R. D., *Phase separation of signaling molecules promotes T cell receptor signal transduction.* Science, 2016. **352**(6285): p. 595-9.
227. Dustin, M. L. and Muller, J., *Liquidity in immune cell signaling.* Science, 2016. **352**(6285): p. 516-7.
228. Tacke, M., Hanke, G., Hanke, T., and Hünig, T., *CD28-mediated induction of proliferation in resting T cells in vitro and in vivo without engagement of the T cell receptor: Evidence for functionally distinct forms of CD28*. Eur J Immunol, 1997. **27**(1): p. 239-47.
229. Lühder, F., Huang, Y., Dennehy, K. M., Guntermann, C., Müller, I., Winkler, E., Kerkau, T., Ikemizu, S., Davis, S. J., Hanke, T., and Hünig, T., *Topological requirements and signaling properties of T cell–activating, anti-CD28 antibody superagonists.* J Exp Med, 2003. **197**(8): p. 955-66.
230. Ball, C., Fox, B., Hufton, S., Sharp, G., Poole, S., Stebbings, R., Eastwood, D., Findlay, L., Parren, P., Thorpe, R., Bristow, A., and Thorpe, S. J., *Antibody C region influences TGN1412-like functional activity in vitro.* J Immunol, 2012. **189**(12): p. 5831-40.
231. Dennehy, K. M., Elias, F., Na, S.-Y., Fischer, K.-D., Hünig, T., and Lühder, F., *Mitogenic CD28 signals require the exchange factor Vav1 to enhance TCR signaling at the SLP-76-Vav-Itk signalosome.* J Immunol, 2007. **178**(3): p. 1363-71.
232. Levin, S. E., Zhang, C., Kadlecek, T. A., Shokat, K. M., and Weiss, A., *Inhibition of ZAP-70 Kinase Activity via an Analog-sensitive Allele Blocks T Cell Receptor and CD28 Superagonist Signaling.* J Biol Chem, 2008. **283**(22): p. 15419-30.
233. Scott, A. M., Wolchok, J. D., and Old, L. J., *Antibody therapy of cancer.* Nat Rev Cancer, 2012. **12**(4): p. 278-87.
234. Bradbury, A. R. M., Sidhu, S., Dübel, S., and McCafferty, J., *Beyond natural antibodies: the power of in vitro display technologies.* Nat Biotechnol, 2011. **29**(3): p. 245-54.
235. Sheppard, K. A., Fitz, L. J., Lee, J. M., Benander, C., George, J. A., Wooters, J., Qiu, Y., Jussif, J. M., Carter, L. L., Wood, C. R., and Chaudhary, D., *PD-1 inhibits T-cell receptor induced phosphorylation of the ZAP70/CD3zeta signalosome and downstream signaling to PKCtheta.* FEBS Lett, 2004. **574**(1-3): p. 37-41.
236. Chen, L. and Han, X., *Anti-PD-1/PD-L1 therapy of human cancer: past, present, and future.* J Clin Invest, 2015. **125**(9): p. 3384-91.
237. Attarwala, H., *TGN1412: From Discovery to Disaster.* J Young Pharm, 2010. **2**(3): p. 332-6.
238. Stebbings, R., Findlay, L., Edwards, C., Eastwood, D., Bird, C., North, D., Mistry, Y., Dilger, P., Liefooghe, E., Cludts, I., Fox, B., Tarrant, G., Robinson, J., Meager, T., Dolman, C., Thorpe, S. J., Bristow, A., Wadhwa, M., Thorpe, R., and Poole, S., *"Cytokine storm" in the phase I trial of monoclonal antibody*

*TGN1412: better understanding the causes to improve preclinical testing of immunotherapeutics*. J Immunol, 2007. **179**(5): p. 3325-31.
239. Suntharalingam, G., Perry, M. R., Ward, S., Brett, S. J., Castello-Cortes, A., Brunner, M. D., and Panoskaltsis, N., *Cytokine storm in a phase 1 trial of the anti-CD28 monoclonal antibody TGN1412*. New Engl J Med, 2006. **355**(10): p. 1018-28.
240. Tabares, P., Berr, S., Römer, P. S., Chuvpilo, S., Matskevich, A. A., Tyrsin, D., Fedotov, Y., Einsele, H., Tony, H. P., and Hünig, T., *Human regulatory T cells are selectively activated by low-dose application of the CD28 superagonist TGN1412/TAB08*. Eur J Immunol, 2014. **44**(4): p. 1225-36.
241. Tyrsin, D., Chuvpilo, S., Matskevich, A., Nemenov, D., Römer, P. S., Tabares, P., and Hünig, T., *From TGN1412 to TAB08: the return of CD28 superagonist therapy to clinical development for the treatment of rheumatoid arthritis*. Clin Exp Rheumatol, 2016. **34**(4 Suppl 98): p. 45-8.
242. Haskins, K., Kubo, R., White, J., Pigeon, M., Kappler, J., and Marrack, P., *The major histocompatibility complex-restricted antigen receptor on T cells. I. Isolation with a monoclonal antibody*. J Exp Med, 1983. **157**(4): p. 1149-69.
243. Marrack, P., Bender, J., Jordan, M., Rees, W., Robertson, J., Schaefer, B. C., and Kappler, J., *Major histocompatibility complex proteins and TCRs: do they really go together like a horse and carriage?* J Immunol, 2001. **167**(2): p. 617-21.
244. Hernandez, J. D., Klein, J., Dyken, S. J., Marth, J. D., and Baum, L. G., *T-cell activation results in microheterogeneous changes in glycosylation of CD45*. Int Immunol, 2007. **19**(7): p. 847-56.
245. Graham, F. L., Smiley, J., Russell, W. C., and Nairn, R., *Characteristics of a human cell line transformed by DNA from human adenovirus type 5*. J Gen Virol, 1977. **36**(1): p. 59-72.
246. Demaison, C., Parsley, K., Brouns, G., Scherr, M., Battmer, K., Kinnon, C., Grez, M., and Thrasher, A. J., *High-level transduction and gene expression in hematopoietic repopulating cells using a human imunodeficiency virus type 1-based lentiviral vector containing an internal spleen focus forming virus promoter*. Hum Gene Ther, 2002. **13**(7): p. 803-13.
247. *BIAevaluation Software Handbook*. 2007, GE Healthcare Bio-Sciences AB. p. 183.
248. Hünig, T. and Dennehy, K., *CD28 superagonists: mode of action and therapeutic potential*. Immunol Lett, 2005. **100**(1): p. 21-8.
249. Morgan, S. H., *Molecular aspects of antibody mediated T cell activation*, in *Nuffield Department of Medicine*. 2009, University of Oxford: Oxford.
250. van der Merwe, P. A. *Surface plasmon resonance*. 1999.
251. Evans, E. J., Castro, M. A. A., O'Brien, R., Kearney, A., Walsh, H., Sparks, L. M., Tucknott, M. G., Davies, E. A., Carmo, A. M., Merwe, P. A., Stuart, D. I., Jones, E. Y., Ladbury, J. E., Ikemizu, S., and Davis, S. J., *Crystal structure and binding properties of the CD2 and CD244 (2B4)-binding protein, CD48*. J Biol Chem, 2006. **281**(39): p. 29309-20.
252. van der Merwe, P. A., Bodian, D. L., Daenke, S., Linsley, P., and Davis, S. J., *CD80 (B7-1) binds both CD28 and CTLA-4 with a low affinity and very fast kinetics*. J Exp Med, 1997. **185**(3): p. 393-403.

253. Fritzsche, M., Fernandes, R. A., Colin-York, H., Santos, A. M., Lee, S. F., Lagerholm, C. B., Davis, S. J., and Eggeling, C., *CalQuo: automated, simultaneous single-cell and population-level quantification of global intracellular Ca2+ responses.* Sci Rep, 2015. **5**: p. 16487.
254. Giannone, G. and Sheetz, M. P., *Substrate rigidity and force define form through tyrosine phosphatase and kinase pathways.* Trends Cell Biol, 2006. **16**(4): p. 213-23.
255. Vogel, V. and Sheetz, M., *Local force and geometry sensing regulate cell functions.* Nat Rev Mol Cell Biol, 2006. **7**(4): p. 265-75.
256. O'Connor, R. S., Hao, X., Shen, K., Bashour, K., Akimova, T., Hancock, W. W., Kam, L. C., and Milone, M. C., *Substrate rigidity regulates human T cell activation and proliferation.* J Immunol, 2012. **189**(3): p. 1330-9.
257. Bhakta, N. R., Oh, D. Y., and Lewis, R. S., *Calcium oscillations regulate thymocyte motility during positive selection in the three-dimensional thymic environment.* Nat Immunol, 2005. **6**(2): p. 143-51.
258. Harriague, J. and Bismuth, G., *Imaging antigen-induced PI3K activation in T cells.* Nat Immunol, 2002. **3**(11): p. 1090-6.
259. Hessell, A. J., Hangartner, L., Hunter, M., Havenith, C. E., Beurskens, F. J., Bakker, J. M., Lanigan, C. M., Landucci, G., Forthal, D. N., Parren, P. W., Marx, P. A., and Burton, D. R., *Fc receptor but not complement binding is important in antibody protection against HIV*. Nature, 2007. **449**(7158): p. 101-4.
260. Akkaya, B., *Modulation of the PD-1 pathway by inhibitory antibody superagonists*, in *Nuffield Department of Medicine*. 2012, University of Oxford: Oxford.
261. Liu, H. and May, K., *Disulfide bond structures of IgG molecules: structural variations, chemical modifications and possible impacts to stability and biological function.* MAbs, 2012. **4**(1): p. 17-23.
262. Harris, L. J., Skaletsky, E., and McPherson, A., *Crystallographic structure of an intact IgG1 monoclonal antibody.* J Mol Biol, 1998. **275**(5): p. 861-72.
263. Sondermann, P., Huber, R., and Jacob, U., *Crystal structure of the soluble form of the human fcgamma-receptor IIb: a new member of the immunoglobulin superfamily at 1.7 A resolution.* EMBO J, 1999. **18**(5): p. 1095-103.
264. Fernandes, R. A., *Controls on T-cell receptor phosphorylation and triggering*, in *Nuffield Department of Medicine*. 2011, University of Oxford: Oxford.
265. Shields, R. L., Namenuk, A. K., Hong, K., Meng, Y. G., Rae, J., Briggs, J., Xie, D., Lai, J., Stadlen, A., Li, B., Fox, J. A., and Presta, L. G., *High resolution mapping of the binding site on human IgG1 for Fc gamma RI, Fc gamma RII, Fc gamma RIII, and FcRn and design of IgG1 variants with improved binding to the Fc gamma R.* J Biol Chem, 2001. **276**(9): p. 6591-604.
266. Tao, M. H. and Morrison, S. L., *Studies of aglycosylated chimeric mouse-human IgG. Role of carbohydrate in the structure and effector functions mediated by the human IgG constant region.* J Immunol, 1989. **143**(8): p. 2595-601.
267. Mimura, Y., Sondermann, P., Ghirlando, R., Lund, J., Young, S. P., Goodall, M., and Jefferis, R., *Role of oligosaccharide residues of IgG1-Fc in Fc gamma RIIb binding.* J Biol Chem, 2001. **276**(49): p. 45539-47.
268. Walker, M. R., Lund, J., Thompson, K. M., and Jefferis, R., *Aglycosylation of human IgG1 and IgG3 monoclonal antibodies can eliminate recognition by human cells*

*expressing Fc gamma RI and/or Fc gamma RII receptors.* Biochem J, 1989. **259**(2): p. 347-53.
269. Mazor, Y., Van Blarcom, T., Mabry, R., Iverson, B. L., and Georgiou, G., *Isolation of engineered, full-length antibodies from libraries expressed in Escherichia coli.* Nat Biotechnol, 2007. **25**(5): p. 563-5.
270. Simmons, L. C., Reilly, D., Klimowski, L., Raju, T. S., Meng, G., Sims, P., Hong, K., Shields, R. L., Damico, L. A., Rancatore, P., and Yansura, D. G., *Expression of full-length immunoglobulins in Escherichia coli: rapid and efficient production of aglycosylated antibodies.* J Immunol Methods, 2002. **263**(1-2): p. 133-47.
271. Palayret, M. G. S., *Applying Single-Molecule Localisation Microscopy to Achieve Virtual Optical Sectioning and Study T-Cell Activation*, in *Department of Chemistry*. 2015, University of Cambridge: Cambridge.
272. Weimann, L., Ganzinger, K. A., McColl, J., Irvine, K. L., Davis, S. J., Gay, N. J., Bryant, C. E., and Klenerman, D., *A Quantitative Comparison of Single-Dye Tracking Analysis Tools Using Monte Carlo Simulations.* PLoS ONE, 2013. **8**(5): p. e64287.
273. Chozinski, T. J., Gagnon, L. A., and Vaughan, J. C., *Twinkle, twinkle little star: Photoswitchable fluorophores for super-resolution imaging.* FEBS Lett, 2014. **588**(19): p. 3603-12.
274. Min-Feandez, M. L., Tynan, C. J., and Webb, S. E. D., *A 'pocket guide' to total internal reflection fluorescence.* J Microsc, 2013. **252**(1): p. 16-22.
275. Zhang, M., Chang, H., Zhang, Y., Yu, J., Wu, L., Ji, W., Chen, J., Liu, B., Lu, J., Liu, Y., Zhang, J., Xu, P., and Xu, T., *Rational design of true monomeric and bright photoactivatable fluorescent proteins.* Nat Methods, 2012. **9**(7): p. 727-29.
276. Manley, S., Gillette, J. M., and Lippincott-Schwartz, J., *Chapter five-single-particle tracking photoactivated localization microscopy for mapping single-molecule dynamics*, in *Methods in Enzymology*, Nils, G.W., Editor. 2010, Academic Press. p. 109-20.
277. Saxton, M. J., *Single-particle tracking: connecting the dots.* Nat Methods, 2008. **5**(8): p. 671-2.
278. Kong, Y. M., Waldmann, H., Cobbold, S., Giraldo, A. A., Fuller, B. E., and Simon, L. L., *Pathogenic mechanisms in murine autoimmune thyroiditis: short-and long-term effects of in vivo depletion of CD4+ and CD8+ cells.* Clin Exp Immunol, 1989. **77**(3): p. 428-33.
279. Watt, S. M., Gilmore, D. J., Davis, J. M., Clark, M. R., and Waldmann, H., *Cell-surface markers on haemopoietic precursors. Reagents for the isolation and analysis of progenitor cell subpopulations.* MCP, 1987. **1**(4): p. 297-326.
280. Malkusch, S., Endesfelder, U., Mondry, J., Gelleri, M., Verveer, P. J., and Heilemann, M., *Coordinate-based colocalization analysis of single-molecule localization microscopy data.* Histochem Cell Biol, 2012. **137**(1): p. 1-10.
281. Bartholomaeus, P., Semmler, L. Y., Bukur, T., Boisguerin, V., Römer, P. S., Tabares, P., Chuvpilo, S., Tyrsin, D. Y., Matskevich, A., Hengel, H., Castle, J., Hünig, T., and Kalinke, U., *Cell contact-dependent priming and Fc interaction with CD32+ immune cells contribute to the TGN1412-triggered cytokine response.* J Immunol, 2014. **192**(5): p. 2091-8.

282. Oh-hora, M. and Rao, A., *Calcium signaling in lymphocytes.* Curr Opin Immunol, 2008. **20**(3): p. 250-8.
283. Jutz, S., Leitner, J., Schmetterer, K., Doel-Perez, I., Majdic, O., Grabmeier-Pfistershammer, K., Paster, W., Huppa, J. B., and Steinberger, P., *Assessment of costimulation and coinhibition in a triple parameter T cell reporter line: Simultaneous measurement of NF-κB, NFAT and AP-1.* J Immunol Methods, 2016. **430**: p. 10-20.
284. Waibler, Z., Sender, L. Y., Merten, C., Hartig, R., Kliche, S., Gunzer, M., Reichardt, P., Kalinke, U., and Schraven, B., *Signaling Signatures and Functional Properties of Anti-Human CD28 Superagonistic Antibodies.* PLoS ONE, 2008. **3**(3): p. e1708.
285. Hussain, K., Hargreaves, C. E., Roghanian, A., Oldham, R. J., Chan, H. T. C., Mockridge, C. I., Chowdhury, F., Frendeus, B., Harper, K. S., Strefford, J. C., Cragg, M. S., Glennie, M. J., Williams, A. P., and French, R. R., *Upregulation of FcγRIIb on monocytes is necessary to promote the superagonist activity of TGN1412.* Blood, 2015. **125**(1): p. 102-10.
286. James, J. R. and Vale, R. D., *Biophysical mechanism of T-cell receptor triggering in a reconstituted system.* Nature, 2012. **487**(7405): p. 64-9.
287. Cartwright, A. N. R., Griggs, J., and Davis, D. M., *The immune synapse clears and excludes molecules above a size threshold.* Nat Commun, 2014. **5**: p. 5479.
288. Alakoskela, J.-M., Koner, A. L., Rudnicka, D., Köhler, K., Howarth, M., and Davis, D. M., *Mechanisms for size-dependent protein segregation at immune synapses assessed with molecular rulers.* Biophys J, 2011. **100**(12): p. 2865-74.
289. Gogishvili, T., Elias, F., Emery, J. L., McPherson, K., Okkenhaug, K., Hünig, T., and Dennehy, K. M., *Proliferative signals mediated by CD28 superagonists require the exchange factor Vav1 but not phosphoinositide 3-kinase in primary peripheral T cells.* Eur J Immunol, 2008. **38**(9): p. 2528-33.
290. Bischof, A., Hara, T., Lin, C. H., Beyers, A. D., and Hünig, T., *Autonomous induction of proliferation, JNK and NF-alphaB activation in primary resting T cells by mobilized CD28.* Eur J Immunol, 2000. **30**(3): p. 876-82.
291. Brodovitch, A., Bongrand, P., and Pierres, A., *T lymphocytes sense antigens within seconds and make a decision within one minute.* J Immunol, 2013. **191**(5): p. 2064-71.
292. Axelrod, D., *Cell-substrate contacts illuminated by total internal reflection fluorescence.* J Cell Biol, 1981. **89**(1): p. 141-5.
293. Chen, B.-C., Legant, W. R., Wang, K., Shao, L., Milkie, D. E., Davidson, M. W., Janetopoulos, C., Wu, X. S., Hammer, J. A., Liu, Z., English, B. P., Mimori-Kiyosue, Y., Romero, D. P., Ritter, A. T., Lippincott-Schwartz, J., Fritz-Laylin, L., Mullins, D. R., Mitchell, D. M., Bembenek, J. N., Reymann, A.-C., Böhme, R., Grill, S. W., Wang, J. T., Seydoux, G., Tulu, S. U., Kiehart, D. P., and Betzig, E., *Lattice light-sheet microscopy: Imaging molecules to embryos at high spatiotemporal resolution.* Science, 2014. **346**(6208): p. 1257998.
294. Chen, W., Zarnitsyna, V. I., Sarangapani, K. K., Huang, J., and Zhu, C., *Measuring Receptor-Ligand Binding Kinetics on Cell Surfaces: From Adhesion Frequency to Thermal Fluctuation Methods.* Cell Mol Bioeng, 2008. **1**(4): p. 276-88.

295. Zhou, Z., Zhang, Y., and Zhu, L., *Theoretical and experimental studies on optical trapping using radially polarized beams.* Opt Quant Electron, 2016. **48**(8): p. 404.
296. Kaizuka, Y., Douglass, A. D., Varma, R., Dustin, M. L., and Vale, R. D., *Mechanisms for segregating T cell receptor and adhesion molecules during immunological synapse formation in Jurkat T cells.* Proc Natl Acad Sci U S A, 2007. **104**(51): p. 20296-301.
297. Davis, S. J. and van der Merwe, P. A., *The structure and ligand interactions of CD2: implications for T-cell function.* Immunol Today, 1996. **17**(4): p. 177-87.
298. van der Merwe, P. A., McNamee, P. N., Davies, E. A., Barclay, A. N., and Davis, S. J., *Topology of the CD2-CD48 cell-adhesion molecule complex: implications for antigen recognition by T cells.* Curr Biol, 1995. **5**(1): p. 74-84.
299. Theodoly, O., Huang, Z. H., and Valignat, M. P., *New modeling of reflection interference contrast microscopy including polarization and numerical aperture effects: application to nanometric distance measurements and object profile reconstruction.* Langmuir, 2010. **26**(3): p. 1940-8.
300. Chizhik, A. I., Rother, J., Gregor, I., Janshoff, A., and Enderlein, J., *Metal-induced energy transfer for live cell nanoscopy.* Nat Photon, 2014. **8**(2): p. 124-7.
301. Cardoso Dos Santos, M., Deturche, R., Vezy, C., and Jaffiol, R., *Topography of Cells Revealed by Variable-Angle Total Internal Reflection Fluorescence Microscopy.* Biophys J, 2016. **111**(6): p. 1316-27.
302. Cartwright, A. N., Griggs, J., and Davis, D. M., *The immune synapse clears and excludes molecules above a size threshold.* Nat Commun, 2014. **5**: p. 5479.
303. Beyersdorf, N., Gaupp, S., Balbach, K., Schmidt, J., Toyka, K. V., Lin, C. H., Hanke, T., Hünig, T., Kerkau, T., and Gold, R., *Selective targeting of regulatory T cells with CD28 superagonists allows effective therapy of experimental autoimmune encephalomyelitis.* J Exp Med, 2005. **202**(3): p. 445-55.
304. Eastwood, D., Findlay, L., Poole, S., Bird, C., Wadhwa, M., Moore, M., Burns, C., Thorpe, R., and Stebbings, R., *Monoclonal antibody TGN1412 trial failure explained by species differences in CD28 expression on CD4+ effector memory T-cells.* Br J Pharmacol, 2010. **161**(3): p. 512-26.